

FLORIDA INTERNATIONAL UNIVERSITY

Miami, Florida

DIPICOLINAMIDE LIGANDS AND ANALOGS FOR LANTHANIDES (Ln),
ACTINIDES (An) AND MERCURY (Hg) FOR APPLICATION TO NUCLEAR FUEL
CYCLE SEPARATIONS AND WASTE MANAGEMENT

A dissertation submitted in partial fulfillment of the

requirements for the degree of

DOCTOR IN PHILOSOPHY

in

CHEMISTRY

by

Ingrid Lehman-Andino

2020

To: Dean Michael R. Heithaus
College of Arts, Sciences, and Education

This dissertation, written by Ingrid Lehman-Andino and entitled Dipicolinamide Ligands and Analogs for Lanthanides (Ln), Actinides (An), and Mercury (Hg) for Application to Nuclear Fuel Cycle Separations and Waste Management, having been approved in respect to style and intellectual content, is referred to you for judgment.

We have read this dissertation and recommend that it be approved.

Christopher J. Dares

Anthony DeCaprio

Raphael G. Raptis

Joerg Reinhold

Konstantinos Kavallieratos, Major Professor

Date of Defense: June 26, 2020

The dissertation of Ingrid Lehman-Andino is approved.

Dean Michael R. Heithaus
College of Arts, Sciences and Education

Andrés G. Gil
Vice President of Research and Economic Development
and Dean of the University Graduate School

Florida International University, 2020

© Copyright 2020 by Ingrid Lehman-Andino

All rights reserved.

DEDICATION

With all my love to my parents, Roberto Lehman-Matos and Jenny Andino-Vergara.

Without their support, this work wouldn't be possible to achieve.

To my grandmothers, Ramona "Monin" Vergara-Nuñez and Luz María Matos-Cruz, and my grandfather Arturo Lehman-Lopez thanks for becoming my angels.

To my friends and family, thanks for always been there for me.

To every person who believed in me.

To myself...

ACKNOWLEDGMENTS

First, I express my profound gratitude to my supervisor, Dr. Konstantinos Kavallieratos, for his support and guidance. I will be eternally grateful to Dr. KK, as we call him at the lab, for his patience and wisdom. Particular thanks to Dr. Christopher J. Dares for guidance and advice during collaboration and travels to Idaho National Laboratory (INL).

We acknowledge the U.S. Nuclear Regulatory Commission (US-NRC) that supported me with a fellowship (NRC-HQ-84-14-G-0040/NRC-HQ-84-15-G-0038/0038B). This research was also supported by the Center for Actinide Science and Technology (CAST), an Energy Frontier Research Center (EFRC) funded by the U.S. Department of Energy (US-DOE), Office of Science, Basic Energy Sciences (BES), under Award DE-SC0016568 and by the US-DOE of Environmental Management-Savannah River Nuclear Solutions (SRNS-MSIPP Contract BOA541 TOA 0000332972 and 0000403067).

We are grateful to Dr. Travis S. Grimes (INL) for solvent extraction experimental collaboration, help, and advice. Thanks to our collaborators Dr. Jing Su, Dr. Enrique R. Batista, and Dr. Ping Yang at Los Alamos National Laboratory (theory), Dr. Teresa M. Eaton, Dr. Jiwen Jian, Dr. Tian Jian, Dr. John K. Gibson at Lawrence Berkeley National Laboratory (Mass Spectrometry), Dr. David Dan, Dr. Thomas E. Albrecht-Schmitt, Dr. Indranil Chakaborty, Dr. Logesh Mathivatanan, Dr. Raphael G. Raptis (X-ray crystallography). Special thanks to labmates and colleagues who make this process easier by their help: Ivis Chaplé, Alvio J. Dominguez, Matthew T. Fortunato, Andres Francisco, Gabriel A. Flores, Ma. Renalyn Gem A. Macias, Gabriella G. Pena, Dr. Tosin M. Jonah, Dr. Rene Panzer, Dr. Xinrui Zhang, Dr. Konstantinos E. Papathanasiou, and Jeffrey R. McLachlan.

ABSTRACT OF THE DISSERTATION

DIPICOLINAMIDE LIGANDS AND ANALOGS FOR LANTHANIDES (Ln), ACTINIDES (An) AND MERCURY (Hg) FOR APPLICATION TO NUCLEAR FUEL CYCLE SEPARATIONS AND WASTE MANAGEMENT

by

Ingrid Lehman-Andino

Florida International University, 2020

Miami, Florida

Professor Konstantinos Kavallieratos, Major Professor

Spent nuclear fuel (SNF) – or used nuclear fuel (UNF) – contains long-lived minor actinides such as ^{241}Am , ^{245}Cm , and ^{237}Np , together with fission products that include lanthanides. Minor actinides are responsible for much of the radiotoxicity and heat generation that limits the capacity of geological repositories. Thus, removing minor actinides from UNF can reduce storage time required for decay to natural levels of activity by several orders of magnitude. Actinide(An)/Lanthanide(Ln) separation processes via solvent extraction by selective complexation with organic or aqueous ligands have to overcome difficulties due to similarities in their ionic radii for the +3 oxidation state. Actinide valence orbitals (5f) allow for a stronger covalent component in metal-ligand interactions with soft-donor ligands, as compared to the 4f orbitals in lanthanides. Therefore, we have synthesized ligands with soft-donor sites that can take advantage of slight differences in hardness between An(III) and Ln(III) for selective An^{3+} separations.

We have investigated the binding and extraction properties of An and Ln with ligands that contain the C=O *vs.* the C=S group, specifically dipicolinamides *vs.* dithiopicolinamides. The *S*-donor thioamide ligand did not show strong binding towards Ln(III) in the UV-visible and NMR spectra in CH₃CN, yet it was shown to extract Am(III) over Ln(III) from highly acidic solutions. Gas-phase studies and theoretical DFT calculations both showed stronger binding of An(III) *vs.* Ln(III) for the thioamide *vs.* the amide ligand in agreement with extraction results. Moreover, a dipyridine-dipicolinamide ligand was also used in an aqueous environment as a holdback reagent that keeps Am(III) selectively in the aqueous phase while HDEHP complexes Ln(III) in the organic phase, taking advantage of the difference in hardness between An(III) and Ln(III).

Our dipicolinamide and dithiopicolinamide results open new possibilities for efficient waste transmutation processes and for minor actinide recycling that can increase uranium utilization. Aside from SNF, dithiopicolinamide ligands also showed promise for addressing the presence of mercury in cold war nuclear waste. As Hg is present in the nuclear waste tanks at the Savannah River Site in several forms, including organic Hg, the mercury problem has been of concern.

TABLE OF CONTENTS

CHAPTER	PAGE
CHAPTER I - Spent Nuclear Fuel: Reprocessing and Management Alternatives.....	1
1.1 Nuclear fuel cycle and spent nuclear fuel	2
1.1.1 The Nuclear Fuel Cycle:.....	2
1.1.2 Reprocessing of spent fuel	6
1.1.3 Americium; properties, separation, and removal	9
1.2 Solvent extraction concepts and theory	11
1.3 Separation processes (An/Ln and An + Ln from fission products).....	13
1.3.1 Overview:	13
1.3.2 DIAMEX Process:.....	14
1.3.3 TALSPEAK and ALSEP:	15
1.3.4 SANEX and GANEX:.....	18
1.4 Development of selective ligands for An(III)/ Ln(III) separation.....	20
1.4.1 Overview:	20
1.4.2 Ligand design criteria	21
1.4.3 Dipicolinamides and Dithiopicolinamides	22
1.5 Legacy waste and integrated salt-waste processing at the Savannah River Site.....	25
1.5.1 Savannah River Site and the CSSX Process:	25
1.5.2 Mercury treatment at Savannah River Site.....	27
1.6 Methodology for quantifying Metal-Ligand interactions.....	28
1.6.1 Binding constant determination by NMR spectroscopy.....	30
1.6.2 Binding constant determination by UV-Visible spectroscopy	30
1.6.3 Binding constant determination by fluorescence spectroscopy	31
1.7 References:	32
 CHAPTER II: Soft-donor dipicolinamide derivatives for selective actinide(III)/lanthanide(III) separation: the role of S- vs. O-donor sites.....	 42
2.1 Abstract:	43

2.2	Introduction:	43
2.3	Results and Discussion	47
2.3.1	Spectrophotometric titrations:	47
2.3.2	X-ray Crystallography	53
2.3.3	Solvent Extraction	54
2.3.4	Gas Phase Studies: CID-ESI-MS	56
2.3.5	DFT Calculations	58
2.4	Experimental	63
2.4.1	Material and Methods:	63
2.4.2	Synthetic procedure for [Nd(3) ₃]I ₃ complex:	66
2.4.3	UV-Visible Titrations:	66
2.4.4	UV-Visible Job plots:	67
2.4.5	Fluorescence titrations:	67
2.4.6	¹ H-NMR Titrations:	68
2.4.7	Solvent Extraction:	68
2.4.8	DFT calculations:	69
2.4.9	Gas phase experiments (CID-ESI-MS):	71
2.4.10	X-Ray Crystallography:	71
2.5	Conclusion	72
2.6	References:	73
CHAPTER III: A bis(pyridine)dipicolinamide derivative as a water-soluble holdback reagent for selective Am(III)/Ln(III) separations.....82		
3.1	Abstract	83
3.2	Introduction	84
3.3	Results and discussion	86
3.3.1	Solvent extraction results	86

3.3.2	Collision Induced Dissociation Electron Spray Ionization Mass Spectroscopy (CID-ESI-MS) results.....	89
3.3.3	Spectrophotometric data - UV-Visible titrations:	93
3.3.4	Potentiometric Titrations:.....	95
3.3.5	Counteranion effects: Isolation and characterization of [Nd(III)L ₃](PF ₆) ₃ complex.....	96
3.4	Experimental Section:	98
3.4.1	Materials and Methods.....	98
3.4.2	Synthesis	99
3.4.1	Solvent extraction:.....	100
3.4.2	Gas-Phase via Collision Induced Dissociation (CID).....	101
3.4.3	UV-visible titrations:.....	102
3.4.4	Potentiometric titrations:.....	103
3.5	Conclusion:.....	103
3.6	References:	104
CHAPTER IV: A dithiopicolinamide ligand complexes and senses Hg(II) selectively via a unique 2:2 Hg ₂ L ₂ coordination pattern.....		
4.1	Abstract:	109
4.2	Introduction	109
4.4	Results and Discussion.....	112
4.4.1	X-ray Crystallography and FT-IR	112
4.4.2	¹ H-NMR titration (complexation analysis)	118
4.4.3	UV-Visible titration.....	119
4.5	Experimental:	122
4.5.1	Materials and Methods:	122
4.5.2	Synthetic procedure.....	123
4.5.3	UV-Visible Titrations and determination of K ₂₂ binding constant:.....	123

4.5.4	¹ H-NMR Titration Experiments:	125
4.5.5	X-ray crystallography:	126
4.6	Conclusion:	128
4.7	References:	129
CHAPTER V: Investigation of Uranyl (UO ₂₂₊) U-O and U-S bonding interaction: Complexation by the Dipicolinamide and Dithiopicolinamide Ligands as Probes for Complexation of AmO ₂₂₊		
		134
5.1	Abstract:	135
5.2	Introduction:	135
5.3	Results and discussion:	138
5.4	Experimental section:	145
5.4.1	Materials and Methods:	145
5.4.2	UV-Visible titrations:	145
5.4.3	Solvent drop grinding Infrared spectroscopy:	146
5.4.4	Gas-phase experiments (CID-ESI-MS) and infrared multiphoton dissociation spectroscopy:	146
5.4.5	Computational details:	147
5.5	Conclusion:	148
5.6	References:	149
Chapter VI: General Conclusions		152
Appendices		155
VITA		209

LIST OF TABLES

TABLE	PAGE
Table 1.1. Am/Eu separation factors for organic extractants with soft-donor atoms for Am(III) extraction from highly acidic media. Br Cosan is a brominated cobalt bis(dicarbollide) anion, used as a synergistic lipophilic anion.	22
Table 2.1. Calculated Gibbs free energies (ΔG in kcal/mol) for the ligand exchange reaction $M(\text{NO}_3)_3(2)(\text{H}_2\text{O}) + \mathbf{1} \rightarrow M(\text{NO}_3)_3(1)(\text{H}_2\text{O}) + \mathbf{2}$, where $M = \text{Nd, Eu and Am}$, in CH_3CN and CH_2Cl_2 , respectively.	60
Table 2.2. Calculated and Experimental Gibbs free energies (ΔG in kcal/mol) of the reactions of the M(III) hydrates and nitrate hydrates ($M = \text{Am and Eu}$) with ligands 1 and 2 in $\text{CH}_2\text{Cl}_2/\text{HNO}_3$	62
Table 3.1. Ln/Am separation factors (SF) in dodecane/ HNO_3 (pH = 2.0) at various concentrations of holdback reagent L. HDEHP concentration is constant at 0.35 M	86
Table 4.1. Crystal data and structure refinement parameters for LH_2 and complex 1.	127
Table A.1. Crystal data and structure refinement parameters for ligand 3.	169
Table A.2. Crystal data and structure refinement parameters for Pb-3.	169
Table B.1. Crystal data and structure refinement for $[\text{Nd}(3)_3]\text{I}_3 \cdot 3\text{CH}_3\text{CN}$	174
Table B.2. Fractional Atomic Coordinates ($\times 10^4$) and Equivalent Isotropic Displacement Parameters ($\text{\AA}^2 \times 10^3$) for Nd(3). U_{eq} is defined as 1/3 of the trace of the orthogonalised U_{IJ} tensor.	175
Table B.3. Anisotropic Displacement Parameters ($\text{\AA}^2 \times 10^3$) for Nd(3). The Anisotropic displacement factor exponent takes the form: $-2\pi^2[\text{h}^2\text{a}^*{}^2U_{11} + 2\text{hka}^*\text{b}^*U_{12} + \dots]$	178
Table B.4. Bond Lengths for Nd(3).	182
Table B.5. Bond Angles for Nd(3).	185

Table B.6. Hydrogen Atom Coordinates ($\text{\AA}\times 10^4$) and Isotropic Displacement Parameters ($\text{\AA}^2\times 10^3$) for Nd(3).....	190
Table B.7. Atomic Occupancy for Nd(3).....	194
Table B.8. Cartesian coordinates of PBE0 optimized geometries of ligands and metal complexes	195

LIST OF FIGURES

FIGURE	PAGE
Figure 1.1. Diagram of nuclear fuel cycle obtained from the Congressional Research Service, Report RL34234. Retrieved from https://fas.org/sgp/crs/nuke/R45880.pdf	3
Figure 1.2. The approximate constituents of the spent nuclear fuel: from The Royal Society Science Policy Center Report. Oct 2011. ISBN: 978-0-85403-891-6.	5
Figure 1.3. Used nuclear fuel radiotoxicity over time: i) under current long-term storage practices, ii) after partitioning and transmutation, including removal and reuse of U/Pu and An/Ln separation iii) after full minor actinide recycling and reuse of reprocessed fuel (including minor An) in fast reactors. (Diagram retrieved from Magill et al. ³)	8
Figure 1.4. Solvent extraction schematic of the liquid-liquid extraction procedure.....	12
Figure 1.5. Molecular structures of TODGA (1), DMDBTDMA (2), and DMDOHEMA (3).....	15
Figure 1.6. Extractants for TALSPEAK process: Diisopropylbenzene (DIPB) (1) and bis(2-ethylhexyl) hydrogen phosphate (HDEHP) (2), are used as organic extractants, while 2-ethylhexylphosphonic acid mono-2-ethylhexyl ester (HEH[EHP]) (3) and diethylenetriamine-N,N,N', N'',N'''- pentaacetic acid (DTPA) (4) are used as stripping agents.....	16
Figure 1.7. Molecular structure of Cyanex 923.	17
Figure 1.8 Organic co-extractants used for the ALSEP separation process octyl(phenyl)-N,N-diisobutylcarbamoylmethylphosphine oxide (CMPO) (1) and N,N,N',N'-tetra(2-ethylhexyl)diglycolamide (T2EHDGA) (2).	18
Figure 1.9 N-Donor ligands used for SANEX and <i>i</i> -SANEX processes: CyMe ₄ -BTBP (1) and BTP type (2) ligands used for SANEX extraction by Geist and Magnusson; ³³ Water-soluble BTP-type ligands (3) used by Geist ^{16,49} and bis-triazolyl pyridines (4) used by Macerata ¹⁵ for <i>i</i> -SANEX processing.	20
Figure 1.10. Extractants used by Nigond and coworkers in 1993.	23
Figure 1.11. Structure of Dipicolinic acid (DPA).	24

Figure 1.12 Structures of thioamide-based Pd(II) pincer complexes.	24
Figure 1.13. Structures of 1,10-phenanthroline ligands used by Galletta et al.	25
Figure 1.14 Cs-loaded extractant (calix[4]arene-bis(4-tert-octylbenzo-crown-6)) used for CSSX.....	27
Figure 2.1 Structure of Cyanex-301.....	44
Figure 2.2. Molecular structures of i) a picolinamide-based calix[6]arene (a), ii) diamides of dipicolinic acid (b), iii)dipicolinamide triazine (c), iv) dipicolinamide- phenanthroline-based ligands (d) and v) rigid pyridine-2,6-dicarboxamide analogs (e).....	45
Figure 2.3. Dipicolinamide and dithiopicolinamide ligands under investigation. N ² ,N ⁶ -bis(phenyl)pyridine-2,6-dicarboxamide (1), N ² ,N ⁶ -bis(phenyl)pyridine-2,6- bis(carbothioamide) (2), N ² ,N ⁶ -bis(4-(tert-butyl)phenyl)pyridine-2,6- dicarboxamide (3) and N ² ,N ⁶ -bis(4-(tert-butyl)phenyl)pyridine-2,6- dicarbothioamide (4).....	46
Figure 2.4. UV-Visible titration in CH ₃ CN of 1 (1.3 x 10 ⁻⁵ M) with Nd(NO ₃) ₃ ·6H ₂ O (1.0 x 10 ⁻³ M).....	47
Figure 2.5. a) UV-Vis titration in CH ₃ CN of ligand 2 (3.4 x 10 ⁻⁵ M) with Nd(NO ₃) ₃ ·6H ₂ O (1.1 x 10 ⁻³ M) (b) UV-Vis titration in CH ₃ CN of ligand 4 (1.0x 10 ⁻⁴ M) with Nd(NO ₃) ₃ ·6H ₂ O (1.1 x 10 ⁻² M)	48
Figure 2.6. UV-visible titration in CH ₃ CN of ligand 3 (2.6 x 10 ⁻⁵ M) with Nd(NO ₃) ₃ ·6H ₂ O (1.0 x10 ⁻³ M).....	48
Figure 2.7. a) UV-Vis titration in CH ₃ CN of ligand 1 (2.6 x 10 ⁻⁵ M) with La(NO ₃) ₃ ·6H ₂ O (1.2 x 10 ⁻³ M). b) UV-Vis titration in CH ₃ CN of ligand 1 (1.3 x 10 ⁻⁵ M) with Eu(NO ₃) ₃ ·6H ₂ O (1.0 x 10 ⁻³ M) c) UV-Vis titration in CH ₃ CN of ligand 1 (2.8 x 10 ⁻⁵ M) with Lu(NO ₃) ₃ ·6H ₂ O (1.9 x 10 ⁻³ M).....	49
Figure 2.8. a. Fluorescence titration in CH ₃ CN of 1 (1.3 x 10 ⁻⁵ M) with La(NO ₃) ₃ ·6H ₂ O (8.8 x 10 ⁻³ M). b. Fluorescence titration in CH ₃ CN of 1 (2.8 x 10 ⁻⁵ M) with Lu(NO ₃) ₃ ·6H ₂ O (1.9 x 10 ⁻³ M). c. Fluorescence titration in CH ₃ CN of 1 (1.2 x 10 ⁻⁴ M) with Ce(NO ₃) ₃ ·6H ₂ O (1.1 x 10 ⁻² M). λ _{exc.} = 282 nm.....	50
Figure 2.9. Fluorescence titration of Eu(III) with ligand 3 and 4. Eu(NO ₃) ₃ ·6H ₂ O at 1.4 mM constant concentration titrated with Ligand 3 23.2 mM in MeCN 10 Slits,	

Photomultiplier Tube (PMT): 1000 Volts (Left). $\text{Eu}(\text{NO}_3)_3 \cdot 6\text{H}_2\text{O}$ at 1.1 mM constant concentration titrated with Ligand 4 20.9 mM in MeCN 10 Slits, PMT: 1000 Volts (Right).	51
Figure 2.10. $^1\text{H-NMR}$ titration (acetone- d_6) of ligands 1 (2.4 mM) and 2 (1.4 mM) with $\text{La}(\text{NO}_3)_3 \cdot 6\text{H}_2\text{O}$	52
Figure 2.11. Job Plot for 1 and $\text{La}(\text{NO}_3)_3$ in CH_3CN showing 1:1 binding stoichiometry.....	52
Figure 2.12. Structure of $[\text{Nd}(\text{CN})_9]^{3-}$ complex with Nd^{3+} , showing a three-face centered trigonal prism (D_{3h}) coordination sphere (CN 9) surrounding the metal center.....	54
Figure 2.13. Distribution values of ligands 1 and 2 after extraction experiments with Am-243 and Eu-154 in $\text{CH}_2\text{Cl}_2/\text{HNO}_3$ (6.5M).....	55
Figure 2.14. Distribution ratios for extraction of Am and Eu by ligands 1 and 2 at 1 M HNO_3 and 6.5 M HNO_3	55
Figure 2.15. CID results for mixed-ligand complexes with 1 and 2 of (a) Am(III), and (b) Eu(III), at nominal CID energies of 0.6 V and 0.5 V, for (a) and (b), respectively.	57
Figure 2.16. Optimized geometries $\text{M}(\text{NO}_3)_3(\text{H}_2\text{O})$ and $\text{M}(\text{NO}_3)_3(\text{H}_2\text{O})_2$ (M=Nd, Eu, Am).....	58
Figure 2.17. DFT/PBE0 simulated UV-Vis spectra of 1 and $\text{Nd}(\text{NO}_3)_3(\text{H}_2\text{O})$ complex (Top left), DFT/PBE0 simulated UV-Vis spectra of 2 and $\text{Nd}(\text{NO}_3)_3(\text{H}_2\text{O})_2$ complex (Top right). DFT/PBE0 simulated UV-Vis spectra of 3 and $\text{Nd}(\text{NO}_3)_3(\text{H}_2\text{O})_3$ complex (Bottom).....	59
Figure 2.18. Optimized geometrical structures of 1, 2 and M(III) hydrate and nitrate hydrate complexes with M=Eu and Am.	61
Figure 3.1. Structure of N,N' -bis(pyridin-2-ylmethyl)pyridine-2,6-dicarboxamide ligand (L).	85
Figure 3.2. Representation of solvent extraction experiments performed at Idaho National Laboratory using L and HDEHP (INL).	86

Figure 3.3. Concentration dependence of solvent extraction distribution showing a slope of 3.43 ± 0.01 . $[\text{HDEHP}]_{\text{org}} = 0.35\text{M}$	87
Figure 3.4. pH dependence of Ln(III)/Am(III) extraction selectivity. $[\text{HDEHP}]_{\text{org}} = 0.20\text{ M}$ and $[\text{L}]_{\text{t}} = 0.0196\text{ M}$	88
Figure 3.5. CID mass spectra of (a) $[\text{Eu}(\text{L})(\text{NO}_3)_2]^+$ and (b) $[\text{Am}(\text{L})(\text{NO}_3)_2]^+$ at 0.4 V; (c) $[\text{Eu}(\text{L})_2(\text{NO}_3)_2]^+$ and (d) $[\text{Am}(\text{L})_2(\text{NO}_3)_2]^+$ at 0.2 V. The parent species are indicated by solid circles, the CID elimination processes by solid lines, and the CID products by solid squares. Also marked with open triangles in (a) and (b) are small peaks resulting from H_2O addition to the CID products, indicated by dotted lines.....	90
Figure 3.6. CID mass spectra of the isolated (a) $[\text{L}+\text{H}]^+$ and (b) $[\text{L}+\text{H}]^+$ at voltage of 0.60 V.....	91
Figure 3.7. CID mass spectra of the isolated (a) $[\text{Eu}(\text{L})(\text{NO}_3)_2]^+$ and (b) $[\text{Am}(\text{L})(\text{NO}_3)_2]^+$ at voltage of 0.40 V.....	93
Figure 3.8. UV-visible titration of L ($6.3 \times 10^{-5}\text{ M}$) with $\text{La}(\text{NO}_3)_3 \cdot 6\text{H}_2\text{O}$ ($1.3 \times 10^{-3}\text{ M}$) in CH_3CN	94
Figure 3.9. UV-visible titration results of L with Gd^{3+} , Ce^{3+} and Eu^{3+} nitrate salts in CH_3CN . a) $[\text{L}]_{\text{t}} = 7.2 \times 10^{-5}\text{M}$ with $\text{Gd}(\text{NO}_3)_3 \cdot 6\text{H}_2\text{O}$ ($1.2 \times 10^{-3}\text{ M}$) b) $[\text{L}]_{\text{t}} = 6.0 \times 10^{-5}\text{ M}$ with $\text{Ce}(\text{NO}_3)_3 \cdot 6\text{H}_2\text{O}$ ($1.5 \times 10^{-3}\text{ M}$) c) $[\text{L}]_{\text{t}} = 7.4 \times 10^{-5}\text{ M}$ with $\text{Eu}(\text{NO}_3)_3 \cdot 6\text{H}_2\text{O}$ ($9.5 \times 10^{-4}\text{ M}$)	95
Figure 3.10. Experimental titration curve for acid dissociation equilibrium for L. ($\text{pK}_a = 5.15, 4.59$ and 1.55).....	96
Figure 3.11. ^1H -NMR spectra of L (top) and isolated product of complexation reaction with NdCl_3 and KPF_6 shown on Scheme 3.1.....	97
Figure 3.12. Infrared spectra of ligand (L) comparison with $[\text{Nd}(\text{L})_3][\text{PF}_6]_3$ complex.	98
Figure 4.1. Structure of N^2, N^6 -diphenyl-2,6-pyridine dicarbothioamide (LH_2) and the dinuclear complex (1) with electronic delocalization scheme.	112
Figure 4.2. Perspective view of 1 with atom labeling scheme. Thermal ellipsoids are shown at 50% probability level. The inset displays the coordination sphere around the mercury (II) centers. Selected interatomic distances (Å): $\text{Hg1-S1}, 2.3798(9)$; $\text{Hg1-S3}, 2.3879(8)$; $\text{Hg1-N1}, 2.566(3)$; $\text{Hg2-S2}, 2.3443(8)$; $\text{Hg2-S4}, 2.3457(9)$;	

Hg2–N4, 2.552(2); Hg...Hg, 4.5143(4) and angles (°): S1–Hg1–S3, 154.83(3); N1–Hg1–S3, 128.25(6); S1–Hg1–N1, 76.92(6); S4–Hg2–S2, 160.24(3); S2–Hg2–N4, 121.35(6); N4–Hg2–S4, 78.27(6).	113
Figure 4.3. Packing pattern of 1 along c axis (the dotted line indicates the C–H...S intermolecular interactions)	113
Figure 4.4. Perspective view of LH ₂ with atom labeling scheme. Thermal ellipsoids are shown at 50% probability level. Selected bond distances (Å): S1–C6, 1.658(2); S2–C13, 1.659(2); C6–N2, 1.324(3); C13–N3, 1.330(3); C6–C5, 1.499(2); C1–C13, 1.494(3)	115
Figure 4.5. Packing pattern of LH ₂ along c axis (the dotted lines indicate C–H...S intermolecular interactions)	116
Figure 4.6. Intermolecular π–π stacking interactions in LH ₂	116
Figure 4.7. FT-IR spectrum of LH ₂ in ATR mode	117
Figure 4.8. FT-IR spectrum of the complex 1 in ATR mode.	117
Figure 4.9. ¹ H-NMR titration of LH ₂ (2.2 x 10 ⁻³ M) with HgCl ₂ and DIPEA (excess) in acetone-d ₆	118
Figure 4.10. UV-Vis absorption of ligand LH ₂ (2.1 x 10 ⁻⁵ M) and N,N'-Diisopropylethylamine (4.0 x 10 ⁻⁴ M) in methanol upon gradual addition of HgCl ₂ (4.4 x 10 ⁻⁴ M).	119
Figure 4.11. UV-Vis absorption spectra for titration of LH ₂ (5.04 x 10 ⁻⁵ M) with HgCl ₂ (3.09 x 10 ⁻⁴ M) in methanol with no base added.....	121
Figure 4.12. Competitive UV-Vis titration experiment in methanol with Hg(II) in the presence or absence of Ca(II): [LH ₂] _t = 4.0 x 10 ⁻⁵ M, [DIPEA] _t = 3.1 x 10 ⁻⁴ M upon gradual addition of HgCl ₂ (3.5 x 10 ⁻⁴ M) in the presence or absence of CaCl ₂ . [Ca(II)] _t = 4.6 x 10 ⁻³ M.	121
Figure 4.13. UV-Visible titration of LH ₂ (3.6 x 10 ⁻⁵ M) with PbCl ₂ (1.0 x 10 ⁻⁴ M) in MeOH.	122
Figure 5.1. X-ray structure of dipicolinamide complex with UO ₂ (NO ₃) ₂ , as previously reported by Lapka <i>et al.</i>	137

Figure 5.2. (A): UV-visible titration of Ligand 1 ($8.0 \times 10^{-5} \text{M}$) with $\text{UO}_2(\text{NO}_3)_3 \cdot 6\text{H}_2\text{O}$ ($4.4 \times 10^{-3} \text{M}$). (B): ΔA (310 nm) vs. $[\text{UO}_2^{2+}]_t$ for titration of 1 ($7.7 \times 10^{-5} \text{M}$) with $\text{UO}_2(\text{NO}_3)_3 \cdot 6\text{H}_2\text{O}$ ($3.0 \times 10^{-3} \text{M}$), with fitting showing the binding constant $K_a = 4970 \text{ M}^{-1}$	138
Figure 5.3. Gas-phase Collision Induced Dissociation (CID), uranyl complexes with neutral and deprotonated ligand studies demonstrated both 1:1 and 2:1 ligand: metal ratios for both ligands (LBL).....	140
Figure 5.4. Optimized geometrical structures of $\text{UO}_2(\text{L-H})(\text{H}_2\text{O})^+$ and $\text{UO}_2(\text{L})(\text{OH})^+$ (L=1,2), as derived by DFT calculations (LANL).....	141
Figure 5.5. FT-IR Multiphoton Dissociation Spectra – A. Free electro-laser $[(\text{UO}_2)(1)_2]^{2+}$ infrared spectra. B. Infrared spectra of $[(\text{UO}_2)(1-\text{H})(\text{H}_2\text{O})]^+$ C. Infrared spectra $[(\text{UO}_2)(1)(\text{OH})]^+$. (FELIX Lab, Netherlands).....	143
Figure 5.6. FT-IR solvent drop grinding experiments: A) Ligand 1 with $\text{UO}_2(\text{NO}_3)_3 \cdot 6\text{H}_2\text{O}$ B) Ligand 2 with $\text{UO}_2(\text{NO}_3)_3 \cdot 6\text{H}_2\text{O}$ vs. spectra of 1 and 2.....	144
Figure A.1. Extraction-based sensing of Pb(II) via an ion-exchange mechanism using a dinitrosulfonamide analog, which leads to organic layer color-change (colorless to yellow) upon metal complexation.....	157
Figure A.2. Extraction-based sensing of Pb(II) via an ion-exchange mechanism using a sulfonamide analog, which leads to fluorescence change in the organic layer (strongly fluorescent to weakly fluorescent) upon metal complexation.....	158
Figure A.3. A (left): PLUTO representation of the extended structure of $\text{Pb}[1,2-\text{C}_6\text{H}_4(\text{NSO}_2\text{C}_6\text{H}_5)_2]$, indicating the formation of a coordination polymer. Hydrogen atoms have been omitted for clarity. B (Right): X-Ray structure of the complex of the dansylated derivative $\text{Pb}[1,2-\text{C}_6\text{H}_4(\text{N-dansyl})_2]$ which gives selective fluorescent sensing. [(dansyl = 5(N,N')-dimethyl amino-naphthylsulfonyl)].....	159
Figure A.4. Molecular structures of studied ligands 4-nitro-N,N'-bis-p-tolylsulphonyl- <i>o</i> -phenylenediamine (1), 1,2-Bis-(<i>p</i> -methylphenylsulfonamido)-4,5-bis-nitrobenzene (2), 1,2-Bis-(<i>p</i> -methylphenylsulfonamido)-4,5-bis-fluorobenzene (3).....	160
Figure A.5. UV-Vis spectra of 2 (0.0005 M) upon contact with Pb(II) (0.005M) vs. higher concentrations of Ca(II) (0.100 M) and Zn(II) (0.050 M) and a picture of the experiment.....	161

Figure A.6. UV-Vis spectra of 1 (0.002 M) upon contact with Pb(II) (0.02 M), Ca(II) (0.4 M) and Zn(II), 0.2 M).....	162
Figure A.7. UV-Vis spectra of 3 (0.002 M) upon contact with Pb(II) (0.02 M), Ca(II) (0.4 M) and Zn(II), 0.2 M).....	162
Figure A.8. X-ray diffraction of ligand 3 in a P-1 space group.	163
Figure A.9. X-ray crystallography of Pb-3 complex ($3 \cdot [2(\text{CH}_3)_2\text{SO}]$), P-1 space group. Hydrogen atoms have been omitted for clarity.	164
Figure B.1. Structure of $[\text{Nd}(\text{3})_3]\text{I}_3 \cdot 3\text{CH}_3\text{CN}$. Hydrogens are omitted for clarity.....	173

LIST OF SCHEMES

SCHEME	PAGE
Scheme 3.1. Reaction for formation of $[\text{Nd}(\text{L})_3][\text{PF}_6]_3$ from L (1 mM) with NdCl_3 (0.3 mM) adding KPF_6 (excess) in $\text{CH}_3\text{OH}/\text{water}$	97
Scheme 5.1. Molecular structure of ligands N',N''-diphenylpyridine-2,6-dicarboxamide (1) and N',N''-diphenylpyridine-2,6-bis(carbothioamide) (2).	138

LIST OF ABBREVIATIONS

ALSEP	Actinide Lanthanide Separation Process
CH ₃ CN or MeCN	Acetonitrile
CID	Collision Induced Dissociation
DFT	Density Functional Theory
DIAMEX	Diamide Extraction
D _m	Distribution ratio
DMF	Dimethylformamide
DTPA	diethylenetriamine- <i>N,N,N', N'', N'''</i> - pentaacetic acid
ESI	Electron Spray Ionization
EtOAc	Ethyl Acetate
FT-IR	Fourier transform infrared spectroscopy
GANEX	Group Actinide Extraction
HDEHP	bis-2-ethyl(hexyl) phosphoric acid
HLW	High Level Waste
LWR	Light Water Reactor
MeOH	Methanol
MOX	Mixed Oxide
MS	Mass Spectroscopy
NMR	Nuclear magnetic resonance
PUREX	Plutonium Uranium Extraction
PWR	Pressurized Water Reactor
SANEX	Selective Actinide Extraction

SF _m	Separation factor
SNF	Spent Nuclear Fuel
TALSPEAK	Trivalent Actinide Lanthanide Separation
TBP	Tributyl phosphate
TRU	Transuranic
TRUEX	Transuranic Extraction
UNF	Used Nuclear Fuel
UREX	Uranium Recovery by Extraction
UV-Vis	Ultraviolet-visible

CHAPTER I

Spent Nuclear Fuel: Reprocessing and Management Alternatives

1.1 Nuclear fuel cycle and spent nuclear fuel

1.1.1 The Nuclear Fuel Cycle:

Martin Heinrich Klaproth discovered uranium in 1789,^{1,2} the heaviest element in the Earth's crust. Radioactivity was discovered later in 1896 right after the discovery of X-rays, playing a big role in nuclear energy exploitation.² Uranium-235 (²³⁵U) is the fissile isotope of uranium, and its natural abundance is 0.711%.²⁻⁴ Bombardment of uranium with neutrons produces a large amount of energy through nuclear fission, which is used for military and peaceful purposes, such as nuclear energy. The nuclear power industry is growing exponentially. At the end of 2015, over 440 nuclear power reactors were operating worldwide, providing up to 380 gigawatts (GW) to the global energy network.⁵ The concept model for most currently used power reactors such as Light Water Reactors (LWRs) or Pressurized Water Reactors (PWR), consists of fuel pins made of stacks of cylindrical enriched uranium dioxide encapsulated in metal tubes.⁵

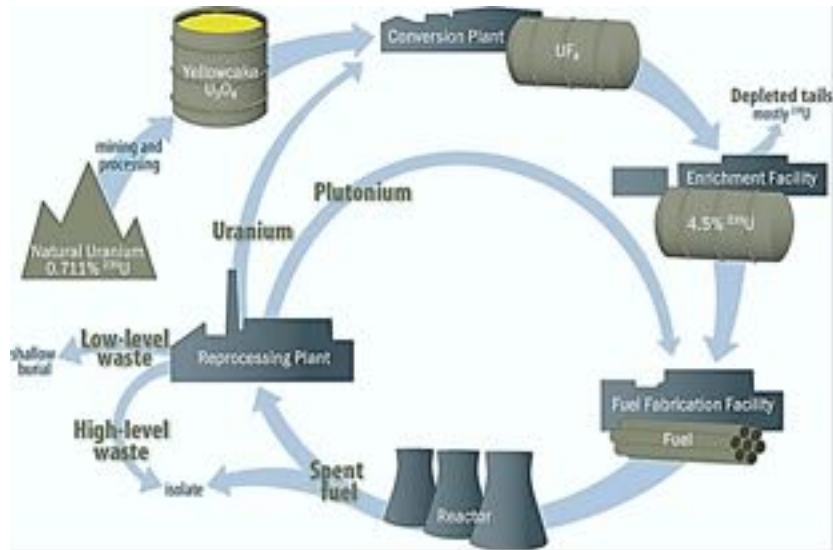


Figure 1.1. Diagram of nuclear fuel cycle obtained from the Congressional Research Service, Report RL34234. Retrieved from <https://fas.org/sgp/crs/nuke/R45880.pdf>⁴

Natural uranium ore undergoes several processes to function as fuel for LWR or PWR reactors. The essential processes for energy generation by nuclear fission of ²³⁵U are mining, milling, conversion, enrichment, and fuel fabrication (Figure 1.1).^{4,6} These five steps or industrial processes involved in the nuclear fuel cycle lead to the production of electricity from ²³⁵U in nuclear power reactors.^{3,4} The nuclear fuel cycle, (Fig. 1.1), can be either an “open fuel cycle” or a “closed fuel cycle.” The current policy in the U.S. employs the “open fuel cycle” concept, which relies on running the nuclear fuel through the reactor once (“once through”), and then isolating and containing the waste in repositories for > 100,000 years until its radiotoxicity reaches the levels of natural uranium (100 mSv).^{5,7} The high cost of storage of UNF on reactor sites or repositories and concerns for leaks or weapons proliferation has led to proposed “closed fuel cycle” concepts. These “closed fuel cycle” alternatives involve reprocessing of spent nuclear fuel by shearing of the fuel rods followed by dissolution in HNO₃.⁵ Then a plutonium and uranium extraction process called

PUREX (Plutonium Uranium REdox eXtraction) partitions the uranium and plutonium nitrates using a tributyl phosphate (TBP) extractant, as well as a reducing agent (such as ferrous sulphamate, or hydrazine) that reduces plutonium (Pu) and facilitates, its separation in a dedicated Pu(III) stream.⁸⁻¹⁰ The fission products and minor actinides (Np, Am, Cm) remain in the aqueous feed are stored in stainless steel canisters.^{5,7} Reintroducing these minor actinides, along with plutonium into the fuel cycle and being able to recycle them could help to finally close the nuclear fuel cycle, which can increase uranium utilization, and reduce the long-term radiotoxicity of nuclear waste.¹¹

The used nuclear fuel (UNF) stream removed from the reactor –and before reprocessing by PUREX–consists mainly of ^{238}U and ^{235}U , and about 1.27% of plutonium nuclides.^{3,5,7,10} The remaining UNF contains other products such as 0.14% of minor actinides,^{9,12} (^{237}Np , ^{241}Am , ^{243}Am , and ^{245}Cm) and several fission products (5.15%),^{3,9,10,12,13} mainly ^{137}Cs and ^{90}Sr , but also lanthanides (^{144}Ce ^{151}Sm ^{144}Nd ^{155}Eu) (Figure 1.2).^{5,7} The minor actinides are produced during reactor operation from neutron capture by ^{235}U and ^{238}U and consecutive nuclear reactions. Specifically, ^{241}Am is formed by neutron capture of ^{239}Pu and ^{240}Pu , forming ^{241}Pu , which then decays by beta decay to ^{241}Am with a half-life of 14.75 years (See Section 1.1.2).

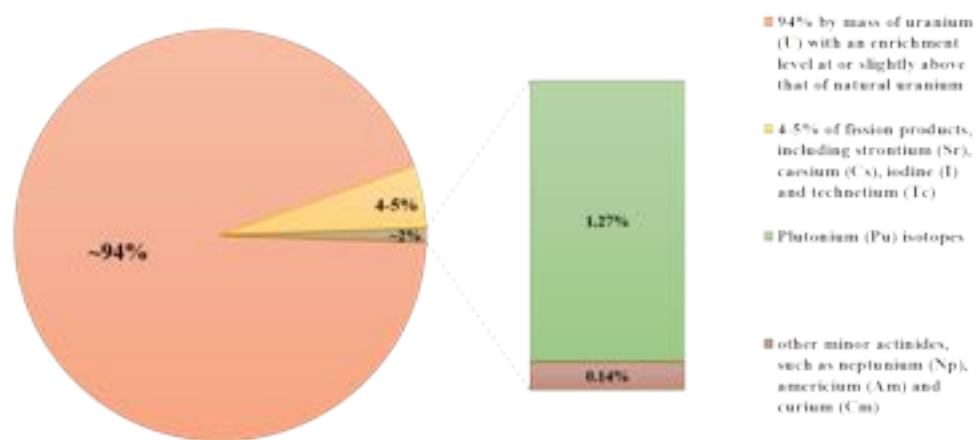


Figure 1.2. The approximate constituents of the spent nuclear fuel: from The Royal Society Science Policy Center Report. Oct 2011. ISBN: 978-0-85403-891-6.^{5,7,10}

Minor actinides, especially ^{241}Am , are responsible for the high amount of radiotoxicity and heat generation of UNF, and unlike fission products, they are very long-lived (^{241}Am 432.2 y; ^{247}Cm 1.5×10^7 y; ^{237}Np 2.14×10^6 y); this limits the capacity of geological repositories.^{3,6,9,10,13-18} Plutonium, which is one of the major contributors of radiotoxicity, can be recovered by the PUREX process, while the minor actinides cannot. As the used nuclear fuel in the U.S. is currently not being reprocessed, it is considered high-level discharge waste (HLW), and the nuclear fuel cycle is termed an “open nuclear fuel cycle.” However, used nuclear fuel can be reprocessed in the future by closing the fuel cycle and increasing uranium utilization. This close nuclear fuel practice –at least partially– is successful in other countries, such as in France, where the plutonium which is isolated by PUREX, is mixed with uranium oxide and is used once again as Mixed Oxide (MOX) nuclear fuel. Removal and burning of minor actinides in next-generation fast reactors, also known as breeder reactors,^{19,20} can reduce the long-term thermal generation, the volume,

and the radiotoxicity level of remaining waste, which –post-processing– will mainly be consisting of fission products. This is expected to increase uranium utilization and capacity of deep geological waste repositories.^{6,9,10,13,15–17} Such a transformation of nuclear energy into a source of carbon-free energy for the future, with less radiotoxic waste is expected to increase the social acceptability of nuclear energy and provide an alternate route in addressing climate change.

1.1.2 Reprocessing of spent fuel

Existing reactors are continuing nuclear energy production, and more nuclear reactors are continuously brought into operation. Therefore, the number of spent fuel rods has increased, with concern about dealing with highly radiotoxic waste as a result. During the nuclear fuel reprocessing cycle, highly acidic waste is accumulated after the reactors are shut down. The PUREX process,⁸ developed in 1949 by Oak Ridge National Laboratory, is (in modified form), the main current UNF processing method in Europe. Some PUREX separation facilities at Savannah River Site and West Valley Reprocessing Plant were closed as consequence of U.S. regulatory requirements.^{5,8,10} After the PUREX process, a raffinate is obtained (recovered aqueous phase post-PUREX after Pu and U removal), containing long-lived radiotoxic minor actinides such as ²⁴¹Am, ²⁴⁵Cm, and ²³⁷Np together with other fission products.^{10,12,13} Since the 70s, the U.S. is just collecting the SNF to be stored in dry cast storage canisters, while the majority of spent fuel is left to decay on the sites of power plants in pools.²¹ Although these storage solutions are temporary, they have essentially become permanent, and turn out to be hazard because of the long-term radiotoxicity of plutonium and minor actinides.²¹

During the cold war years, PUREX reprocessing of used nuclear fuel was extensively practiced in the U.S. and the former Soviet Union, in order to produce weapons-grade plutonium.²¹ Proliferation concerns and increased threats from terrorism have decreased interest in reprocessing, even though methods other than PUREX can address proliferation concerns by achieving separation of minor actinides without creating a pure plutonium stream.^{16,21} In the U.S., UREX (Uranium Recovery by Extraction) process was developed to avoid proliferation concerns. The UREX is a modification of PUREX with addition of acetohydroxamic acid, which prevents a pure plutonium extract by oxidizing it to Pu⁴⁺.⁷ As UREX was not considered ecologically viable, because of several stripping stages and problems in the removal of ⁹⁹Tc (2.212 x10⁵ y), which is present as the highly mobile pertechnetate (TcO₄⁻) under oxidizing conditions, spent fuel rods continue to be stored.²² Fast breeder reactors that can utilize fission of plutonium and minor actinides to produce energy were developed several years ago, and their more comprehensive fuel utilization, than LWR and PWR, could maximize future fuel resources while minimizing the accident and proliferation concerns.^{6,7} Therefore, there is a need for minor actinide recycling strategies to make the SNF suitable as fuel for next-generation breeder reactors, but also to accomplish partitioning and transmutation strategies for advanced safe long-term geological disposal.^{3,13}

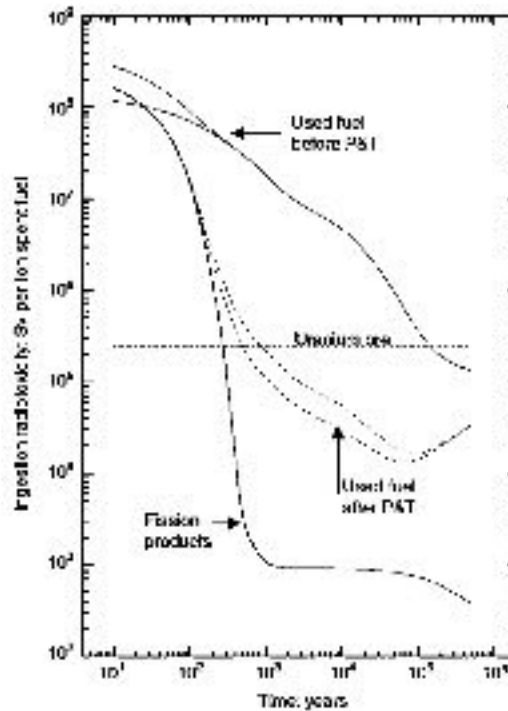


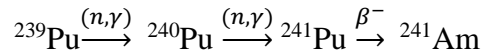
Figure 1.3. Used nuclear fuel radiotoxicity over time: i) under current long-term storage practices, ii) after partitioning and transmutation, including removal and reuse of U/Pu and An/Ln separation iii) after full minor actinide recycling and reuse of reprocessed fuel (including minor An) in fast reactors. (Diagram retrieved from Magill *et al.* ³)

Other approaches, and transmutation, such as homogeneous recycling of actinides, are also being considered and studied for future radioactive waste management.^{3,13} Even within the once-through open fuel cycle, An/Ln separations can provide innovative long-term disposal strategies, through partitioning and transmutation (Fig. 1.3, ii), which can substantially reduce long-term radiotoxicity and waste volume thus improving sustainability, economics, safety, and reliability.¹³ The SNF that goes through partitioning and transmutation involving An/Ln separation followed by dry storage in ecologically viable geologic repositories could lead to a long-term solution for the problem of SNF from nuclear power plants. The used nuclear fuel that goes through partitioning and transmutation can reach a safe uranium ore radiotoxicity in less than 2,000 years (Figure

1.3). Moreover, it would significantly reduce the volume and amount of waste and thus would increase the repository capacity.²¹ The transmutation process is a suitable strategy after partitioning because of the possibility of transmute the troublesome long-lived transuranic radionuclides in a neutron flux to shorter-lived and less radiotoxic species.²¹ The necessity of lanthanide removal prior to transmutation arises from the lanthanide high neutron cross-sections, which can decrease the neutron flux in the reactor and increase by-product formation during transmutation.⁷

1.1.3 Americium; properties, separation, and removal

Americium (Am) is a ductile silvery-white dense metal with various isotopes. Americium-241 (²⁴¹Am, t_{1/2}=432.7 years) for example, is a product of the irradiation of Plutonium by neutrons:



The Am nuclides found in SNF are ²⁴¹Am, ^{242m}Am, ²⁴³Am, and are all highly radioactive and pose an extreme health hazard to humans.¹⁸ Americium nuclides represent a major health concern because of highly energetic α-particle emission and exposure to its intense γ-radiation when working with ²⁴¹Am.¹⁸ It has been calculated that there is 594 g of Am per metric ton of uranium (MTU) in spent fuel (503g of ²⁴¹Am, 0.66g of ^{242m}Am, 90.6g of ²⁴³Am). Americium-241 exhibits an α-spectrum peak at 5.486 MeV (85%) and 5.443 MeV (13%) meanwhile for ²⁴³Am is 5.277 MeV¹⁸. The α-spectroscopy is usually used for determination of Am, but separation and purification are required to avoid any overlapping of α-peaks from other radionuclides. The characteristic γ-ray emission by ²⁴¹Am at

59.6keV, can also be used for identification of this isotope, but mostly for its quantitative analysis¹⁸.

The solution chemistry of Am is primarily determined by its different oxidation states. For Am the most stable americium oxidation state under environmental conditions is the III; however, IV, V, and VI oxidation states have been reported in aqueous solution and in the solid state.^{18,23} In alkaline solutions, Am can exist in any of the four oxidation states (III, IV, V, and VI) while in dilute acid only III and V, (and rarely VI) are stable. The aqueous cations of V and VI oxidation states are unstable, and they hydrolyze to form the linear *trans* dioxo americium cations AmO_2^+ and AmO_2^{2+} .¹⁸ Recent studies demonstrated that the hexavalent americium cation (AmO_2^{2+}) can be successfully extracted from highly acidic solutions using diamylamylphosphonate (DAAP), bis(2,6-dimethyl-4-heptyl) phosphoric acid (H.D. (DIBM)P), and tributylphosphate (TBP).²³ These types of extraction systems depend entirely on the efficiency of the oxidation of Am(V) to Am(VI).^{24,25} Our extraction chemistry, however, is directed towards the Am(III) oxidation state, which is abundant and stable on acidic solutions, and shows many similarities with the chemistry of trivalent lanthanides.

Americium can be transmuted to less hazardous materials in a reactor, but only after most of the lanthanides have been removed to ensure efficiency of the process. The similarity of Am(III) with Ln(III) create a challenge on their separation, making it essential to understand Am(III) vs. Ln(III) coordination and extraction properties by synthetic ligands. Separation efforts for Am with various methods have been studied, but its separation is mainly dominated by the stability of its +III oxidation state and selective

extractants or stripping agents for Am(III) vs. Ln(III).²⁶ Only at relatively extreme conditions, such as high chloride concentrations and high radiation fields, higher oxidation states become more important.^{18,23}

1.2 Solvent extraction concepts and theory

The solvent extraction concept, which is mostly used for selective extraction of dissolved metallic species in hydrometallurgical processes,²⁷⁻²⁹ has many advantages for new reprocessing and partitioning/transmutation strategies. As organic extractants are typically recycled, no large quantities of organic reagents and solvents are required, and it is possible to scale-up, while maintaining fast contact times and excellent selectivity in centrifugal contactors.^{7,29} The previous mention concept involves the distribution of a solute among two immiscible liquid phases.^{7,30} In a typical liquid-liquid extraction standard procedure an organic and an aqueous phase are contacted (Figure 1.4). For SNF extraction processes, the nitric acid dissolution post-PUREX keeps actinides and lanthanides at the aqueous phase, and a selective extractant is added in the organic phase for separation. After separation, the stripping stage follows, in which the organic phase is contacted once again with an aqueous phase (typically of higher pH), that may contain a stripping agent. (Figure 1.4). Solvent extraction is highly influenced by pH variations and the oxidation state of the metal in the species involved.³⁰

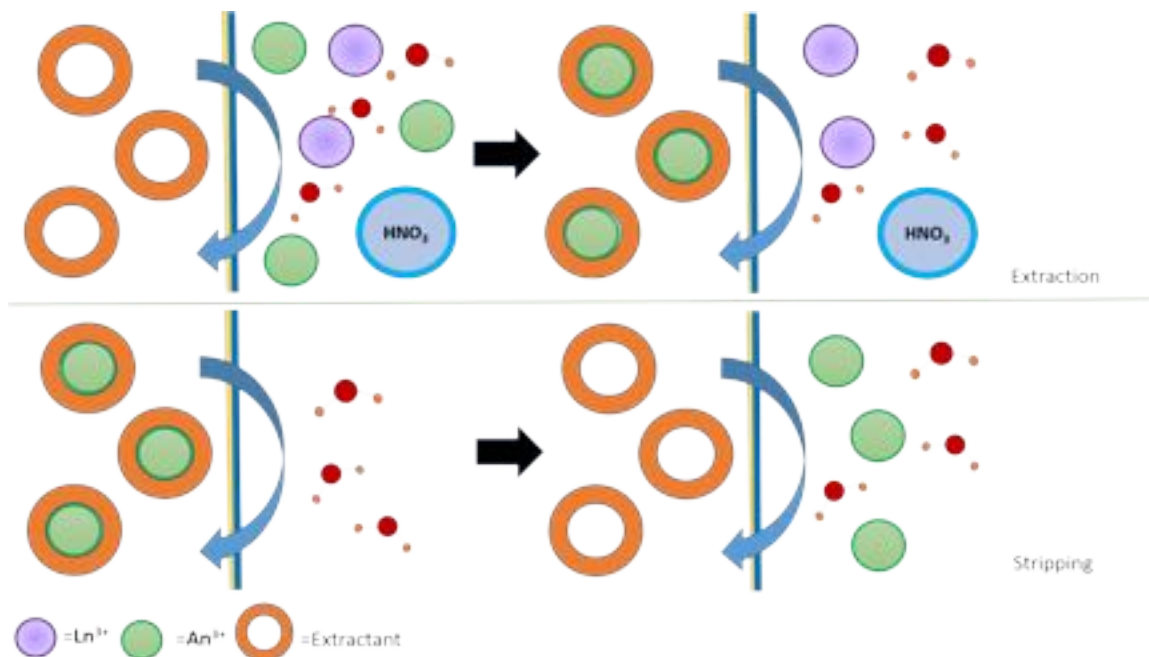


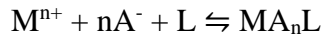
Figure 1.4. Solvent extraction schematic of the liquid-liquid extraction procedure.

Ideally, the solute at solvent extraction separations does not undergo a chemical transformation. When modelling such a situation, there is a distribution equilibrium of the species between the two phases. The total concentration will be constant according to the Nernst distribution law. The distribution ratio will be described as:

$$D_M = \frac{[M^{3+}]_{org.}}{[M^{3+}]_{aq.}} = \frac{[M^{3+}]_{init.Aq} - [M^{3+}]_{final.Aq}}{[M^{3+}]_{final.Aq}}$$

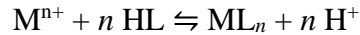
$SF_{An/Ln} = \frac{D_{An}}{D_{Ln}}$, will be the separation factor, derived from distribution ratios, which is indicative of ligand extraction selectivity. Adherence to thermodynamic extraction results can be optimized by variation of the extractant, which can improve kinetics. Oftentimes, for solutions of high ionic strength that simulate real-life practical examples, equilibria

calculations need to take account for activity coefficients. The equilibrium treatment assumes that species do not chemically react or are transform to other byproducts during extraction.^{7,28} The mechanism for extraction by solvation using neutral extracting agents that co-extract a metal cation is:



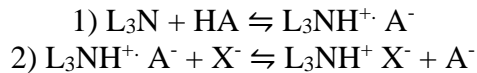
and involves the co-extracted anion.

Other types of extractions relevant to our work, include extraction by cation exchange:



which occurs at low acidity, with back-extraction at high acidity.

The extraction by ion exchange occurs via an extractant that can be protonated (or deprotonated), such as in the example below that involves protonation. The second step is the reverse stripping process which allows the solute to return into the aqueous phase and the organic solvent to be recycled:⁷



1.3 Separation processes (An/Ln and An + Ln from fission products)

1.3.1 Overview:

Several solvent extraction processes have been designed for separation of actinides from lanthanides. Unlike PUREX, UREX and TRUEX (TRansUranic EXtraction) which

aim to separate uranium, plutonium, and transuranics from SNF, none of the current An/Ln separation processes have achieved the maturity of a scaled-up industrial process. These processes include DIAMEX,^{31,32} SANEX,^{33,34} *i*-SANEX,³⁵ GANEX,^{15,34,36,37} TALKSPEAK^{17,38} and ALSEP.^{11,39} These solvent extraction processes provide An(III) separation, either by selective An(III) extraction into an organic solvent, or by selective An(III) stripping into an aqueous phase by aqueous ligands.⁹ Solvent extraction and stripping stages using stable ligands are essential for efficient separation processes; with subsequent transmutation into shorter-lived or stable nuclides by neutron irradiation.^{15,16,40} An efficient An/Ln separation process by partitioning followed by transmutation,^{13,16} is a widely studied strategy for improvement and optimization of SNF management.

1.3.2 DIAMEX Process:

The DIAMEX (DIAMide Extraction) process is used for the separation of trivalent actinides together with lanthanides from the fission products by using diamide extractants such as *N,N,N',N'*-tetraoctyldiglycolamide (TODGA) or *N,N'*-Dimethyl-*N,N'*-dibutyltetradecylmalonamide (DMDBTDMA), which is considered to be the reference extractant for the process.³¹ Madic, Nigond and coworkers, developed this process in the early '90s, which was later modified for better solubility using dimethyl-*N,N'*-dioctyl-hexylethoxy-malonamide (DMDOHEMA).^{31,32,41} The advantage of these diamide ligands is that they consist of C, H, O, and N atoms that create an entirely combustible waste stream, following the CHON principle. These diamide extractants open new possibilities for use of diamide framework ligands on separations. For example, in 2000 Sasaki *et al.* reported a diverse family of diglycolamides showing low to moderate Eu/Am and Am/Cm separation ($SF_{Eu/Am} = 8.8$, $SF_{Cm/Am} = 2.6$) at 1 M HNO₃.⁴²

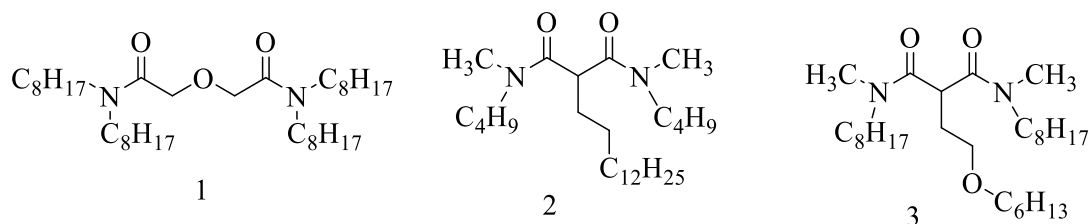


Figure 1.5. Molecular structures of TODGA (1), DMDBDTMA (2), and DMDOHEMA (3).

1.3.3 TALSPEAK and ALSEP:

In general, the TALSPEAK (Trivalent Actinide Lanthanide Separation with Phosphorus-Reagent Extraction from Aqueous Complexes)^{17,38} and ALSEP (Actinide Lanthanide Separation Process)^{11,39} processes have been developed in the U.S. for An/Ln separation, in which An(III) are selectively stripped from an organic phase that contains both An and Ln, concentrating the An(III) in the aqueous phase. The TALSPEAK was developed in 1960 at Oak Ridge National Laboratory and depends on the balance of the relative affinity of cation-exchange solvent extraction reagents (Section 1.2) and comparably powerful aqueous complexants for separating An(III) from Ln(III). The extractant has a strong affinity for both lanthanides and actinides, while the actinide selective aqueous complexant binds stronger to An(III) than Ln(III), such as Am(III).³⁸

During an effort to approach an efficient transuranic (TRU) separation and avoid any variation on pH during the stripping process, some researchers combine extractants from different methods. In 1999 Dhimi *et al.*⁴³ started working with a mixture of HDEHP (Figure 1.6) and CMPO (octyl(phenyl)-N,N-diisobutylcarbamoyl-methylphosphine oxide or Carbamoyl Methyl Phosphine Oxide) as extractants for separation. Gregg J. Lumetta

and co-workers⁴⁴ continued Dhami's work with the TRUSPEAK process, which is a combination of TRUEX (Transuranic elements Extraction) and TALSPEAK. The TRUEX process extracts different transuranic elements, such as Am and Cm, from the HLW solution by using CMPO together with TBP (*tert*-butyl phosphate). The TRUSPEAK demonstrated the feasibility of combining CMPO and HDEHP into a single solvent extraction step to recover Am from UNF and separating it from lanthanides.⁴⁴

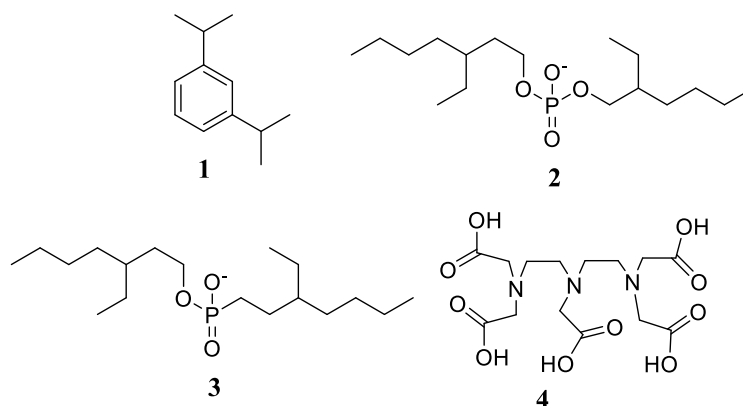


Figure 1.6. Extractants for TALSPEAK process: Diisopropylbenzene (DIPB) (**1**) and bis(2-ethylhexyl) hydrogen phosphate (HDEHP) (**2**), are used as organic extractants, while 2-ethylhexylphosphonic acid mono-2-ethylhexyl ester (HEH[EHP]) (**3**) and diethylenetriamine-*N,N,N',N'',N'''*-pentaacetic acid (DTPA) (**4**) are used as stripping agents.

In 2007, Nilsson and Nash reviewed the TALSPEAK process and its complex chemistry, extensively.⁴⁵ The aqueous phase in TALSPEAK combines multiple acid/base equilibria, which makes the speciation of DTPA and lactic acid very susceptible to pH variations. The extraction efficiency of HDEHP is also vulnerable to pH fluctuations, as the phase transfer mechanism depends on the dissociation of three H^+ to accommodate a trivalent metal such as Am(III).^{17,45} To improve TALSPEAK, variations have been investigated, such as TALSPEAK-MME⁴⁶, which involves an alternative mixed extractant system that features a weak organic phase extractant interaction. In the case of

TALSPEAK-MME, a commercially available extractant like Cyanex-923, was used (Figure 1.7). The liquid extractant was composed of a mixture of four trialkylphosphine oxides and was combined with HEH[EHP] (Figure 1.6). Johnson and Nash⁴⁶ demonstrated that both the lanthanide and trivalent actinides can be efficiently extracted from nitric acid solutions, and after coextraction, the minor actinides are selectively stripped from the organic phase by the polyaminopolycarboxylate ligand.

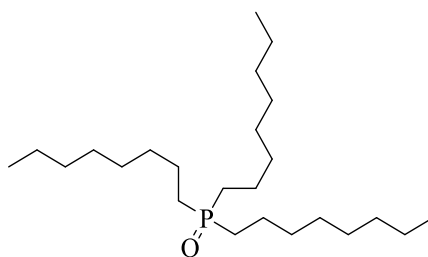


Figure 1.7. Molecular structure of Cyanex 923.

Recent investigations with several solvent combinations have led to Advanced-TALSPEAK, which aims to address the pH dependence and kinetics issues on TALSPEAK. Recently, Braley and co-workers⁴⁷ showed rapid phase transfer kinetics for the heavier lanthanides without higher concentrations of lactate buffer, just by combining HEDTA (*N*-(2-hydroxyethyl)ethylenediamine-*N,N',N'*-triacetic acid) and HEH[EHP]. Furthermore, in 2017, Wilden *et al.*⁴⁸ presented an advanced TALSPEAK process using HEH[EHP] to extract Am(III) and Cm(III) to the organic phase and using HEDTA on the aqueous phase to hold back the lanthanides.

The latest step in An/Ln separations processes using selective An stripping or holdback, has been ALSEP, which has resulted from a collaboration between Argonne National

Laboratory and Pacific Northwest National Laboratory. The ALSEP uses the commercially available neutral donor TODGA, CMPO, or T2EHDGA (Figure 1.8), as co-extractants for selective separation under conditions analogous to TALSPEAK.³⁹ Recent efforts for ALSEP separation demonstrated high distribution ratios with an increase in HNO₃ concentration, and stripping that is less sensitive to pH variations, specifically with combinations of extractants such as TODGA or T2EHDGA with HEH[EHP].³⁹

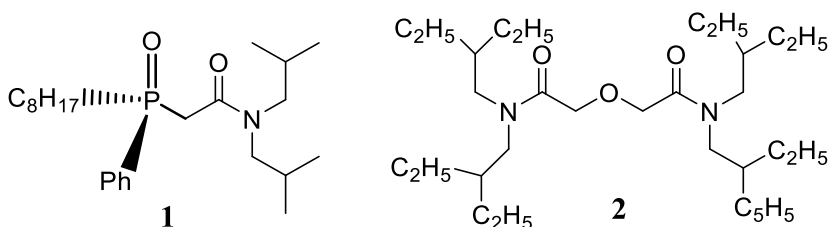


Figure 1.8 Organic co-extractants used for the ALSEP separation process octyl(phenyl)-N,N-diisobutylcarbamoylmethylphosphine oxide (CMPO) (**1**) and N,N,N',N'-tetra(2-ethylhexyl)diglycolamide (T2EHDGA) (**2**).

1.3.4 SANEX and GANEX:

In the SANEX (Selective ActiNide Extraction) and GANEX (Group ActiNide Extraction) processes, which were developed in Europe, An(III) are selectively complexed in the organic medium, while Ln(III) are remaining in the aqueous phase.^{15,33,34} These methods use an organic soft-donor ligands, such as the triazinyl ligands **1** and **2** (Figure 1.9). The SANEX process was designed to separate the minor actinides from the lanthanides from the DIAMEX raffinate.^{15,33} The CyMe₄-BTBP remains the reference molecule for the SANEX process because it has shown the most promising results while being hydrolytically and radiolytically stable.³³ The BTP ligands by Kolarik *et al*²⁶ were

able to impressively recover >99% of Am(III) with separation factors between Am(III) and Eu(III) ≤ 150 , however, some ligand degradation was observed.

Geist and coworkers have developed the innovative SANEX process (*i*-SANEX), that uses water-soluble An(III) complexants (3 and 4, Figure 1.9) and utilizes An(III) selective stripping.⁴⁹ Analogs of ligand **4**, were reported by Macerata¹⁵ and presented an impressive selectivity for Am(III) with a $SF_{Eu/Am}$ of 240, which is substantially higher than for SANEX ligands. These ligands are hydrolytically stable at low pH conditions and have shown some resistance to radiolysis under the intense radiation fields, which is a great advantage for UNF extraction process development.¹⁵

The GANEX process is an expansion of SANEX, which can be used directly on spent fuel and separate plutonium together with minor actinides from uranium without the need for PUREX, and thus without the proliferation risk of a pure Pu stream.³⁴ The GANEX process consists of two cycles and combines the BTBP and TBP (tributyl phosphate) ligands into one solvent. Most of the uranium is recovered on the first cycle, while the second cycle recovers all the remaining actinides separating them from the fission products, including lanthanides.^{34,37}

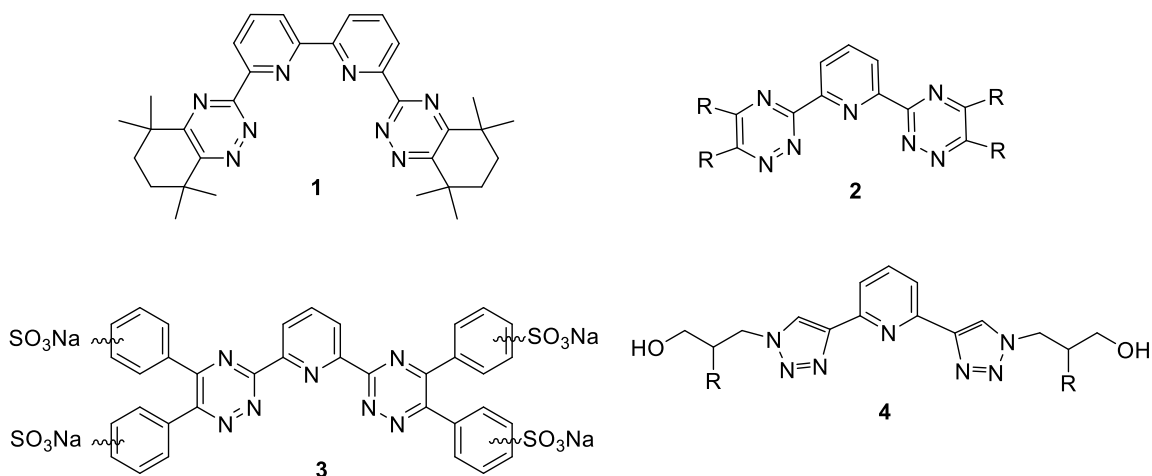


Figure 1.9 *N*-Donor ligands used for SANEX and *i*-SANEX processes: CyMe₄-BTBP (**1**) and BTP type (**2**) ligands used for SANEX extraction by Geist and Magnusson;³³ Water-soluble BTP-type ligands (**3**) used by Geist^{16,49} and bis-triazolyl pyridines (**4**) used by Macerata¹⁵ for *i*-SANEX processing.

1.4 Development of selective ligands for An(III)/ Ln(III) separation

1.4.1 Overview:

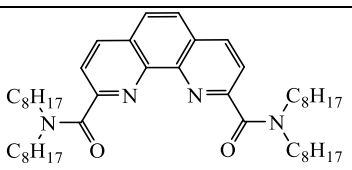
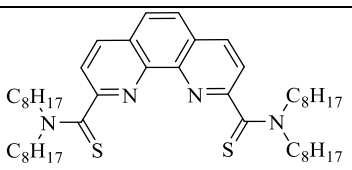
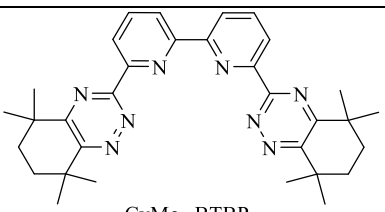
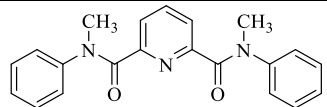
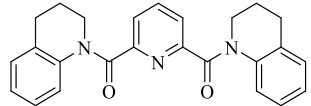
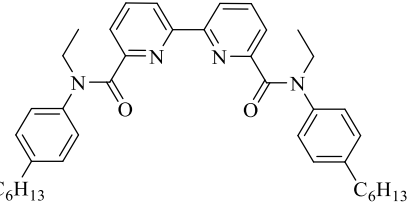
The separation processes previously mentioned demonstrate that both An(III) and Ln(III) have strong interactions with families of organic ligands, containing electronegative donor atoms typically O, N, P and S. These main interactions are determined by electrostatic and steric factors.⁵⁰ During the early 1980's Musikas and coworkers observed that soft-donor ligands containing *N* and *S* based moieties (azides or ortho-phenanthroline) complexed An(III) over Ln(III) selectively.^{9,51} A key point to consider in ligand design is that An(III) are “less hard” Lewis acids than Ln(III) according to HSAB theory, and thus a stronger covalent character interaction with softer Lewis bases than hard Lewis bases is expected.^{38,52} Participation of actinide valence *5f* orbitals in

bonding provides a stronger electronic effect; they are lower in energy and less spatially expanded than compared to the lanthanide *4f* orbitals.^{25,50}

1.4.2 Ligand design criteria

The development of an ideal organic extractant for separation of trivalent actinides from lanthanides needs to follow certain criteria, as such separation has proven to be challenging because of their similar properties and oxidation states: Ligands must exhibit good solubility in the organic diluent used for solvent extraction methods, for example, *n*-octanol or *n*-dodecane. The ligand/metal complex has to be soluble in the organic diluent in order to remove the An(III) or Ln(III) and prevent a third phase formation. Other essential criteria are: (i) Ligand must be highly selective. (ii) Chemical bonding between ligand and metal should be sufficiently labile to allow fast stripping and recycling of the ligand. (iii) Ligand has to show stability under hydrolytic and radiolytic conditions under extraction. (iv) The extraction must be effective under highly acidic pH. (v) Synthesis of the ligand must be economically viable and able to be scaled up.^{7,10,28} It is also desirable for the ligand to follow the CHON principle (Section 1.3.1). This principle means that it should contain only carbon (C), hydrogen (H), oxygen (O) and nitrogen (N) atoms to allow incineration without byproduct formation.^{7,35} Ligands shown on Table 1.1 satisfy the previous criteria for ligand design and have demonstrated excellent separation capabilities by extracting Am(III) over Eu(III) at highly acidic conditions with high separation factors.

Table 1.1. Am/Eu separation factors for organic extractants with soft-donor atoms for Am(III) extraction from highly acidic media. Br Cosan is a brominated cobalt bis(dicarbollide) anion, used as a synergistic lipophilic anion.

Extractant	Solvent	[HNO ₃] _t (M)	SF _{Am/Eu}	Reference
	o-nitrophenyl hexyl ether (NPHE) + Br Cosan*	1.00	3.96	Galletta <i>et al.</i> ⁵³
		3.82	8.71	
	NPHE + Br Cosan*	1.00	2.31	Galletta <i>et al.</i> ⁵³
		3.82	4.87	
 CyMe ₄ -BTBP	<i>n</i> -octanol + DMDOHEMA (catalyst)	1.00	120	Geist <i>et al.</i> ²⁸
	CH ₂ Cl ₂	6.00	3.13	Babain <i>et al.</i> ⁵⁴
	CH ₂ Cl ₂ + Metanitrobenzotri fluoride	6.00	3.00	Babain <i>et al.</i> ⁵⁴
	1,2-dichloroethane	3.00	7.6	Alyapyshev <i>et al.</i> ⁵⁵
		6.00	12	

1.4.3 Dipicolinamides and Dithiopicolinamides

Our research was focussed on organic ligands with soft donor atoms using pyridine-derived frameworks, such as dipicolinamides (diamides of dipicolinic acid) and dithiopicolinamides (dithioamides of dipicolinic acid) for selective actinide complexation

and extraction. Dipicolinamides have been investigated before as possible extractants for reprocessing.^{31,40,53} Amides offer the advantage of following the CHON principle, unlike organophosphorus ligands such as TBP or CMPO.⁵⁶ During the early 1990s Nigond and coworkers used picolinamides and dipicolinamide extractants (Figure 1.10) on the DIAMEX type process.³¹ The presence of the soft-donor nitrogen allowed co-extraction of Am(III) but rejected Eu(III) to the aqueous phase in the case of picolinamide **1** ($SF_{Am/Eu} \sim 7.7$) (Figure 1.10). In the case of picolinamide **2** solubility problems were encountered but complexation with Nd(III) was confirmed by UV-visible and IR. The dipicolinamide **3** (Figure 1.10), was not as effective as **1** for Am(III)/Eu(III) separation, showing a $SF_{Am/Eu}$ of 1.3. It was observed that dipicolinamides present properties similar to DMDBTDMA and TODGA used for DIAMEX (Section 1.4.2).

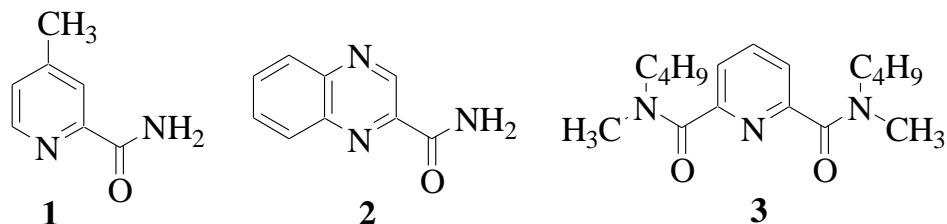


Figure 1.10. Extractants used by Nigond and coworkers in 1993.³¹

Lapka and co-workers⁵⁶ in the early 2000's showed the great potential of dipicolinamide ligands for selective extraction of U(VI) from HNO₃ solutions. Spectroscopic data suggest that a 1:1 metal/ligand complex through the amide (C=O) groups is formed, as confirmed in 2009 by the same group with x-ray crystallography.⁵⁷ Following the work by Kolarik,²⁶ Nigond,^{31,32} and Sasaki,⁴² other dipicolinamides derived from 2,6-dicarboxylic acid were studied as potential extractants of minor actinides from 1-4 M HNO₃ solutions, most of them using fluorinated diluents.^{52,54,55,58} Dipicolinic acid,

known as DPA, has also been studied on TALSPEAK-like processes by Nash and Heathman.⁵⁹ Dipicolinic acid forms strong complexes with many metal ions, including Ln(III). The stability constants for Am(III) complex formation with the tridentate mixed donor complexant DPA were reported to be $\log(\beta_{101})=8.90(\pm 0.02)$, $\log(\beta_{101})=15.87(\pm 0.03)$, and $\log(\beta_{101})=21.88(\pm 0.04)$ when DPA was used as a substitute of DTPA under TALKSPEAK-like conditions (Section 1.4.3, Figure 1.6).⁵⁹

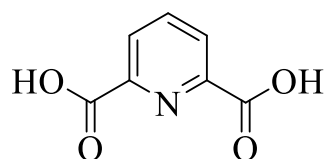


Figure 1.11. Structure of Dipicolinic acid (DPA).

Selectivity of these ligands for An(III) vs. Ln(III) complexation is expected because of a slight increase in covalent character for An-ligand interactions, compared to Ln-ligand ones.⁶⁰ Dithiopicolinamide ligands have been well-studied in transition-metal coordination chemistry.⁵² These ligands have the charge versatility needed for transition metal binding.^{61,62} Bowman-James and co-workers reported a thioamide-based pincer ligand that works as catalyst for carbon-carbon coupling reactions.⁶²

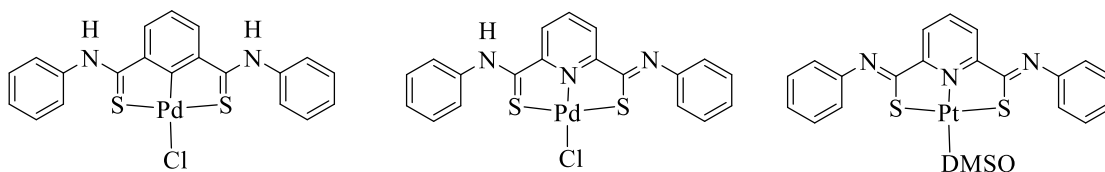


Figure 1.12 Structures of thioamide-based Pd(II) pincer complexes.⁶²

This framework has received surprisingly little attention for An/Ln separations processes, even though thioamides are more resistant to oxidation than other thio-ligands.⁶³ The binding versatility of the thioamide group is determined by the two active centers, the nitrogen atom with the unshared pair of electrons, and the thiocarbonyl group.⁶⁴ Sulfur sites offer reasonably high basicity, high polarizability, and higher covalent character than Oxygen sites.⁶⁵ These properties give the thioamide moiety a soft Lewis-base character. In 2013 Galletta and coworkers, studied the selectivity of C=O vs C=S 1,10-phenanthroline ligands (Figure 1.12).⁵³ The extraction studies were performed in the presence of Br-Cosan, acting as a synergistic agent. (Table 1.1). Promising separation factors were obtained for solvent extraction at high acidic conditions (0.001 M-3.82 M), with ESI-MS and DFT calculations supporting these results.

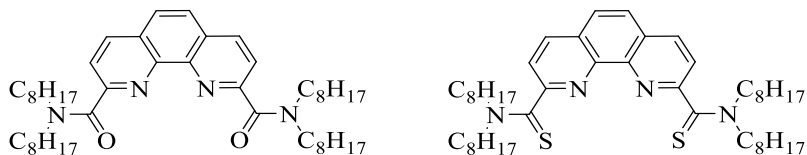


Figure 1.13. Structures of 1,10-phenanthroline ligands used by *Galletta et al.*⁵³

1.5 Legacy waste and integrated salt-waste processing at the Savannah River Site

1.5.1 Savannah River Site and the CSSX Process:

Weapons manufacturing during the cold war required plutonium and tritium production at the Savannah River Site (SRS) as part of an integrated Department of Energy (DOE) effort. The SRS was the primary provider of plutonium and tritium from 1953 through 1988, generating a large quantity of nuclear waste by the end of the cold war. The commercial nuclear power industry is mainly concerned about storing and disposing the

spent fuel, but at Savannah River, and also at Hanford, the concern is specifically the processing of MGal quantities of accumulated nuclear waste during years of weapons production.^{8,68,69}

One of the major HLW issues has to do with the construction of the first Savannah River waste tanks. The PUREX process is performed in highly acidic nitric acid streams, so the tanks needed stainless steel which is more expensive than regular carbon steel.^{8,67,68} As there was a shortage of stainless steel during the war (which was expended for the war effort) reprocessed fuel at Savannah River and Hanford was treated with sodium hydroxide, resulting to highly alkaline solutions, so that carbon steel could be used.⁸ As a result, several metals including transition metals and actinides are precipitated as a sludge that settles at the bottom of the tanks, making eventual treatment and disposal complicated.^{66,68} Soluble alkali and alkaline earth metal salts are concentrated in the supernate and saltcake phases. Single-shell carbon steel tanks have shown indications of leakage and escape of radioactive components into the surrounding environment, especially at the Hanford site. The supernate is mostly comprised of various alkali and alkaline earth metal salt solutions, with ¹³⁷Cs as the main concern in terms of activity. Most waste tanks contain combinations of sludge/saltcake/supernate, but the ratios have changed over time.^{68,69}

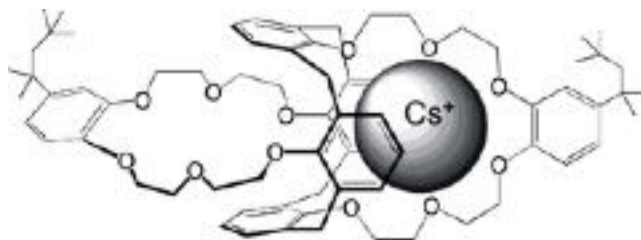


Figure 1.14 Cs-loaded extractant (calix[4]arene-bis(4-tert-octylbenzo-crown-6)) used for CSSX.⁶⁸⁻⁷⁰

Fission products such as zirconium, ruthenium, cesium-137, and strontium-90 are present at HLW. Cesium-137 and Strontium-90 have moderately long half-lives of 30 and 28 years, respectively.^{4,5} Different efforts to remove these fission products have been undertaken, with success finally achieved with the Caustic-Side Solvent Extraction Process (CSSX), specifically developed to separate cesium.⁶⁸⁻⁷⁰ The CSSX process uses the calixarene-crown ether calix[4] arene-bis-(*tert*-octylbenzo-crown-6 (Figure 1.14) as a selective Cs extractant. This previous mention extractant is dissolved at 0.01 M in an aliphatic diluent and can extract Cesium from high-level liquid waste quantitatively, while being fully recycled.⁶⁸

1.5.2 Mercury treatment at Savannah River Site

Savannah River site has used mercury in the past as a catalyst for acidic dissolution of aluminum cladding from target fuels within the uranium and plutonium processing operations, before the tanks were made alkaline.^{66,67} Mercury in the high-level waste (HLW) tanks is present to an amount of about 60 metric tons in various forms, including metallic mercury (Hg^0), mercurous (Hg_2^{2+}), mercuric salts (Hg^{2+}), and organic mercury (e.g., CH_3Hg^+), with the latter being an extremely hazardous pollutant that can have a profound impact on the environment if released.⁷¹ The presence of organic mercury in the

saltstone at the Savannah River Site (SRS) has been increasing because the integrated salt-waste processing through the ARP-CSSX process sequence effectively recycles the Hg back to the tanks, resulting to an increasing amount of Hg in Low Activity Waste (LAW),^{66,67} as additional supernate is processed. As result of its high toxicity and environmental concerns, the integrated-salt waste processing is in jeopardy unless efficient separation methods from alkaline environments are derived. The present project aims to complex, extract and sense Hg(II) from alkaline environments so that Hg is removed prior to disposal of LAW in saltstone. Savannah River Site has been working on a treatment by steam stripping prior to sludge processing where they reduce Hg(II) to Hg with formic acid.^{66,67} Other examples of Hg removal efforts include cation exchange at the effluent treatment plant, sulfide precipitation, coagulation with aluminum sulfate, and membrane separation. It is noted that the conventional sulfide treatment for inorganic Hg precipitation typically fails to stabilize Hg(II) sufficiently.⁶⁷ Therefore, the design of suitable extractants for Hg(II) embedded within a high pH environment is warranted.⁶⁶

1.6 Methodology for quantifying Metal-Ligand interactions

The literature describes several methods available for the determination of association constants K_a .^{2,72,73} In a simple 1:1 equilibrium system, where the receptor S is complexing the ligand L resulting in the 1:1 complex S.L., we have:



Evidently, any complex can be constructed in this manner and to define an overall binding constant:

$$K_a = K_{mn} = \frac{[S_m L_n]}{[S]^m [L]^n} \quad (\text{eq. 2})$$

The 1:1 binding isotherm can be derived from the equilibrium constant to give:

$$f_{11} = \frac{K_a [L]}{1 + K_a [L]} \quad (\text{eq. 3})$$

f_{11} represents the fraction of the receptor that has been complexed:

$$f_{11} = \frac{[SL]}{[S]_t} = \frac{[L]_t - [L]}{[S]_t} \quad (\text{eq. 4})$$

The value L from equation (4) is substituted into equation (3) and solving for f_{11} we get equation 5 that contains total ligand concentration $[L]_t$, as the only variable. The equation 5 is possible if we assume that experimental conditions $[S]_t$ is kept stable:

$$f_{11} = \frac{[S]_t + [L]_t + K_a^{-1} - \left(\sqrt{([S]_t + [L]_t + K_a^{-1})^2 - 4[L]_t [S]_t} \right)}{2[S]_t} \quad (\text{eq. 5})$$

The f_{11} value is directly related to the measured property, and therefore non-linear fitting of the expression $f_{11} = f([L]_t)$ via equation (5) allows direct determination of the association constant.⁷⁴

1.6.1 Binding constant determination by NMR spectroscopy

In an NMR titration experiment in which the complex and the components are in fast exchange, the chemical shift c observed is the weighted average of the chemical shifts of the components.

Let a = chemical shift of a specific resonance at the start of the titration when $[L]_t = 0$

Then, $[S] = [S]_t$ or $f_{11} = 0$

Let b = the chemical shift of the same resonance at the end of the titration when $[L]_t = \infty$

Then, $[S] = 0$ or $f_{11} = 1$.

By defining $\Delta\delta_{\max} = b - a$

And defining $\Delta\delta = c - a$

And substituting f_{11} (equation 5) into equation 6,

Equation 7 can be used in order to fit the data which allows for the calculation of K_a as

and $\Delta\delta_{\max}$. This model can also be used for complicated equilibrium systems^{73,74}.

$$f_{11} = \Delta\delta/\Delta\delta_{\max} = (c-a)/(b-a) \quad (\text{eq. 6})$$

$$\Delta\delta = \frac{([S]_t + [L]_t + K_a^{-1}) - \left(\left(\sqrt{([S]_t + [L]_t + K_a^{-1})^2 - (4[L]_t [S]_t)} \right) \right) \Delta\delta_{\max}}{2[S]_t} \quad (\text{eq. 7})$$

1.6.2 Binding constant determination by UV-Visible spectroscopy

In a UV-Visible titration experiment that showed a decrease of A_x and an increase at A_y with clear isosbestic points, the binding constant can be determined directly from the 1:1 or 2:2 binding equilibria (eq. 1) by applying Beer's law to the maximum absorption, assuming that the only species that absorb at that wavelength are the $[L]$ and the $[C]$ complex, for example let use 2:2 binding equilibria:⁷⁴

$$[C] = \frac{C_{Lt} - [L]}{2} \quad (\text{eq. 8})$$

Where C_{Lt} is the total ligand concentration, which is constant during the titration.

$$[M^+] = C_{Mt} - 2[M] \text{ (eq. 9)}$$

Where C_{Mt} is the total Metal concentration, calculated for each titration point after the addition of solution B.

$$A_x = \varepsilon_L b [L] + \varepsilon_C b [C] \text{ (eq. 10)}$$

Where ε_L is the molar extinction coefficient for the ligand L at the selected absorption (found from the initial point of the titration) ε_C is the molar extinction coefficient for the complex at the same absorption, calculated from the last post-saturation titration point in which the M is in excess and assuming all ligand is complexed. The constant b is the path length (1 cm).

Substituting [C] on eq. 3 from eq. 1 and solving for [L] gives:

$$[L] = \frac{2 A_x - \varepsilon_C b C_{Lt}}{(2\varepsilon_L - \varepsilon_C) b} \text{ (eq. 11)}$$

Then by substituting on equation 2, the binding constant is derived.

1.6.3 Binding constant determination by fluorescence spectroscopy

For fluorescence spectroscopy, in the case that a fluorescence enhancement is observed, the Benesi-Hildebrand analysis can be applied:⁷⁴ In a typical fluorescence titrations experiment, the receptor is titrated with the analyte at constant receptor concentration. When the addition of analyte to receptor shows an increase in fluorescence emission upon binding, the Benesi-Hildebrand equation is used to fit the data.

$$I_0/I - I_0 = \beta/(\alpha - \beta)[1/K_\alpha[M] + 1] \text{ (eq. 12)}$$

Where I_0 is the fluorescence intensity of the sensor in the absence of guest; I is the fluorescence intensity of the sensor in the presence of guest; $[M]$ is the concentration of the substrates, and K_a is the association constant between the receptor and the substrate. In the equation, a and b are constants. The value of $b/(a - b)$ can be found out by plotting $I_0/(I - I_0)$ against the inverse of the concentration term, M^{-1} . The intercept of the graph gives $b/(a - b)$; I_0 and I are determined experimentally.

In the case of fluorescence quenching, at lower concentrations of the analyte, a plot of I_0/I vs. $[Q]$ is plotted and the slope obtained gives the Stern-Volmer constant (K_{sv}). Fluorescence quenching is measured with the Stern-Volmer quantitatively by equation 13 where the quencher concentration is $[Q]$, the Stern-Volmer constant is K_{sv} , I_0 is the measured fluorescence intensity without quencher present, and I is measured fluorescence intensity with $[Q]$ present.

$$I_0/I = 1 + K_{sv}[Q] \quad (\text{eq. 13})$$

1.7 References:

- (1) Scuettmann, W. The discovery of uranium by Martin Heinrich Klaproth 200 year ago. *Kernenergie* **1989**, *32*, 416–420.
- (2) Ramos, M. L.; Justino, L. L. G.; Barata, R.; Costa, T.; Nogueira, B. A.; Fausto, R.; Burrows, H. D. Oxocomplexes of U(VI) with 8-Hydroxyquinoline-5-Sulfonate in Solution: Structural Studies and Photophysical Behaviour. *Dalton Trans.* **2017**, *46*, 9358–9368.
- (3) Magill, J.; Berthou, V.; Haas, D.; Galy, J.; Schenkel, R.; Heusener, G. Impact Limits of Partitioning and Transmutation Scenarios on the Radiotoxicity of Actinides in Radioactive Waste. *Nuclear Energy* **2003**, *42*, 263–277.

- (4) Nikitin, M.B.D., Managing the Nuclear Fuel Cycle: Policy Implications of Expanding Global Access to Nuclear Power U.S. Nuclear Regulatory Commission. Generic Environmental Impact Statement on Uranium Milling; Report RL34234, Washington, D.C. USA, **2019**. Retrieved from <https://fas.org/sgp/crs/nuke/R45880.pdf>
- (5) Rodriguez-Penalonga, L. and Moratilla-Soria, Y. A Review of the Nuclear Fuel Cycle Strategies and the Spent Nuclear Fuel Management Technologies. *Energies*, **2017**, *10*, 1235.
- (6) Edwards, A. C.; Wagner, C.; Geist, A.; Burton, N. A.; Sharrad, C. A.; Adams, R. W.; Pritchard, R. G.; Panak, P. J.; Whitehead, R. C.; Harwood, L. M. Exploring Electronic Effects on the Partitioning of Actinides(III) from Lanthanides(III) Using Functionalised Bis-Triazinyl Phenanthroline Ligands. *Dalton Trans.* **2016**, *45*, 18102-18112.
- (7) Edwards, A. C. The development of 1,10-phenanthroline-derived extractants for advance future nuclear fuel cycles, PhD. Dissertation, *The University of Manchester*, **2017**.
- (8) Orth, D. A. Purex: Process and Equipment Performance; Report DP-MS-86-28; Savannah River Laboratory: Aiken, SC. USA, **1986**.
- (9) Panak, P. J.; Geist, A. Complexation and Extraction of Trivalent Actinides and Lanthanides by Triazinylpyridine *N*-Donor Ligands. *Chem. Rev.* **2013**, *113*, 1199–1236.
- (10) Hudson, M. J.; Harwood, L. M.; Laventine, D. M.; Lewis, F. W. Use of Soft Heterocyclic *N*-Donor Ligands To Separate Actinides and Lanthanides. *Inorganic Chemistry* **2013**, *52*, 3414–3428.
- (11) Gelis, A. V.; Lumetta, G. J. Actinide Lanthanide Separation Process—ALSEP. *Ind. Eng. Chem. Res.* **2014**, *53*, 1624–1631.
- (12) Bhattacharyya, A.; Mohapatra, P. K.; Manchanda, V. K. Separation of Americium(III) and Europium(III) from Nitrate Medium Using a Binary Mixture of

Cyanex-301 with N-donor Ligands. *Solvent Extraction and Ion Exchange* **2006**, *24*, 1–17.

(13) Salvatores, M.; Palmiotti, G. Radioactive Waste Partitioning and Transmutation within Advanced Fuel Cycles: Achievements and Challenges. *Progress in Particle and Nuclear Physics*. **2011**, *66*, 144–166.

(14) Demir, S.; Brune, N. K.; Van Humbeck, J. F.; Mason, J. A.; Plakhova, T. V.; Wang, S.; Tian, G.; Minasian, S. G.; Tyliczszak, T.; Yaita, T.; Kobayashi, T.; Kalmykov, S. N.; Shiwaku, H.; Shuh, D. K.; Long, J. R. Extraction of Lanthanide and Actinide Ions from Aqueous Mixtures Using a Carboxylic Acid-Functionalized Porous Aromatic Framework. *ACS Cent Sci*. **2016**, *2*, 253–265.

(15) Macerata, E.; Mossini, E.; Scaravaggi, S.; Mariani, M.; Mele, A.; Panzeri, W.; Boubals, N.; Berthon, L.; Charbonnel, M.-C.; Sansone, F.; Arduini, A.; Casnati, A. Hydrophilic Clicked 2,6-Bis-Triazolyl-Pyridines Endowed with High Actinide Selectivity and Radiochemical Stability: Toward a Closed Nuclear Fuel Cycle. *J. Am. Chem. Soc.* **2016**, *138*, 7232–7235.

(16) Geist, A.; Müllich, U.; Magnusson, D.; Kaden, P.; Modolo, G.; Wilden, A.; Zevaco, T. Actinide(III)/Lanthanide(III) Separation Via Selective Aqueous Complexation of Actinides(III) Using a Hydrophilic 2,6-Bis(1,2,4-Triazin-3-Yl)-Pyridine in Nitric Acid. *Solvent Extraction and Ion Exchange* **2012**, *30*, 433–444.

(17) Zalupski, P. R.; Nash, K. L.; Martin, L. R. Thermodynamic Features of the Complexation of Neodymium(III) and Americium(III) by Lactate in Trifluoromethanesulfonate Media. *J Solution Chem.* **2010**, *39*, 1213–1229.

(18) Runde, W. Americium and Curium: Radionuclides. *Encyclopedia of Inorganic Chemistry* **2005**.

(19) Minor Actinide Burning in Thermal Reactors: A Report by the Working Party on Scientific Issues of Reactor Systems; *Nuclear Science*; NEA No. 6997; Nuclear Energy Agency, **2013**, 82. Retrieved from <https://www.oecd-nea.org/science/pubs/2013/6997-minor-actinide.pdf>

- (20) Murray, R. L.; Holbert, K. E. Chapter 25 - Breeder Reactors. In *Nuclear Energy (Eighth Edition)*; Murray, R. L., Holbert, K. E., Eds.; Butterworth-Heinemann, **2020**, 505–523.
- (21) Vandenbosch, R.; Vandenbosch, S. E. Nuclear Waste Stalemate: Political and Scientific Controversies, 1st ed.; *The University of Utah Press*, **2007**.
- (22) Croff, A. G.; Wymer, R. G.; Tavlarides, L. L.; Flack, J. H.; Larson, H. G. Background, Status and Issues Related to the Regulation of Advanced Spent Nuclear Fuel Recycle Facilities. *NUREG* **2008**, Report No. 1909, 219.
- (23) Mincher, B. J.; Martin, L. R.; Schmitt, N. C. Tributylphosphate Extraction Behavior of Bismuthate-Oxidized Americium. *Inorg. Chem.* **2008**, *47*, 6984–6989.
- (24) Richards, J. M.; Sudowe, R. Separation of Americium in High Oxidation States from Curium Utilizing Sodium Bismuthate. *Anal. Chem.* **2016**, *88*, 4605–4608.
- (25) Mincher, B. J.; Martin, L. R.; Schmitt, N. C. Diamylamylphosphonate Solvent Extraction of Am(VI) from Nuclear Fuel Raffinate Simulant Solution. *Solvent Extraction and Ion Exchange* **2012**, *30*, 445–456.
- (26) Kolarik, Z.; Müllich, U.; Gassner, F. Extraction of Am(III) and Eu(III) nitrates by 2,6-(5,6-dipropyl-1,2,4-triazin-3-yl)pyridines. *Solvent Extr. Ion Exch.* **1999**, *17*, 1155–1170.
- (27) Kolarik, Z.; Müllich, U.; Gassner, F. Selective extraction of Am(III) over Eu(III) by 2,6-ditriazolyl and 2,6-ditriazinylpyridines. *Solvent Extr. Ion Exch.* **1999**, *17*, 23–32.
- (28) Geist, A.; Hill, C.; Modolo, G.; Foreman, M. R. S. J.; Weigl, M.; Gompper, K.; Hudson, M. J. 6,6'-Bis(5,5,8,8-tetramethyl-5,6,7,8-tetrahydro-benzo[1,2,4]Triazin-3-yl) [2,2']Bipyridine, an Effective Extracting Agent for the Separation of Americium(III) and Curium(III) from the Lanthanides. *Solvent Extraction and Ion Exchange* **2006**, *24*, 463–483.

- (29) Geist, A.; Taylor, R.; Ekberg, C.; Guilbaud, P.; Modolo, G.; Bourg, S. The SACSESS Hydrometallurgy Domain — An Overview. *Procedia Chemistry* **2016**, *21*, 218–222.
- (30) Ahmed, W. Solvent Extraction Principle and Factors Affecting on It Chemistry, *Funda*, **2019**. Retrieved from <https://chemistryfunda.com/solvent-extraction-principle/>
- (31) Nigond, L. Recent Advances in the Treatment of Nuclear Wastes by the Use of Diamide and Picolinamides Extractants. *Sep.Sci.Technol.* **1993**, *30*, 2075–2099.
- (32) Nigond, L.; Musikas, C.; Cuillardier, C. Extraction by *N,N,N',N''*-Tetraalkyl-2-Alkyl Propane-1,3-Diamines. U(VI) and Pu(IV). *Solvent Extraction and Ion Exchange* **1994**, *12*, 297–323.
- (33) Magnusson, D.; Christiansen, B.; Foreman, M. R. S.; Geist, A.; Glatz, J. -P.; Malmbeck, R.; Modolo, G.; Serrano-Purroy, D.; Sorel, C. Demonstration of a SANEX Process in Centrifugal Contactors Using the CyMe₄-BTBP Molecule on a Genuine Fuel Solution. *Solvent Extraction and Ion Exchange* **2009**, *27*, 97–106.
- (34) Whittaker, D. M.; Griffiths, T. L.; Helliwell, M.; Swinburne, A. N.; Natrajan, L. S.; Lewis, F. W.; Harwood, L. M.; Parry, S. A.; Sharrad, C. A. Lanthanide Speciation in Potential SANEX and GANEX Actinide/Lanthanide Separations Using Tetra-N-Donor Extractants. *Inorg. Chem.* **2013**, *52*, 3429–3444.
- (35) Modolo, G.; Wilden, A.; Kaufholz, P.; Bosbach, D.; Geist, A. Development and Demonstration of Innovative Partitioning Processes (*i*-SANEX and *l*-Cycle SANEX) for Actinide Partitioning. *Progress in Nuclear Energy* **2014**, *72*, 107–114.
- (36) Carrott, M.; Maher, C.; Mason, C.; Sarsfield, M.; Taylor, R. “TRU-SANEX”: A Variation on the EURO-GANEX and *i*-SANEX Processes for Heterogeneous Recycling of Actinides Np-Cm. *Separation Science and Technology* **2016**, 1–16.
- (37) Aneheim, E.; Ekberg, C.; Fermvik, A.; Foreman, M. R. S. Development of a Novel GANEX Process. In Nuclear Energy and the Environment; ACS Symposium Series; American Chemical Society, **2010**; *1046*, 119–130.

- (38) Nash, K. L. The Chemistry of TALSPEAK: A Review of the Science. *Solvent Extraction and Ion Exchange* **2015**, *33*, 1–55.
- (39) Lumetta, G. J.; Gelis, A. V.; Carter, J. C.; Niver, C. M.; Smoot, M. R. The Actinide-Lanthanide Separation Concept. *Solvent Extraction and Ion Exchange* **2014**, *32*, 333–347.
- (40) Galletta, M.; Baldini, L.; Sansone, F.; Ugozzoli, F.; Ungaro, R.; Casnati, A.; Mariani, M. Calix[6]Arene-Picolinamide Extractants for Radioactive Waste: Effect of Modification of the Basicity of the Pyridine N Atom on the Extraction Efficiency and An/Ln Separation. *Dalton Trans.* **2010**, *39*, 2546–2553.
- (41) Weßling, P.; Trumm, M.; Geist, A.; Panak, P. J. Stoichiometry of An(III)–DMDOHEMA Complexes Formed during Solvent Extraction. *Dalton Trans.* **2018**, *47*, 10906–10914.
- (42) Sasaki, Y.; Sugo, Y.; Suzuki, S.; Tachimori, S. The novel extractants, diglycolamides, for the extraction of lanthanides and actinides in HNO₃-n-dodecane system. *Solvent Extraction and Ion Exchange* **2001**, *19*, 91–103.
- (43) Dhama, P. S.; Chitnis, R. R.; Gopalakrishnan, V.; Wattal, P. K.; Ramanujam, A.; Bauri, A. K. Studies on the Partitioning of Actinides from High Level Waste Using a Mixture of HDEHP and CMPO as Extractant. *Separation Science and Technology* **1999**, *36*, 325–335.
- (44) Lumetta, G. J.; Gelis, A. V.; Braley, J. C.; Carter, J. C.; Pittman, J. W.; Warner, M. G.; Vandegrift, G. F. The TRUSPEAK Concept: Combining CMPO and HDEHP for Separating Trivalent Lanthanides from the Transuranic Elements. *Solvent Extraction and Ion Exchange* **2013**, *31*, 223–236.
- (45) Nilsson, M.; Nash. Review Article: A Review of the Development and Operational Characteristics of the TALSPEAK Process: *Solvent Extraction and Ion Exchange*. **2007**, *25*, 665–701.

- (46) Johnson, A. T.; Nash, K. L. Mixed Monofunctional Extractants for Trivalent Actinide/Lanthanide Separations: TALSPEAK-MME. *Solvent Extraction and Ion Exchange* **2015**, *33*, 642–655.
- (47) Braley, J. C.; Grimes, T. S.; Nash, K. L. Alternatives to HDEHP and DTPA for Simplified TALSPEAK Separations. *Ind. Eng. Chem. Res.* **2012**, *51*, 629–638.
- (48) Wilden, A.; Lumetta, G. J.; Sadowski, F.; Schmidt, H.; Schneider, D.; Gerdes, M.; Law, J. D.; Geist, A.; Bosbach, D.; Modolo, G. An Advanced TALSPEAK Concept for Separating Minor Actinides. Part 2. Flowsheet Test with Actinide-Spiked Simulant. *Solvent Extraction and Ion Exchange* **2017**, *35*, 396–407.
- (49) Geist, A.; Weigl, M.; Müllich, U.; Gompper, K. Actinide(III)/Lanthanide(III) Partitioning Using n-Pr-BTP as Extractant: Extraction Kinetics and Extraction Test in a Hollow Fiber Module. *Nuclear Fuel Cycle And Fuel Materials* **2001**, *32*, 641–647.
- (50) Marie, C.; Miguirditchian, M.; Guillaumont, D.; Tosseng, A.; Berthon, C.; Guilbaud, P.; Duvail, M.; Bisson, J.; Guillaneux, D.; Pipelier, M.; Dubreuil, D. Complexation of Lanthanides(III), Americium(III), and Uranium(VI) with Bitopic N,O Ligands: An Experimental and Theoretical Study. *Inorg. Chem.* **2011**, *50*, 6557–6566.
- (51) Musikas, C.; LeMarois, G.; Fitoussi, R.; Cuillardier, C.; Navratil, J. D.; Schulz, W. W. Actinide Separations. In *Actinide Separations; ACS Symposium Series 117*: Washington, D.C., **1980**.
- (52) Ustynyuk, Y. A.; Gloriov, I. P.; Kalmykov, S. N.; Mitrofanov, A. A.; Babain, V. A.; Alyapyshev, M. Yu.; Ustynyuk, N. A. Pyridinedicarboxylic Acid Diamides as Selective Ligands for Extraction and Separation of Trivalent Lanthanides and Actinides: DFT Study. *Solvent Extraction and Ion Exchange* **2014**, *32*, 508–528.
- (53) Galletta, M.; Scaravaggi, S.; Macerata, E.; Famulari, A.; Mele, A.; Panzeri, W.; Sansone, F.; Casnati, A.; Mariani, M. 2,9-Dicarbonyl-1,10-Phenanthroline Derivatives with an Unprecedented Am(III)/Eu(III) Selectivity under Highly Acidic Conditions. *Dalton Trans.* **2013**, *42*, 16930–16938.

- (54) Babain, V. A.; Alyapyshev, M. Yu.; Kiseleva, R. N. Metal Extraction by *N,N'*-Dialkyl-*N,N'*-Diaryl-Dipicolinamides from Nitric Acid Solutions. *Radiochimica Acta* **2007**, *95*, 217–223.
- (55) Alyapyshev, M. Y.; Babain, V. A.; Tkachenko, L. I.; Paulenova, A.; Popova, A. A.; Borisova, N. E. New Diamides of 2,2'-Dipyridyl-6,6'-Dicarboxylic Acid for Actinide-Lanthanide Separation. *Solvent Extraction and Ion Exchange* **2014**, *32*, 138–152.
- (56) Lapka, J. L.; Paulenova, A.; Alyapyshev, M. Yu.; Babain, V. A.; Herbst, R. S.; Law, J. D. Extraction of Uranium(VI) with Diamides of Dipicolinic Acid from Nitric Acid Solutions. *Radiochimica Acta International journal for chemical aspects of nuclear science and technology* **2008**, *97*, 291–296.
- (57) Lapka, J. L.; Paulenova, A.; Zakharov, L. N.; Alyapyshev, M. Y.; Babain, V. A. Coordination of Uranium(VI) with *N, N'*-Diethyl-*N, N'*-Ditolyldipicolinamide. *IOP Conf. Ser.: Mater. Sci. Eng.* **2009**, *9*, 20-29.
- (58) Babain, V. A.; Alyapyshev, M. Y.; Smirnov, I. V.; Shadrin, A. Y. Extraction of Am and Eu with *N,N'*-Substituted Pyridine-2,6-Dicarboxamides in Fluorinated Diluents. *Radiochemistry* **2006**, *48*, 369–373.
- (59) Heathman, C. R.; Nash, K. L. Characterization of Europium and Americium Dipicolinate Complexes. *Separation Science and Technology* **2012**, *47*, 2029–2037.
- (60) Maiwald, M. M.; Wagner, A. T.; Kratsch, J.; Skerencak-Frech, A.; Trumm, M.; Geist, A.; Roesky, P. W.; Panak, P. J. 4,4'-Di-Tert-Butyl-6-(1H-Tetrazol-5-Yl)-2,2'-Bipyridine: Modification of a Highly Selective N-Donor Ligand for the Separation of Trivalent Actinides from Lanthanides. *Dalton Trans.* **2017**, *46*, 9981–9994.
- (61) Wang, Q.-Q.; Ara Begum, R.; Day, V. W.; Bowman-James, K. Molecular Thioamide ↔ Iminothiolate Switches for Sulfur Mustards. *Inorg. Chem.* **2012**, *51*, 760–762.
- (62) Begum, R. A.; Powell, D.; Bowman-James, K. Thioamide Pincer Ligands with Charge Versatility. *Inorg. Chem.* **2006**, *45*, 964–966.

- (63) Modolo, G.; Odoj, R. The Separation of Trivalent Actinides from Lanthanides by Dithiophosphinic Acids from HNO₃ Acid Medium. *Journal of Alloys and Compounds* **1998**, *271*, 248–251.
- (64) Jagodziński, T. S. Thioamides as Useful Synthons in the Synthesis of Heterocycles. *Chem. Rev.* **2003**, *103*, 197–228.
- (65) Berny, F.; Wipff, G. Interaction of M³⁺ Lanthanide Cations with Amide, Urea, Thioamide and Thiourea Ligands: A Quantum Mechanical Study. *J. Chem. Soc., Perkin Trans. 2.* **2001**, *1*, 73–82.
- (66) (a) Bannochie, C. J.; Fellingner, T. L.; Garcia-Strickland, P.; Shah, H. B.; Jain, V.; Wilmarth, W. R. Mercury in Aqueous Tank Waste at the Savannah River Site: Facts, Forms, and Impacts. *Separation Science and Technology* **2018**, *53*, 1935–1947.
(b) Fellingner, T.L.; Bannochie, C.J. Phase 2 Report: Mercury Behavior in the Defense Waste Processing Facility, X-ESR-S-00279, Savannah River Site, Aiken, SC. **2016**.
- (67) Jain, V.; Shah, H. B.; Occhipinti, J. E.; Wilmarth, W. R.; Edwards, R. E. *Evaluation of Mercury in Liquid Waste Processing Facilities*; Phase I Report, SRR-CES-2015-00012 Rev.1; Savannah River Site, Aiken, SC., **2015**.
- (68) Bonnesen, P. V.; Delmau, L. H.; Moyer, B. A.; Leonard, R. A. A Robust Alkaline-Side Csex Solvent Suitable for Removing Cesium from Savannah River High Level Waste. *Solvent Extraction and Ion Exchange* **2000**, *18*, 1079–1107.
- (69) Bonnesen, P. V.; Delmau, L. H.; Moyer, B. A.; Lumetta, G. J. Development of Effective Solvent Modifiers for the Solvent Extraction of Cesium from Alkaline High-Level Tank Waste. *Solvent Extraction and Ion Exchange* **2003**, *21*, 141–170.
- (70) Wang, J.; Zhuang, S. Cesium Separation from Radioactive Waste by Extraction and Adsorption Based on Crown Ethers and Calixarenes. *Nuclear Engineering and Technology* **2019**, *52*, 328–336.
- (71) Rodríguez, O.; Padilla, I.; Tayibi, H.; López-Delgado, A. Concerns on Liquid Mercury and Mercury-Containing Wastes: A Review of the Treatment Technologies for the Safe Storage. *J Environ Manage* **2012**, *101*, 197–205.

(72) Rodrigues, F.; Boubals, N.; Charbonnel, M.-C.; Morel-Desrosiers, N. Thermodynamic Approach of Uranium(VI) Extraction by N,N-(2-Ethylhexyl)Isobutyramide. *Procedia Chemistry* **2012**, *7*, 59–65.

(73) Jonah, T. M.; Mathivathanan, L.; Morozov, A. N.; Mebel, A. M.; Raptis, R. G.; Kavallieratos, K. Remarkably Selective NH_4^+ Binding and Fluorescence Sensing by Tripodal Tris(Pyrazolyl) Receptors Derived from 1,3,5-Triethylbenzene: Structural and Theoretical Insights on the Role of Ion Pairing. *New J. Chem.* **2017**, *41*, 14835–14838.

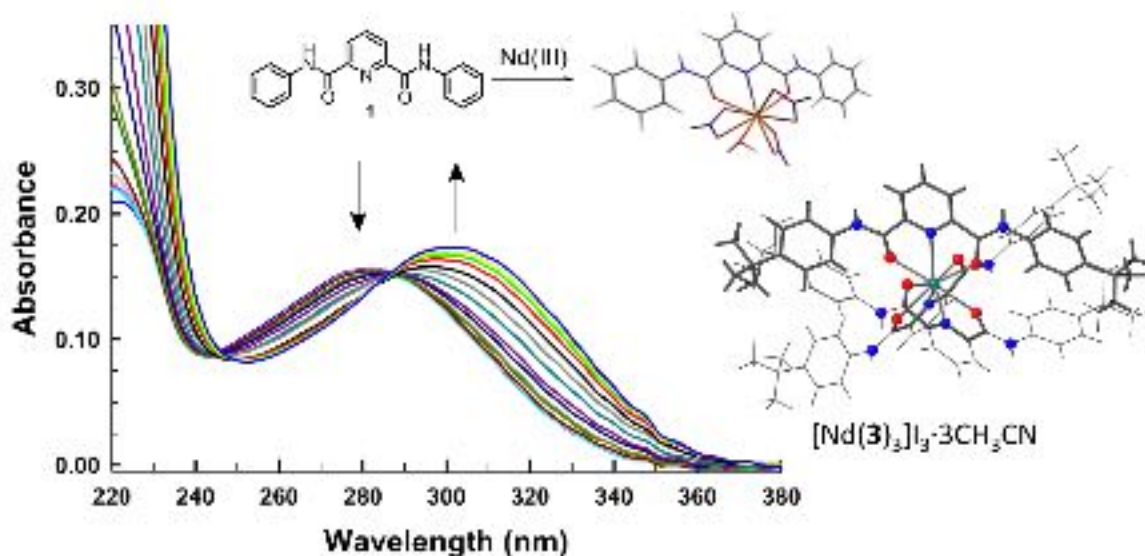
(74) Connors, K. A. *Binding Constants: The Measurement of Molecular Complex Stability*; John Wiley and Sons Inc., **1987**.

CHAPTER II

Soft-donor dipicolinamide derivatives for selective actinide(III)/lanthanide(III) separation: the role of S- vs. O-donor sites

Ingrid Lehman-Andino,^a Jing Su,^b Konstantinos E. Papathanasiou,^a Teresa M. Eaton,^c
Jiwen Jian,^c David Dan,^d Thomas E. Albrecht-Schmitt,^d Christopher J. Dares,^a Enrique R.
Batista,^{*b} Ping Yang,^{*b} John K. Gibson^{*c} and Konstantinos Kavallieratos^{*a}

^a Department of Chemistry and Biochemistry and Biomolecular Sciences Institute,
Florida International University, USA. ^b Theoretical Division, Los Alamos National
Laboratory, USA. ^c Chemical Sciences Division, Lawrence Berkeley National
Laboratory, USA. ^d Department of Chemistry and Biochemistry, Florida State University,
USA.



This Chapter was reproduced and adapted from Lehman-Andino, I.; Su, J.; Papathanasiou, K. E.; Eaton, T. M.; Jian, J.; Dan, D.; Albrecht-Schmitt, T. E.; Dares, C. J.; Batista, E. R.; Yang, P.; et al. *Chem. Commun.* **2019**, 55 (17), 2441–2444. <https://doi.org/10.1039/C8CC07683A> with permission from The Royal Society of Chemistry.

2.1 Abstract:

Removal of long-lived minor actinides from used nuclear fuel might be the pathway towards the sustainability of nuclear energy. Continuous efforts on research and development of new compounds for removing minor actinides by extraction has attracted extensive research interest. Several organic and aqueous ligands have been recently investigated for An(III)/Ln(III) separation. The purpose of our investigation is to demonstrate the selectivity for An(III) vs. Ln(III) binding and extraction using dipicolinamide analogs containing the C=O vs. C=S groups. The binding selectivity of these ligands is investigated in solution, gas-phase, and by DFT theoretical calculations. Extraction studies of the lipophilic ligands **1** and **2** were conducted with acidic aqueous media containing ^{243}Am . The results show higher selectivity for complex formation and extraction for Am(III) vs. Eu(III) for the softer dithioamide **2** vs. the diamide **1**, while in CH_3CN , the diamide binds more strongly than the thioamide to several Ln(III), forming 1:1 complexes.

2.2 Introduction:

Long-lived minor actinides (An) such as ^{241}Am , ^{245}Cm , and ^{237}Np are present together with fission products in used nuclear fuel (UNF) and are responsible for much of the radiotoxicity and heat generation that limit the capacity of geological repositories.¹⁻⁹ Thus, removing minor An from UNF can reduce storage time from thousands of years to a few hundred years.^{1,10} Furthermore, the large neutron cross-sections of lanthanide (Ln) fission products interfere with transmutation and compromise long-term geological disposal.^{4,11} Selective An(III)/Ln(III) separation based on complexation and extraction

must overcome difficulties due to similar properties of these elements in their dominant +III oxidation state.^{4,12,13} The An(III) *5f* valence orbitals allow for a stronger covalent component in metal-ligand interactions with soft donor ligands, as compared to Ln(III) *4f* orbitals.^{14–18}

Since the 1980s a variety of soft- *N*- and *O*-donor ligands have been introduced for selective An(III) vs. Ln(III) complexation and extraction, some with excellent separation properties.^{2,11,19–24} S-donors, such as the P=S ligand Cyanex 301[bis(2,4,4-trimethylpentyl) dithiophosphinic acid] (Figure 2.1) used for SANEX-type separations, have been studied less, with concerns including stability under the highly acidic and oxidizing conditions of UNF, as well as adherence to the CHON principle for safe disposal.^{12,13,25}

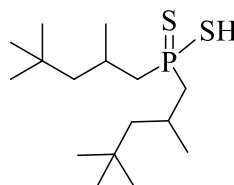


Figure 2.1. Structure of Cyanex-301.

Ligands containing O-donor sites, such as picolinamide-based calix[6]arenes,²⁶ diamides of dipicolinic acid,²⁷ dipicolinamide triazine derivatives,^{1,8} phenanthroline-based dipicolinamides²⁸ and rigid analogs of pyridine-2,6-dicarboxamides²⁹ (Figure 2.2) have demonstrated excellent actinide extraction selectivity on different SANEX and GANEX processes. These ligands have been broadly studied under acidic nuclear fuel conditions from 1 to 4 M HNO₃. However, the addition of a phase transfer catalyst is needed in most cases for these ligands to accomplish stronger extraction and higher An/Ln separation factors.³⁰ Thioamide derivatives of dipicolinic acid have been known to complex softer

transition metals, but their An(III) vs. Ln(III) coordination chemistry remains poorly explored, even though they are more stable than other thio-ligands.³¹ The N-C=S group^{32,33} offers higher basicity, polarizability, and covalent character than the analogous N-C=O.³⁴

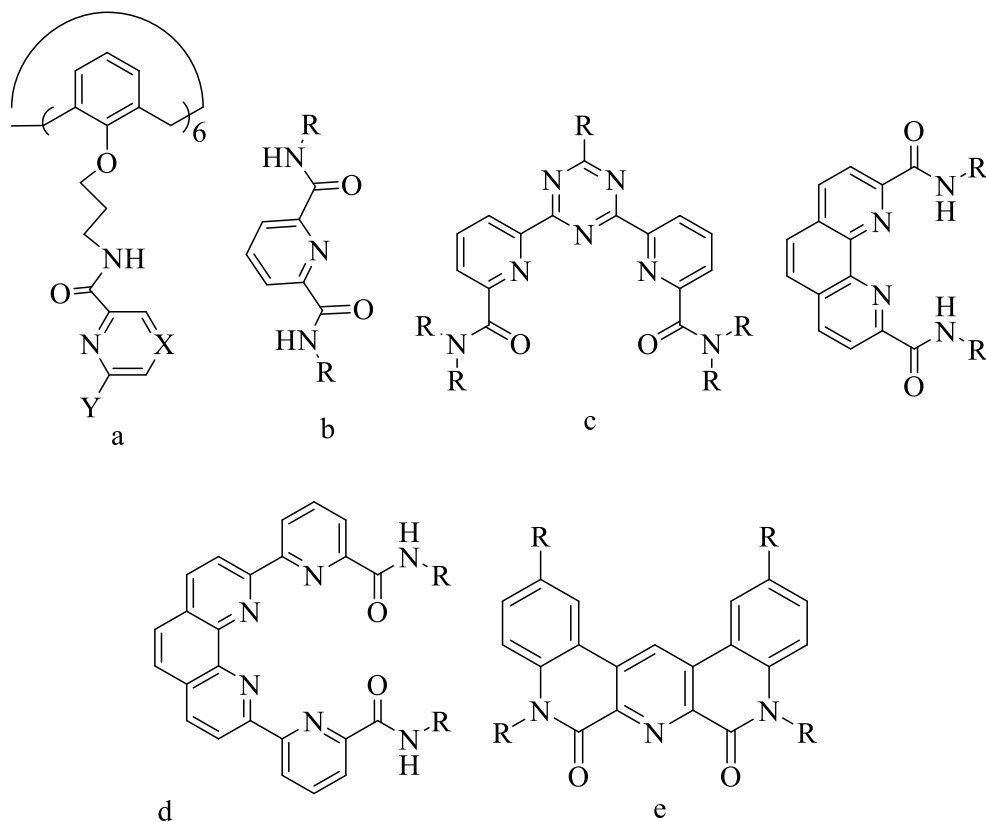


Figure 2.2. Molecular structures of i) a picolinamide-based calix[6]arene (**a**), ii) diamides of dipicolinic acid (**b**), iii) dipicolinamide triazine (**c**), iv) dipicolinamide-phenanthroline-based ligands (**d**) and v) rigid pyridine-2,6-dicarboxamide analogs (**e**).

Herein we present a selective dithioamide ligand (**2** in Fig. 2.3) for An(III) vs. Ln(III) separation from highly acidic aqueous media via solvent extraction, a detailed Ln(III) binding study of the diamide (**1** in Fig. 2.3), and a direct comparison of C=O vs. C=S analogs and their complexation properties. Experiments and theory indicate 1:1 binding

stoichiometry in solution in the presence of coordinating NO_3^- , while the X-ray structure of the Nd(III) complex of the *t*-Bu analog **3** in the presence of I⁻ reveals a 1:3 metal:ligand binding stoichiometry. Collision Induced Dissociation Electrospray Ionization Mass Spectrometry (CID-ESI-MS) and DFT theoretical calculations corroborate the extraction and solution complexation studies. This N-C=S vs. N-C=O comparison points to potential future applicability of optimized thioamide analogs for selective minor actinide separations.

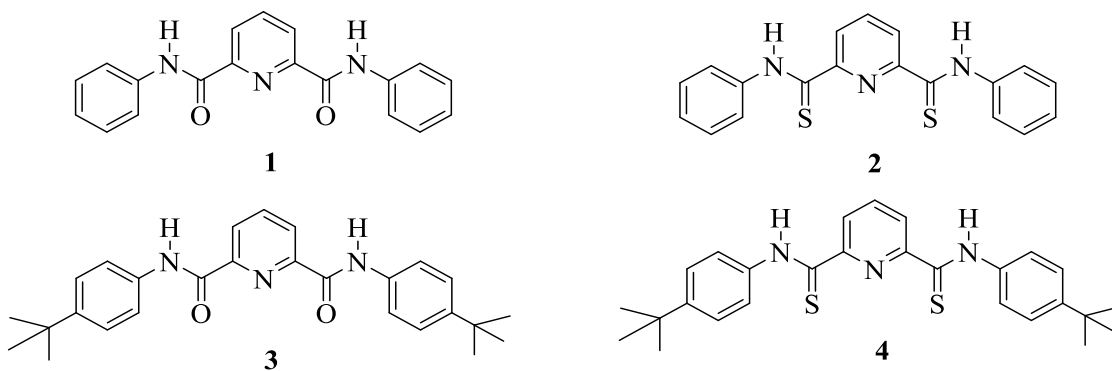


Figure 2.3. Dipicolinamide and dithiopicolinamide ligands under investigation. *N*²,*N*⁶-bis(phenyl)pyridine-2,6-dicarboxamide (**1**), *N*²,*N*⁶-bis(phenyl)pyridine-2,6-bis(carbothioamide) (**2**), *N*²,*N*⁶-bis(4-(tert-butyl)phenyl)pyridine-2,6-dicarboxamide (**3**) and *N*²,*N*⁶-bis(4-(tert-butyl)phenyl)pyridine-2,6-dicarbothioamide (**4**)

2.3 Results and Discussion

2.3.1 Spectrophotometric titrations:

Ln(III) binding experiments were carried out by NMR, UV-Vis, and fluorescence titrations. The diamide **1** shows maximum absorption at $\lambda_{\text{max}} = 282$ nm and fluorescence emission at $\lambda_{\text{em}} = 338$ nm, while the dithioamide **2** shows an absorption maximum at $\lambda_{\text{max}} = 311$ nm and no significant fluorescence emission. Spectroscopic UV-Vis titrations in acetonitrile were performed in order to understand the binding properties of **1** vs. **2** in solution. Upon addition of several Ln(III) salts in CH₃CN (under constant concentration of **1**), a new lower energy band was observed, with clear isosbestic points. Figure 2.4 shows the UV-Vis titration with Nd(NO₃)₃·6H₂O ($K_a = 6900$ M⁻¹), with similar results obtained for La(III), Eu(III), and Lu(III) (Figure 2.7). Figure 2.5 shows no significant changes upon the titration of the dithiopicolinamide ligands **2** and **4** with Nd(NO₃)₃·6H₂O. The di(*t*-Bu)diamide analog **3** showed similar spectroscopic changes as **1** upon Ln(III) addition (Nd(III), $K_a = 70700$ M⁻¹, Eu(III), $K_a = 1.07 \times 10^5$ M⁻¹) (Figure 2.6).

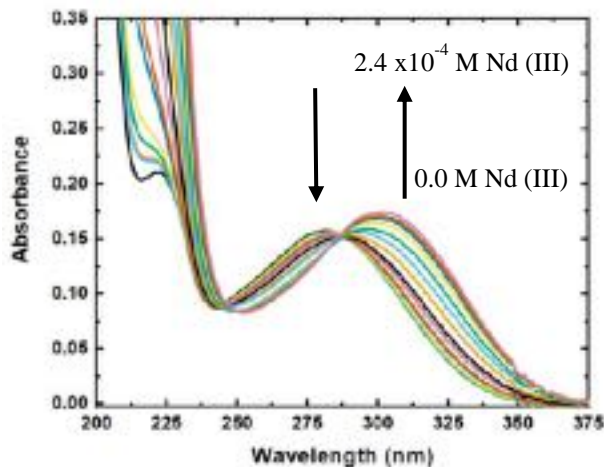


Figure 2.4. UV-Visible titration in CH₃CN of **1** (1.3×10^{-5} M) with Nd(NO₃)₃·6H₂O (1.0×10^{-3} M).

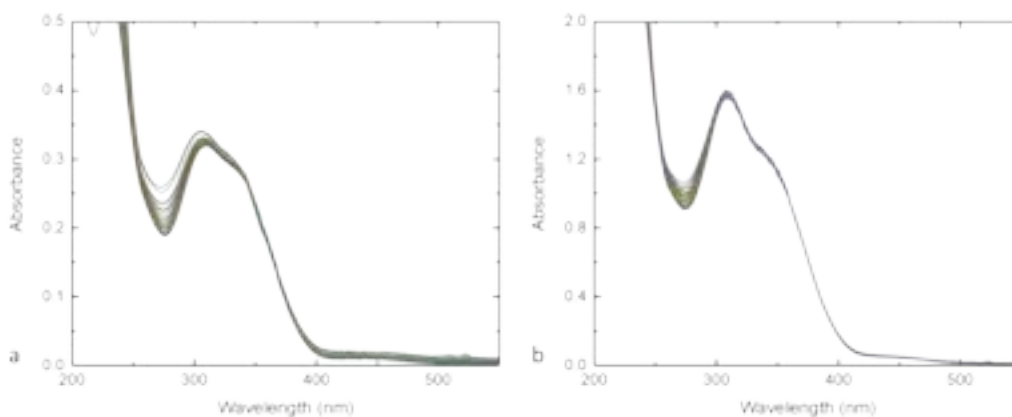


Figure 2.5. a) UV-Vis titration in CH_3CN of ligand **2** ($3.4 \times 10^{-5} \text{ M}$) with $\text{Nd}(\text{NO}_3)_3 \cdot 6\text{H}_2\text{O}$ ($1.1 \times 10^{-3} \text{ M}$) (b) UV-Vis titration in CH_3CN of ligand **4** ($1.0 \times 10^{-4} \text{ M}$) with $\text{Nd}(\text{NO}_3)_3 \cdot 6\text{H}_2\text{O}$ ($1.1 \times 10^{-2} \text{ M}$)

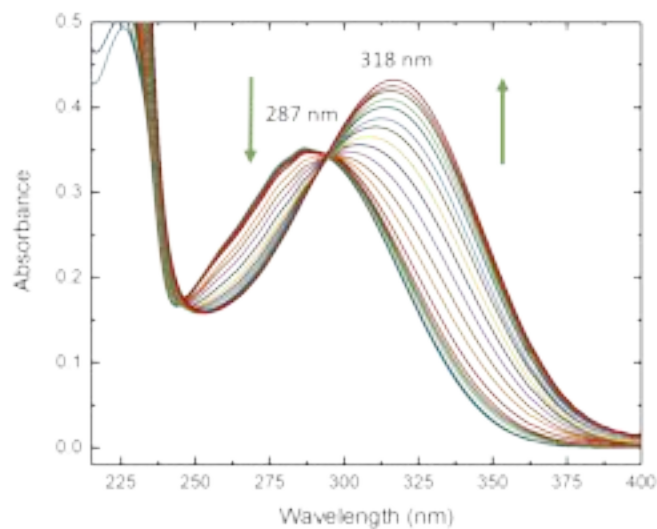


Figure 2.6. UV-visible titration in CH_3CN of ligand **3** ($2.6 \times 10^{-5} \text{ M}$) with $\text{Nd}(\text{NO}_3)_3 \cdot 6\text{H}_2\text{O}$ ($1.0 \times 10^{-3} \text{ M}$).

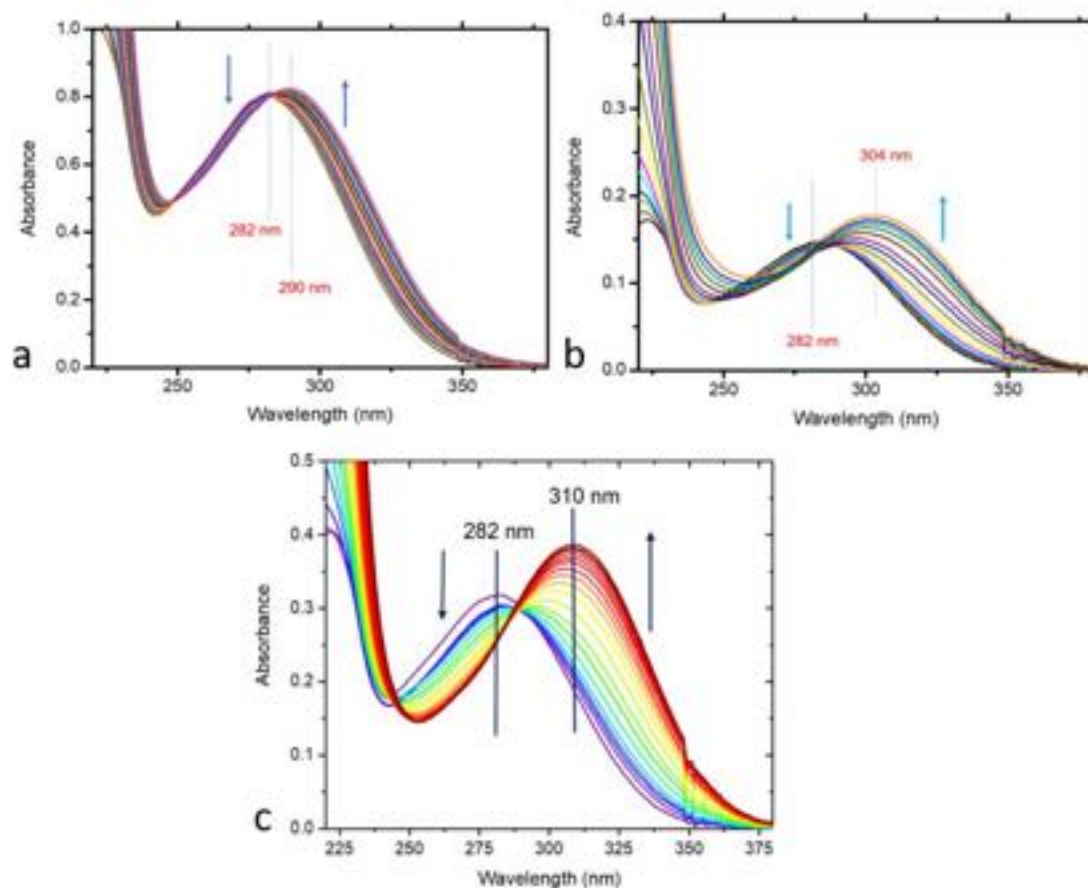


Figure 2.7. a) UV-Vis titration in CH_3CN of ligand **1** ($2.6 \times 10^{-5} \text{ M}$) with $\text{La}(\text{NO}_3)_3 \cdot 6\text{H}_2\text{O}$ ($1.2 \times 10^{-3} \text{ M}$). b) UV-Vis titration in CH_3CN of ligand **1** ($1.3 \times 10^{-5} \text{ M}$) with $\text{Eu}(\text{NO}_3)_3 \cdot 6\text{H}_2\text{O}$ ($1.0 \times 10^{-3} \text{ M}$) c) UV-Vis titration in CH_3CN of ligand **1** ($2.8 \times 10^{-5} \text{ M}$) with $\text{Lu}(\text{NO}_3)_3 \cdot 6\text{H}_2\text{O}$ ($1.9 \times 10^{-3} \text{ M}$).

Fluorescence titrations of ligand **1** with Ln(III) nitrate salts showed fluorescence quenching at 338 nm with a slight red shift (Figure 2.8). Fitting of fluorescence titration curves was also found consistent with a 1:1 Ln(III):**1** binding stoichiometry. Stern-Volmer analysis was used for determination of the Stern-Volmer binding constant (K_{sv}). The K_{sv} determined for different Ln(III) salts; for La(III):**1** 48500 M^{-1} ; Ce(III):**1** 1700 M^{-1} ; Lu(III):**1** 6200 M^{-1} .

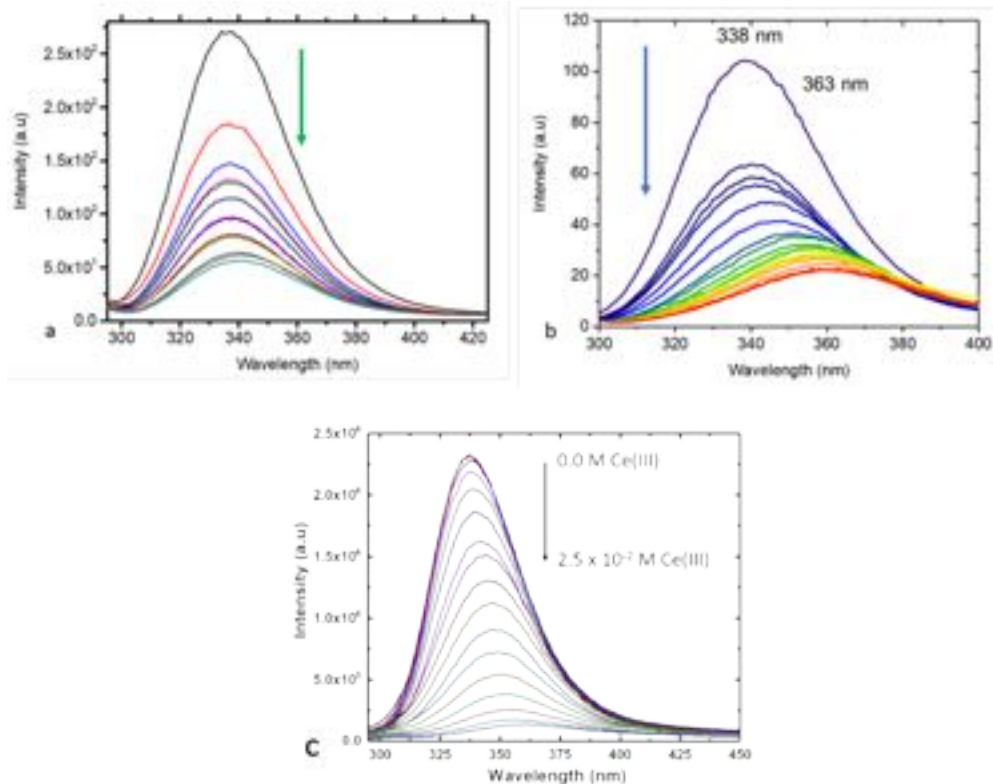


Figure 2.8. a. Fluorescence titration in CH_3CN of **1** (1.3×10^{-5} M) with $\text{La}(\text{NO}_3)_3 \cdot 6\text{H}_2\text{O}$ (8.8×10^{-3} M). b. Fluorescence titration in CH_3CN of **1** (2.8×10^{-5} M) with $\text{Lu}(\text{NO}_3)_3 \cdot 6\text{H}_2\text{O}$ (1.9×10^{-3} M). c. Fluorescence titration in CH_3CN of **1** (1.2×10^{-4} M) with $\text{Ce}(\text{NO}_3)_3 \cdot 6\text{H}_2\text{O}$ (1.1×10^{-2} M). $\lambda_{\text{exc.}} = 282$ nm.

Fluorescence titrations of $\text{Eu}(\text{NO}_3)_3 \cdot 6\text{H}_2\text{O}$ were performed with the *tert*-butyl analogs **3** and **4** (for better solubility). A solution of constant concentration of $\text{Eu}(\text{NO}_3)_3 \cdot 6\text{H}_2\text{O}$ was titrated with increasing concentrations of ligands. At excitation wavelength of 394 nm, Europium fluorescence emissions are expected at 579 nm ($^5\text{D}_0 \rightarrow ^7\text{F}_0$), 594 nm ($^5\text{D}_0 \rightarrow ^7\text{F}_1$), 619 nm ($^5\text{D}_0 \rightarrow ^7\text{F}_2$), 651 nm ($^5\text{D}_0 \rightarrow ^7\text{F}_3$), and 702 nm ($^5\text{D}_0 \rightarrow ^7\text{F}_4$).^{35–37} This experiment gives us the opportunity to observe with clarity if there is binding with thioamide ligand **4**, vs. oxoamide ligand **3**. It should be noted that the thioamide ligand **4** shows no fluorescence emission ($\lambda_{\text{exc}} = 394$ nm), on its own, unlike oxoamide ligand **3**. In Figure 2.9, a comparison of fluorescence titrations of $\text{Eu}(\text{III})$ with ligands **3** and **4** is provided, showing quenching

of Eu(III) prominent emission at 594 nm, with clear isosbestic points at 582 nm, 595 nm, and 630 nm for ligand **3**. The isosbestic points on titration of Eu(III) with the dithiopicolinamide ligand **4** were not as clear, and no saturation in quenching was shown, indicative of weaker binding interaction for **4** vs. **3**, and possible the presence of other processes, as the quenching extrapolates to almost 0 rather than a finite value. $^1\text{H-NMR}$ titrations with $\text{La}(\text{NO}_3)_3 \cdot 6\text{H}_2\text{O}$ in acetone- d_6 showed chemical shift changes for diamide **1** but no observable changes for dithioamide **2** under the same conditions (Figure 2.11). UV-Vis continuous variation method (Job plot) experiments (plots of $\text{Abs} \times [\mathbf{1}]/([\text{Ln}(\text{III})]+[\mathbf{1}])$ vs. mol. fraction) showed maxima at 0.5, consistent with 1:1 binding stoichiometry for ligand **1** and La(III) (Figure 2.12).

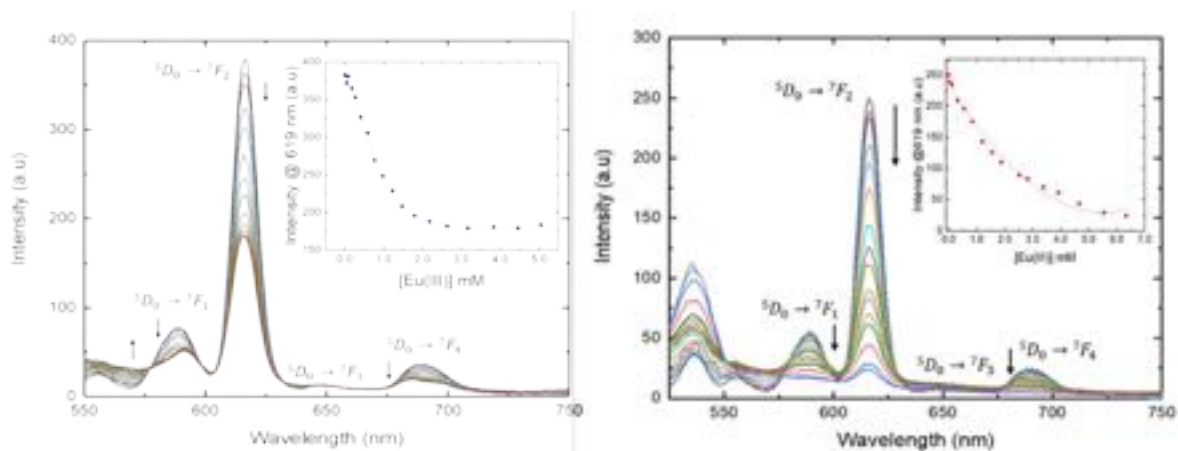


Figure 2.9. Fluorescence titration of Eu(III) with ligand **3** and **4**. $\text{Eu}(\text{NO}_3)_3 \cdot 6\text{H}_2\text{O}$ at 1.4 mM constant concentration titrated with Ligand **3** 23.2 mM in MeCN 10 Slits, Photomultiplier Tube (PMT): 1000 Volts (Left). $\text{Eu}(\text{NO}_3)_3 \cdot 6\text{H}_2\text{O}$ at 1.1 mM constant concentration titrated with Ligand **4** 20.9 mM in MeCN 10 Slits, PMT: 1000 Volts (Right).

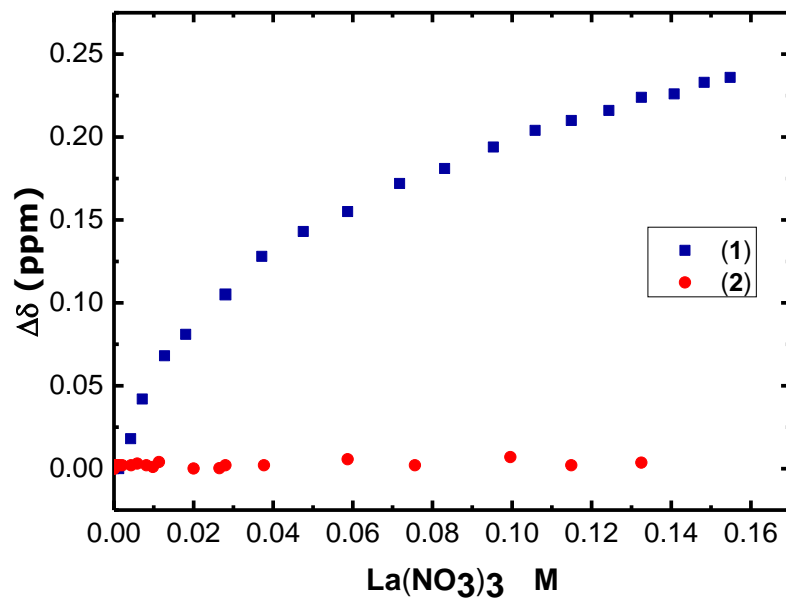


Figure 2.10. ¹H-NMR titration (acetone-d₆) of ligands **1** (2.4 mM) and **2** (1.4 mM) with La(NO₃)₃·6H₂O.

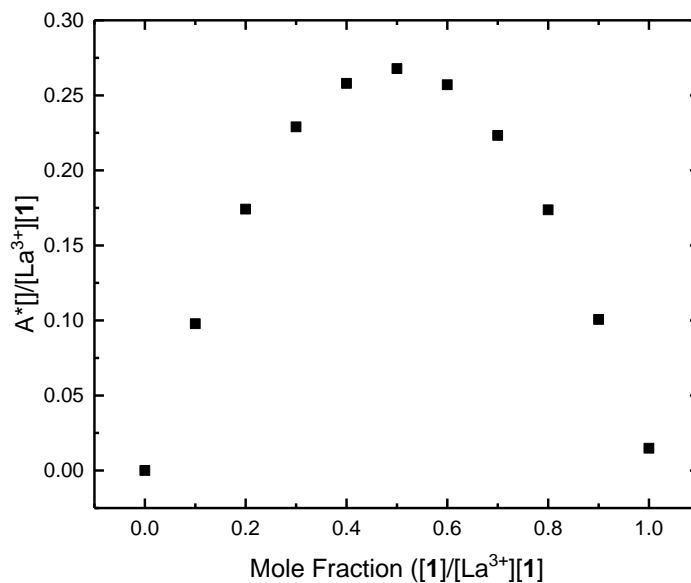


Figure 2.11. Job Plot for **1** and La(NO₃)₃ in CH₃CN showing 1:1 binding stoichiometry.

2.3.2 X-ray Crystallography

Attempts to crystallize the Ln(III) complexes with ligands **1-4** in the presence of Ln(III)-nitrate salts were unsuccessful. However, when the more weakly-coordinating I⁻ salt was used, instead of NO₃⁻, crystals of the complex of diamide **3** with Nd(III) were obtained. The structure of [Nd(**3**)₃]I₃·3CH₃CN (Figure 2.13) consists of Nd³⁺, an Am³⁺ structural surrogate,^{38,39} complexed by three tridentate ligands creating a distorted, 9-coordinate environment. The I⁻ anions are in the outer sphere, with the closest contacts between the three I⁻ anions and the arene rings at 3.67(6), 3.52(6), and 3.53(6) Å.⁴⁰⁻⁴² The average Nd-N and Nd-O bond distances are 2.518(3) and 2.593(3) Å respectively. The structure is instructive of how distortions due to bulky donors allow for high M:L coordination ratios. The bulky nature of the ligand creates challenges in packing three such ligands around a single metal center. One of the three complexed ligand molecules of **3** is relatively co-planar; whereas the other two ligands both have substantial distortions. For the ligand **3**, there is substantial twisting of one of the peripheral phenyl rings by 55.08(5)° with respect the rest of the ligand, which is roughly co-planar. The second distorted molecule of ligand (**3**), accommodates the bulky ligand packing by twisting at one of the amide-pyridine linkages 23.69(5)° with respect the plane of the pyridine ring. These distortions allow for improved packing of the *t*-butyl groups on adjacent ligands. Remarkably, even though there are substantial distortions of two of the three complexed ligand molecules, the Nd-N and Nd-O bond distances do not reflect these features, and even in the most pronounced example, the Nd-O bond distances are not statistically different at the 3σ limit.

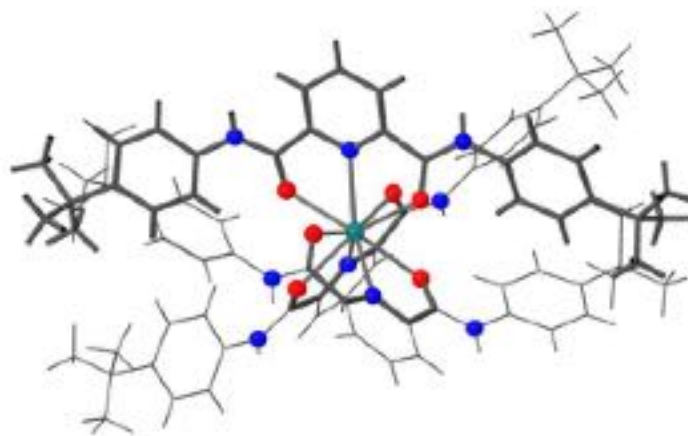


Figure 2.12. Structure of $[\text{Nd}(\mathbf{3})_3]\text{I}_3 \cdot 3\text{CH}_3\text{CN}$. N^2, N^6 -bis(4-(tert-butyl)phenyl)pyridine-2,6-dicarboxamide complex with Nd^{3+} , showing a three-face centered trigonal prism (D_{3h}) coordination sphere (CN 9) surrounding the metal center.

2.3.3 Solvent Extraction

The ligand ability to extract Am(III) vs. Eu(III) under acidic conditions was investigated by solvent extraction experiments with ^{243}Am and ^{154}Eu in $\text{CH}_2\text{Cl}_2/\text{HNO}_3$ (6.5 M). Both **1** and **2** exhibit stronger extraction for Am(III) vs. Eu(III) into dichloromethane solutions saturated with ligand. Specifically, an Am/Eu separation factor (SF) of 5 (± 2) was determined for C=O ligand **1**, while a SF of 17 (± 3) was measured for C=S ligand **2** (Figure 2.14), with the thioamide ligand **2** also showing substantially higher solubility, and thus stronger extraction. Slightly weaker extraction is observed from 1.0 M HNO_3 (Figure 2.15). Our $\text{SF}_{\text{Am/Eu}}$ of 17 while lower than the system reported by Geist,¹ it is slightly higher than most reported systems for extraction from highly acidic media (Section 1.4.2, Table 1.1)

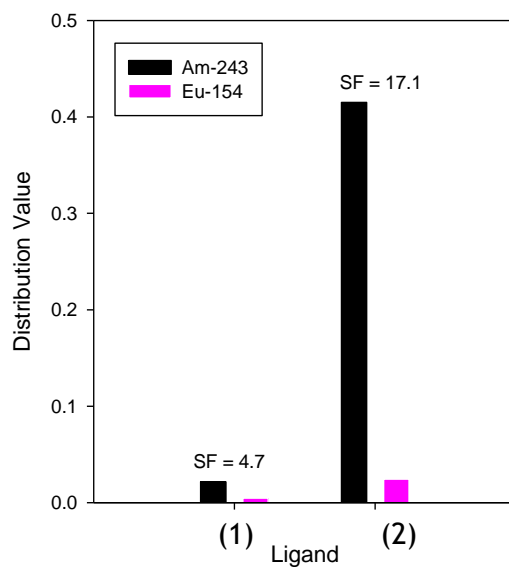


Figure 2.13. Distribution values of ligands **1** and **2** after extraction experiments with Am-243 and Eu-154 in $\text{CH}_2\text{Cl}_2/\text{HNO}_3$ (6.5M)

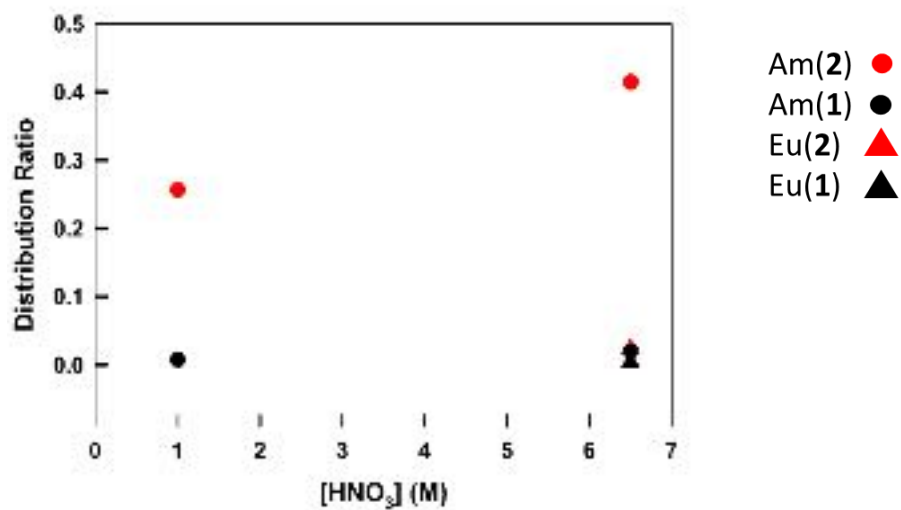
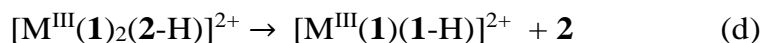
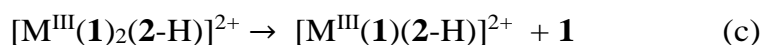
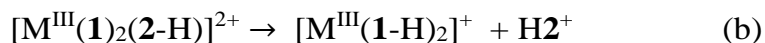
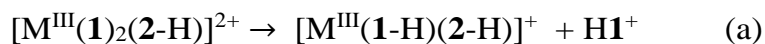


Figure 2.14. Distribution ratios for extraction of Am and Eu by ligands **1** and **2** at 1 M HNO_3 and 6.5 M HNO_3 .

2.3.4 Gas Phase Studies: CID-ESI-MS

Although solvent effects, including entropy, may be important in actual separations, fragmentation of bare gas-phase coordination complexes can offer fundamental insights into metal-ligand binding in the absence of such effects. The CID-ESI-MS of mixed ligand complexes with Am(III) and Eu(III) show: i) Higher relative stability of the Am(III) vs. Eu(III) complex, and ii) a higher tendency of Eu(III) for **2** vs **1** ligand loss, as determined by the relative intensity ratios, based on the four different decomposition pathways for ligand loss. The gas-phase complexes $[M(\mathbf{1})_2(\mathbf{2-H})]^{2+}/[M(\mathbf{1})(\mathbf{2})(\mathbf{1-H})]^{2+}$ (these two isomers are denoted hereafter as $[M(\mathbf{1})_2(\mathbf{2-H})]^{2+}$), where M = Am or Eu, were produced by ESI and subjected to CID in a quadrupole ion trap. The L-H notation (for L = **1** or **2**) indicates H⁺ loss. The tricationic gas-phase complexes $[M(\mathbf{1})_2(\mathbf{2})]^{3+}$, which might be more directly comparable to solution species, were not produced in appreciable yields by ESI. CID of mixed-ligand complexes such as $[M(\mathbf{1})_2(\mathbf{2-H})]^{2+}$ can illuminate relative binding strengths of the two ligands **1** and **2**. The dominant CID fragmentation pathways apparent in figure 2.16 for $[M(\mathbf{1})_2(\mathbf{2-H})]^{2+}$ are given by reactions **a-d**. Reactions **b** and **c** were dominant over **a** and **d** for both M = Am and M = Eu.



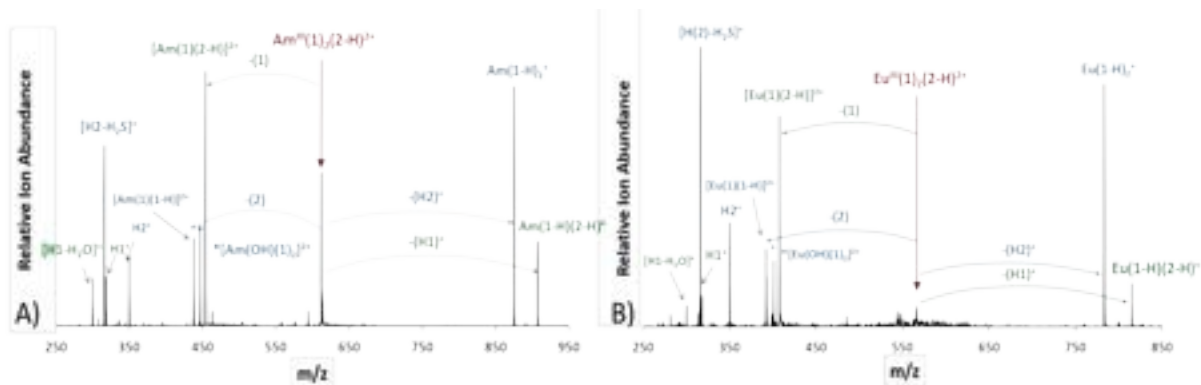


Figure 2.15. CID results for mixed-ligand complexes with **1** and **2** of (a) Am(III), and (b) Eu(III), at nominal CID energies of 0.6 V and 0.5 V, for (a) and (b), respectively.

The results (Figure 2.16) show that the Eu(III) complex fragments more easily, as revealed by near complete depletion of the parent peak (Figure 2.16B) at a lower CID energy, nominally 0.5 V, than Am(III), nominally 0.6 V (Figure 2.16A), where substantial unfragmented Am(III) parent complex remains. This more facile fragmentation of the Eu(III) complex is in accord with the greater affinity of both **1** and **2** for Am(III) versus Eu(III) in solution. Another apparent difference is that the contribution of reaction **a** relative to reaction **b** is greater for Am(III) versus Eu(III). Even though the change from an O- to an S- ligand affects not only the relative covalency of M-L bonding, these gas-phase results suggest that the direct bonding interactions between ligands and metal center are the dominant factor determining metal-ligand affinities, and the solvation and/or entropy may be secondary effects. Notably, this is precisely the effect observed in solution, where the Am/Eu SF is higher for **2** vs. **1**. The key gas-phase fragmentation results, and the remarkable parallels with the observed solution affinities, suggest that the SFs are, at least partly, governed by intrinsic differences in binding of Am(III) and Eu(III) to **1** and **2**.

2.3.5 DFT Calculations

To understand the complexation thermodynamics of the ligands **1** and **2** with Nd(III), and the UV-Vis absorption spectral changes in the titrations, DFT calculations were performed on the reactant $\text{Nd}(\text{NO}_3)_3(\text{H}_2\text{O})_4$, obtained by removing two H_2O molecules in the 2nd coordination sphere in the X-ray structure of $\text{Nd}(\text{NO}_3)_3 \cdot 6\text{H}_2\text{O}$,⁴³ to form a model 1:1 Nd(III):L product, $\text{Nd}(\text{NO}_3)_3(\text{L})(\text{H}_2\text{O})$ (L= **1** or **2**). Even though we can't claim that these 1:1 M-L species are exclusively formed under extraction conditions and higher complexation is also possible, these products are likely formed in the extraction experiment as shown in prior work with analogous tridentate ligands.^{22,44} The optimized structures (Figure 2.17) show tridentate coordination. The calculated Gibbs free energies (ΔG) of the complexation reaction 1 are -15.49 and -3.77 kcal/mol for ligands **1** and **2**, respectively; meaning that the ligand complexation with Nd(III) is thermodynamically favorable, with **1** as the stronger complexant.

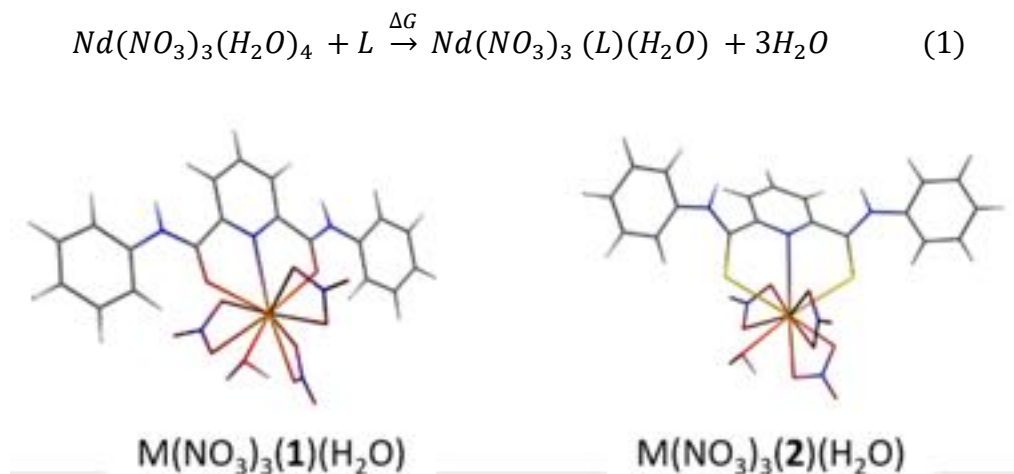


Figure 2.16. Optimized geometries $\text{M}(\text{NO}_3)_3(\mathbf{1})(\text{H}_2\text{O})$ and $\text{M}(\text{NO}_3)_3(\mathbf{2})(\text{H}_2\text{O})$ (M=Nd, Eu, Am).

The calculated UV-Vis spectra (Figure 2.18) show a red shift of the lowest energy absorption band from 267 nm for unbound **1** to 288 nm for $\text{Nd}(\text{NO}_3)_3(\mathbf{1})(\text{H}_2\text{O})$, which is consistent with the UV-Vis titration results. The DFT-derived UV-Vis for **2** and $\text{Nd}(\text{NO}_3)_3(\mathbf{2})(\text{H}_2\text{O})$ show a slight blue shift of the maximum absorption band from 304 nm in **2** to 294 nm in the complex, also in accord with the minimal changes in UV-Vis titrations.

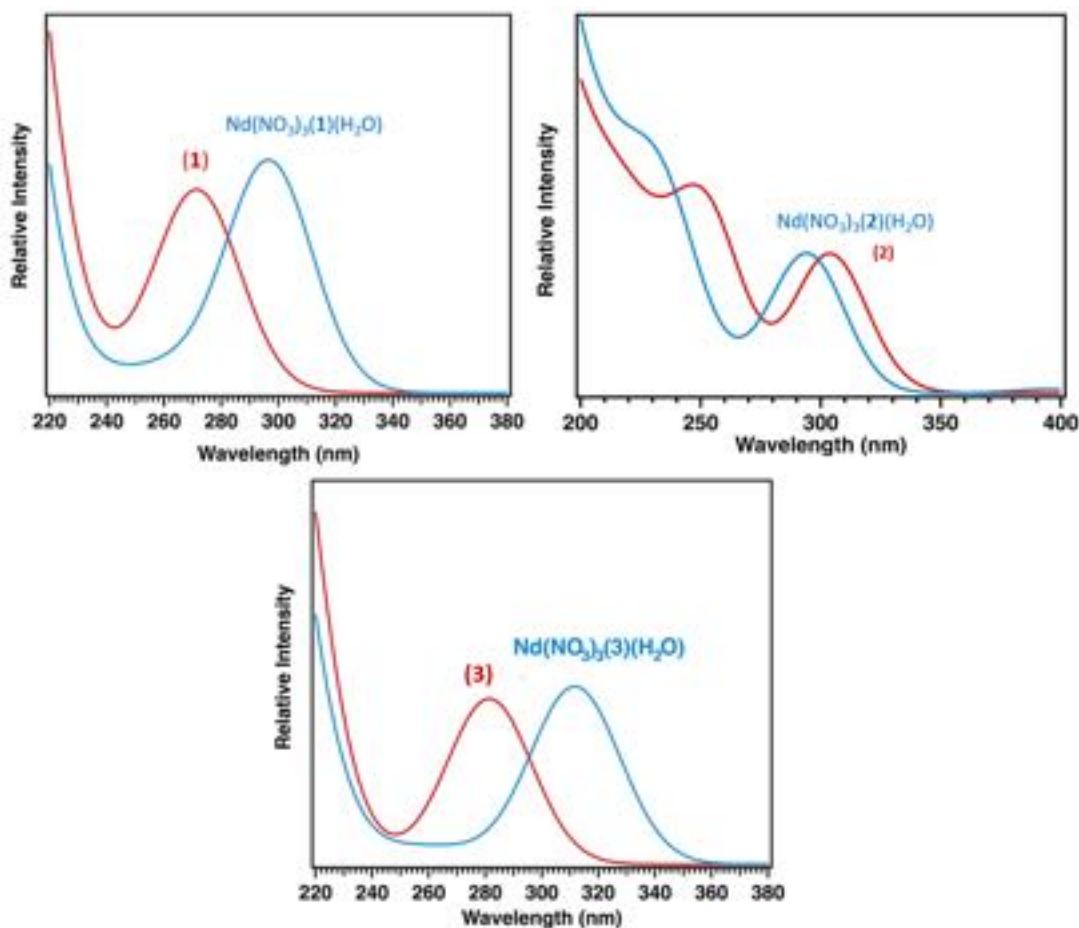
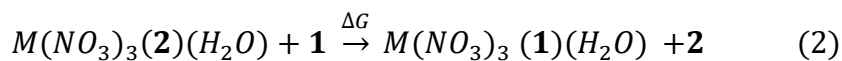


Figure 2.17. DFT/PBE0 simulated UV-Vis spectra of **1** and $\text{Nd}(\text{NO}_3)_3(\mathbf{1})(\text{H}_2\text{O})$ complex (Top left), DFT/PBE0 simulated UV-Vis spectra of **2** and $\text{Nd}(\text{NO}_3)_3(\mathbf{2})(\text{H}_2\text{O})$ complex (Top right). DFT/PBE0 simulated UV-Vis spectra of **3** and $\text{Nd}(\text{NO}_3)_3(\mathbf{3})(\text{H}_2\text{O})$ complex (Bottom).

The binding affinity of **1** versus **2** towards M(III) (M=Nd, Eu, Am) was evaluated from the ligand exchange reaction 2:

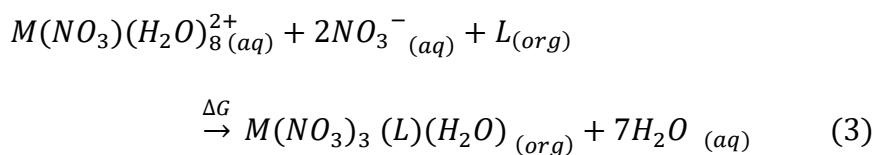


The calculated ΔG values in Table 2.1 are negative with the values slightly different depending on solvents; the ΔG for solvent CH_2Cl_2 are -11.93 , -15.10 and -14.53 kcal/mol for M=Nd, Eu and Am, respectively, which suggests stronger binding of **1** vs. **2** towards both Ln(III) and An(III).

Table 2.2. Calculated Gibbs free energies (ΔG in kcal/mol) for the ligand exchange reaction $M(NO_3)_3(\mathbf{2})(H_2O) + \mathbf{1} \rightarrow M(NO_3)_3(\mathbf{1})(H_2O) + \mathbf{2}$, where M=Nd, Eu and Am, in CH_3CN and CH_2Cl_2 , respectively.

Solvents	Nd	Eu	Am
CH_3CN	-11.72	-15.11	-14.63
CH_2Cl_2	-11.93	-15.10	-14.53

The extraction selectivity of **1** vs. **2** for Eu(III) and Am(III) in CH_2Cl_2/HNO_3 was also assessed in a two-phase extraction system by the reaction 3 where $M(NO_3)(H_2O)_8^{2+}$ (optimized structure in Figure 2.19) and $M(NO_3)_3(L)(H_2O)$ are taken as the dominant species of both Am(III) and Eu(III) in aqueous and organic phases, respectively (M=Am/Eu and L= **1** or **2**):¹¹



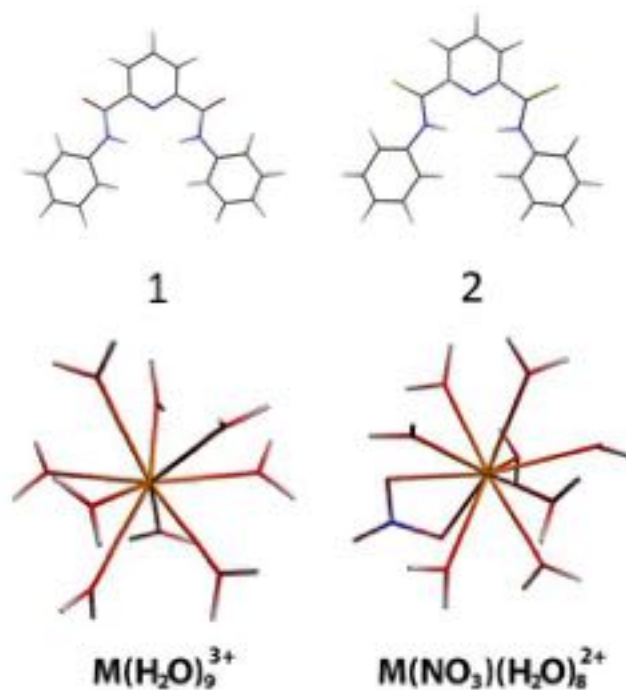


Figure 2.18. Optimized geometrical structures of **1**, **2** and M(III) hydrate and nitrate hydrate complexes with M=Eu and Am.

From the $\Delta G(\text{Eu})$, $\Delta G(\text{Am})$ and $\Delta\Delta G(\text{Am-Eu})$ values (Table 2.2), it is shown that $\Delta G(\text{Am})$ is more negative than $\Delta G(\text{Eu})$, resulting in $\Delta\Delta G(\text{Am-Eu})$ of -1.03 and -1.60 kcal/mol, for **1** and **2**, respectively. These values are in excellent agreement with the corresponding experimental results of -0.93 and -1.68 kcal/mol, which follow from SFs 5 for **1** and 17 for **2**, according to the formula $\Delta\Delta G = -RT \ln SF_{\text{Am/Eu}}$ ($T = 298$ K). The calculated $\Delta\Delta G(\text{Am-Eu}) = -1.03$ kcal/mol for **1** is also very close to the previously computed value of -0.76 kcal/mol for Et-Tol-PyDA,¹¹ which is an analog of **1**. The Am(III)/Eu(III) extraction selectivity into CH_2Cl_2 was evaluated according to reaction 4:

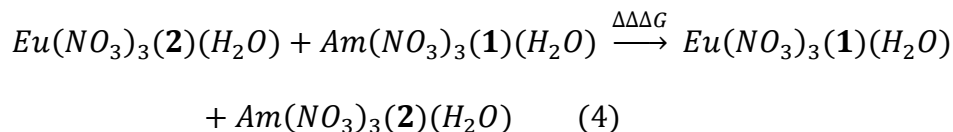


Table 2.3. Calculated and Experimental Gibbs free energies (ΔG in kcal/mol) of the reactions of the M(III) hydrates and nitrate hydrates (M=Am and Eu) with ligands **1** and **2** in CH_2Cl_2/HNO_3

Reaction	ΔG_{Eu}	ΔG_{Am}	$\Delta\Delta G_{(Am-Eu)}$	
	Theory	Theory	Theory	Expt
$M(H_2O)_9^{3+}_{(aq)} + 3NO_3^-_{(aq)} + \mathbf{1}_{(org)} \rightarrow M(NO_3)_3(\mathbf{1})(H_2O)_{(org)} + 8H_2O_{(aq)}$	-50.36	-51.83	-1.47	-0.92
$M(H_2O)_9^{3+}_{(aq)} + 3NO_3^-_{(aq)} + \mathbf{2}_{(org)} \rightarrow M(NO_3)_3(\mathbf{2})(H_2O)_{(org)} + 8H_2O_{(aq)}$	-35.26	-37.30	-2.04	-1.68
$M(NO_3)(H_2O)_8^{2+}_{(aq)} + 2NO_3^-_{(aq)} + \mathbf{1}_{(org)} \rightarrow M(NO_3)_3(\mathbf{1})(H_2O)_{(org)} + 7H_2O_{(aq)}$	-37.92	-38.95	-1.03	-0.92
$M(NO_3)(H_2O)_8^{2+}_{(aq)} + 2NO_3^-_{(aq)} + \mathbf{2}_{(org)} \rightarrow M(NO_3)_3(\mathbf{2})(H_2O)_{(org)} + 7H_2O_{(aq)}$	-22.82	-24.42	-1.60	-1.68

The $\Delta\Delta G$ is calculated to be -0.57 kcal/mol, which is consistent with the experimental value of -0.77 kcal/mol for Am(III) vs. Eu(III) extraction (Figure 2.13). The reason for higher selectivity of **2** towards Am(III) is that replacement of thioamide **2** with oxoamide **1** stabilizes Eu(III) vs. Am(III) (-15.10 versus -14.53 kcal/mol - Eq. 2). This thermodynamic preference is possibly due to increased covalency in Am-S vs. Eu-S bonding, as discussed elsewhere.⁴⁵⁻⁴⁷ Although replacing $M(NO_3)(H_2O)_8^{2+}$ with $M(H_2O)_9^{3+}$ in Eq. 3 significantly changes ΔG , it has

an insignificant overall influence on $\Delta\Delta G(\text{Am-Eu})$ or $\Delta\Delta\Delta G$ (Eq. 4). $\Delta\Delta\Delta G$ values have been valuable for evaluating relative separation selectivities.⁴⁸

2.4 Experimental

2.4.1 Material and Methods:

All chemicals and solvents were purchased from Aldrich Chemical Company or ACROS Organics, were standard reagent grade and were used without further purification unless otherwise noted. 2,6-pyridinedicarbonyl dichloride was purchased from ACROS Organics (CAS: 3739-94-4). (*N*²,*N*⁶-diphenyl)pyridine-2,6-dicarboxamide (**1**)⁴⁹ was prepared from 2,6-pyridinedicarbonyl dichloride and aniline in DMF by a modification of previously published procedures.⁴⁹ (*N*²,*N*⁶-diphenyl)pyridine-2,6-bis(carbothioamide) (**2**)³¹ was prepared by an improved method from (**1**) by reaction with Lawesson's reagent in toluene, and was found to be spectroscopically identical to the reported compound.^{31,49} ¹H and ¹³C NMR spectra were recorded on a 400 MHz Bruker NMR spectrometer and referenced to the residual solvent resonances. All chemical shifts, δ , are reported in ppm. Fluorescence spectra recorded on a Cary Eclipse fluorescence spectrophotometer and UV-Vis spectra were recorded on a Cary 100 UV-Visible spectrophotometer. X-ray crystallography was carried out on a Bruker D8 Quest diffractometer equipped with PHOTON II detector.

(*N*²,*N*⁶-diphenyl)pyridine-2,6-dicarboxamide (1**):**⁴⁹ Pyridine-2,6-dicarbonyl chloride (503 mg, 2.46 mmol) was dissolved in 10 mL of DMF. Aniline (2.00 mL, 21.9 mmol) was added dropwise to the stirring solution and was allowed to react for 3h, at room temperature under N₂. Deionized water (150 mL) was added, and a white precipitate formed. The

formed solid was filtered, and dried (350.1 mg, 1.10 mmol, 45% yield). The same method was also used for a gram scale preparation at slightly lower yields, after recrystallization from DMSO. ¹H NMR (400 MHz, DMSO-*d*₆): δ 11.05 (s, 2H), 8.41 (d, *J* = 7.7 Hz, 2H), 8.31 (t, *J* = 8.0 Hz, 1H), 7.92 (d, *J* = 8.4 Hz, 4H), 7.45 (t, *J* = 7.7 Hz, 4H), 7.20 (t, *J* = 7.5 Hz, 2H). FT-IR (ATR) cm⁻¹: 1655 (m, C=O), 3271 (bd m, N-H). UV/Vis(CH₃CN): λ_{max} 282 nm.

(*N*²,*N*⁶-diphenyl)pyridine-2,6-bis(carbothioamide) (2):² (*N*²,*N*⁶-diphenyl)pyridine-2,6-dicarboxamide **1** (200.8 mg, 0.633 mmol) was dissolved in dry and distilled toluene under a flow of N₂. A solution of Lawesson's reagent (503 mg, 1.24 mmol) in dry-distilled toluene was added dropwise under N₂ to the stirring solution. After 2 h the volatiles were evaporated and the residue was purified by silica gel column chromatography in EtOAc/Hexane (1:4). A yellow crystalline compound was obtained that was recrystallized from dichloromethane/hexane to give the pure product (64 mg, 0.182 mmol, 30% yield): ¹H NMR (400 MHz, CH₂Cl₂-*d*₂) δ 11.17 (s, 2H), 8.95 (d, *J* = 7.9 Hz, 2H), 8.09 (t, *J* = 7.9 Hz, 1H), 7.97 (d, *J* = 7.6 Hz, 4H), 7.52 (t, *J* = 7.9 Hz, 4H), 7.32 (t, *J* = 7.4 Hz, 2H). ¹³C-NMR (400 MHz, CH₂Cl₂-*d*₂) δ 189.21 (s), 150.7 (s), 139.4 (s), 139.2 (s), 129.7 (s), 128.2 (s), 127.7 (s), 124.1 (s). FT-IR (ATR) cm⁻¹: 1078 (m, C=S), 3210 (bd m, N-H). UV/Vis(CH₃CN): λ_{max} 311 nm.

***N*²,*N*⁶-bis(4-(*tert*-butyl)phenyl)pyridine-2,6-dicarboxamide (3):**⁵⁰ 2,6-Pyridinedicarboxylic acid dichloride, 97% (500 mg; 2.9 mmol) and 4-*tert*-Butylaniline 98% (CAS: 769-92-6; Oakwood Chemical) (0.94 mL; 5.8 mmol) were mixed together in 3 mL of DMF. The 5 mL conical flask remained uncapped and under stirring for 48 h at

room temperature. The reaction mixture was poured into 500 mL of water causing formation of a white powder. The solid was filtered out, dried under vacuum and recrystallized from hot ethanol (Yield: 1.08 g; 82%). ^1H NMR (400 MHz, $\text{CH}_2\text{Cl}_2\text{-}d_2$) δ 9.53 (2H, s), 8.51 (d, $J = 7.8$ Hz, 2H), 8.19 (t, $J = 7.8$ Hz, 1H), 7.74 (d, $J = 8.7$ Hz, 4H), 7.49 (d, $J = 8.7$ Hz, 4H), 1.39 (s, 18H). ^{13}C -NMR (400 MHz, $\text{CH}_2\text{Cl}_2\text{-}d_2$) δ 161.4 (s), 149.5 (s), 148.4 (s), 140.3 (s), 135.1 (s), 126.3 (s), 125.7 (s), 120.3 (s), 34.8 (s), 31.5 (s). FT-IR(ATR) cm^{-1} : 1673 (m, C=O), 3358 (bd m, N-H). UV/Vis(CH_3CN): λ_{max} 287 nm. Elemental analysis: Anal. Calcd. for $\text{C}_{27}\text{H}_{31}\text{N}_3\text{O}_2$: C, 75.49; H, 7.27; N, 9.78. Found: C, 75.15; H, 7.25; N, 9.72.

N^2, N^6 -bis(4-(tert-butyl)phenyl)pyridine-2,6-dicarbothioamide (4): N^2, N^6 -bis(4-(tert-butyl)phenyl)pyridine-2,6-dicarboxamide (3) (514.6 mg, 1.20 mmol) was dissolved in dry and distilled toluene under a flow of N_2 . A solution of Lawesson's reagent (1.54 g, 3.82 mmol) in dry-distilled toluene was added under N_2 to solution. After 4 h the toluene were evaporated and the residue was washed with methanol. The precipitate was filtered and purified thorough silica gel column chromatography in EtOAc/Hexane (3:7). A yellow crystalline compound was obtained that was recrystallized from dichloromethane/hexane to give the pure product (430 mg, 0.965 mmol, 78% yield): ^1H -NMR (400 MHz, $\text{DMSO-}d_6$) δ 12.42 (s, 2H), 8.83 (d, $J = 7.9$ Hz, 2H), 8.24 (t, $J = 7.9$ Hz, 2H), 7.69 (d, $J = 8.5$ Hz, 4H), 7.52 (d, $J = 8.6$ Hz, 4H), 1.32 (s, 18H). ^{13}C NMR (101 MHz, DMSO) δ 189.06 (s), 149.94 (s), 149.62 (s), 138.82 (s), 136.68 (s), 127.56 (s), 125.40 (s), 125.19 (s), 124.80 (s), 34.42 (s), 31.11 (s). FT-IR (ATR) cm^{-1} : 1078 (m, C=S), 3210 (bd m, N-H).

UV/Vis(CH₃CN): λ_{\max} 308 nm. Anal. Calcd. for C₂₇H₃₁N₃S₂: C, 70.24; H, 6.77; N, 9.10. Found: C, 69.04; H, 6.60; N, 8.89.

2.4.2 Synthetic procedure for [Nd(3)₃]I₃ complex:

NdI₃: 0.2 mL of concentrated HI (without stabilizer) was added to 3.0 mg (8.92 μ mol) of Nd₂O₃ in a 6 mL glass vial. The suspension was then heated at 150 °C until the excess HI evaporated off, leaving 9.4 mg of putative NdI₃·nH₂O.

[Nd(3)₃]I₃·3CH₃CN: In a 6 mL glass vial, 9.4 mg (17.8 μ mol) of NdI₃ was added to 23.0 mg (53.5 μ mol) of **3**. This mixture was then dissolved in 2 mL of acetonitrile and was allowed to evaporate slowly over a 24 h period resulting in yellow, acicular crystals (30% yield). ¹H NMR (400 MHz, CH₃CN-*d*₃) δ 10.00 (s, 4H), 9.31 (d, *J* = 6.0 Hz, 2H), 9.08 (d, *J* = 4.7 Hz, 4H), 8.85 (t, *J* = 7.5 Hz, 1H), 8.80 (s, 2H), 8.42 (d, *J* = 7.8 Hz, 4H), 8.22 (t, *J* = 7.4 Hz, 2H), 7.79 (d, *J* = 8.3 Hz, 8H), 7.66 (d, *J* = 5.7 Hz, 4H), 7.48 (d, *J* = 8.6 Hz, 8H), 1.39 (s, 18H), 1.34 (s, 36H). FT-IR (ATR) cm⁻¹: 1620 (m, C=O), 3186 (bd m, N-H). Elemental analysis: Anal. Calcd. For C₈₁H₉₃I₃N₉NdO₆·HI·3H₂O: C, 48.75; H, 5.05; N, 6.32. Found: C, 48.38; H, 5.00; N, 6.41.

2.4.3 UV-Visible Titrations:

Solutions of ligands **1**, **2**, or **3** in CH₃CN were titrated with solutions of lanthanide salts, including La(NO₃)₃·6H₂O, Nd(NO₃)₃·6H₂O, Eu(NO₃)₃·6H₂O and Lu(NO₃)₃·6H₂O at constant ligand concentration. In a typical experiment, a solution of **1** (2.0 x 10⁻⁵ M) in CH₃CN (solution A) was titrated with a solution of Ln(NO₃)₃·6H₂O (1.0 x 10⁻³ M) and **1** (2.0 x 10⁻⁵ M) (solution B) prepared by accurately weighing approximately 1.80 mg of Ln(NO₃)₃·6H₂O in a 5.00 mL volumetric flask and diluting with solution A. For spectra

collection, 2.30 mL of solution A were added to the UV-Visible cuvette and solution B was added in 2-150 μL increments until a total of 1000 μL had been added.

2.4.4 UV-Visible Job plots:

Solutions of the ligand **1** (4.7×10^{-5} M) and $\text{La}(\text{NO}_3)_3 \cdot 6\text{H}_2\text{O}$ (4.5×10^{-5} M) in CH_3CN were prepared. Eleven vials were filled with 1000 μL of solutions that contain ligand and metal in the following volume ratios (in μL). 1000:0, 900:100, 800:200, 700:300, 600:400, 500:500, 400:600, 300:700, 200:800, 100:900 and 0:1000. Each of them was transferred to the cuvette and spectra were recorded. Job plots were obtained by plotting mol. fraction against $\text{Abs} \times [\text{L}]_t / ([\text{M}] + [\text{L}]_t)$ (where **L** is ligand **1** and **M** is La^{3+}).

2.4.5 Fluorescence titrations:

i) Titration of Ligands with Ln(III): Solutions of ligands in CH_3CN were titrated with solutions of lanthanide salts, including $\text{La}(\text{NO}_3)_3 \cdot 6\text{H}_2\text{O}$, $\text{Ce}(\text{NO}_3)_3 \cdot 6\text{H}_2\text{O}$ and $\text{Lu}(\text{NO}_3)_3 \cdot 6\text{H}_2\text{O}$ at constant ligand concentration. Fluorescence emission was measured at increments of 0.5 nm, and integration time of 0.1 s, excitation slit width of 10 nm, emission slit width of 5 nm. For ligand **1** excitation at 282 nm produces an emission at 338 nm and ligand **3** excitation at 287 nm produce an emission 350 nm. In a typical experiment, a solution of **1** (2×10^{-5} M) in CH_3CN (solution A) was titrated with a solution of $\text{Ln}(\text{NO}_3)_3 \cdot 6\text{H}_2\text{O}$ (1×10^{-3} M) and **1** (2×10^{-5} M) (solution B) prepared by accurately weighing 18.0 mg of $\text{Ln}(\text{NO}_3)_3 \cdot 6\text{H}_2\text{O}$ in a 5.00 mL volumetric flask and diluting with solution A. For spectra collection, 2.3 mL of solution A were added to the cuvette and solution B was added in 2.0-150 μL increments until a total of 1000 μL had been added. The Stern-Volmer fluorescence quenching method⁵¹ was used to determine the Stern-

Volmer quenching constant of the fluorescence titrations. A more sensitive system will have a steeper slope and, as a result, a higher K_{sv} value.

ii) Titration of Eu(III) with Ligands: Solutions of $\text{Eu}(\text{NO}_3)_3 \cdot 6\text{H}_2\text{O}$ were titrated with solutions of ligands **3** or **4** at constant Eu(III) concentration ($\lambda_{\text{exc}} = 394\text{nm}$). In a typical experiment, a solution of $\text{Eu}(\text{NO}_3)_3 \cdot 6\text{H}_2\text{O}$ (1.4 mM) in CH_3CN (solution A) was titrated with a solution of **3** (23.2 mM) and $\text{Eu}(\text{NO}_3)_3 \cdot 6\text{H}_2\text{O}$ (1.4 mM) (solution B) prepared by accurately weighing 47.98 mg of **3** in a 5.00 mL volumetric flask and diluting with solution A prepared by weighing 16.07 mg of $\text{Eu}(\text{NO}_3)_3 \cdot 6\text{H}_2\text{O}$ in a 25.00 mL volumetric flask. For spectra collection, 2.30 mL of solution A were added to the cuvette and solution B was added in 2-150 μL increments until a total of 1000 μL had been added.

2.4.6 $^1\text{H-NMR}$ Titrations:

Solutions of ligands ($2.4 \times 10^{-3} \text{ M}$) were titrated in acetone- d_6 with solutions of $\text{La}(\text{NO}_3)_3 \cdot 6\text{H}_2\text{O}$ ($2 \times 10^{-1} \text{ M}$) at constant ligand concentration. In a typical experiment, a solution of **1** ($2.4 \times 10^{-3} \text{ M}$) in acetone d_6 was prepared in a 2.00 mL volumetric flask (solution A). A $\text{La}(\text{NO}_3)_3 \cdot 6\text{H}_2\text{O}$ solution (Solution B) was prepared by a dilution of an accurately weighed amount of $\text{La}(\text{NO}_3)_3 \cdot 6\text{H}_2\text{O}$ with solution A in a 1.00 mL volumetric flask (Solution B). Solution A (0.700 mL) was placed in an NMR tube. Solution B was added in increments with a μL syringe until a total of 950 μL was added.

2.4.7 Solvent Extraction:

Extraction experiments for ligands **1** and **2** with Am-243 and Eu-154 were carried out as follows: Initially saturated dichloromethane solutions of each ligand (10 mL for each) were prepared. To assist in ensuring that each ligand was saturated, the solutions were

sonicated for 5 min, and then filtered to remove any undissolved ligand. An aliquot of an Am-243 or Eu-154 solution was added to 1.5 mL of 1.0 M or 6.5 M nitric acid. 1.5 mL of the ligand in organic solvent was then added to the aqueous solution containing the radionuclide and was mixed on a vortex stirrer for 5 min. After the layers were allowed to separate, 1.00 mL of each phase was pipetted out into scintillation vials and counted for 10 min. using an ORTEC GEM50P4 coaxial HPGe detector and DSPEC gamma spectrometer. The average dead time for each sample was 8.5 %. Distribution values for the extraction were obtained by the ratio of the number of counts of the desired radionuclide in the organic phase relative to the amount in the aqueous phase. The separation factor (SF) is the ratio of the distribution values for Am-243 relative to Eu-154. In 6.5 M nitric acid, **1** had a distribution ratio of 0.02 (123 counts in the organic phase, and 5739 in the aqueous phase), while **2** had an Am-243 distribution ratio of 0.42 (3724 counts organic phase, 1546 counts aqueous phase). In 6.5 M nitric acid, **1** did not extract any Eu-154 (28 counts in the organic phase, 6150 counts in the aqueous phase). Under similar conditions (6.5 M nitric acid), **2** also did not extract Eu-154 (133 counts in the organic phase, 5482 counts in the aqueous phase – D value of 0.02). In 1.0 M nitric acid, the Am-243 extraction with both ligands was lower than in 6.5 M nitric acid; **2** had a measured distribution ratio of 0.26 (756 organic counts, 2941 aqueous counts), and **1** showed no extraction (D value of 0.01).

2.4.8 DFT calculations:

DFT calculations were performed on the following molecules: **1**, **2**, **3**, $\text{Nd}(\text{NO}_3)_3(\text{H}_2\text{O})_4$, $\text{Nd}(\text{NO}_3)_3(\mathbf{3})(\text{H}_2\text{O})$, $\text{M}(\text{NO}_3)_3(\text{L})(\text{H}_2\text{O})$ (M=Nd, Eu, Am; L= **1** or **2**), $\text{M}(\text{H}_2\text{O})_9^{3+}$ and $\text{M}(\text{NO}_3)(\text{H}_2\text{O})_8^{2+}$ (M=Eu, Am). Geometry optimizations were performed

by employing the hybrid functional PBE0⁵² as implemented in the Amsterdam Density Functional (ADF 2016.104).⁵³⁻⁵⁵ The Slater basis sets with the quality of triple- ζ plus two polarization functions (TZ2P) were used.⁵⁶ The frozen core approximation was applied to the $[1s^2-4f^{14}]$ cores of Am, and $[1s^2-4d^{10}]$ cores of Nd and Eu, and $[1s^2]$ cores of C, N and O, and $[1s^2-2p^6]$ core of S, with the rest of the electrons explicitly treated variationally. All the geometric structures were fully optimized by DFT/PBE0 at the scalar-relativistic (SR) zero-order-regular approximation (ZORA)⁵⁷ with the gradient convergence of 10^{-4} in gas phase. In the vibrational frequency calculations, all frequencies were real, indicating that the structures were true minima on the energy surface. To account for the solvation effects, a subsequent single-point calculation for the above molecules was performed at PBE0 level using the implicit COSMO^{58,59} solvation model with the default Delley surface⁶⁰ and a radius of 2.045 for Am and of 1.870 for Nd and of 1.820 for Eu and the default van der Waals radius from the MM3 method divided by 1.2 for other atoms.⁶¹ The UV-Vis spectra of ligand and $\text{Nd}(\text{NO}_3)_3(\text{ligand})(\text{H}_2\text{O})$ (ligand=**1**, **2**, **3**) were simulated as the Kohn-Sham orbital energy differences from SR-DFT/PBE0 calculations, i.e., the energy difference between an occupied orbital and a virtual orbital of the ground state. All the calculated transition intensities were evenly broadened with a Gaussian function of full-width at half-maximum of 35 nm (i.e., peak width) to emulate the experimental spectra. For a specific electronic excitation, the oscillator strength was calculated using the transition-dipole approximation between this occupied MO and the virtual MOs.

2.4.9 Gas phase experiments (CID-ESI-MS):

$[\text{Eu}^{\text{III}}(\mathbf{1})_2(\mathbf{2-H})]^{2+}$ and $[\text{Am}^{\text{III}}(\mathbf{1})_2(\mathbf{2-H})]^{2+}$ dicationic complexes were produced by electrospray ionization (ESI) of ethanol solutions containing 100 μM of either AmCl_3 or EuCl_3 , and 100 μM of both **1** and **2** ligands. The employed ^{243}Am isotope has an alpha-decay half-life of 7370 y. The gas phase experiments were performed using an Agilent 6340 quadrupole ion trap mass spectrometer (QIT/MS) with the ESI source located inside a radiological containment glovebox.⁶² The gas-phase cation complex of interest was isolated and subjected to collision induced dissociation (CID) whereby ions are excited and undergo multiple energetic collisions with helium to ultimately induce dissociation. As discussed elsewhere, the background H_2O and O_2 pressures in the ion trap are estimated to be on the order of 10^{-6} Torr, while the helium buffer gas pressure in the trap is constant at $\sim 10^{-4}$ Torr.⁶³ Cation mass spectra were acquired using the following instrumental parameters: solution flow rate, 60 $\mu\text{L min}^{-1}$; nebulizer gas pressure, 18 psi; capillary voltage, -3500 V; end plate voltage offset, -500 V; dry gas flow rate, 4 L/min; dry gas temperature, 325 $^\circ\text{C}$; capillary exit, 94.0 V; skimmer, 40.0 V; octopole 1 and 2 dc, 12.0 and 1.7 V; octopole RF amplitude, 171.0 Vpp; lens 1 and 2, -5.0 and -60.0 V; trap drive, 52.0. The high-purity nitrogen gas for nebulization and drying in the ion transfer capillary was the boil off from a liquid nitrogen Dewar.

2.4.10 X-Ray Crystallography

Light yellow-dark block-shaped crystals of $[\text{Nd}(\mathbf{3})_3]\text{I}_3$ complex were obtained by slow evaporation of a MeCN solution. The crystals were formed after one week. NMR characterization of the dissolved formed crystals perfectly matched the spectrum of the

complex $[\text{Nd}(\mathbf{3})_3]\text{I}_3$ formed by bulk synthesis. The crystal was selected and mounted on a Bruker D8 Quest diffractometer equipped with PHOTON II detector operating at $T = 120$ K. Data were collected with ω shutter less scan technique using graphite monochromated Mo-K α radiation ($\lambda = 0.71073 \text{ \AA}$). The total number of runs and images for both data collections was based on the strategy calculation from the program *APEX3* (Bruker)⁶⁴. Cell parameters were retrieved using the *SAINTE* (Bruker) software⁶⁵ and refined using *SAINTE* (Bruker) on 132580 reflections for $[\text{Nd}(\mathbf{3})_3]\text{I}_3$. Data reduction was performed using the *SAINTE* (Bruker) software, which corrects for Lorentz and polarization effects. Hydrogen atom positions were calculated geometrically and refined using the riding model. Good quality single crystals of complex $[\text{Nd}(\mathbf{3})_3]\text{I}_3$ have also been isolated upon slow evaporation of the final solution of the NMR titration experiments. One of such single crystals was selected for data collection and upon the solution and refinement this revealed the same molecular structure as $[\text{Nd}(\mathbf{3})_3]\text{I}_3$ albeit in a different crystal system and space group. Calculations and molecular graphics were performed using *SHELXTL* 2014 and *Olex2*⁶⁶ programs.

2.5 Conclusion

In conclusion, our investigation of binding and An(III) vs. Ln(III) extraction selectivity of C=O vs. C=S dipicolinamide analogs demonstrates the potential of simple dithiopicolinamides as selective extractants for minor actinides under highly acidic conditions consistent with UNF reprocessing. DFT results reveal a stronger affinity of diamide **1** (C=O) vs. dithioamide **2** (C=S) for both Ln(III) and An(III), while also demonstrating that **2** has a higher Am(III)/Eu(III) separation selectivity. Titrations with

NO₃⁻ salts show strong Ln(III) binding by the diamide ligands **1** and **3** with 1:1 metal-to-ligand stoichiometry, while X-ray crystallography indicates a 1:3 stoichiometry when I⁻ is used. Different crystallization attempts with different counter cations such as PF₆⁻, Cl⁻ and NO₃⁻, were unsuccessful under different conditions. Such solvent and counteranion-dependent coordination effects^{67–69} can affect speciation under UNF extraction conditions.

2.6 References:

- (1) Geist, A.; Hill, C.; Modolo, G.; Foreman, M. R. S. J.; Weigl, M.; Gompper, K.; Hudson, M. J. 6,6'-Bis(5,5,8,8-tetramethyl-5,6,7,8-tetrahydro-benzo[1,2,4]Triazin-3-yl)[2,2'] Bipyridine, an Effective Extracting Agent for the Separation of Americium(III) and Curium(III) from the Lanthanides. *Solvent Extraction and Ion Exchange*. **2006**, *24*, 463–483.
- (2) Panak, P. J.; Geist, A. Complexation and Extraction of Trivalent Actinides and Lanthanides by Triazinylpyridine *N*-Donor Ligands. *Chem. Rev.* **2013**, *113*, 1199–1236.
- (3) Salvatores, M.; Palmiotti, G. Radioactive Waste Partitioning and Transmutation within Advanced Fuel Cycles: Achievements and Challenges. *Progress in Particle and Nuclear Physics* **2011**, *66*, 144–166.
- (4) Edwards, A. C.; Wagner, C.; Geist, A.; Burton, N. A.; Sharrad, C. A.; Adams, R. W.; Pritchard, R. G.; Panak, P. J.; Whitehead, R. C.; Harwood, L. M. Exploring Electronic Effects on the Partitioning of Actinides(III) from Lanthanides(III) Using Functionalised Bis-Triazinyl Phenanthroline Ligands. *Dalton Trans.* **2016**, *45*, 18102-18112.
- (5) Hudson, M. J.; Harwood, L. M.; Laventine, D. M.; Lewis, F. W. Use of Soft Heterocyclic *N*-Donor Ligands to Separate Actinides and Lanthanides. *Inorganic Chemistry* **2013**, *52*, 3414–3428.

- (6) Demir, S.; Brune, N. K.; Van Humbeck, J. F.; Mason, J. A.; Plakhova, T. V.; Wang, S.; Tian, G.; Minasian, S. G.; Tyliczszak, T.; Yaita, T.; Kobayashi, T.; Kalmykov, S. N.; Shiwaku, H.; Shuh, D. K.; Long, J. R. Extraction of Lanthanide and Actinide Ions from Aqueous Mixtures Using a Carboxylic Acid-Functionalized Porous Aromatic Framework. *ACS Cent Sci.* **2016**, *2*, 253–265.
- (7) Macerata, E.; Mossini, E.; Scaravaggi, S.; Mariani, M.; Mele, A.; Panzeri, W.; Boubals, N.; Berthon, L.; Charbonnel, M.C.; Sansone, F.; Arduini, A.; Casnati, A. Hydrophilic Clicked 2,6-Bis-Triazolyl-Pyridines Endowed with High Actinide Selectivity and Radiochemical Stability: Toward a Closed Nuclear Fuel Cycle. *J. Am. Chem. Soc.* **2016**, *138*, 7232–7235.
- (8) Geist, A.; Müllich, U.; Magnusson, D.; Kaden, P.; Modolo, G.; Wilden, A.; Zevaco, T. Actinide(III)/Lanthanide(III) Separation Via Selective Aqueous Complexation of Actinides(III) Using a Hydrophilic 2,6-Bis(1,2,4-Triazin-3-Yl)-Pyridine in Nitric Acid. *Solvent Extraction and Ion Exchange* **2012**, *30*, 433–444.
- (9) Zalupski, P. R.; Nash, K. L.; Martin, L. R. Thermodynamic Features of the Complexation of Neodymium(III) and Americium(III) by Lactate in Trifluoromethanesulfonate Media. *J Solution Chem* **2010**, *39*, 1213–1229.
- (10) Magill, J.; Berthou, V.; Haas, D.; Galy, J.; Schenkel, R.; Heusener, G. Impact Limits of Partitioning and Transmutation Scenarios on the Radiotoxicity of Actinides in Radioactive Waste. *Nuclear Energy* **2003**, *42*, 263–277.
- (11) Wu, Q.-Y.; Song, Y.-T.; Ji, L.; Wang, C.-Z.; Chai, Z.-F.; Shi, W.-Q. Theoretically Unraveling the Separation of Am(III)/Eu(III): Insights from Mixed *N,O*-Donor Ligands with Variations of Central Heterocyclic Moieties. *Phys. Chem. Chem. Phys.* **2017**, *19*, 26969–26979.
- (12) Modolo, G.; Odoj, R. The Separation of Trivalent Actinides from Lanthanides by Dithiophosphinic Acids from HNO₃ Acid Medium. *Journal of Alloys and Compounds* **1998**, *271*, 248–251.

- (13) Bhattacharyya, A.; Mohapatra, P. K.; Manchanda, V. K. Separation of Americium(III) and Europium(III) from Nitrate Medium Using a Binary Mixture of Cyanex-301 with *N*-donor Ligands. *Solvent Extraction and Ion Exchange* **2006**, *24*, 1–17.
- (14) Nash, K. L. The Chemistry of TALSPEAK: A Review of the Science. *Solvent Extraction and Ion Exchange* **2015**, *33*, 1–55.
- (15) Ustynyuk, Y. A.; Gloriov, I. P.; Kalmykov, S. N.; Mitrofanov, A. A.; Babain, V. A.; Alyapyshev, M. Yu.; Ustynyuk, N. A. Pyridinedicarboxylic Acid Diamides as Selective Ligands for Extraction and Separation of Trivalent Lanthanides and Actinides: DFT Study. *Solvent Extraction and Ion Exchange* **2014**, *32*, 508–528.
- (16) Marie, C.; Miguiritchian, M.; Guillaumont, D.; Tosseng, A.; Berthon, C.; Guilbaud, P.; Duvail, M.; Bisson, J.; Guillaneux, D.; Pipelier, M.; Dubreuil, D. Complexation of Lanthanides(III), Americium(III), and Uranium(VI) with Bitopic N,O Ligands: An Experimental and Theoretical Study. *Inorg. Chem.* **2011**, *50*, 6557–6566.
- (17) Mincher, B. J.; Martin, L. R.; Schmitt, N. C. Diamylmethylphosphonate Solvent Extraction of Am(VI) from Nuclear Fuel Raffinate Simulant Solution. *Solvent Extraction and Ion Exchange* **2012**, *30*, 445–456.
- (18) Braley, J. C.; Grimes, T. S.; Nash, K. L. Alternatives to HDEHP and DTPA for Simplified TALSPEAK Separations. *Ind. Eng. Chem. Res.* **2012**, *51*, 629–638.
- (19) Whittaker, D. M.; Griffiths, T. L.; Helliwell, M.; Swinburne, A. N.; Natrajan, L. S.; Lewis, F. W.; Harwood, L. M.; Parry, S. A.; Sharrad, C. A. Lanthanide Speciation in Potential SANEX and GANEX Actinide/Lanthanide Separations Using Tetra-*N*-Donor Extractants. *Inorg. Chem.* **2013**, *52*, 3429–3444.
- (20) Wang, J.; Su, D.; Wang, D.; Ding, S.; Huang, C.; Huang, H.; Hu, X.; Wang, Z.; Li, S. Selective Extraction of Americium(III) over Europium(III) with the

Pyridylpyrazole Based Tetradentate Ligands: Experimental and Theoretical Study. *Inorg. Chem.* **2015**, *54*, 10648–10655.

- (21) Kolarik, Z.; Müllich, U.; Gassner, F. *Solvent Extr. Ion Exch.* **1999**, *17*, 1155–1170.
- (22) Alyapyshev, M. Y.; Babain, V. A.; Tkachenko, L. I.; Paulenova, A.; Popova, A. A.; Borisova, N.E. New Diamides of 2,2'-Dipyridyl-6,6'-Dicarboxylic Acid for Actinide-Lanthanide Separation. *Solvent Extraction and Ion Exchange* **2014**, *32*, 138–152.
- (23) Xiao, C.-L.; Wang, C.-Z.; Yuan, L.-Y.; Li, B.; He, H.; Wang, S.; Zhao, Y.-L.; Chai, Z.-F.; Shi, W.-Q. Excellent Selectivity for Actinides with a Tetradentate 2,9-Diamide-1,10-Phenanthroline Ligand in Highly Acidic Solution: A Hard–Soft Donor Combined Strategy. *Inorg. Chem.* **2014**, *53*, 1712–1720.
- (24) Bisson, J.; Dehaut, J.; Charbonnel, M.-C.; Guillaneux, D.; Miguiditchian, M.; Marie, C.; Boubals, N.; Dutech, G.; Pipelier, M.; Blot, V.; Dubreuil, D. 1,10-Phenanthroline and Non-Symmetrical 1,3,5-Triazine Dipicolinamide-Based Ligands for Group Actinide Extraction. *Chemistry* **2014**, *20*, 7819–7829.
- (25) Geist, A.; Weigl, M.; Müllich, U.; Gompper, K. Actinide(III)/Lanthanide(III) Partitioning Using n-Pr-BTP as Extractant: Extraction Kinetics and Extraction Test in a Hollow Fiber Module. *Nuclear Fuel Cycle and Fuel Materials* **2001**, *32*, 641–647.
- (26) Galletta, M.; Baldini, L.; Sansone, F.; Ugozzoli, F.; Ungaro, R.; Casnati, A.; Mariani, M. Calix[6]Arene-Picolinamide Extractants for Radioactive Waste: Effect of Modification of the Basicity of the Pyridine *N* Atom on the Extraction Efficiency and An/Ln Separation. *Dalton Trans.* **2010**, *39*, 2546–2553.
- (27) Babain, V. A.; Alyapyshev, M. Yu.; Kiseleva, R. N. Metal Extraction by *N,N'*-Dialkyl-*N,N'*-Diaryl-Dipicolinamides from Nitric Acid Solutions. *Radiochimica Acta.* **2007**, *95*, 217–223.

- (28) Bisson, J.; Berthon, C.; Berthon, L.; Boubals, N.; Dubreuil, D.; Charbonnel, M.-C. Effect of the Structure of Amido-Polynitrogen Molecules on the Complexation of Actinides. *Procedia Chemistry* **2012**, *7*, 13–19.
- (29) Lavrov, H. V.; Ustynyuk, N. A.; Matveev, P. I.; Gloriozov, I. P.; Zhokhov, S. S. A Novel Highly Selective Ligand for Separation of Actinides and Lanthanides in the Nuclear Fuel Cycle. *Dalton Trans.* **2017**, *46*, 10926-10934.
- (30) Galletta, M.; Scaravaggi, S.; Macerata, E.; Famulari, A.; Mele, A.; Panzeri, W.; Sansone, F.; Casnati, A.; Mariani, M. 2,9-Dicarbonyl-1,10-Phenanthroline Derivatives with an Unprecedented Am(III)/Eu(III) Selectivity under Highly Acidic Conditions. *Dalton Trans.* **2013**, *42*, 16930–16938.
- (31) Komiyama, Y.; Kuwabara, J.; Kanbara, T. Deprotonation-Induced Structural Changes in SNS-Pincer Ruthenium Complexes with Secondary Thioamide Groups. *Organometallics* **2014**, *33*, 885–891.
- (32) Jagodziński, T. S. Thioamides as Useful Synthons in the Synthesis of Heterocycles. *Chem. Rev.* **2003**, *103*, 197–228.
- (33) Wang, Q.-Q.; Ara Begum, R.; Day, V. W.; Bowman-James, K. Molecular Thioamide ↔ Iminothiolate Switches for Sulfur Mustards. *Inorg. Chem.* **2012**, *51*, 760–762.
- (34) Berny, F.; Wipff, G. Interaction of M^{3+} Lanthanide Cations with Amide, Urea, Thioamide and Thiourea Ligands: A Quantum Mechanical Study. *J. Chem. Soc., Perkin Trans. 2.* **2001**, *1*, 73–82.
- (35) Puntus, L. N.; Zolin, V. F.; Kudryashova, V. A.; Tsaryuk, V. I.; Legendziewicz, J.; Gawryszewska, P.; Szostak, R. Charge Transfer Bands in the Eu^{3+} Luminescence Excitation Spectra of Isomeric Europium Pyridine-Dicarboxylates. *Phys. Solid State* **2002**, *44*, 1440–1444.

- (36) Maiwald, M. M.; Wagner, A. T.; Kratsch, J.; Skerencak-Frech, A.; Trumm, M.; Geist, A.; Roesky, P. W.; Panak, P. J. 4,4'-Di-Tert-Butyl-6-(1H-Tetrazol-5-Yl)-2,2'-Bipyridine: Modification of a Highly Selective N-Donor Ligand for the Separation of Trivalent Actinides from Lanthanides. *Dalton Trans.* **2017**, *46*, 9981–9994.
- (37) Boubals, N.; Wagner, C.; Dumas, T.; Chanèac, L.; Manie, G.; Kaufholz, P.; Marie, C.; Panak, P. J.; Modolo, G.; Geist, A.; Guilbaud, P. Complexation of Actinide(III) and Lanthanide(III) with H4tpaen for a Separation of Americium from Curium and Lanthanides. *Inorg. Chem.* **2017**, *56*, 7861–7869.
- (38) Lundberg, D. An Overview of Eight- and Nine-Coordinate N-Donor Solvated Lanthanoid(III) and Actinoid(III) Ions. *J Radioanal Nucl Chem* **2018**, *316*, 849–854.
- (39) Cross, J. N.; Villa, E. M.; Wang, S.; Diwu, J.; Polinski, M. J.; Albrecht-Schmitt, T. E. Syntheses, Structures, and Spectroscopic Properties of Plutonium and Americium Phosphites and the Redetermination of the Ionic Radii of Pu(III) and Am(III). *Inorg. Chem.* **2012**, *51*, 8419–8424.
- (40) Albrecht, M.; Wessel, C.; de Groot, M.; Rissanen, K.; Lüchow, A. Structural Versatility of Anion– π Interactions in Halide Salts with Pentafluorophenyl Substituted Cations. *J. Am. Chem. Soc.* **2008**, *130*, 4600–4601.
- (41) Garau, C.; Frontera, A.; Quiñonero, D.; Ballester, P.; Costa, A.; Deyà, P. M. Cation– π versus Anion– π Interactions: Energetic, Charge Transfer, and Aromatic Aspects. *J. Phys. Chem. A* **2004**, *108*, 9423–9427.
- (42) Hay, B. P.; Custelcean, R. Anion– π Interactions in Crystal Structures: Commonplace or Extraordinary. *Crystal Growth & Design.* **2009**, *9*, 2539–2545.
- (43) Quarton, M.; Svoronos, D. Crystallographic Study of Neodymium Nitrate Hexahydrate. *J. Solid State Chem.* **1982**, *42*, 325–327.
- (44) Drew, M. G. B.; Iveson, P. B.; Hudson, M. J.; Liljenzin, J. O.; Spjuth, L.; Cordier, P.-Y.; Enarsson, Å.; Hill, C.; Madic, C. Separation of Americium(III) from

- Europium(III) with Tridentate Heterocyclic Nitrogen Ligands and Crystallographic Studies of Complexes Formed by 2,2'-6',2''-Terpyridine with the Lanthanides. *J. Chem. Soc., Dalton Trans.* **2000**, 5, 821–830.
- (45) Ingram, K. I. M.; Tassell, M. J.; Gaunt, A. J.; Kaltsoyannis, N. Covalency in the *f*-Element-Chalcogen Bond. Computational Studies of M[N(EPR₂)(₂)](₃) (M = La, Ce, Pr, Pm, Eu, U, Np, Pu, Am, Cm; E = O, S, Se, Te; R = H, Pr-i, Ph). *Inorg. Chem.* **2008**, 47, 7824–7833.
- (46) Spencer, L. P.; Yang, P.; Scott, B. L.; Batista, E. R.; Boncella, J. M. Uranium(VI) Bis(Imido) Chalcogenate Complexes: Synthesis and Density Functional Theory Analysis. *Inorg. Chem.* **2009**, 48, 2693–2700.
- (47) Kaneko, M.; Watanabe, M. Correlation between Am(III)/Eu(III) Selectivity and Covalency in Metal–Chalcogen Bonds Using Density Functional Calculations. *J Radioanal Nucl Chem.* **2018**, 316, 1129–1137.
- (48) Keith, J. M.; Batista, E. R. Theoretical Examination of the Thermodynamic Factors in the Selective Extraction of Am³⁺ from Eu³⁺ by Dithiophosphinic Acids. *Inorg. Chem.* **2012**, 51, 13–15.
- (49) Malone, J. F.; Murray, C. M.; Dolan, G. M.; Docherty, R.; Lavery, A. J. Intermolecular Interactions in the Crystal Chemistry of *N,N'*-Diphenylisophthalamide, Pyridine-2,6-Dicarboxylic Acid Bisphenylamide, and Related Compounds. *Chem. Mater.* **1997**, 9, 2983–2989.
- (50) Kimura, I.; Tsuji, M.; Tojo, M.; Asakai, M. Pyridine dicarboxylic acid derivative charge control agent and toner. Patent WO 2013129015, September 6, **2013**.
- (51) Keizer, J. Nonlinear Fluorescence Quenching and the Origin of Positive Curvature in Stern-Volmer Plots. *J. Am. Chem. Soc.* **1983**, 105, 1494–1498.

- (52) Adamo, C.; Barone, V. Toward Reliable Density Functional Methods without Adjustable Parameters: The PBE0 Model. *The Journal of Chemical Physics* **1999**, *110*, 6158–6170.
- (53) Guerra, C. F.; Snijders, J. G.; te Velde, G.; Baerends, E. J. Towards an Order-N DFT Method. *Theor. Chem. Acc.* **1998**, *99*, 391–403.
- (54) te Velde, G.; Bickelhaupt, F. M.; Baerends, E. J.; Guerra, C. F.; Van Gisbergen, S. J. A.; Snijders, J. G.; Ziegler, T. Chemistry with ADF. *J. Comput. Chem.* **2001**, *22*, 931–967.
- (55) ADF: accurate & efficient DFT, with great GUI & expert support <https://www.scm.com/product/adf/> (accessed Aug 10, **2018**).
- (56) Lenthe, E. V.; Baerends, E. J. Optimized Slater-Type Basis Sets for the Elements 1–118. *Journal of Computational Chemistry* **2003**, *24*, 1142–1156.
- (57) Lenthe, E. van; Baerends, E. J.; Snijders, J. G. Relativistic Regular Two-component Hamiltonians. *The Journal of Chemical Physics* **1993**, *99*, 4597–4610.
- (58) Klamt, A.; Schüürmann, G. COSMO: A New Approach to Dielectric Screening in Solvents with Explicit Expressions for the Screening Energy and Its Gradient. *J. Chem. Soc., Perkin Trans. 2.* **1993**, *5*, 799–805.
- (59) Pye, C. C.; Ziegler, T. An Implementation of the Conductor-like Screening Model of Solvation within the Amsterdam Density Functional Package. *Theor. Chem. Acc.* **1999**, *101*, 396–408.
- (60) Delley, B. The Conductor-like Screening Model for Polymers and Surfaces. *Mol. Simul.* **2006**, *32*, 117–123.
- (61) Allinger, N.; Zhou, X.; Bergsma, J. Molecular Mechanics Parameters. *Theochem-J. Mol. Struct.* **1994**, *118*, 69–83.

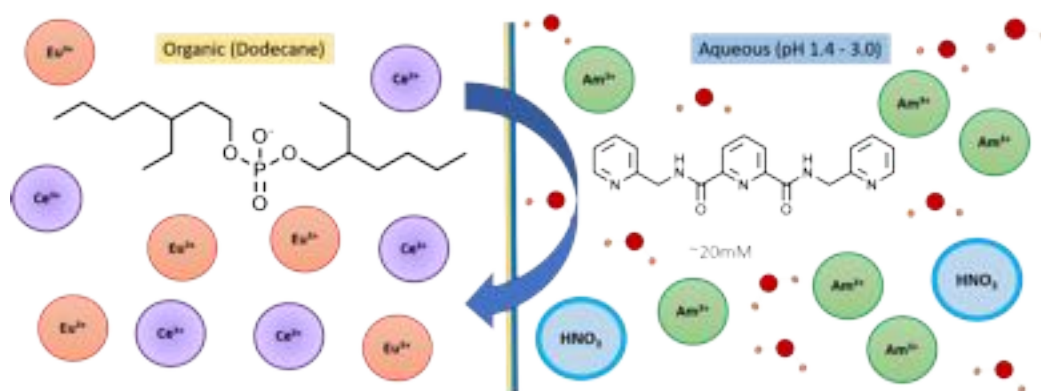
- (62) Rios, D.; Rutkowski, P. X.; Shuh, D. K.; Bray, T. H.; Gibson, J. K.; Van Stipdonk, M. J. Electron Transfer Dissociation of Dipositive Uranyl and Plutonyl Coordination Complexes. *J Mass Spectrom.* **2011**, *46*, 1247–1254.
- (63) Rios, D.; Michelini, M. C.; Lucena, A. F.; Marçalo, J.; Bray, T. H.; Gibson, J. K. Gas-Phase Uranyl, Neptunyl, and Plutonyl: Hydration and Oxidation Studied by Experiment and Theory. *Inorg Chem.* **2012**, *51*, 6603–6614.
- (64) *Bruker APEX 3*; Bruker AXS Inc.: Madison, Wisconsin, USA, **2014**.
- (65) *Bruker SAINT*; Bruker AXS Inc.: Madison, Wisconsin, USA, **2012**.
- (66) Dolomanov, O. V.; Bourhis, L. J.; Gildea, R. J.; Howard, J. A. K.; Puschmann, H. OLEX2: A Complete Structure Solution, Refinement and Analysis Program. *Journal of Applied Crystallography* **2009**, *42*, 339–341.
- (67) Qiao, B.; Sengupta, A.; Liu, Y.; McDonald, K. P.; Pink, M.; Anderson, J. R.; Raghavachari, K.; Flood, A. H. Electrostatic and Allosteric Cooperativity in Ion-Pair Binding: A Quantitative and Coupled Experiment–Theory Study with Aryl–Triazole–Ether Macrocycles. *J. Am. Chem. Soc.* **2015**, *137*, 9746–9757.
- (68) Mahoney, J. M.; Beatty, A. M.; Smith, B. D. Selective Recognition of an Alkali Halide Contact Ion-Pair. *J. Am. Chem. Soc.* **2001**, *123*, 5847–5848.
- (69) Jonah, T. M.; Mathivathanan, L.; Morozov, A. N.; Mebel, A. M.; Raptis, R. G.; Kavallieratos, K. Remarkably Selective NH_4^+ Binding and Fluorescence Sensing by Tripodal Tris(Pyrazolyl) Receptors Derived from 1,3,5-Triethylbenzene: Structural and Theoretical Insights on the Role of Ion Pairing. *New J. Chem.* **2017**, *41*, 14835–14838.

CHAPTER III

A bis(pyridine)dipicolinamide derivative as a water-soluble holdback reagent for selective Am(III)/Ln(III) separations

Ingrid Lehman-Andino^a, Christopher J. Dares^a, Tian Jian^b, John K. Gibson^b, Travis S. Grimes^{c*}, Konstantinos Kavallieratos^{a*}

^aDepartment of Chemistry and Biochemistry, Florida International University, 11200 SW 8th St, Miami, Florida 33199. ^bChemical Sciences Division, Lawrence Berkeley National Laboratory, USA. ^cAqueous Separations and Radiochemistry Group, Idaho National Laboratory, Idaho Falls, Idaho, 83415



3.1 Abstract

The TALSPEAK An/Ln process uses diethylenetriamine-*N,N,N',N'',N'''*-pentaacetic acid (DTPA) as a holdback reagent for keeping the An(III) selectively in the aqueous phase, while bis-2-ethyl(hexyl) phosphoric acid (HDEHP) acts as an organic Ln(III) complexant.¹ We introduce a water-soluble diamide of dipicolinic acid (**L**), as a holdback reagent, that can be used in conditions similar to TALSPEAK, instead of DTPA, for improved separation of ²⁴¹Am from lanthanides. Solvent extraction experiments with HDEHP dissolved in *n*-dodecane (0.35 M) and *N',N''*-bis(pyridin-2-ylmethyl)pyridine-2,6-dicarboxamide (**L**) (20 mM) dissolved in acidic aqueous media with spikes of ²⁴¹Am, ¹⁵⁴Eu, and ¹³⁹Ce demonstrated excellent separation between Eu/Am ($SF_{Eu/Am} = 74$) and Ce/Am ($SF_{Ce/Am} = 202$) at pH = 2.0. Slope analysis of logD vs. log[**L**] in various concentrations suggest a 1:3 metal/**L** complexation ratio in solution, which was also observed on the isolated and characterized complex [Nd(**L**)₃][PF₆]₃·2CH₃OH (by NMR, FT-IR and Elemental Analysis). Unlike in the solvent extraction system, and in accordance with our prior work with analogous dipicolinamides UV-Vis titrations of **L** with M(NO₃)₃·6H₂O in MeCN were consistent with 1:1 complexation. A binding constant of $K_{11} = (2.03 \pm 0.06) \times 10^4 \text{ M}^{-1}$ for La(III)/**L** complexation was obtained from non-linear regression analysis of the absorbance changes, with similar binding constants for the other lanthanides studied.

3.2 Introduction

Separation of minor actinides (Am, Cm, Np) from lanthanides is of importance for efficient transmutation after uranium and plutonium removal from used nuclear fuel.²⁻⁵ Lanthanides compete with actinides for the neutron flux on the transmutation step, and both are formed during fuel use in nuclear reactors.¹ An effective transmutation process can increase the capacity of geological repositories by reducing overall heat load and radiotoxicity. Furthermore, An/Ln separation processes can eventually lead to practical minor actinide recycling that can increase uranium utilization, and lead to potential applicability of nuclear energy as a carbon-free alternative to fossil fuels.^{3,4} Americium-241 is the primary long-lived Am isotope ($t_{1/2}=433$ years) in UNF that mainly contributes to its radiotoxicity and heat generation.⁶⁻⁹ Separating Ln(III) from An(III) is a challenging separation problem because of their similar properties. Actinide $5f$ orbitals allow for a stronger covalent component in metal-ligand interactions with soft-donor ligands, than the $4f$ orbitals in lanthanides.^{1,3,4,10,11}

The TALSPEAK process has encountered many challenges over the years; i) relatively low $SF_{Ln/An}$ because of the similarity of trivalent oxidation state between Ln and An that limits the selectivity of the DTPA holdback reagent ii) radiolytic degradation of the reagents, and iii) high SF variations associated with pH differences, that dominate the separation effectiveness.³ Most of the TALSPEAK improvement efforts have been focused on modification of the aqueous media (section 1.3.3). In 1954, Seaborg *et al.*, demonstrated the applicability of the TALKSPEAK concept by using a strong cation-exchange resin and hydrochloric acid as eluent to separate Am(III) from lanthanides.¹⁰ Ligands with soft sites

can take advantage of the slight difference in hardness between An^{3+} and Ln^{3+} either as organic complexants or as aqueous holdback or stripping agents.³ The *N*- or *S*-donor ligands have been used previously for An(III) separations.^{1,9,11-14} Dipicolinic acid and picolinate derivatives have been found to act as efficient An stripping agents at a pH 2.0-4.0 with Ln/Am separation factors between 30 to 73.^{15,16}

Our group recently studied the extraction and complexation properties of a dithiopicolinamide ligand *vs.* the analogous dipicolinamide.¹² We are now introducing an aqueous bis(pyridine) dipicolinamide *N*-donor ligand (**L**) (Figure 3.1) that selectively holds back Am-241 in the aqueous phase with Eu/Am separation factors as high as 74 and Ce/Am separation factors as high as 289, at a relatively broad pH range (1.4 - 3.1). Slope analysis of extraction data suggested a 1:3 M:L ratio and the Nd(III) complex of **L**, $[Nd(L)_3][PF_6]_3$ was isolated and characterized (by NMR, IR and elemental analysis), confirming this stoichiometry. The mixed *N*-, *O*- donor ligand presented has potential for further structural modification for improved Am(III)/Ln(III) separations.

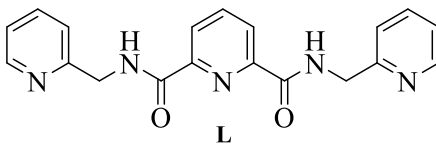


Figure 3.1. Structure of *N',N''*-bis(pyridin-2-ylmethyl)pyridine-2,6-dicarboxamide ligand (**L**).

3.3 Results and discussion

3.3.1 Solvent extraction results

Solvent extraction experiments were carried out at Idaho National Lab at with **L** in the aqueous phase and HDEHP as the organic extractant in conditions simulating TALSPEAK (Fig. 3.2). Distribution for Am(III) and Ln(III) was investigated as a function of the total concentration of **L** ($[L]_t$) in the presence of HDEHP. Figure 3.3 demonstrates the extraction capability of **L** for Am(III), Eu(III) and Ce(III) under acidic conditions at pH 2.0. The summary of the separation factors values is shown in Table 1:

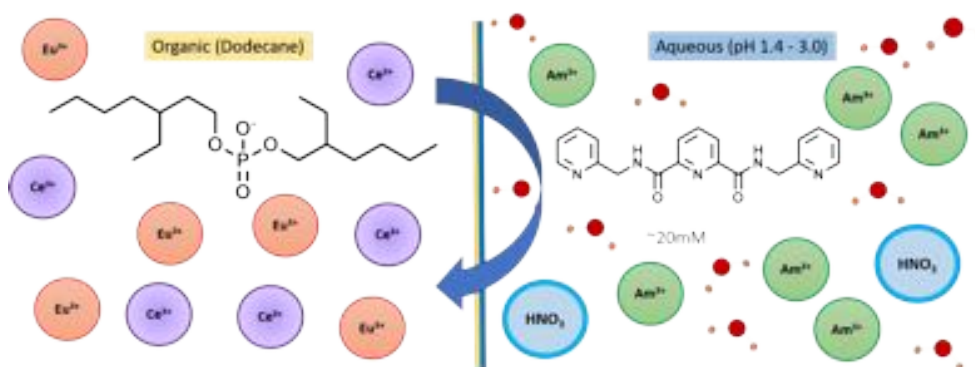


Figure 3.2. Representation of solvent extraction experiments performed at Idaho National Laboratory using **L** and HDEHP (INL).

Table 3.1. Ln/Am separation factors (SF) in dodecane/HNO₃ (pH = 2.0) at various concentrations of holdback reagent **L**. HDEHP concentration is constant at 0.35 M

$[L]_t$, M	SF _{Eu/Am}	SF _{Ce/Am}
0.010	54	40
0.015	65	158
0.020	74	202
0.025	40	230
0.030	44	289

The highest D_{Eu}/D_{Am} separation factor is observed at $[L]_t = 0.020$ M (Figure 3.3, Table 1). The slope of 3.43 is suggestive of a 3:1 L /Am(III) binding stoichiometry (Figure 3.3). The correct balance between the strong cation exchanger HDEHP (0.35 M in dodecane) and the aqueous holdback reagent L (20 mM) is needed in order to give low extraction of Am(III) into the organic phase and low partitioning of Ce(III) and Eu(III) in the aqueous phase.

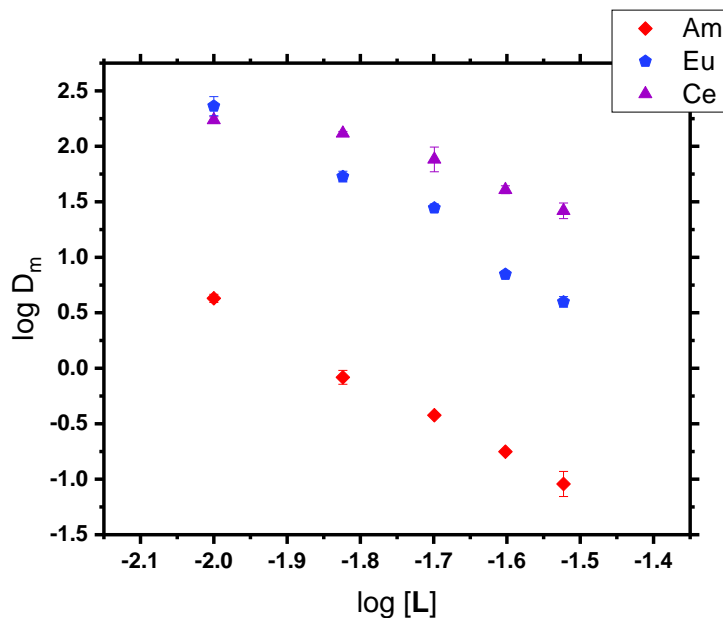


Figure 3.3. Concentration dependence of solvent extraction distribution showing a slope of 3.43 ± 0.01 . $[HDEHP]_{org} = 0.35M$. Slope $m=3.43$.

Beside understanding the capability of L at different concentrations, it is also necessary to identify the lowest pH for which our ligand has the highest efficiency for Ln(III)/Am(III) separation. The pH dependence experiment demonstrated the capability of L to holdback Am(III), selectively in the aqueous phase at low pH. As observed in Figure 3.4, at pH = 1.4, SFs for Eu/Am, using ligand L , as high as 50 for pH = 1.4 were observed (Table 2).

Most of the ligands reported in the literature work well on a pH range of 2.5-4.0.¹⁷ The importance of this experiment relies on the influence of the pH for the separation, knowing that separation at highly acidic environments is crucial for practical applicability to UNF.

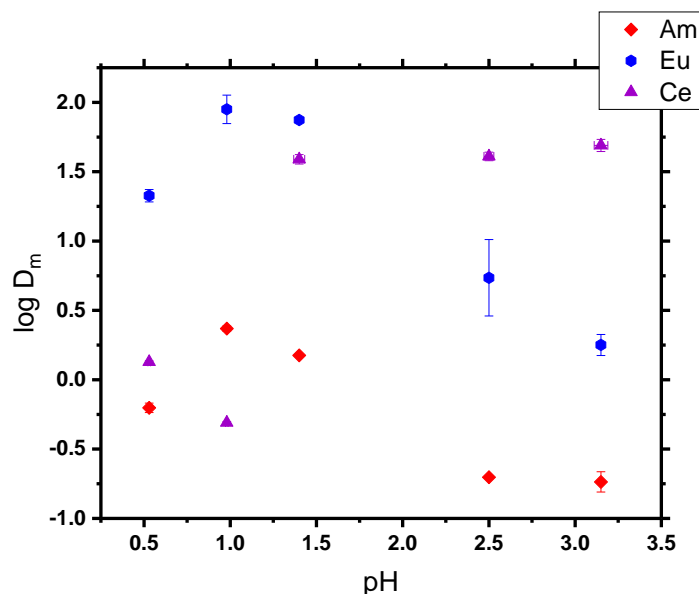


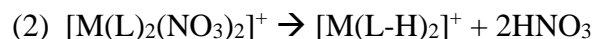
Figure 3.4. pH dependence of Ln(III)/Am(III) extraction selectivity. $[\text{HDEHP}]_{\text{org}} = 0.20$ M and $[\text{L}]_{\text{t}} = 0.0196$ M.

Table 3.2. Ln/Am separation factors (SF) in dodecane/ HNO_3 at various pH concentrations with holdback reagent L (0.019M). HDEHP concentration is constant at 0.20 M

pH	SF _{Eu/Am}	SF _{Ce/Am}
0.5	34	2
1	38	0
1.4	50	26
2.5	27	206
3.1	10	267

3.3.2 Collision Induced Dissociation Electron Spray Ionization Mass Spectroscopy (CID-ESI-MS) results

Solvent effects, including entropy, are important in actual separations. Still, the fragmentation of gas-phase coordination complexes can offer fundamental understandings into metal-ligand binding in the absence of such effects. The CID-ESI-MS of ligand **L** with Am(III) and Eu(III) show higher relative stability of the Am(III) *vs.* Eu(III) complex. The observed primary dissociation processes apparent in Figure 3.5 are given by reaction (1) (for (a) and (b)), and reaction (2) (for (c) and (d)).



Assignment in (2) of two singly deprotonated (**L-H**), rather than a doubly-deprotonated (**L-2H**) and an intact (**L**), is assumed from the absence of (**L-2H**) for the single **L** species. The relative abundances in Figure 3.4 reveal that both reactions (1) and (2) are more facile for $M = \text{Am}$ *vs.* $M = \text{Eu}$. Assuming the barriers for proton transfer from **L** to NO_3 are small, and/or similar for $M = \text{Am}$ and $M = \text{Eu}$, then we can conclude that the more facile process is less endothermic; in fact, reactions (1) and (2) are both lower energy processes for $M = \text{Am}$ *vs.* $M = \text{Eu}$. Thus, the net increase in energy of the formed *vs.* broken bonding interactions is lower for $M = \text{Am}$ *vs.* $M = \text{Eu}$. In other words, in (1) a $M\text{-(L-H)}$ bonding interaction is created, while a $M\text{-(L)}$ and a $M\text{-(NO}_3\text{)}$ interaction is destroyed. The formed $\text{H-(NO}_3\text{)}$ interactions are constant and thus neglected in comparing metal-ligand binding. Similarly, in (2) two $M\text{-(L-H)}$ bonds are formed, while two $M\text{-(L)}$ and two $M\text{-(NO}_3\text{)}$ bonds are broken.

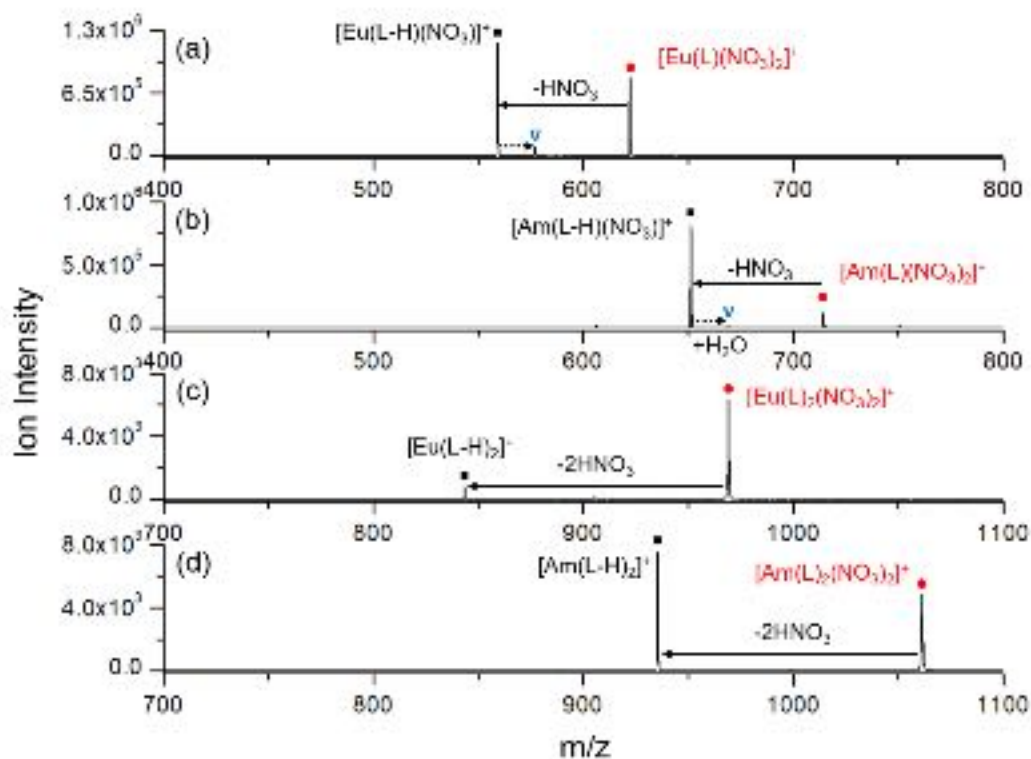


Figure 3.5. CID mass spectra of (a) $[\text{Eu}(\text{L})(\text{NO}_3)_2]^+$ and (b) $[\text{Am}(\text{L})(\text{NO}_3)_2]^+$ at 0.4 V; (c) $[\text{Eu}(\text{L})_2(\text{NO}_3)_2]^+$ and (d) $[\text{Am}(\text{L})_2(\text{NO}_3)_2]^+$ at 0.2 V. The parent species are indicated by solid circles, the CID elimination processes by solid lines, and the CID products by solid squares. Also marked with open triangles in (a) and (b) are small peaks resulting from H_2O addition to the CID products, indicated by dotted lines.

The overall significance of the results does not point to preferential binding of Am(III) versus Eu(III) with **L**, but shows instead a difference in the chemistry of Am(III) and Eu(III) complexes with (**L**), (**L-H**) and (NO_3^-). Finally, reaction (3) is evidently spontaneous and exothermic for both $M = \text{Am}$ and $M = \text{Eu}$, with the present results providing no apparent differentiation between these M(III) complexes.



Both the indicated hydroxide and hydrate product structures are reasonable.

To understand the chemistry behavior of **L** a comparison was necessary with the parent dipicolinamide ligand **1** (Chapter 2). In both cases the protonated ligands are abundant in the ESI mass spectra. Figure 3.6 displays the CID results for protonated ligands. In Figure 3.6a, the CID of $[1+H]^+$ shows four dissociation channels, which are tentatively assigned as below. The most intense one is the loss of 18 Da, which corresponds to the elimination of water. The loss of 93 and 121 Da can be attributed to the elimination of aniline and formanilide, respectively. The last channel shows the loss of 147 Da, which may arise from the elimination of N-Phenylacrylamide. In Figure 3.6b, three main CID channels are observed with the corresponding loss of 18, 36 and 126 Da. The first two channels are assigned to the elimination of one and two water molecules. The third channel represents the loss of water and 2-picolylamine.

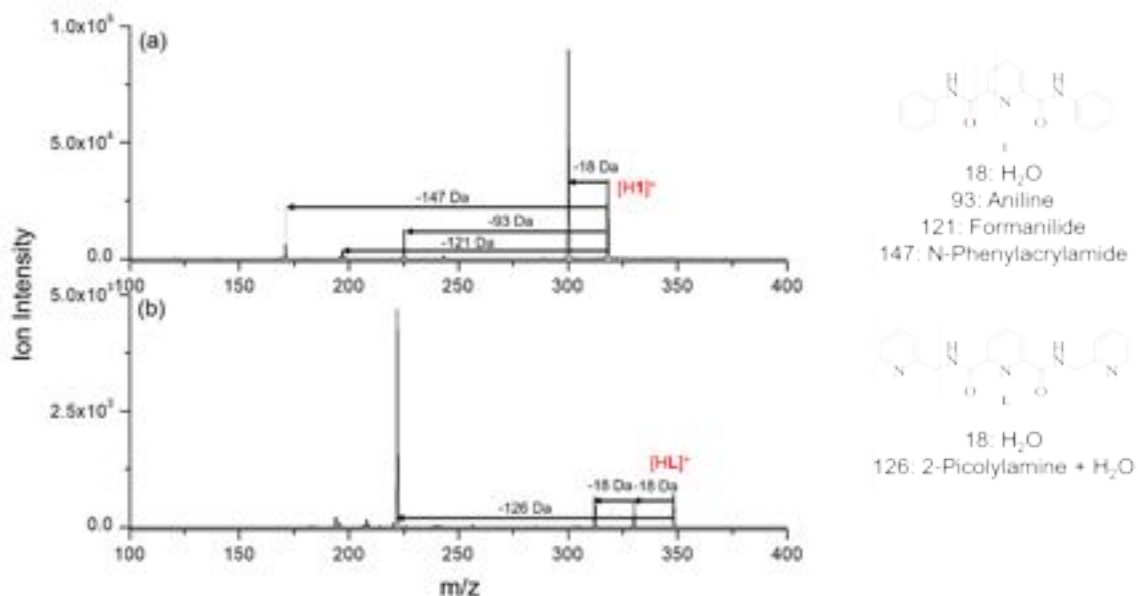
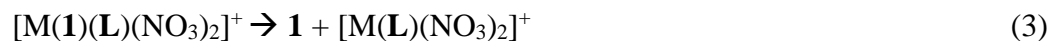
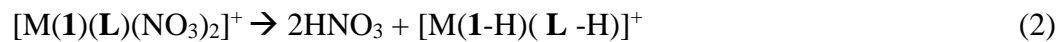
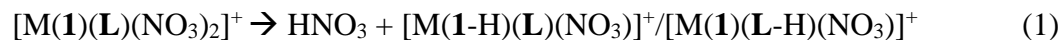


Figure 3.6. CID mass spectra of the isolated (a) $[1+H]^+$ and (b) $[L+H]^+$ at voltage of 0.60 V.

The Figure 3.7 displays the CID results of $[M(\mathbf{1})(\mathbf{L})(\text{NO}_3)_2]^+$ ($M = \text{Eu}, \text{Am}$) complexes, which can be summarized in reactions (1) - (3). The major dissociation channels result from the sequential elimination of HNO_3 via reactions (1) and (2). A minor but important dissociation channel is the elimination of neutral $\mathbf{1}$ to generate $[M(\mathbf{L})(\text{NO}_3)_2]^+$ via reaction (3). Meanwhile, no such \mathbf{L} elimination was observed at the same experimental condition. The more facile elimination of $\mathbf{1}$ over \mathbf{L} suggests the binding strength of metal- \mathbf{L} is stronger than that of metal- $\mathbf{1}$. The $[M(\mathbf{L})(\text{NO}_3)_2]^+$ complex can further eliminate HNO_3 to generate $[M(\mathbf{L}-\text{H})(\text{NO}_3)]^+$.



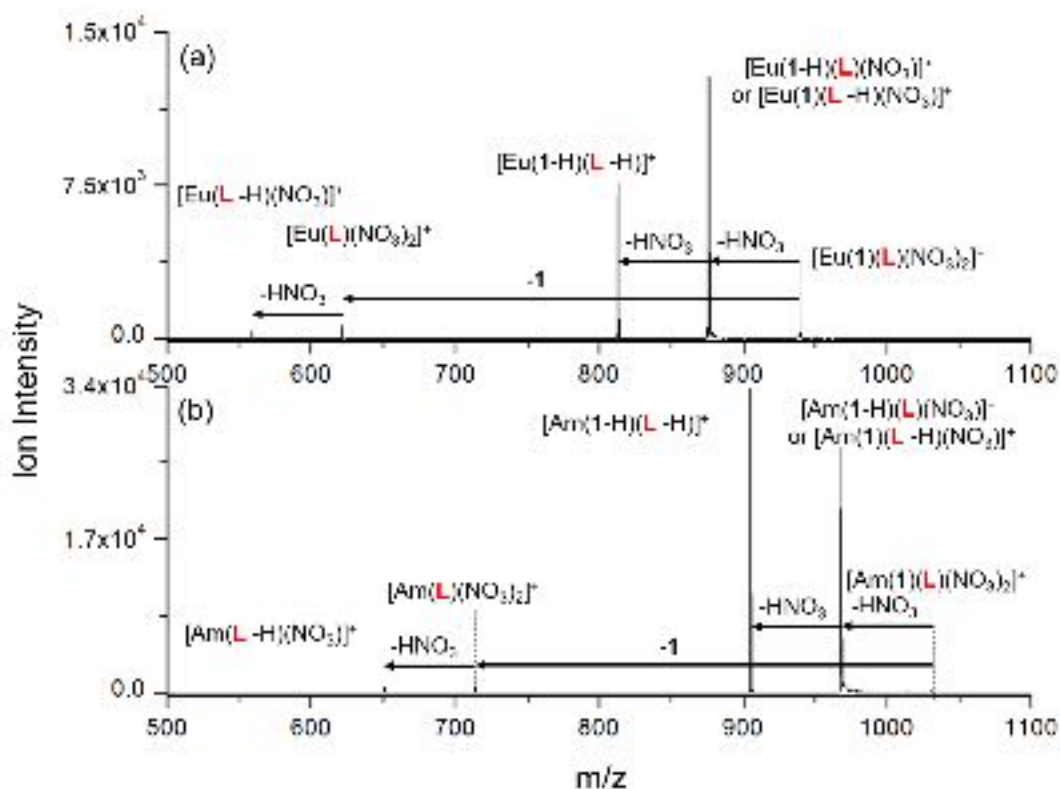


Figure 3.7. CID mass spectra of the isolated (a) $[\text{Eu}(\mathbf{1})(\text{L})(\text{NO}_3)_2]^+$ and (b) $[\text{Am}(\mathbf{1})(\text{L})(\text{NO}_3)_2]^+$ at voltage of 0.40 V.

3.3.3 Spectrophotometric data - UV-Visible titrations:

Ligand **L** was titrated with various lanthanide salts (La^{3+} , Gd^{3+} , Ce^{3+} , and Eu^{3+}) in acetonitrile and demonstrated significant changes in the UV-visible spectra with the formation of new bands. Plotting of $A_{276 \text{ nm}}$ vs. $[\text{Ln}(\text{III})]_t$ and fitting to the 1:1 binding isotherm using non-linear regression analysis gave a binding constant a $K_{11} = 2.03 \pm 0.06 \times 10^4 \text{ M}^{-1}$ for the $\text{La}(\text{NO}_3)_3$ titration, (Figure 3.8). Other lanthanide salts that were studied gave similar results (Figure 3.9) with Gd^{3+} , Ce^{3+} and Eu^{3+} nitrate salt titrations giving binding constants of $K_{11} = 8.16 \pm 0.04 \times 10^4 \text{ M}^{-1}$, $K_{11} = 1.22 \pm 0.06 \times 10^4 \text{ M}^{-1}$, and $K_{11} = 1.36 \pm 0.06 \times 10^4 \text{ M}^{-1}$ respectively. As CH_3CN is a highly-coordinating solvent, it is

understandable why a 1-1 Ln-L complexation would be favorable under the extraction conditions. Such results would be in agreement with our prior studies with the parent dipicolinamide.¹²

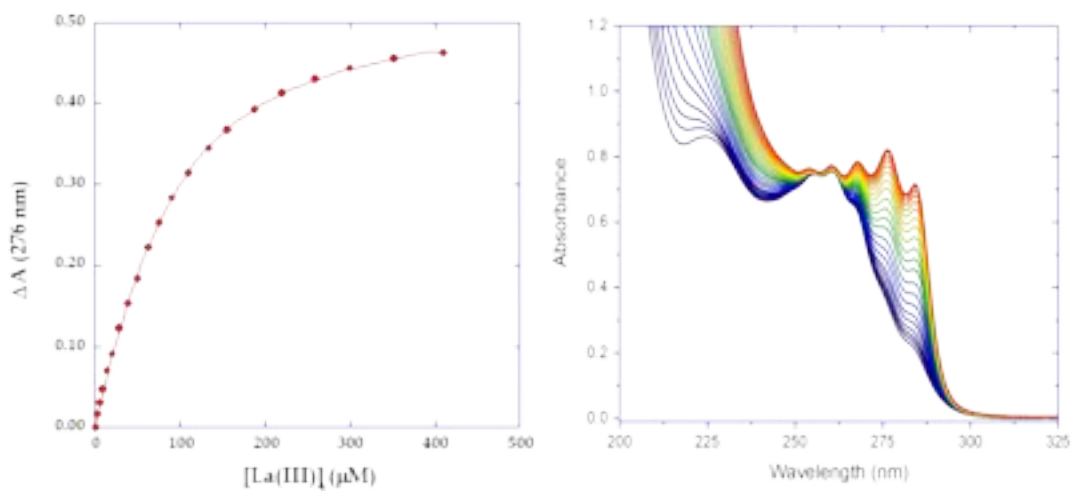


Figure 3.8. UV-visible titration of **L** (6.3×10^{-5} M) with $La(NO_3)_3 \cdot 6H_2O$ (1.3×10^{-3} M) in CH_3CN

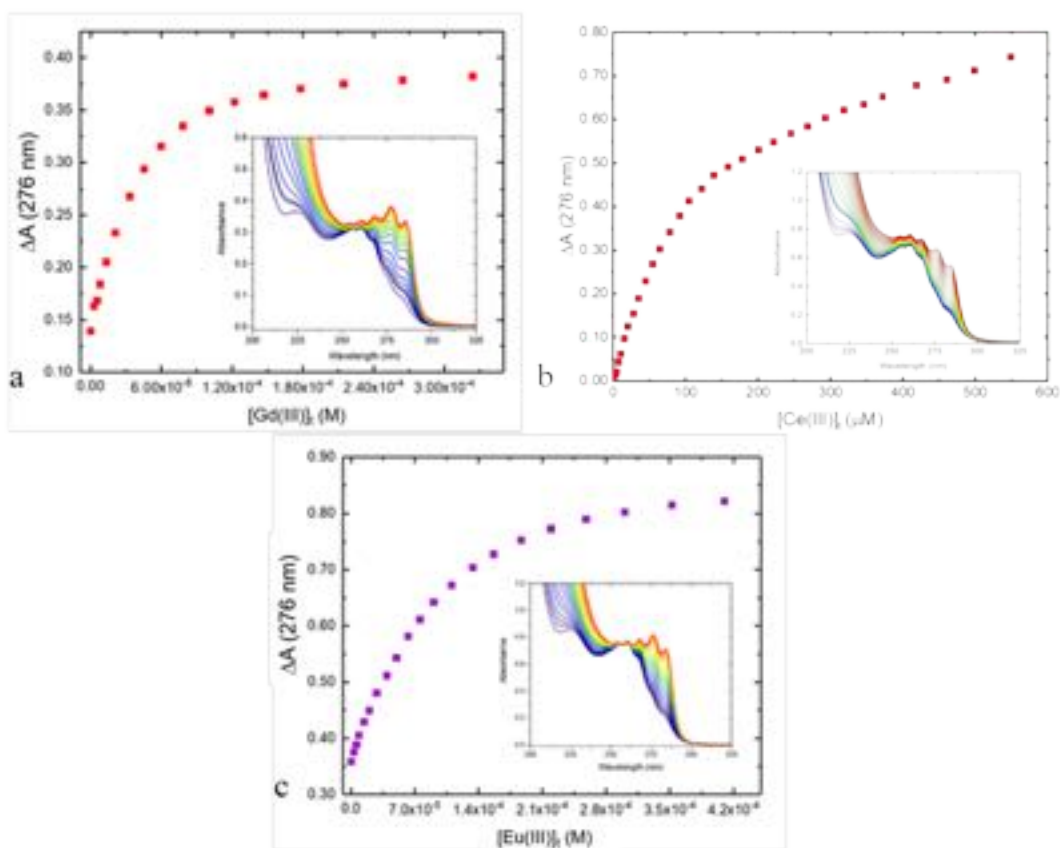


Figure 3.9. UV-visible titration results of **L** with Gd^{3+} , Ce^{3+} and Eu^{3+} nitrate salts in CH_3CN . a) $[\text{L}]_t = 7.2 \times 10^{-5} \text{ M}$ with $\text{Gd}(\text{NO}_3)_3 \cdot 6\text{H}_2\text{O}$ ($1.2 \times 10^{-3} \text{ M}$) b) $[\text{L}]_t = 6.0 \times 10^{-5} \text{ M}$ with $\text{Ce}(\text{NO}_3)_3 \cdot 6\text{H}_2\text{O}$ ($1.5 \times 10^{-3} \text{ M}$) c) $[\text{L}]_t = 7.4 \times 10^{-5} \text{ M}$ with $\text{Eu}(\text{NO}_3)_3 \cdot 6\text{H}_2\text{O}$ ($9.5 \times 10^{-4} \text{ M}$)

3.3.4 Potentiometric Titrations:

A potentiometric titration of **L** was performed in order to provide insight about the binding mode of **L** with Am and Ln. There are three acid dissociation equilibria on **L** to be considered. The two wingtip pyridine nitrogens of **L** are expected to protonate at higher pH, while the pyridine of central ring at lower pH. The distribution of protonated species throughout the titration experiment is shown in Figure 3.10. This potentiometric titration is consistent with the hypothesis that the central pyridine nitrogen can bind Americium

(Am) even at pH as low as 1.4. The terminal pyridines should be protonated at this pH, allowing ligand **L** to bind on a 3:1 stoichiometry in the same O,N,O configuration as shown previously for parent dipicolinamides.¹²

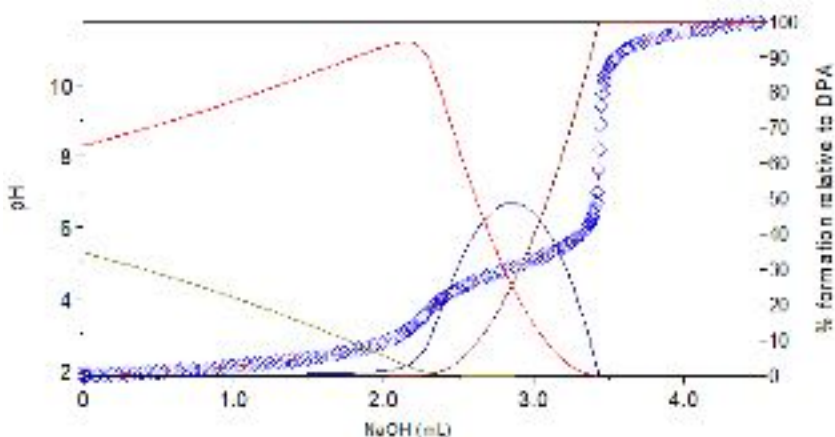
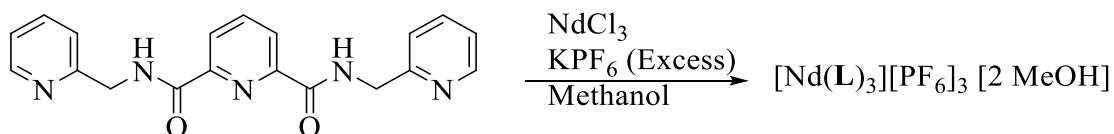


Figure 3.10. Experimental titration curve for acid dissociation equilibrium for **L**. ($pK_a = 5.15, 4.59$ and 1.55)

3.3.5 Counteranion effects: Isolation and characterization of $[\text{Nd}(\text{III})\text{L}_3](\text{PF}_6)_3$ complex

The solvent and counteranion-dependent coordination effects can affect speciation under UNF extraction conditions.^{18–20} Previous work with dipicolinamides¹² demonstrated that different crystallization attempts with various counteranions such as PF_6^- , Cl^- and NO_3^- , were unsuccessful, however using I^- as counteranion a 1:3 Metal/Ligand complex was obtained. Due to solubility problems with ligand (**L**) in organic solvents, water is needed to be used for crystallization attempts. We were successfully isolating the $[\text{Nd}(\text{L})_3][\text{PF}_6]_3$ complex by using PF_6^- as counter anion, however crystals suitable for X-ray characterization could not be obtained. Nevertheless, the $[\text{Nd}(\text{L})_3][\text{PF}_6]_3$ complex was

isolated and characterized by reaction of **L** with NdCl_3 in $\text{CH}_3\text{OH}/\text{water}$ with excess of KPF_6 (Scheme 3.1). Figure 3.11 shows the $^1\text{H-NMR}$ data for **L** vs. $[\text{Nd}(\text{L})_3][\text{PF}_6]_3$. (Scheme 3.1). Elemental analysis was found consistent with this formulation, with two molecules of residual CH_3OH added.



Scheme 3.1. Reaction for formation of $[\text{Nd}(\text{L})_3][\text{PF}_6]_3$ from **L** (1mM) with NdCl_3 (0.3 mM) adding KPF_6 (excess) in $\text{CH}_3\text{OH}/\text{water}$.²¹

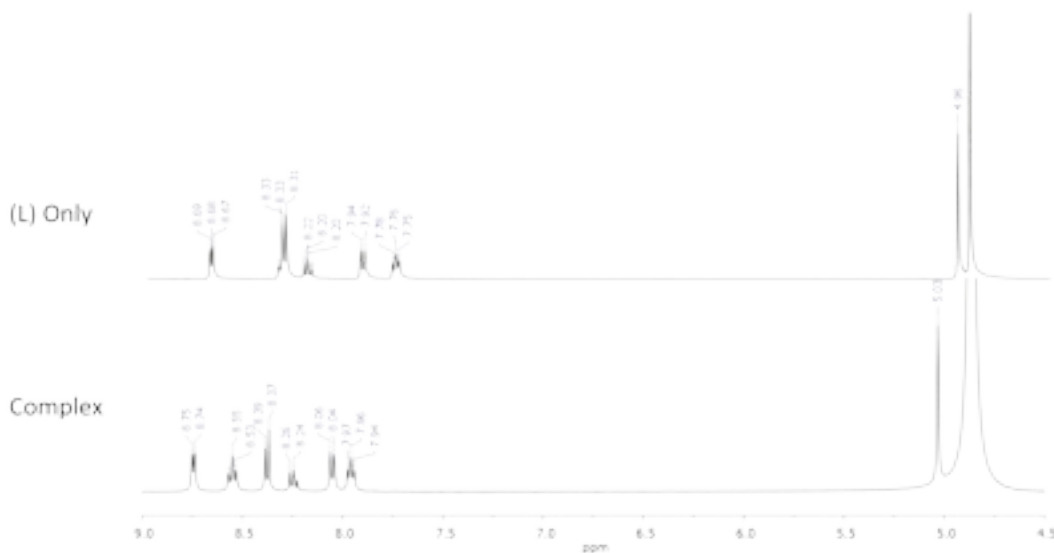


Figure 3.11. $^1\text{H-NMR}$ spectra of **L** (top) and isolated product of complexation reaction with NdCl_3 and KPF_6 shown on Scheme 3.1.

The spectra shown in Figure 3.11 demonstrate the complex formation from the reaction (Scheme 3.1) which give $[\text{Nd}(\text{L})_3][\text{PF}_6]_3$ consistently with prior work for the analogous dipicolinamide ligand¹² and in accordance with the slope analysis of our solvent extraction data. The $^1\text{H-NMR}$ shifts correspond to a 3:1 symmetric complex with PF_6^- as counteranion. The infrared spectra show the presence of the Nd-O=C vibrational bands

around the fingerprint area between 750-825 cm^{-1} for $[\text{Nd}(\mathbf{L})_3][\text{PF}_6]_3$, which also agreed with the previously reported dipicolinamide complex¹². The presence of the 3306 cm^{-1} on both spectra demonstrated no deprotonation for binding of Nd, while the C=O stretches of dipicolinamide shift from 1676 cm^{-1} (in \mathbf{L}) to 1661 cm^{-1} (in $[\text{Nd}(\mathbf{L})_3][\text{PF}_6]_3$).

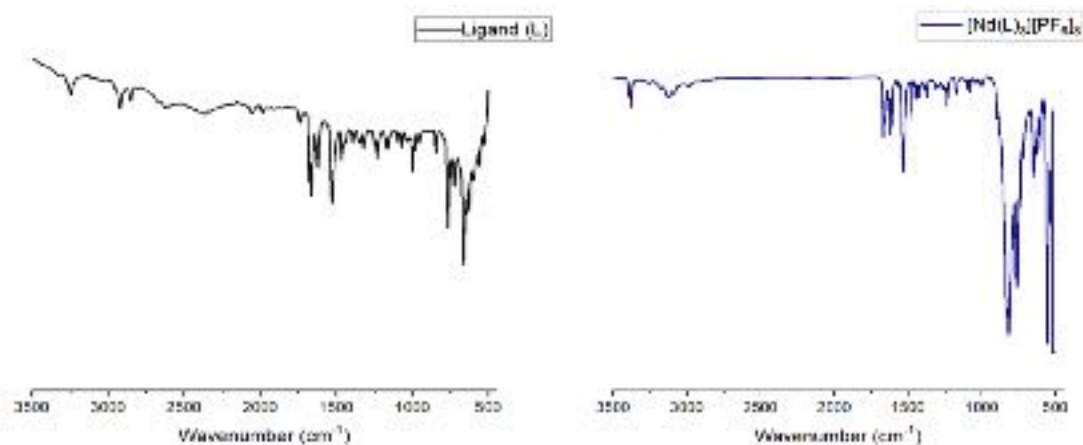


Figure 3.12. Infrared spectra of ligand (\mathbf{L}) comparison with $[\text{Nd}(\mathbf{L})_3][\text{PF}_6]_3$ complex.

3.4 Experimental Section:

3.4.1 Materials and Methods

All chemicals and solvents were purchased from Aldrich Chemical Company or ACROS Organics, were standard reagent grade and were used without further purification unless otherwise noted. The 2,6-pyridinedicarbonyl dichloride was purchased from ACROS Organics (CAS: 3739-94-4). The N',N' -bis(pyridin-2-ylmethyl)pyridine-2,6-dicarboxamide (\mathbf{L})²² was prepared from 2,6-pyridinedicarbonyl dichloride and 2-picolilamine by a modification of previously published procedures and was found to be spectroscopically identical to the reported compound.²² The NMR spectra were recorded

on a 400 MHz Bruker NMR spectrometer and referenced to the residual solvent resonances. All chemical shifts, δ , are reported in ppm. Fluorescence spectra recorded on a Cary Eclipse fluorescence spectrophotometer and UV-Vis spectra were recorded on a Cary 100 UV-Visible spectrophotometer. For extraction experiments, the HDEHP (97%) used was purchased from Aldrich. The n-dodecane was obtained from Alfa-Aesar (99% pure), and both were used as received. The organic-phase samples were prepared by dissolving weighed amounts of the HDEHP (97%). The aqueous phases were prepared using Actinide and lanthanides stock solutions. All solvent extraction experiments were completed using the same procedure and equal volume of each phase. Nitric acid solutions were prepared from Trace Metal grade HNO₃ (Fisher Scientific) using deionized water.

3.4.2 Synthesis

N',N''-bis(pyridin-2-ylmethyl)pyridine-2,6-dicarboxamide²² (L):

Ligand (L) N',N''-bis(pyridin-2-ylmethyl)pyridine-2,6-dicarboxamide²² was synthesized by an improvement of previously published method. The 2,6-pyridinedicarbonyl dichloride was dissolved in a mixture 20:1 Chloroform:DMF at room temperature under nitrogen. Afterwards, the 2-picolyamine was added dropwise. (70% yield). The product was found spectroscopically identical to the one reported previously.²² ¹H NMR (600 MHz, D₂O) δ 8.71 (d, J = 5.3 Hz, 1H), 8.55 (td, J = 8.1, 1.4 Hz, 1H), 8.35 – 8.28 (m, 1H), 8.25 (dd, J = 8.6, 7.0 Hz, 1H), 8.05 (d, J = 8.2 Hz, 1H), 7.97 (t, J = 6.8 Hz, 1H), 5.06 (s, 2H). ¹³C NMR (101 MHz, CD₃OD) δ 166.44 (s), 156.71 (s), 149.62 (s), 145.05 (s), 144.94 (s), 140.78 (s), 126.31 (s), 126.05 (s), 125.97 (s), 43.17 (s). Selected IR bands (cm⁻¹): 3306m (vNH), 1676s (vCO).

[Nd(L)₃][PF₆]₃

A solution of NdCl₃·6H₂O (0.33 mmol) and **L** (0.21 g, 1 mmol) in methanol was stirred for 30 min. A solution of excess KPF₆ in distilled water was then added, resulting in a white precipitate.²¹ After overnight cooling to allow complete precipitation, the solid was filtered off and dried *in vacuo* to give [Nd(L)₃][PF₆]₃ in 85% yield. ¹H NMR (400 MHz, CD₃OD) δ 8.74 (d, J = 5.6 Hz, 1H), 8.55 (t, J = 7.4 Hz, 1H), 8.38 (d, J = 7.8 Hz, 1H), 8.25 (d, J = 7.4 Hz, 1H), 8.05 (d, J = 8.2 Hz, 1H), 7.96 (t, J = 6.5 Hz, 1H), 5.03 (s, 2H). ¹³C NMR (101 MHz, CD₃OD) δ 185.72 (s), 166.80 (s), 155.60 (s), 149.58 (s), 147.84 (s), 142.83 (s), 141.04 (s), 126.94 (s), 126.88 (m), 126.65 (s), 42.24 (s). ¹⁹F NMR (376 MHz, CD₃OD) δ -74.52 (d, J = 707.9 Hz). ³¹P NMR (162 MHz, CD₃OD) δ -130.97 – -159.38 (m). FT-IR (Selected bands, cm⁻¹): 3306m (ν_{NH}), 1661s (ν_{CO}). Anal. Calcd. For C₅₇H₅₁N₁₅NdO₆[PF₆]₃·2CH₃OH: C, 42.23; H, 3.17; N, 12.96. Found: C, 42.05; H, 3.53; N, 12.47.

3.4.1 Solvent extraction:

3.4.1.1 Concentration-dependent extraction procedure:

For all triplicated samples, HDEHP was dissolved in the organic phase (*n*-dodecane) to a concentration of 0.35M, and the solution was contacted with an aqueous phase containing only HNO₃ (pH = 2.0) for pre-equilibration by vigorous shaking for 10 minutes. The aqueous phases containing ligand **L** of various concentrations (0.010M, 0.015 M, 0.020 M, 0.025 M, 0.030 M) were also pre-equilibrated for 10 min. by contact with *n*-dodecane. Equal volumes of the pre-equilibrated phases were contacted, and a 10.0 μL spike of a concentrated solution radiotracers ²⁴¹Am (~ 15mM= 1.41 x10³ Bq.), ¹⁵²Eu, and ¹³⁹Ce was added to the aqueous solutions. After vigorous shaking of 30 minutes, the

extraction vials were centrifuge for five minutes. Each of the phases was separated, and a 300 μL sample of each phase was taken for radiometric counting to determine metal ion concentration. The γ -counting was performed using a DSPEC gamma spectrometer with a HPGe detector.

3.4.1.2 pH dependent extraction procedure:

The pH dependence extraction experiments were performed with pre-determined ratios of HDEHP and **L**. For all triplicated samples HDEHP was dissolved in the organic phase (*n*-dodecane) to a concentration of 0.20 M, and the different solutions were contacted with an aqueous phase containing only HNO_3 (pH 0.5, 1.0, 1.4, 2.5, 3.1) for pre-equilibration by vigorous shaking for 10 minutes. The aqueous phases containing ligand **L** of 0.0196 M were also pre-equilibrated for 10 minutes by contact with *n*-dodecane. Equal volumes of the pre-equilibrated phases were contacted, and a 10.0 μL spike of a concentrated solution radiotracers ^{241}Am ($\sim 15\text{mM} = 1.41 \times 10^3 \text{ Bq.}$), ^{152}Eu , and ^{139}Ce was added to the aqueous solutions. After vigorous shaking of 30 minutes, the extraction vials were centrifuge for 5 minutes. Each of the phases was separated, and a 300 μL sample of each phase was taken for radiometric counting to determine metal ion concentration. The γ -counting was performed using a DSPEC gamma spectrometer with an HPGe detector.

3.4.2 Gas-Phase via Collision Induced Dissociation (CID)

The experiments were carried out using an Agilent 6340 quadruple ion trap mass spectrometer (QIT/MS) with MS^n collision induced dissociation (CID) capabilities. The electrospray ionization source inside a radiological contaminant glovebox, details of which

has been described elsewhere.²⁵ Cation complexes $[M(\mathbf{1})(\mathbf{L})(\text{NO}_3)_2]^+$ (M=Eu, Am) were produced by electrospray ionization (ESI) of tetrahydrofuran (THF) solution containing 100 μM $M(\text{NO}_3)_3$ (M=Eu, Am), 1 mM of **1** and 1 mM **L**. The cation complex of interest was isolated in the QIT and subjected CID, during which an ion undergo multiple energetic collisions with helium to eventually induce dissociation. The CID energy under these conditions is not quantified but increases with the CID voltage. Collision Induced Dissociation of two ions with similar mass (m/z) under the same instrumental conditions result in comparable excitation such that a higher CID yield indicates a more efficient reaction. For a simple ligand-elimination process that can be considered to be essentially barrierless. As a result, a higher efficiency indicates a lower energy process, which indicates lower endothermicity and lower ligand binding energy. The mass spectra were acquired using the following instrumental parameters in the positive ion mode: solution flow rate, 60 $\mu\text{L}/\text{min}$; nebulizer gas pressure, 15 psi; capillary voltage, -3500 V; end plate voltage offset, -500 V; dry gas flow rate, 2 L/min; dry gas temperature, 325 $^\circ\text{C}$; capillary exit, 137.7 V; skimmer, 40.0 V; octopole 1 and 2 dc, 12.00 and 0.00 V; octopole RF amplitude, 229.2 Vpp; lens 1 and 2, -5.0 and -82.0 V; trap drive, 66.8. High-purity nitrogen gas for nebulization and drying in the ion transfer capillary was the boil off from a liquid nitrogen Dewar. The helium buffer gas pressure in the QIT was constant at $\sim 10^{-4}$ Torr.

3.4.3 UV-visible titrations:

The UV-Vis titrations were performed in solutions at a constant concentration of ligand (**L**) with different lanthanides such as $\text{La}(\text{NO}_3)_3 \cdot 6\text{H}_2\text{O}$, $\text{Gd}(\text{NO}_3)_3 \cdot 6\text{H}_2\text{O}$,

Ce(NO₃)₃·6H₂O and Eu(NO₃)₃·6H₂O. In a typical experiment, solution A of **L** (6.3 x 10⁻⁵ M) in CH₃CN was titrated with solution B containing Ln(NO₃)₃·6H₂O (1.3 x 10⁻³ M). Solution B was prepared by dilution with solution A, thus keeping a constant concentration of ligand upon titration of solution A with solution B. 2.3 mL of solution A were added to the UV-visible cuvette and solution B was added in increments to a total of 1,000 μL. The absorbance changes were monitored, with the results plotted and fitted to the 1:1 binding isotherm using non-linear regression analysis:

$$\Delta A = A_{\text{obs}} - A_{\text{init.}} = ([\mathbf{L}]_t + [\mathbf{X}^-]_t + K_a^{-1} - ((([\mathbf{L}]_t + [\mathbf{X}^-]_t + K_a^{-1})^2 - 4[\mathbf{X}^-]_t [\mathbf{L}]_t)^{1/2})) \Delta\delta_{\text{max.}} / (2[\mathbf{L}]_t)^{23}$$

3.4.4 Potentiometric titrations:

All measurements were performed using a glass electrode filled with 5.0 M NaCl for stabilization of junction potential. All titrations were performed at room temperature 25.0 ± 0.1 °C and under fixed ionic strength media to monitor changes in free [H⁺] for aqueous solutions of **L**. The fitting software Hyperquad2013²⁴ was used in order to determine the acid dissociation equilibria.

3.5 Conclusion:

The bis(pyridine) dipicolinamide ligand (**L**) demonstrated strong and selective holdback of ²⁴¹Am vs. Eu(III) and Ce(III), even at very low pHs of 0.5-2.0, with Eu/Am separation factors between 27 and 74 at TALSPEAK-like conditions, and a 3:1 ligand to metal binding stoichiometry, as indicated both by extraction slope analysis and by the isolation and characterization of [M(**L**)₃][PF₆]₃. Potentiometric titrations experiments explain the good performance of **L** at low pHs with three acid dissociation equilibria

involved. UV-visible spectroscopic data gave 1:1 complexation in acetonitrile solutions. The difference in stoichiometry depending on solvent and counteranion-dependent coordination effects is consistent with our prior work (Chapter 2). The gas-phase CID ESI-MS results demonstrate a difference in the chemistry of Am(III) vs. Eu(III) with (**L**), (**L**-H) and (NO₃). Furthermore, CID-ESI-MS result with mixed ligand complexes of type [M(**1**)(**L**)(NO₃)₂]⁺ (M = Eu, Am) reveal stronger binding for **L** than the non-pyridine simpler dipicolinamide **1**. Theoretical calculations and X-ray structural studies are needed to elucidate the underpinnings of the observed differences.

3.6 References:

- (1) Heathman, C. R.; Grimes, T. S.; Zalupski, P. R. Coordination Chemistry and f-Element Complexation by Diethylenetriamine-*N,N'*-Bis(Acetylglycine)-*N,N',N''*-Triacetic Acid. *Inorg. Chem.* **2016**, *55*, 11600–11611.
- (2) Lumetta, G. J.; Gelis, A. V.; Carter, J. C.; Niver, C. M.; Smoot, M. R. The Actinide-Lanthanide Separation Concept. *Solvent Extraction and Ion Exchange.* **2014**, *32*, 333–347.
- (3) Nash, K. L. The Chemistry of TALSPEAK: A Review of the Science. *Solvent Extraction and Ion Exchange.* **2015**, *33*, 1–55.
- (4) Braley, J. C.; Grimes, T. S.; Nash, K. L. Alternatives to HDEHP and DTPA for Simplified TALSPEAK Separations. *Ind. Eng. Chem. Res.* **2012**, *51*, 629–638.
- (5) Geist, A.; Hill, C.; Modolo, G.; Foreman, M. R. S. J.; Weigl, M.; Gompper, K.; Hudson, M. J. 6,6'-Bis(5,5,8,8-tetramethyl-5,6,7,8-tetrahydro-benzo[1,2,4]Triazin-3-yl) [2,2']Bipyridine, an Effective Extracting Agent for the Separation of Americium(III) and Curium(III) from the Lanthanides. *Solvent Extraction and Ion Exchange.* **2006**, *24*, 463–483.
- (6) Geist, A.; Müllich, U.; Magnusson, D.; Kaden, P.; Modolo, G.; Wilden, A.; Zevaco, T. Actinide(III)/Lanthanide(III) Separation Via Selective Aqueous Complexation of Actinides(III) Using a Hydrophilic 2,6-Bis(1,2,4-Triazin-3-Yl)-Pyridine in Nitric Acid. *Solvent Extraction and Ion Exchange.* **2012**, *30*, 433–444.

- (7) Demir, S.; Brune, N. K.; Van Humbeck, J. F.; Mason, J. A.; Plakhova, T. V.; Wang, S.; Tian, G.; Minasian, S. G.; Tyliszczak, T.; Yaita, T.; Kobayashi, T.; Kalmykov, S. N.; Shiwaku, H.; Shuh, D. K.; Long, J. R. Extraction of Lanthanide and Actinide Ions from Aqueous Mixtures Using a Carboxylic Acid-Functionalized Porous Aromatic Framework. *ACS Cent Sci.* **2016**, *2*, 253–265.
- (8) Zalupski, P. R.; Nash, K. L.; Martin, L. R. Thermodynamic Features of the Complexation of Neodymium(III) and Americium(III) by Lactate in Trifluoromethanesulfonate Media. *J Solution Chem.* **2010**, *39*, 1213–1229.
- (9) Macerata, E.; Mossini, E.; Scaravaggi, S.; Mariani, M.; Mele, A.; Panzeri, W.; Boubals, N.; Berthon, L.; Charbonnel, M.-C.; Sansone, F.; Arduini, A.; Casnati, A. Hydrophilic Clicked 2,6-Bis-Triazolyl-Pyridines Endowed with High Actinide Selectivity and Radiochemical Stability: Toward a Closed Nuclear Fuel Cycle. *J. Am. Chem. Soc.* **2016**, *138*, 7232–7235.
- (10) Diamond, R. M.; Street, K.; Seaborg, G. T. An Ion-Exchange Study of Possible Hybridized 5f Bonding in the Actinides I. *J. Am. Chem. Soc.* **1954**, *76*, 1461–1469.
- (11) Grimes, T. S.; Heathman, C. R.; Jansone-Popova, S.; Ivanov, A. S.; Roy, S.; Bryantsev, V. S.; Zalupski, P. R. Influence of a Heterocyclic Nitrogen-Donor Group on the Coordination of Trivalent Actinides and Lanthanides by Aminopolycarboxylate Complexants. *Inorg. Chem.* **2018**, *57*, 1373–1385.
- (12) Lehman-Andino, I.; Su, J.; Papathanasiou, K. E.; Eaton, T. M.; Jian, J.; Dan, D.; Albrecht-Schmitt, T. E.; Dares, C. J.; Batista, E. R.; Yang, P.; Gibson, J. K.; Kavallieratos, K. Soft-Donor Dipicolinamide Derivatives for Selective Actinide(III)/Lanthanide(III) Separation: The Role of S- vs. O-Donor Sites. *Chem. Commun.* **2019**, *55*, 2441–2444.
- (13) Hudson, M. J.; Harwood, L. M.; Laventine, D. M.; Lewis, F. W. Use of Soft Heterocyclic N-Donor Ligands To Separate Actinides and Lanthanides. *Inorganic Chemistry.* **2013**, *52*, 3414–3428.
- (14) Galletta, M.; Scaravaggi, S.; Macerata, E.; Famulari, A.; Mele, A.; Panzeri, W.; Sansone, F.; Casnati, A.; Mariani, M. 2,9-Dicarbonyl-1,10-Phenanthroline Derivatives with an Unprecedented Am(III)/Eu(III) Selectivity under Highly Acidic Conditions. *Dalton Trans.* **2013**, *42*, 16930–16938.
- (15) Heathman, C. R.; Grimes, T. S.; Jansone-Popova, S.; Roy, S.; Bryantsev, V. S.; Zalupski, P. R. Influence of a Pre-Organized N-Donor Group on the Coordination

of Trivalent Actinides and Lanthanides by an Aminopolycarboxylate Complexant. *Chemistry – A European Journal*. **2019**, *25*, 2545–2555.

- (16) Heathman, C. R.; Nash, K. L. Characterization of Europium and Americium Dipicolinate Complexes. *Separation Science and Technology*. **2012**, *47*, 2029–2037.
- (17) Grimes, T. S.; Jensen, M. P.; Debeer-Schmidt, L.; Littrell, K.; Nash, K. L. Small-Angle Neutron Scattering Study of Organic-Phase Aggregation in the TALSPEAK Process. *J. Phys. Chem. B*. **2012**, *116*, 13722–13730.
- (18) Qiao, B.; Sengupta, A.; Liu, Y.; McDonald, K. P.; Pink, M.; Anderson, J. R.; Raghavachari, K.; Flood, A. H. Electrostatic and Allosteric Cooperativity in Ion-Pair Binding: A Quantitative and Coupled Experiment–Theory Study with Aryl–Triazole–Ether Macrocycles. *J. Am. Chem. Soc.* **2015**, *137*, 9746–9757.
- (19) Mahoney, J. M.; Beatty, A. M.; Smith, B. D. Selective Recognition of an Alkali Halide Contact Ion-Pair. *J. Am. Chem. Soc.* **2001**, *123*, 5847–5848.
- (20) Jonah, T. M.; Mathivathanan, L.; Morozov, A. N.; Mebel, A. M.; Raptis, R. G.; Kavallieratos, K. Remarkably Selective NH_4^+ Binding and Fluorescence Sensing by Tripodal Tris(Pyrazolyl) Receptors Derived from 1,3,5-Triethylbenzene: Structural and Theoretical Insights on the Role of Ion Pairing. *New J. Chem.* **2017**, *41*, 14835–14838.
- (21) Bardwell, D. A.; Jeffery, J. C.; Jones, P. L.; McCleverty, J. A.; Psillakis, E.; Reeves, Z.; Ward, M. D. Lanthanide Complexes of the Tetradentate *N*-Donor Ligand dihydrobis[3-(2-Pyridyl)Pyrazolyl]Borate and the Terdentate *N*-Donor ligand 2,6-Bis(1H-Pyrazol-3-Yl)Pyridine: Syntheses, Crystal structures and Solution Structures Based on Luminescence Lifetime Studies. *J. Chem. Soc., Dalton Trans.* **1997**, 2079–2086.
- (22) Jain, S. L.; Bhattacharyya, P.; Milton, H. L.; Slawin, A. M. Z.; Crayston, J. A.; Woollins, J. D. New Pyridine Carboxamide Ligands and Their Complexation to Copper(II). X-Ray Crystal Structures of Mono-, Di, Tri- and Tetranuclear Copper Complexes. *Dalton Trans.* **2004**, 862–871.
- (23) Connors, K. A. *Binding Constants: The Measurement of Molecular Complex Stability*; John Wiley and Sons Inc., **1987**.
- (24) Gans, P.; Sabatini, A.; Vacca, A. *Hyperquad2013*; **1996**.

- (25) Rios, D.; Rutkowski, P. X.; Shuh, D. K.; Bray, T. H.; Gibson, J. K.; Van Stipdonk, M. J., Electron transfer dissociation of dipositive uranyl and plutonyl coordination complexes. *J Mass Spectrom* **2011**, *46*, 1247-1254.

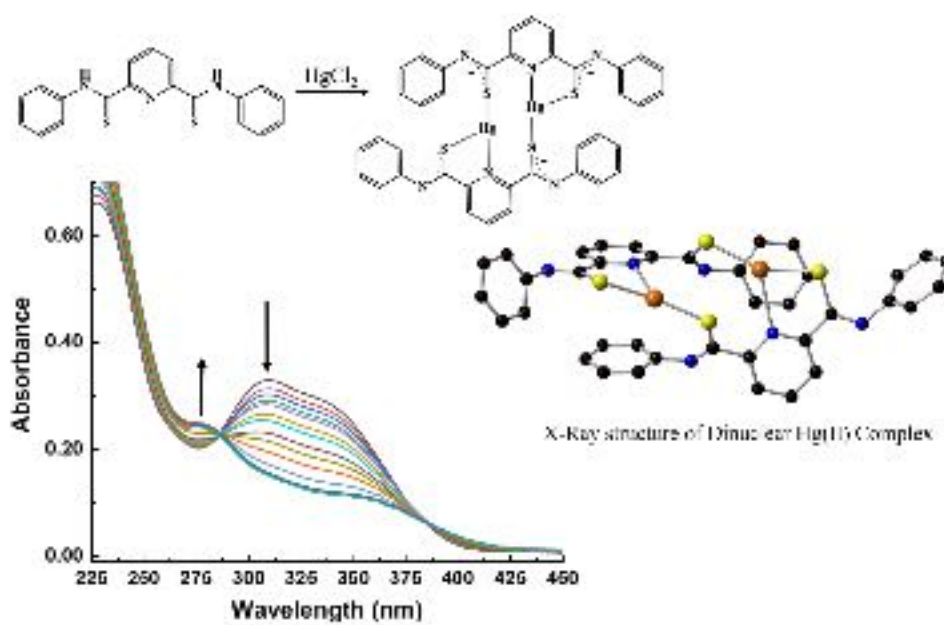
CHAPTER IV

A dithiopicolinamide ligand complexes and senses Hg(II) selectively via a unique 2:2 Hg₂L₂ coordination pattern

Ingrid Lehman-Andino, Indranil Chakraborty, Matthew T. Fortunato, René Panzer,
Raphael G. Raptis, Konstantinos Kavallieratos*

Department of Chemistry and Biochemistry, Florida International University, Miami, FL

33199



4.1 Abstract:

Toxic mercury used for processing operations as a catalyst for dissolution of aluminum cladding at the Savannah River Site (SRS) could become a problem for our health and the environment if released. This work presents Hg(II) complexation and sensing via the formation of an unusual dinuclear $\text{Hg}^{\text{II}}_2\text{L}_2$ complex, derived from the potentially tridentate (SNS) pincer ligand N^2, N^6 -diphenyl-2,6-pyridine dicarbothioamide (**LH₂**), that precipitated from alkaline solution. The structurally characterized dinuclear Hg(II) complex (**1**) shows an *S,S,N*- T-shaped coordination in a 2:2 Hg_2L_2 unique coordination pattern. In solution, the formation of the Hg(II) complex was monitored by ^1H -NMR and UV-Vis titration experiments. ^1H -NMR spectroscopic changes in acetone and UV-Vis titrations in methanol both confirm Hg_2L_2 2:2 binding with a binding constant K_{22} as high as $1.5 \times 10^{16} \text{ M}^{-3}$ (by UV-Vis in methanol).

4.2 Introduction

Mercury is toxic in all its oxidation states, with Hg(II) being of particular interest due to its high environmental mobility.¹⁻⁴ Inorganic mercury can be converted by bacteria to organic mercury forms, such as methyl mercury, which are especially toxic and can be introduced to biological food chains.^{3,5} Recently, the presence of large amounts of mercury in high-level alkaline nuclear waste tanks, as a result of its use as a catalyst for the dissolution of aluminum cladding for nuclear fuel, has led to increasing organic Hg accumulation post-processing into the low-activity stream.^{6,7} Therefore, the design of suitable chemosensors and extractants for Hg(II) at both neutral and alkaline pH environments can be influential in addressing these issues. Over the years several optical

chemosensors have been designed for Hg(II) showing great results as fluorescent and colorimetric sensors.⁸⁻¹⁴ In 2008, Das *et al.*¹⁵, reported a rhodamine-based chemosensor that exhibits a detectable color change in aqueous methanol upon 1:2 Hg(II)/L binding ($K_{12} = 8 \times 10^5 \text{ M}^{-2}$).

The biochemical mechanism of interaction of Hg(II) with S-containing proteins⁴ and known high-affinity binding of Hg(II) by inorganic sulfides due to its softer nature,^{16,17} point to the potential of the thioamide group as a component of selective sensors and extractants for Hg(II). There are several reported transition metal complexes with carbodithioamide derivatives,¹⁸⁻²² typically involving mononuclear complexes. Thioamide pincer complexes with several metals have been studied extensively,^{23,24} with the binding behavior being highly-dependent on the state of protonation of the thioamide group.^{20-23,25,26} In a seminal study, K. Bowman-James and coworkers²⁴ have attributed the “switch-like” behavior of the thioamide pincer ligands to a reversible transformation between the thioamide and the iminothiolate. There have been relatively few reported thioamide sensors for Hg(II) in the literature, and the application of C=S ligands for binding and sensing Hg(II) is also relatively rare: Song *et al.*²⁷ have reported nanocomposite rhodamine chemosensors containing the C=S group with Hg(II) binding constants in the range of 10^5 M^{-1} , as determined by absorption and emission spectroscopy. Yang, Y. *et al.*²⁸ have reported similar rhodamine-containing C=S ligands for strong Hg(II) binding in water-methanol at pH 7 with colorimetric changes and fluorescence sensing selectivity against transition metals and Ca^{2+} . Coronado, E. *et al.*⁵ achieved high Hg(II)-binding and sensing selectivity in water using Ru complexes with NCS groups. Hg(II) complexes of

thiosemicarbazide derivatives have also been reported as extractants for aqueous separation and preconcentration applications.²⁹

We are now reporting remarkably strong binding and selective optical sensing of Hg(II) over Ca(II), an abundant species, both in high-level waste and biological systems, with a potentially tridentate pyridinedicarbothioamide (SNS) pincer ligand (**LH₂**).²² This ligand, which has been previously studied by our group for actinide/lanthanide separations,³⁰ binds Hg(II) when deprotonated via both its N- and S- atoms, via formation of a unique 2:2 Hg(II)₂L₂ complex which was characterized both in solution by ¹H-NMR and UV-Vis, and in the solid-state by X-ray crystallography. The conformational changes of the thioamide ligand upon complexation with Hg(II) were monitored by ¹H-NMR as the ligand, and the complex are in slow exchange on the NMR timescale. The binding constant for the formation of Hg₂L₂ ($K_{22} = 1.5 \times 10^{16} \text{ M}^{-3}$) was determined directly from the UV-Vis titration spectra in methanol.

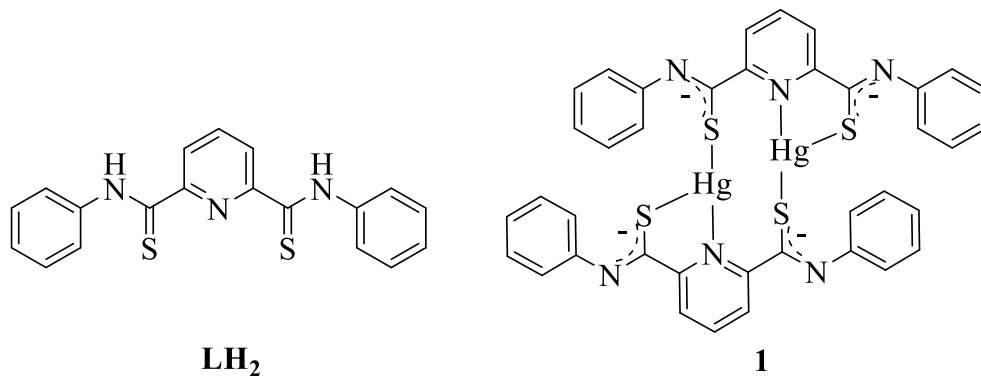


Figure 4.1. Structure of *N*²,*N*⁶-diphenyl-2,6-pyridine dicarbothioamide (**LH₂**) and the dinuclear complex (**1**) with electronic delocalization scheme.

4.4 Results and Discussion

4.4.1 X-ray Crystallography and FT-IR

The reaction of **LH₂** with HgCl₂ in the presence of diisopropylethylamine (DIPEA) in methanol at ambient temperature resulted in a pale yellow precipitate. Recrystallization from DCM/Hexane afforded needle-like crystals within a week. Single crystal X-ray crystallography revealed a 2:2 dinuclear neutral Hg(II)₂L₂ complex (**1**) with *N,S,S*-coordination around each Hg(II) center (Figure 4.2), which is unprecedented for a distinct non-polymeric species. Complex **1** crystallized in a triclinic *P-1* space group with a complete molecule in the asymmetric unit. The X-ray structure of free ligand **LH₂** was also determined (Figure 4.3) and showed a *syn-syn* conformation, which is likely favored due to intermolecular N-H⋯N interactions with the pyridine N.^{31–34}

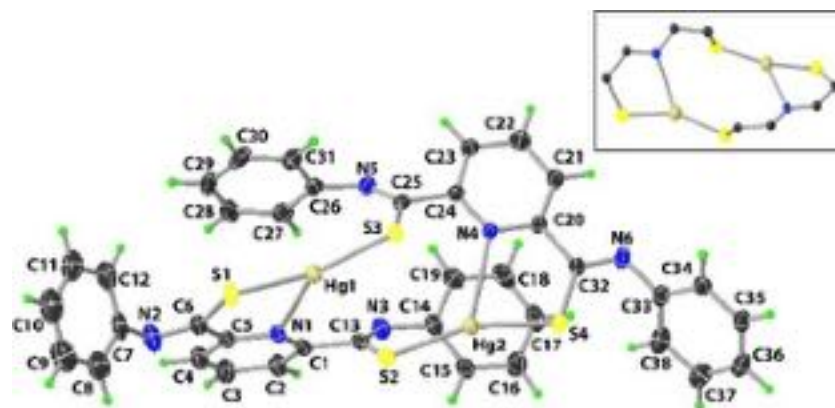


Figure 4.2. Perspective view of **1** with atom labeling scheme. Thermal ellipsoids are shown at 50% probability level. The inset displays the coordination sphere around the mercury (II) centers. Selected interatomic distances (Å): Hg1–S1, 2.3798(9); Hg1–S3, 2.3879(8); Hg1–N1, 2.566(3); Hg2–S2, 2.3443(8); Hg2–S4, 2.3457(9); Hg2–N4, 2.552(2); Hg...Hg, 4.5143(4) and angles (°): S1–Hg1–S3, 154.83(3); N1–Hg1–S3, 128.25(6); S1–Hg1–N1, 76.92(6); S4–Hg2–S2, 160.24(3); S2–Hg2–N4, 121.35(6); N4–Hg2–S4, 78.27(6).

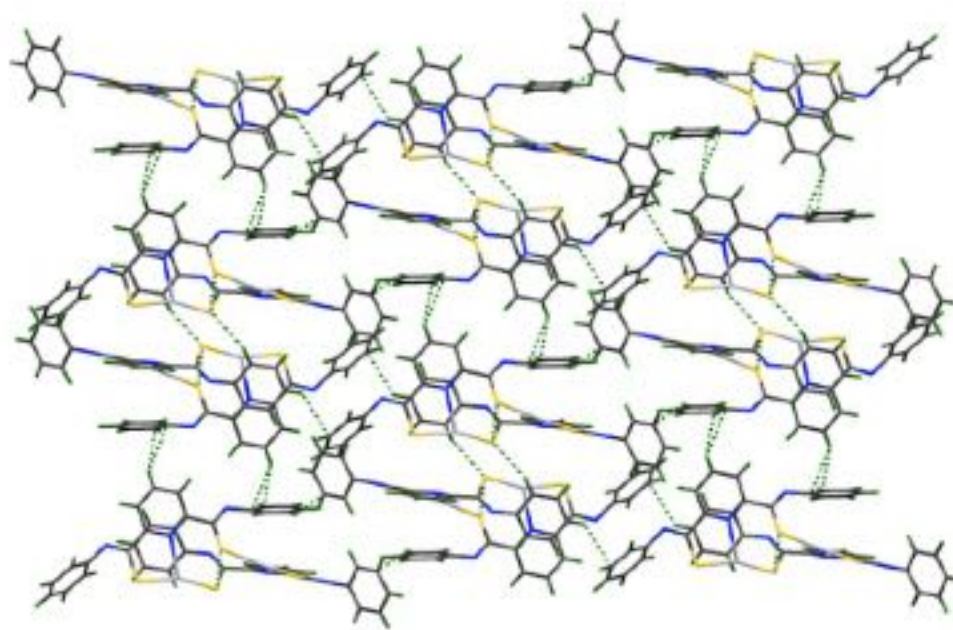


Figure 4.3. Packing pattern of **1** along *c* axis (the dotted line indicates the C–H...S intermolecular interactions)

In contrast to the structure of the free **LH₂** (Figure 4.4), the structure of complex **1** shows a ligand conformation that lies between the non-symmetric *syn-anti* and the symmetric *anti-anti* extremes, which facilitates binding to two Hg(II) centers. Each ligand forms one 5-membered chelate ring with a Hg center through the pyridyl *N*- and the *S*-atom of one of the thioamide functionalities, while the remaining *S*-atom of the second thioamide function for each ligand binds to a different Hg(II) center, resulting to a tri-coordinated environment (Figure 4.2, inset). To our knowledge, this is the first example of a distinct dinuclear Hg(II) complex with an *N,S,S*-tricoordinated pattern, also showing a unique T-shaped coordination environment. The equatorial planes constituted by N1,S1,S3, and N4,S2,S4 atoms represent two perfect planes. The average Hg–S and Hg–N distances in **1** are 2.3644(8) and 2.559(3) Å, respectively, which are comparable with those found in [Hg(SC₆H₂Bu₃^t)₂(py)]³⁵ and the Hg(II) benzenethiolate-nicotinate complex [Hg(Tab)₂(nico)]⁺ reported recently.³⁶ However, the S–Hg–S bond angles in complex **1** (154.83(3)° and 160.24(3)°) are noticeably more acute than those found in these mononuclear complexes (172.1(1)° and 166.69(4)°).^{35,36} In the polymeric [Hg₂(SPh)₄(□-4,4'-bpy)]_n,³⁷ which also shows *S,S,N* tri-coordination the S–Hg–S angles (average value, 169.45(4)°) are also significantly more obtuse than in **1**. Thus, our reported structure represents a unique pseudo T-shaped geometry for Hg(II) in a 2:2 complex, presumably facilitated by the disposition of the donor atoms of the dithiopicolinamide. This configuration also brings the two Hg(II) centers in a relatively proximal distance (Hg---Hg, 4.5143(4) Å). The two negative charges on each ligand are delocalized (Figure 4.1), as shown by bond length comparisons for **1** vs. the free ligand (**LH₂**). For example, N5–C25 and N6–C32 distances in **1** are 1.273(4) and 1.261(4) Å, both shorter than the

corresponding distances in **LH₂** (1.324(3) and 1.330 (4) Å), while S3–C25 and S4–C32 distances in **1** (1.773(3) and 1.771(3) Å) are longer than in **LH₂** (1.658(2) and 1.659(2) Å).

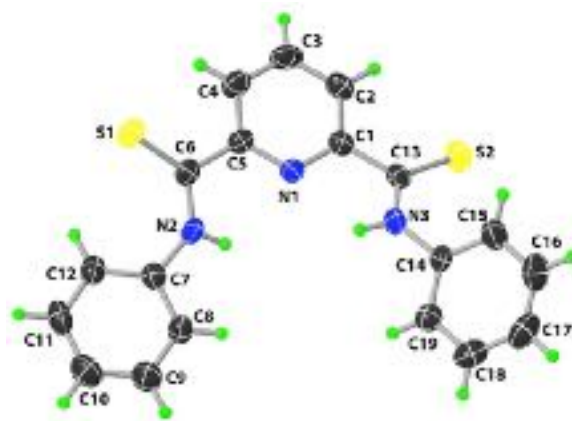


Figure 4.4. Perspective view of **LH₂** with atom labeling scheme. Thermal ellipsoids are shown at 50% probability level. Selected bond distances (Å): S1–C6, 1.658(2); S2–C13, 1.659(2); C6–N2, 1.324(3); C13–N3, 1.330(3); C6–C5, 1.499(2); C1–C13, 1.494(3)

FT-IR spectroscopy (Figures 4.7 and 4.8) also shows shift of the C=S stretching frequency from **LH₂** (1596 cm⁻¹) to the complex (1571 cm⁻¹), consistent with the partial reduction of C–S bond order in **1**. The packing diagram for **1** (Figure 4.3) reveals no classical hydrogen bonding interactions, neither π - π stacking interactions, as we observed on **LH₂** (Figure 4.6). However, moderate to weak intermolecular C–H...S contacts consolidate the extended structure of **1** (Figure 4.3) and also for **LH₂** (Figure 4.5). A search of the Cambridge Structural Database (CSD) revealed no other Hg complexes of **LH₂** or any analogous dithiopicolinamide derivatives. The only reported Hg(II) complexes with –N–C=S frameworks are with dithione derivatives of type [HgI₂(dithione)],³⁸ in which the thioamide function is a part of a ring system.

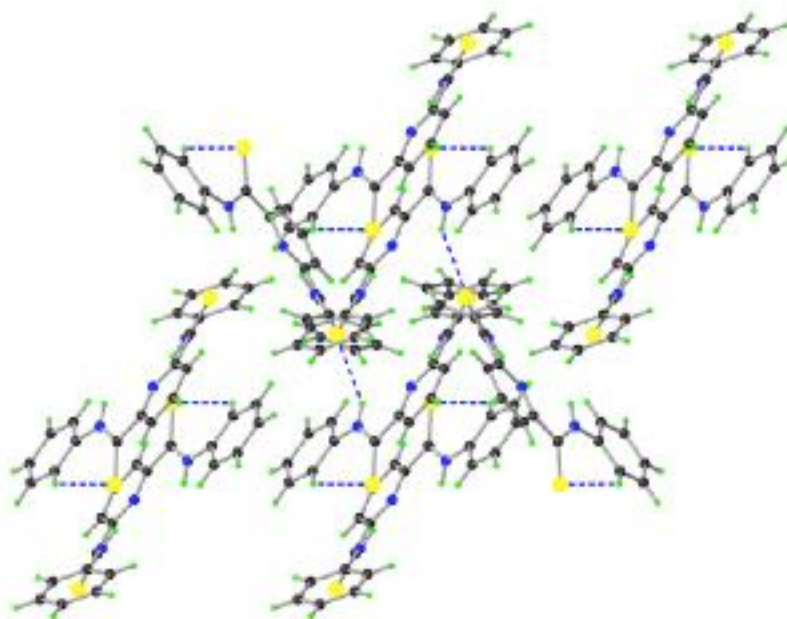


Figure 4.5. Packing pattern of **LH₂** along c axis (the dotted lines indicate C-H...S intermolecular interactions)

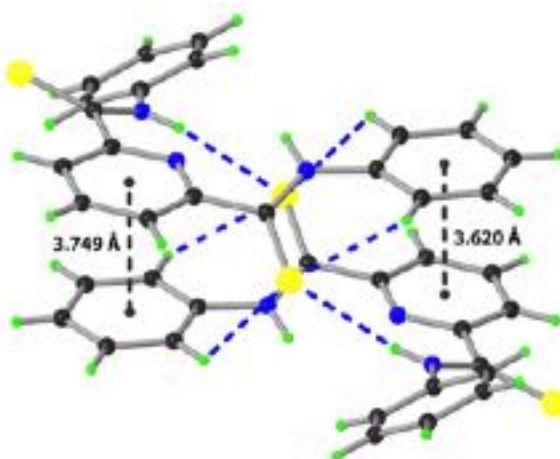


Figure 4.6. Intermolecular π - π stacking interactions in **LH₂**.

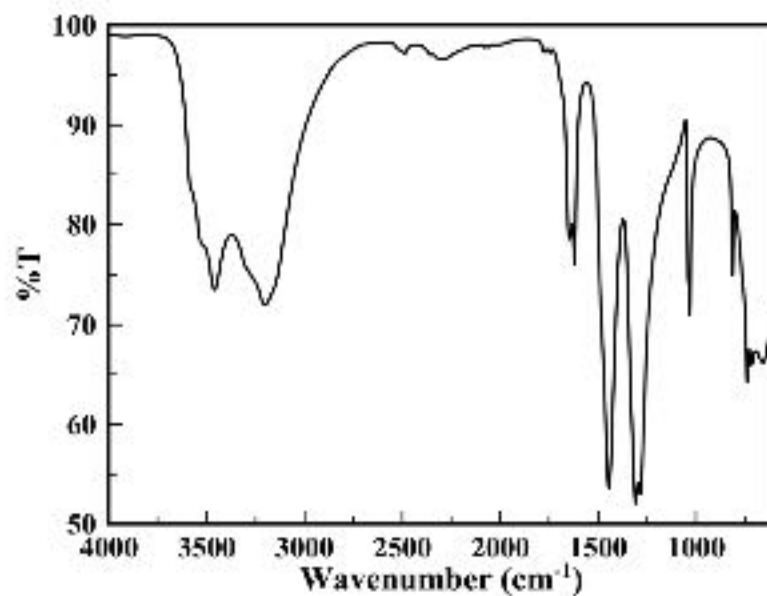


Figure 4.7. FT-IR spectrum of LH₂ in ATR mode

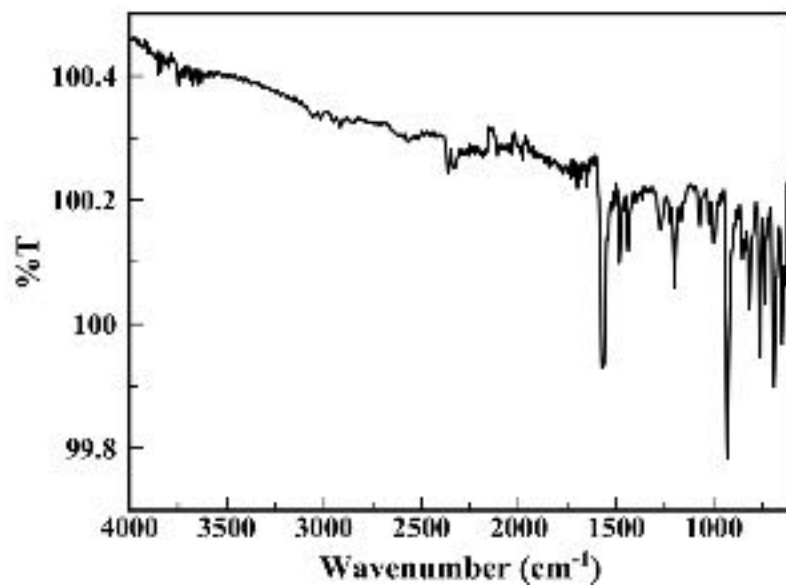


Figure 4.8. FT-IR spectrum of the complex 1 in ATR mode.

4.4.2 ^1H -NMR titration (complexation analysis)

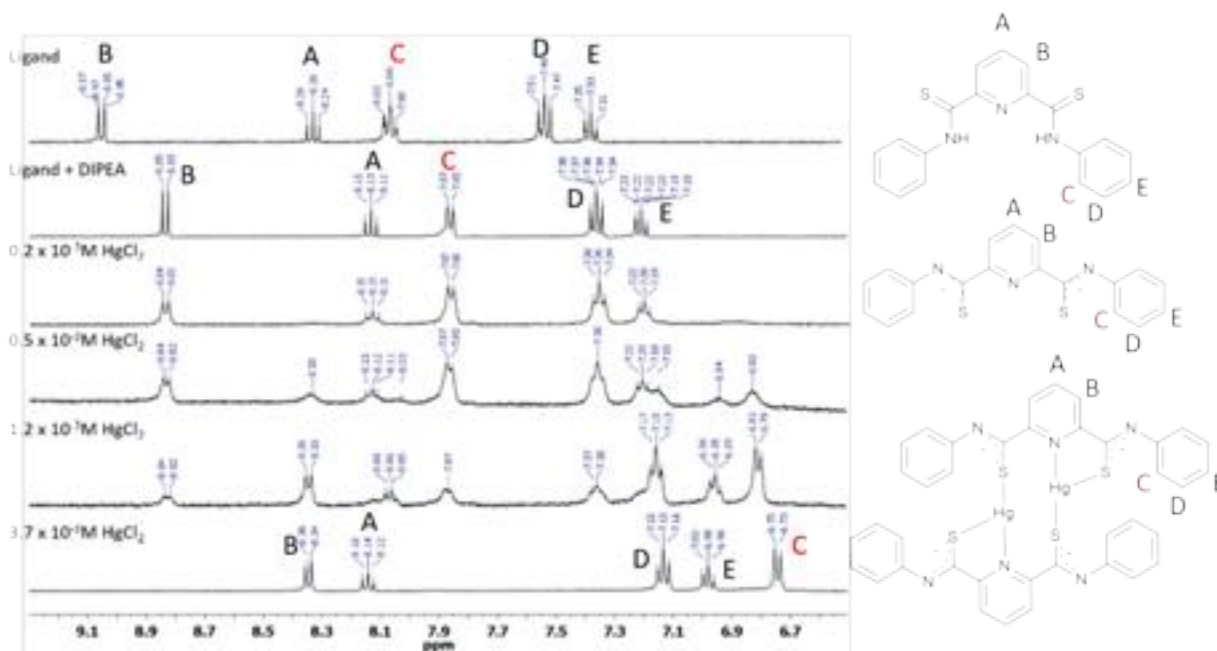


Figure 4.9. ^1H -NMR titration of LH_2 ($2.2 \times 10^{-3} \text{ M}$) with HgCl_2 and DIPEA (excess) in acetone- d_6 .

Complexation of $\text{Hg}(\text{II})$ in solution was confirmed spectroscopically both by ^1H NMR and UV-Vis titrations. ^1H -NMR titration of LH_2 ($2.2 \times 10^{-3} \text{ M}$) with HgCl_2 ($1.9 \times 10^{-2} \text{ M}$) in acetone- d_6 with an excess of DIPEA at constant ligand concentration (Figure 4.9) showed gradual disappearance of the deprotonated ligand L^{2-} resonances and appearance of new resonances for the $\text{Hg}(\text{II})$ complex. The last ^1H -NMR titration point (Figure 4.9, bottom) was identical with the spectrum obtained upon dissolution of the single crystals used for the collection of the X-ray structure data for **1**. The ^1H -NMR resonance shifts during the titration provide further evidence that the solution structure closely resembles the X-ray structure: Specifically, free LH_2 in both the solid-state and solution possesses a

syn-syn conformation for the two thioamide groups, due to intermolecular hydrogen bonding (Figure 4.9, top). Both the X-ray structure and the $^1\text{H-NMR}$ spectra (Figure 4.9, bottom) suggest a conformation between *syn-anti* and *anti-anti*, which places the sulfur atoms in a preferable disposition for binding Hg(II) . Specifically, the protons assigned to the carbons that are closer to the thioamide group on both the wingtip aromatic ring and central aromatic rings show large upfield shifts from 7.85 to 6.74 ppm and from 8.80 to 8.35 ppm, respectively, as the deprotonated ligand L^{2-} is complexed and changes conformation, while the *para* protons (triplets at 7.0 and 8.1 ppm) show only slight movements, as they are further away from the thioamide group. The fact that the final titration point shows a symmetrical structure is consistent with the conformation shown in the scheme from figure 4.1 and implies possible rapid exchange in NMR timescale between two structures that result in an overall symmetric spectrum.

4.4.3 UV-Visible titrations

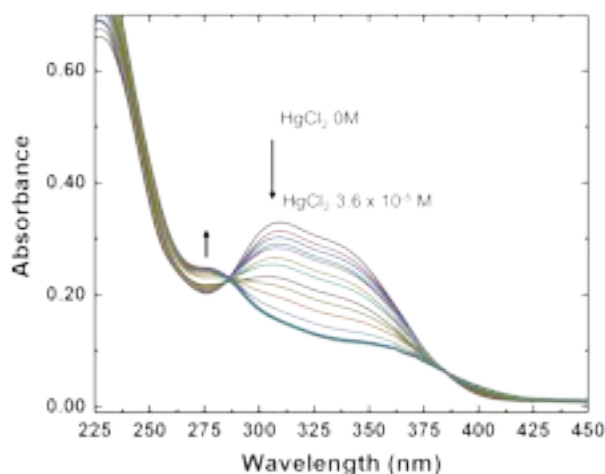


Figure 4.10. UV-Vis absorption of ligand LH_2 ($2.1 \times 10^{-5} \text{ M}$) and N,N' -Diisopropylethylamine ($4.0 \times 10^{-4} \text{ M}$) in methanol upon gradual addition of HgCl_2 ($4.4 \times 10^{-4} \text{ M}$).

UV-Vis titrations of a 2.1×10^{-5} M methanolic solution of **LH₂** containing excess DIPEA with a solution of HgCl₂ (4.0×10^{-4} M) under constant ligand concentrations showed two clear isosbestic points (Figure 4.10) with the final spectrum resembling the one acquired upon dissolution of the single crystals of complex **1**. A binding constant of $1.5 (\pm 0.9) \times 10^{16} \text{ M}^{-3}$ was obtained from the spectra (Section 4.5.3). Further control experiments were performed without the presence of DIPEA showing the same results on the UV-Visible data. This result confirms the formation of the same complex **1** even without the presence of base. Some scattering due to precipitation was observed (Figure 4.11), with the precipitate confirmed by ¹H-NMR to be the complex **1**.

UV-Vis competitive titration experiments with HgCl₂, both in the absence and presence of NaCl, KCl, CsF, CaCl₂, and SrCl₂ (at constant mM concentration levels of the ligand), showed very high selectivity towards HgCl₂, as the response is completely unaffected by the high concentrations of Na(I), K(I), Cs(I), Ca(II), and Sr(II) in the mixture at the early points of the titration (Figure 4.12). Another observation is the sharp saturation point obtained at 1:1 Hg/L ratio, which is consistent with the direct formation of the 2:2 complex. This level of selectivity against the variety of metals is significant compared to prior examples.^{1,39,40} These metals usually found on the HLW tanks seems to unaffected the selectivity of LH₂ to the Hg(II). In a separate experiment only in the presence of Pb(II) no significant changes at the UV-visible were observed at 1.0×10^{-4} M concentration of PbCl₂ (Figure 4.13). The observed selectivity is ascribed to the formation of a unique 2:2 dinuclear Hg(II)₂L₂ complex that has been isolated and characterized. Further selectivity studies are underway to optimize this system for extraction, separation, and sensing applications in the fields of energy and the environment.

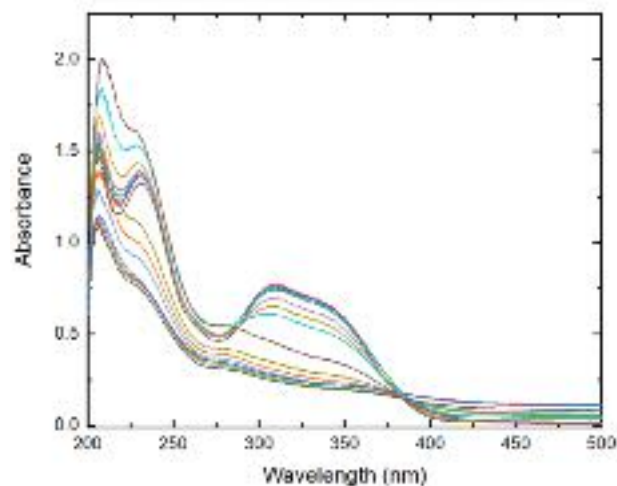


Figure 4.11. UV-Vis absorption spectra for titration of **LH₂** (5.04×10^{-5} M) with **HgCl₂** (3.09×10^{-4} M) in methanol with no base added.

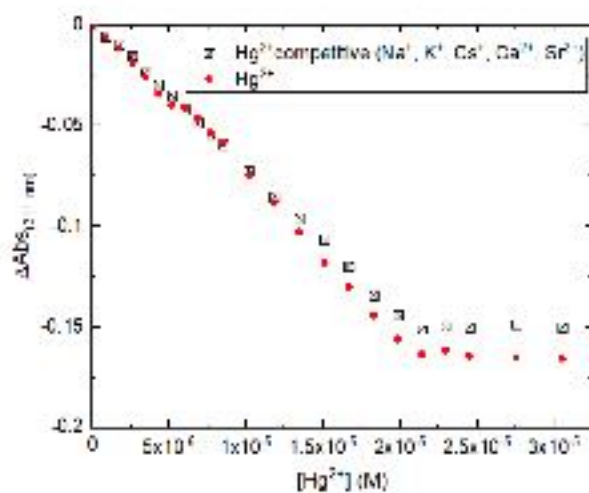


Figure 4.12. Competitive UV-Vis titration experiment in methanol with Hg(II) in the presence or absence of Ca(II), Na(I), K(I), Cs(I) and Sr(II): $[\text{LH}_2]_t = 2.06 \times 10^{-5}$ M, $[\text{DIPEA}]_t = 4.4 \times 10^{-4}$ M upon gradual addition of **HgCl₂** (4.02×10^{-4} M) in the presence or absence of the different metal mixture. $[\text{Ca(II)}]_t = 4.47 \times 10^{-3}$ M), $[\text{Na(I)}]_t = 1.03 \times 10^{-1}$ M), $[\text{K(I)}]_t = 1.04 \times 10^{-2}$ M), $[\text{Cs(I)}]_t = 4.77 \times 10^{-3}$ M), $[\text{Sr(II)}]_t = 4.03 \times 10^{-3}$ M).

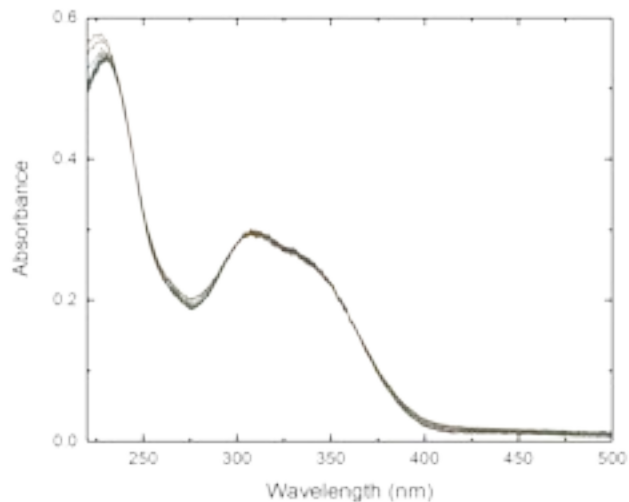


Figure 4.13. UV-Visible titration of **LH₂** (3.6×10^{-5} M) with **PbCl₂** (1.0×10^{-4} M) in MeOH.

4.5 Experimental:

4.5.1 Materials and Methods:

All chemicals were purchased from Aldrich Chemical Company, ACROS Organics, or Fisher Scientific, were standard reagent grade and were used without further purification unless otherwise noted. *N*²,*N*⁶-diphenyl-2,6-pyridinedicarbothioamide (**LH₂**)^{22,30} was synthesized by modification of previously reported procedures. *N*²,*N*⁶-diphenyl-2,6-pyridinedicarboxamide was synthesized from 2,6-pyridinedicarbonyl dichloride, as previously reported.^{30,41} ¹H NMR spectra were recorded on a 400 MHz Bruker NMR spectrometer and referenced to the residual solvent resonances. All chemical shifts, δ , are reported in ppm. UV-Vis spectra were recorded on an Agilent Technologies Cary 8454 UV-Visible spectrophotometer.

4.5.2 Synthetic procedure

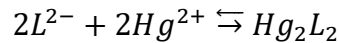
Bis-(*m-h-S,S'*,*N-N*²,*N*⁶-diphenyl-2,6-pyridinedicarbothioamido)-mercury(II)-

(Hg₂L₂)·H₂O (1): *N*²,*N*⁶-diphenyl-2,6-pyridinedicarbothioamide (**LH₂**) (95.0 mg, 0.271 mmol) was dissolved in methanol. *N,N'*-diisopropylethylamine (DIPEA) (100 μL, 0.574 mmol) was added to the solution. Then solid HgCl₂ (78.5 mg, 0.289 mmol) was added slowly to the stirring solution at room temperature. After 1 h a precipitate was formed and recrystallized from CH₂Cl₂/hexanes (136 mg, 0.109 mmol, 41% yield): ¹H NMR (400 MHz, acetone-*d*₆): δ 8.36 (d, *J*=7.7 Hz, 2H), 8.14 (t, *J*=7.8 Hz, 1H), 7.13 (t, *J*=7.7 Hz, 4H), 6.98 (t, *J*=7.4 Hz, 2H), 6.75 (d, *J*=7.4, Hz 4H). UV/Vis (CH₃OH): λ_{max} 276 nm, FT-IR (ATR) cm⁻¹: 1571(m, C=S), 1481(m), 1438(m), 1200(m), 929(s), 759(m), 688(m), 696(m). Elemental analysis: Anal Calcd. for C₃₈H₂₆Hg₂N₆S₄·H₂O: C, 40.97; H, 2.53; N, 7.54. Found: C, 40.87; H, 2.43; N, 7.47.

4.5.3 UV-Visible Titrations and determination of K₂₂ binding constant

Solutions of **LH₂**/DIPEA in MeOH were titrated with solutions of excess HgCl₂ at constant ligand concentration. In a typical experiment, a solution of **LH₂** (3.5 × 10⁻⁵ M) and DIPEA (4.2 × 10⁻⁴ M) in MeOH (solution A) was titrated with a solution of HgCl₂ (4.4 × 10⁻⁴ M), **LH₂** (3.5 × 10⁻⁵ M), and DIPEA (4.2 × 10⁻⁴ M) (solution B) prepared by weighing 0.60 mg of HgCl₂ in a 5.0 mL volumetric flask and diluting with solution A. For spectral collection, 2.3 mL of solution A were added to the UV-Visible cuvette and solution B was added in 2-150 μL increments.

As the UV-Vis spectra showed a decrease of A_{311} and an increase at A_{275} with clear isosbestic points at 287 nm and 386 nm, and a control experiment with DIPEA showed no absorption at 311 nm, the binding constant was determined directly from the 2:2 binding equilibria (eq. 5) by applying Beer's law to the absorption at 311 nm assuming that the only species that absorb at that wavelength are the deprotonated ligand L^{2-} and the Hg_2L_2 complex:⁴²



$$[Hg_2L_2] = \frac{C_{Lt} - [L^{2-}]}{2} \quad (1)$$

Where C_{Lt} is the total ligand concentration, which is constant during the titration.

$$[Hg^{2+}] = C_{Hgt} - 2[Hg_2L_2] \quad (2)$$

Where C_{Hgt} is the total Hg concentration, calculated for each titration point after the addition of solution B.

$$A_{311nm} = \varepsilon_{L^{2-}} b [L^{2-}] + \varepsilon_{Hg_2L_2} b [Hg_2L_2] \quad (3)$$

Where $\varepsilon_{L^{2-}}$ is the molar extinction coefficient for the deprotonated ligand L^{2-} at $\lambda = 311$ nm (found from the initial point of the titration) $\varepsilon_{Hg_2L_2}$ is the molar extinction coefficient for the Hg_2L_2 complex at $\lambda = 311$ nm, calculated from the last post-saturation titration point in which the Hg(II) is in excess and assuming all ligand is complexed and b is the path length (1 cm).

Substituting $[\text{Hg}_2\text{L}_2]$ on eq. 3 from eq. 1 and solving for $[\text{L}^{2-}]$ gives:

$$[\text{L}^{2-}] = \frac{2 A_{311nm} - \varepsilon_{\text{Hg}_2\text{L}_2} b C_{\text{L}t}}{(2\varepsilon_{\text{L}^{2-}} - \varepsilon_{\text{Hg}_2\text{L}_2}) b} \quad (4)$$

Then eq. 1 and eq. 2 are used to find the values $[\text{Hg}_2\text{L}_2]$ and $[\text{Hg}^{2+}]$

$$K_{22} = \frac{[\text{Hg}_2\text{L}_2]}{[\text{L}^{2-}]^2 [\text{Hg}^{2+}]^2} \quad (5)$$

Based on these calculations, the K_{22} for the formation of Hg_2L_2 complex was found to be $1.5 (+/- 0.9) \times 10^{16} \text{ M}^{-3}$.

4.5.4 $^1\text{H-NMR}$ Titration Experiments

The formation of Hg_2L_2 complex was also observed in acetone- d_6 by titration of **LH₂** ($2.2 \times 10^{-3} \text{ M}$) and DIPEA ($4.2 \times 10^{-2} \text{ M}$) with HgCl_2 solutions ($1.9 \times 10^{-2} \text{ M}$) at constant ligand concentration, in which Hg_2L_2 and L^{2-} show separate resonances (slow exchange at NMR timescale). A $2.2 \times 10^{-3} \text{ M}$ solution of **LH₂** and DIPEA in acetone d_6 was prepared in a 2.00 mL volumetric flask (solution A). A HgCl_2 solution (Solution B) was prepared by dilution of 6.08 mg of HgCl_2 with 1.2 mL of Solution A. The solution A (0.500 mL) was placed in an NMR tube. Solution B was added in increments with a μL syringe until a total of 200 μL was added.

4.5.5 X-ray crystallography

Light yellow block-shaped crystals of **LH₂** were obtained by slow evaporation of a methanolic solution. Crystals for the Hg complex **1** were obtained by slow diffusion of hexanes into a dichloromethane (CH₂Cl₂) solution. Pale yellow crystals were formed after one week. NMR characterization of the dissolved formed crystals perfectly matched the spectrum of the complex **Hg₂L₂** formed by bulk synthesis (*vide infra*). In both cases, a suitable crystal was selected and mounted on a Bruker D8 Quest diffractometer equipped with PHOTON II detector operating at T = 298 K. Data were collected with ω shutter less scan technique using graphite monochromated Mo-K α radiation ($\lambda = 0.71073 \text{ \AA}$). The total number of runs and images for both data collections was based on the strategy calculation from the program *APEX3* (Bruker)⁴³. The maximum resolution achieved was $\theta = 26.4^\circ$ for **LH₂** and $\theta = 26.5^\circ$ for **1**. Cell parameters were retrieved using the *SAINTE* (Bruker) software⁴⁴ and refined using *SAINTE* (Bruker) on 7113 reflections for **LH₂** and on 9993 reflections for **1**. Data reduction was performed using the *SAINTE* (Bruker) software, which corrects for Lorentz and polarization effects. The final completeness is 99.7% out to 26.4° in θ for **LH₂** and 99.1% out to 26.5° in θ for **1**. Multi-scan absorption corrections were performed with both data sets using *SADABS* 2014/5 and *SADABS* 2016/2 respectively for **LH₂** and **1**⁴⁵. The absorption coefficient for **LH₂** is 0.32 mm^{-1} and for **1** is 8.60 mm^{-1} and the minimum and maximum transmissions for **LH₂** are 0.716 and 0.745 and the corresponding values for **1** are 0.539 and 0.745. The structures for **LH₂** and **1** were solved in the space group P2₁/c (No. 14) and P-1 (No. 2) respectively by intrinsic phasing using the *ShelXT* (Sheldrick, 2015)⁴⁶ structure solution program and refined by full matrix least

squares on F^2 using version 2016/6 of *ShelXL* (Sheldrick, 2015)⁴⁷. All non-hydrogen atoms were refined anisotropically in both cases. Hydrogen atom positions were calculated geometrically and refined using the riding model. Good quality single crystals of complex **1** have also been isolated upon slow evaporation of the final solution of the NMR titration experiments. One of such single crystals was selected for data collection upon the solution and refinement. This revealed the same molecular structure as **1** albeit in a different crystal system and space group.

Calculations and molecular graphics were performed using *SHELXTL* 2014 and *Olex2*⁴⁸ programs.

Crystal data and structure refinement parameters are listed in Table 4.1.

Table 4.1. Crystal data and structure refinement parameters for **LH₂** and complex **1**

	(LH ₂)	(1)
Formula	C ₁₉ H ₁₅ N ₃ S ₂	C ₃₈ H ₂₆ N ₆ S ₄ Hg ₂
$D_{calc.}/\text{g cm}^{-3}$	1.366	1.978
μ/mm^{-1}	0.32	8.60
Formula Weight	349.46	1096.07
Color	Yellow	Yellow
Shape	Block	Block
T/K	298(2)	298(2)
Crystal System	Monoclinic	Triclinic
Space Group	P2 ₁ /c	P-1
$a/\text{\AA}$	9.6674(4)	10.6053(6)
$b/\text{\AA}$	9.5326(4)	12.2800(8)
$c/\text{\AA}$	18.9876(9)	15.9977(10)
$\alpha/^\circ$	90	111.388(2)
$\beta/^\circ$	103.829(1)	101.577(2)
$\gamma/^\circ$	90	98.882(2)
$V/\text{\AA}^3$	1699.09(13)	1840.4(2)

<i>Z</i>	4	2
Wavelength/Å	0.71073	0.71073
Radiation type	Mo-Kα	Mo-Kα
$2\theta_{min}/^{\circ}$	6.20	5.80
$2\theta_{max}/^{\circ}$	52.80	53.00
Measured Refl.	21717	30281
Independent Refl.	3452	7603
Reflections Used	2433	6333
R_{int}	0.041	0.025
Parameters	217	451
^a GooF	1.040	1.060
^c wR_2	0.106	0.043
^b R_1	0.046	0.020

^aGOF = $[\Sigma[\omega(F_o^2 - F_c^2)^2]/(N_o - N_v)]^{1/2}$ (N_o = number of observations, N_v = number of variables). ^b $R_1 = \Sigma ||F_o| - |F_c|| / \Sigma |F_o|$. ^c $wR_2 = [(\Sigma\omega(F_o^2 - F_c^2)^2 / \Sigma |F_o|^2)]^{1/2}$

CCDC 1825082 (**LH₂**), CCDC 1825083 (complex **1**) contain the supplementary crystallographic data for this paper. These data can be obtained free of charge from The Cambridge Crystallographic Data Center via www.ccdc.cam.ac.uk/data_request.cif.

A CSD (accessed on November 02, 2018) survey revealed Hg complexes with mixed N, S coordination spheres are dominated by octahedral and tetrahedral coordination geometry and mixed N, S tri-coordination in discrete systems is found to be relatively rare (excluding oligomeric species).

4.6 Conclusion:

In conclusion, a relatively simple dithiopicolinamide ligand was found to be an optical sensor for Hg(II) with very strong binding and remarkable selectivity against Na(I), K(I), Cs(I), Ca(II), and Sr(II) together in a mixture (Figure 4.12). The observed selectivity is

ascribed to the formation of a unique 2:2 dinuclear Hg(II)₂L₂ complex that has been isolated and characterized. Further selectivity studies are underway to optimize this system for extraction, separation, and sensing applications in the fields of energy and the environment.

4.7 References:

- (1) Chen, C.; Wang, R.; Guo, L.; Fu, N.; Dong, H.; Yuan, Y. A Squaraine-Based Colorimetric and “Turn on” Fluorescent Sensor for Selective Detection of Hg²⁺ in an Aqueous Medium. *Org. Lett.* **2011**, *13*, 1162–1165.
- (2) Ramesh, G. V.; Radhakrishnan, T. P. A Universal Sensor for Mercury (Hg, HgI, HgII) Based on Silver Nanoparticle-Embedded Polymer Thin Film. *ACS Appl. Mater. Interfaces* **2011**, *3*, 988–994.
- (3) Clarkson, T. W. The Toxicology of Mercury. *Crit. Rev. Clin. Lab. Sci.* **1997**, *34*, 369–403.
- (4) Fernandes Azevedo, B.; Barros Furieri, L.; Peçanha, F. M.; Wiggers, G. A.; Frizera Vassallo, P.; Ronacher Simões, M.; Fiorim, J.; Rossi de Batista, P.; Fioresi, M.; Rossoni, L.; Stefanon, I.; Alonso, M. J.; Salaices, M.; Valentim Vassallo, D. Toxic Effects of Mercury on the Cardiovascular and Central Nervous Systems. *BioMed Res. Int.* **2012**, *2*, 1–11.
- (5) Coronado, E.; Galán-Mascarós, J. R.; Martí-Gastaldo, C.; Palomares, E.; Durrant, J. R.; Vilar, R.; Gratzel, M.; Nazeeruddin, Md. K. Reversible Colorimetric Probes for Mercury Sensing. *J. Am. Chem. Soc.* **2005**, *127*, 12351–12356.
- (6) Bannochie, C. J.; Fellingner, T. L.; Garcia-Strickland, P.; Shah, H. B.; Jain, V.; Wilmarth, W. R. Mercury in Aqueous Tank Waste at the Savannah River Site: Facts, Forms, and Impacts. *Sep. Sci. Technol.* **2018**, *53*, 1935–1947.
- (7) Jain, V.; Shah, H. B.; Occhipinti, J. E.; Wilmarth, W. R.; Edwards, R. E. *Evaluation of Mercury in Liquid Waste Processing Facilities*; Phase I Report, SRR-CES-2015-00012, 1; Savannah River Site, Aiken, SC., **2015**.
- (8) Li, S.; Zhao, X.; Tao, D.; Zhang, W.; Zhang, K. Hg(II)-Activated Emission “Turn-on” Chemosensors Excited by up-Conversion Nanocrystals: Synthesis,

- Characterization and Sensing Performance. *Spectrochim. Acta. A. Mol. Biomol. Spectrosc.* **2015**, *137*, 581–588.
- (9) Xu, Z.-H.; Hou, X.-F.; Xu, W.-L.; Guo, R.; Xiang, T.-C. A Highly Sensitive and Selective Fluorescent Probe for Hg²⁺ and Its Imaging Application in Living Cells. *Inorg. Chem. Commun.* **2013**, *34*, 42–46.
- (10) Tsai, H.-J.; Su, Y.; Wan, C.-F.; Wu, A.-T. A Selective Colorimetric Fluorescent Chemosensor for Hg²⁺ in Aqueous Medium and in the Solid State. *J. Lumin.* **2018**, *194*, 279–283.
- (11) Sie, Y.-W.; Li, C.-L.; Wan, C.-F.; Chen, J.-H.; Hu, C.-H.; Yan, H.; Wu, A.-T. A Colorimetric Probe for Dual Sensing of Hg²⁺ and Cu²⁺ Ions in Water. *Inorganica Chim. Acta* **2017**, *467*, 325–329.
- (12) Sie, Y.-W.; Li, C.-L.; Wan, C.-F.; Chen, J.-H.; Hu, C.-H.; Wu, A.-T. 1,10-Phenanthroline Based Colorimetric and Fluorescent Sensor for Hg²⁺ in Water: Experimental and DFT Study. *Inorganica Chim. Acta* **2018**, *469*, 397–401.
- (13) Nolan, E. M.; Lippard, S. J. A “Turn-On” Fluorescent Sensor for the Selective Detection of Mercuric Ion in Aqueous Media. *J. Am. Chem. Soc.* **2003**, *125*, 14270–14271.
- (14) Wang, C.; Wong, K. M.-C. Selective Hg²⁺ Sensing Behaviors of Rhodamine Derivatives with Extended Conjugation Based on Two Successive Ring-Opening Processes. *Inorg. Chem.* **2013**, *52*, 13432–13441.
- (15) Suresh, M.; Shrivastav, A.; Mishra, S.; Suresh, E.; Das, A. A Rhodamine-Based Chemosensor That Works in the Biological System. *Org. Lett.* **2008**, *10*, 3013–3016.
- (16) Ali, Z.; Ahmad, R.; Khan, A.; Adalata, B. Complexation of Hg(II) Ions with a Functionalized Adsorbent: A Thermodynamic and Kinetic Approach. *Prog. Nucl. Energy* **2018**, *105*, 146–152.
- (17) Bailey, S. E.; Olin, T. J.; Bricka, R. M.; Adrian, D. D. A Review of Potentially Low-Cost Sorbents for Heavy Metals. *Water Res.* **1999**, *33*, 2469–2479.
- (18) Bates, G. W.; Gale, P. A.; Light, M. E.; Ogden, M. I.; Warriner, C. N. Structural Diversity in the First Metal Complexes of 2,5-Dicarboxamidopyrroles and 2,5-Dicarbothioamidopyrroles. *Dalton Trans.* **2008**, 4106–4112.

- (19) Teratani, T.; Koizumi, T.; Yamamoto, T.; Tanaka, K.; Kanbara, T. Deprotonation/Protonation of Coordinated Secondary Thioamide Units of Pincer Ruthenium Complexes: Modulation of Voltammetric and Spectroscopic Characterization of the Pincer Complexes. *Dalton Trans.* **2011**, *40*, 8879–8886.
- (20) Suzuki, T.; Kajita, Y.; Masuda, H. Deprotonation/Protonation-Driven Change of the σ -Donor Ability of a Sulfur Atom in Iron(II) Complexes with a Thioamide SNS Pincer Type Ligand. *Dalton Trans.* **2014**, *43*, 9732–9739.
- (21) Suzuki, T.; Matsumoto, J.; Kajita, Y.; Inomata, T.; Ozawa, T.; Masuda, H. Nitrosyl and Carbene Iron Complexes Bearing a K3-SNS Thioamide Pincer Type Ligand. *Dalton Trans.* **2014**, *44*, 1017–1022.
- (22) Komiyama, Y.; Kuwabara, J.; Kanbara, T. Deprotonation-Induced Structural Changes in SNS-Pincer Ruthenium Complexes with Secondary Thioamide Groups. *Organometallics* **2014**, *33*, 885–891.
- (23) Albrecht, M.; van Koten, G. Platinum Group Organometallics Based on “Pincer” Complexes: Sensors, Switches, and Catalysts. *Angew. Chem. Int. Ed.* **2001**, *40*, 3750–3781.
- (24) Wang, Q.-Q.; Ara Begum, R.; Day, V. W.; Bowman-James, K. Molecular Thioamide \leftrightarrow Iminothiolate Switches for Sulfur Mustards. *Inorg. Chem.* **2012**, *51*, 760–762.
- (25) OgawaYasuyuki; TaketoshiAyako; KuwabaraJunpei; OkamotoKen; FukudaTakashi; KanbaraTakaki. Luminescence Study of Thioamide-Based Pincer Palladium Complexes in Poly(Vinylpyrrolidone) Matrix. *Chem. Lett.* **2010**, *4*, 385–387.
- (26) Arras, J.; Speth, H.; Mayer, H. A.; Wesemann, L. Different Coordination Modes of the Ph₂PCsp³PPh₂ Pincer Ligand in Rhodium Complexes as a Consequence of Csp³–H Metal Interaction. *Organometallics* **2015**, *34*, 3629–3636.
- (27) Song, K.; Mo, J.; Lu, C. Hg(II) Sensing Platforms with Improved Photostability: The Combination of Rhodamine Derived Chemosensors and up-Conversion Nanocrystals. *Spectrochim. Acta. A. Mol. Biomol. Spectrosc.* **2017**, *179*, 125–131.
- (28) Yang, Y.-K.; Yook, K.-J.; Tae, J. A Rhodamine-Based Fluorescent and Colorimetric Chemodosimeter for the Rapid Detection of Hg²⁺ Ions in Aqueous Media. *J. Am. Chem. Soc.* **2005**, *127*, 16760–16761.

- (29) Hassanien, M. M.; Hassan, A. M.; Mortada, W. I.; El-Asmy, A. A. A New Thioamide Derivative for Separation and Preconcentration of Multi Elements in Aquatic Environment by Cloud Point Extraction. *Am. J. Anal. Chem.* **2011**, *2*, 697.
- (30) Lehman-Andino, I.; Su, J.; Papathanasiou, K. E.; Eaton, T. M.; Jian, J.; Dan, D.; Albrecht-Schmitt, T. E.; Dares, C. J.; Batista, E. R.; Yang, P.; Gibson, J. K.; Kavallieratos, K. Soft-Donor Dipicolinamide Derivatives for Selective Actinide(III)/Lanthanide(III) Separation: The Role of S- vs. O-Donor Sites. *Chem. Commun.* **2019**, *55*, 2441–2444.
- (31) Geib, S. J.; Vicent, C.; Fan, E.; Hamilton, A. D. A Self-Assembling, Hydrogen-Bonded Helix. *Angew. Chem. Int. Ed.* **1993**, *32*, 119–121.
- (32) Kavallieratos, K.; de Gala, S. R.; Austin, D. J.; Crabtree, R. H. A Readily Available Non-Preorganized Neutral Acyclic Halide Receptor with an Unusual Nonplanar Binding Conformation. *J. Am. Chem. Soc.* **1997**, *119*, 2325–2326.
- (33) Hossain, Md. A.; Kang, S. O.; Llinares, J. M.; Powell, D.; Bowman-James, K. Elite New Anion Ligands: Polythioamide Macrocycles. *Inorg. Chem.* **2003**, *42*, 5043–5045.
- (34) Kang, S.-O.; Johnson, T. S.; Day, V. W.; Bowman-James, K. Pyridine-2,6-Dicarboxamide Pincer-Based Macrocyclic: A Versatile Ligand for Oxoanions, Oxometallates, and Transition Metals. *Supramol. Chem.* **2018**, *30*, 305–314.
- (35) Bochmann, M.; Webb, K. J.; Powell, A. K. Synthesis and Structure of [Hg(SC₆H₂But₃)₂(Py)]: A T-Shaped Complex of Mercury. *Polyhedron* **1992**, *11*, 513–516.
- (36) Tang, X.-Y.; Yu, H.; Gao, B.-B.; Lang, J.-P. [Cd(H₂O)₆]Cd₆Cl₄ (Nico)₁₂ [Hg(Tab)₂ (μ-Cl)₂]: A Heterometallic Host–Guest Icosidodecahedron Cage via Hierarchical Assembly. *Dalton Trans.* **2017**, *46*, 14724–14727.
- (37) Ng, M. T.; Deivaraj, T. C. D.; Vittal, J. J. Structure of [Hg₂(SPh)₄(μ-4,4'-Bpy)]_n. *Main Group Met. Chem.* **2002**, *25*, 581–582.
- (38) Bigoli, F.; Cabras, M. C.; Deplano, P.; Mercuri, M. L.; Marchiò, L.; Serpe, A.; Trogu, E. F. On the Use of the Bis(Diodine) Adduct of 1,4-Dimethylperhydro-1,4-Diazepine-2,3-Dithione (Me₂dazdt) to Recover Liquid Mercury Producing [Hg(Me₂dazdt)₂] in a One-Step Reaction. *Eur. J. Inorg. Chem.* **2004**, *1*, 960–963.

- (39) Ros-Lis, J. V.; Martínez-Máñez, R.; Rurack, K.; Sancenón, F.; Soto, J.; Spieles, M. Highly Selective Chromogenic Signaling of Hg^{2+} in Aqueous Media at Nanomolar Levels Employing a Squaraine-Based Reporter. *Inorg. Chem.* **2004**, *43*, 5183–5185.
- (40) Shaily; Kumar, A.; Ahmed, N. Indirect Approach for CN^- Detection: Development of “Naked-Eye” Hg^{2+} -Induced Turn-Off Fluorescence and Turn-On Cyanide Sensing by the Hg^{2+} Displacement Approach. *Ind. Eng. Chem. Res.* **2017**, *56*, 6358–6368.
- (41) Malone, J. F.; Murray, C. M.; Dolan, G. M.; Docherty, R.; Lavery, A. J. Intermolecular Interactions in the Crystal Chemistry of $\text{N,N}'$ -Diphenylisophthalamide, Pyridine-2,6-Dicarboxylic Acid Bisphenylamide, and Related Compounds. *Chem. Mater.* **1997**, *9*, 2983–2989.
- (42) Connors, K. A. *Binding Constants: The Measurement of Molecular Complex Stability*; John Wiley and Sons Inc., **1987**.
- (43) *Bruker APEX 3*; Bruker AXS Inc.: Madison, Wisconsin, USA, **2014**.
- (44) *Bruker SAINT*; Bruker AXS Inc.: Madison, Wisconsin, USA, **2012**.
- (45) *Bruker SADABS*; Bruker AXS Inc.: Madison, Wisconsin, USA, **2014**.
- (46) Sheldrick, G. M. SHELXT – Integrated Space-Group and Crystal-Structure Determination. *Acta Crystallogr. Sect. Found. Adv.* **2015**, *71*, 3–8.
- (47) Sheldrick, G. M. Crystal Structure Refinement with SHELXL. *Acta Crystallogr. Sect. C Struct. Chem.* **2015**, *71*, 3–8.
- (48) Dolomanov, O. V.; Bourhis, L. J.; Gildea, R. J.; Howard, J. A. K.; Puschmann, H. OLEX2: A Complete Structure Solution, Refinement and Analysis Program. *J. Appl. Crystallogr.* **2009**, *42*, 339–341.

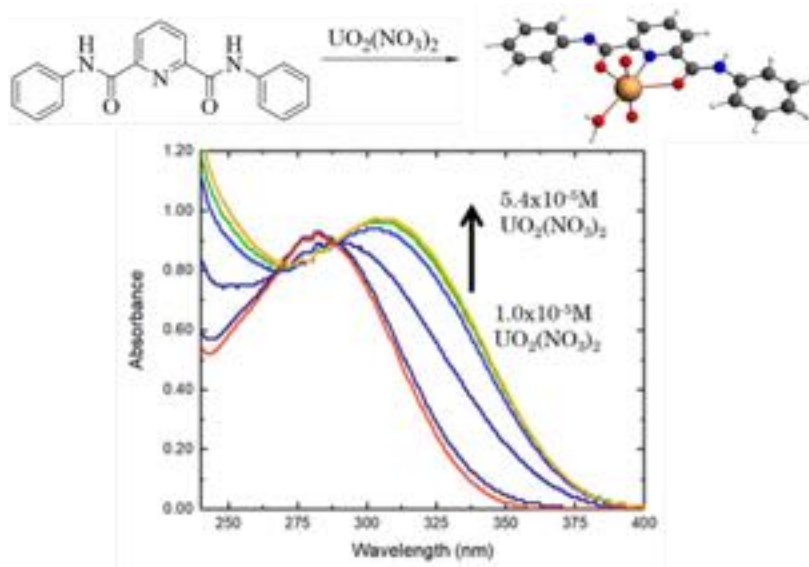
CHAPTER V

Investigation of Uranyl (UO_2^{2+}) U-O and U-S bonding interaction:

Complexation by the Dipicolinamide and Dithiopicolinamide Ligands as Probes for Complexation of AmO_2^{2+}

Jing Su^a, Ingrid Lehman-Andino^b, Teresa Eaton^c, Ping Yang^{a,*}, Enrique R. Batista^a, John K. Gibson^{c,*}, Jonathan Martens^d, Christopher J. Dares^b, and Konstantinos Kavallieratos^{b*}

^aTheoretical Division, Los Alamos National Laboratory, USA (LANL). ^bDepartment of Chemistry and Biochemistry and Biomolecular Sciences Institute, Florida International University, USA. ^cChemical Sciences Division, Lawrence Berkeley National Laboratory, USA (LBNL). ^dFELIX Facility, Radboud University, Netherlands.



This work was performed in collaboration with: Jing Su, Ping Yang and Enrique R. Batista Theoretical calculations from LANL. The Gas-phase CID experiments were performed John K. Gibson and Teresa Eaton at LBNL. Multiphoton FT-IR dissociation spectra were collected at FELIX Lab Netherlands (J. Gibson and J. Martens).

5.1 Abstract

The study and understanding of the fundamental chemistry of actinides and lanthanides with O- and S- donor ligands, is critical for separations related to nuclear energy sustainability. Dipicolinamides and dithiopicolinamides have demonstrated excellent potential for actinide separation and *f*-element coordination chemistry. Herein we report an experimental and theoretical study of uranyl complexation with isostructural O- and S-dipicolinamide and dithiopicolinamide ligands. UV-Vis titration experiments in MeCN were carried out to characterize the structures and to validate calculated thermodynamic properties. Gas-phase complexation properties were measured through collision-induced dissociation (CID) experiments, and infrared multiphoton dissociation spectroscopy, corroborated by density functional theory calculations. Consistent with experimental findings, theoretical calculations show that (*N'*,*N''*-diphenyl)pyridine-2,6-dicarboxamide (**1**) has a stronger binding affinity for UO_2^{2+} than (*N'*,*N''*-diphenyl)pyridine-2,6-bis(carbothioamide) (**2**), due to greater steric interactions, while ligand **2** forms stronger orbital interactions with uranyl than ligand **1**.

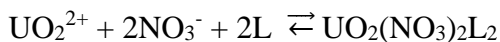
5.2 Introduction

Uranium primarily exists, in aqueous media, as a linear dioxocation with charge 2+ because the stability of the uranium-oxygen bonds tightens the geometric conformation to the planar equatorial region.¹⁻⁴ Recently, research interest in recognition of uranyl ion (UO_2^{2+}) for environmental remediation, water purification, and metallurgical extraction has increased.^{2,3} The chemistry of uranium is also essential in areas such as nuclear fuel reprocessing and treatment of uranium waste, likewise, it can be used as a surrogate for

AmO_2^{2+} because of its specific linear geometry and similarity.³ Oxidation of Am(III) to AmO_2^{2+} provides an alternative pathway for selective separations in the hexavalent state.⁵ In dilute acid, only the Am^{3+} and AmO_2^{2+} are stable (Section 1.1.3). Given the difficulty handling hexavalent americium, uranyl can be used as a surrogate to develop potential new extractants in such cases.⁵

Various reprocessing schemes, such as PUREX, have been established to separate elements that can be reused in reactors, including uranium, plutonium, and neptunium.⁶ These different processes do not separate minor actinides such as Am or Cm, where americium is of particular concern (Section 1.1.2). If Am is allowed to remain in the waste, it will constitute the majority of the long-term heat load and radiotoxicity.⁷⁻¹⁰ Therefore, there is a pressing need to develop materials and molecules that can efficiently separate americium from lanthanides. This includes understanding the bonding properties of actinides with ligands to aid in the development of new extractants.

Previous studies have shown monoamide ligands can extract and complex UO_2^{2+} under mildly acidic conditions through the following reaction mechanism:^{1,11}



Bonding mechanisms of uranium (VI) are usually ionic and preferred complexation takes place through the oxygen donor atoms.¹ Compensation of the metal cation with the anionic charge of nitrates occurs when complexes form. Monoamides facilitate the extraction of the uranyl ion with the carbonyl group, but there is a requirement for charge balance from the two nitrate ions as well as two extractant molecules positioned on opposing sides of the

formed $\text{UO}_2(\text{NO}_3)_2$ complex.¹ Previously reported dipicolinamides containing two amide groups which are more rigid relative to those seen in monoamides and can exhibit differences in characteristics such as bond lengths and angles due to the allowed geometry of the entire complex, thus making them candidates for further studies on uranyl complexation (Figure 5.1).^{1,4,12-14}

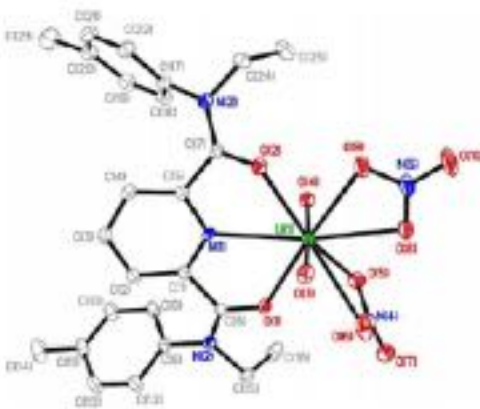
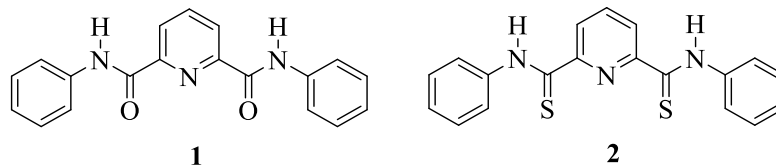


Figure 5.1. X-ray structure of dipicolinamide complex with $\text{UO}_2(\text{NO}_3)_2$, as previously reported by Lapka *et al.*¹

The O- and S- donor ligands under investigation were previously studied for Am(III)/Ln(III) separation under acidic conditions (Chapter 2). Chemical bonding analyses show a dominated U-O / U-S σ bonding between uranyl and ligand **1** and **2**, respectively. The S-donor ligand **2** was shown to have a better actinide/lanthanide separation efficiency than the ligand **1** due to stronger orbital interactions. Herein, UV-visible spectroscopy, gas-phase collision-induced dissociation (CID) experiments, and infrared multiphoton dissociation spectroscopy, corroborated by density functional theory calculations, elucidate the coordination structure, binding energy, and chemical bonding of **1** and **2** with UO_2^{2+} .



Scheme 5.1. Molecular structure of ligands N',N''-diphenylpyridine-2,6-dicarboxamide (**1**) and N',N''-diphenylpyridine-2,6-bis(carbothioamide) (**2**).

5.3 Results and discussion

To evaluate the binding of uranyl to ligands **1** vs. **2**, a UV-Vis titration study was undertaken, in which CH₃CN solutions of ligand (8.0×10^{-5} M) were titrated with UO₂(NO₃)₂·6H₂O (4.4×10^{-3} M) at constant concentration of **1** or **2**. For **1**, the titration showed a gradual decrease of the ligand absorption band at 282 nm with a concurrent appearance of a new strong absorption at 310 nm and two isosbestic points (Figure 5.2).

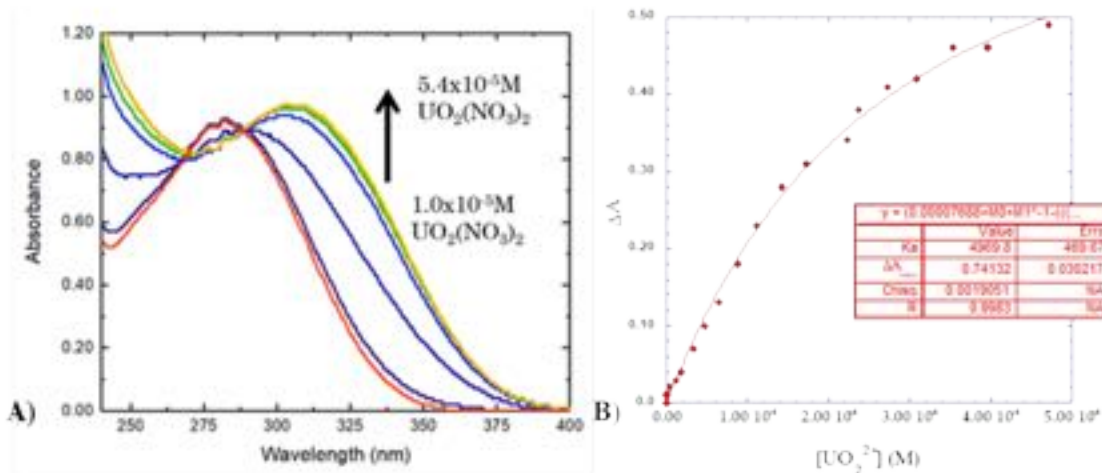


Figure 5.2. (A): UV-visible titration of Ligand **1** (8.0×10^{-5} M) with UO₂(NO₃)₂·6H₂O (4.4×10^{-3} M). (B): ΔA (310 nm) vs. [UO₂²⁺]_t for titration of **1** (7.7×10^{-5} M) with UO₂(NO₃)₂·6H₂O (3.0×10^{-3} M), with fitting showing the binding constant $K_a = 4970$ M⁻¹.

The new absorption is not due to uranyl itself and is ascribed to the formation of a uranyl-**1** complex in solution.¹² Repetition of experiment with a slightly more dilute (1.4×10^{-3} M) uranyl solution and monitoring the change in absorbance at 310 nm for the formation of the complex with subsequent non-linear regression analysis and fitting to the 1:1 binding isotherm gave a K_{11} of $4970 (\pm 470) \text{ M}^{-1}$. This strongly suggests the formation of the 1:1 UO_2^{2+} -**1** complex is dominant under these conditions. Based on prior work by Lapka *et al.*^{1,13} (for uranyl nitrate) and Duval *et al.*⁴ (for uranyl chloride) and the fact that the complex is soluble in CH_3CN , it is reasonable to assume that two nitrates are also coordinated to the uranyl with the complex having the overall formula $[\text{UO}_2(\text{NO}_3)_2(\mathbf{1})]$. Nevertheless, the presence of CH_3CN in the coordination sphere of uranyl is also a possibility. In sharp contrast with **1**, titrations with **2** under identical conditions, did not give any significant changes at the UV-Vis spectrum, with the absorption of the **2** at 311 nm maintained upon titration, suggesting no measureable complex formation between **2** and UO_2^{2+} or, alternatively much weaker complexation under these conditions.

A theoretical and experimental study including first-principle theory (at LANL), and gas-phase CID (At LBNL) and IRMPD experiments (at FELIX lab, Netherlands), was performed in order to investigate the structures of uranyl complexes with neutral and mono-deprotonated ligands **1** or **2** (Scheme 5.1), i.e., **1**, **1-H**, **2** and **2-H**, and the binding ability of ligands, and the nature of metal-ligand bonding. Specifically, the gas-phase uranyl complexation, on figure 5.3, shows formation of these uranyl complexes; $\text{UO}_2(\text{L})_2^{2+}$, $\text{UO}_2(\mathbf{1})(\mathbf{2-H})^+$, $\text{UO}_2(\mathbf{1-H})(\mathbf{2})^+$, $\text{UO}_2(\text{L-H})^+$, $\text{UO}_2(\text{L-H})(\text{H}_2\text{O})^+$ and $\text{UO}_2(\text{L})(\text{OH})^+$ ($\text{L}=\mathbf{1}, \mathbf{2}$), as they are involved in ESI, CID and/or IRMPD experiments.

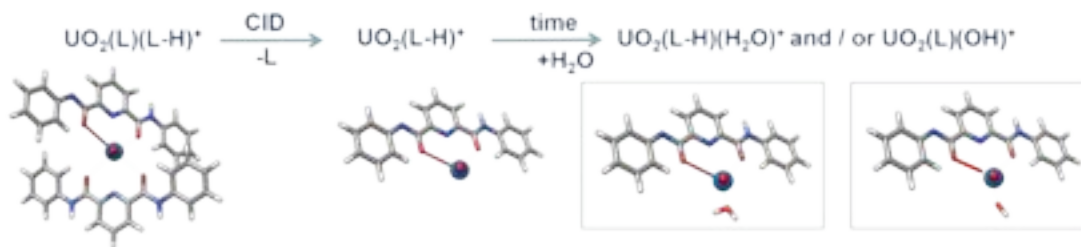


Figure 5.3. Gas-phase Collision Induced Dissociation (CID), uranyl complexes with neutral and deprotonated ligand studies demonstrated both 1:1 and 2:1 ligand: metal ratios for both ligands (LBL).

The optimized geometrical structures (Figure 5.4) were compared with experimental IR spectra and available crystal structure data, and a good agreement was achieved. The relative binding ability of **1** versus **2** was evaluated by calculating the thermodynamics of ligand dissociation reactions. The calculation results are consistent with the Electro Spray Ionization (ESI) species and the relative abundance of the Collision Induced Dissociation (CID) products. The bonding interaction between uranyl and ligands **1** or **2** was analyzed to understand the nature of U-O and U-S bonds. The U-S orbital interaction is stronger than U-O orbital interaction suggesting that ligands of type **2** have potential applications in actinide/lanthanide separation.

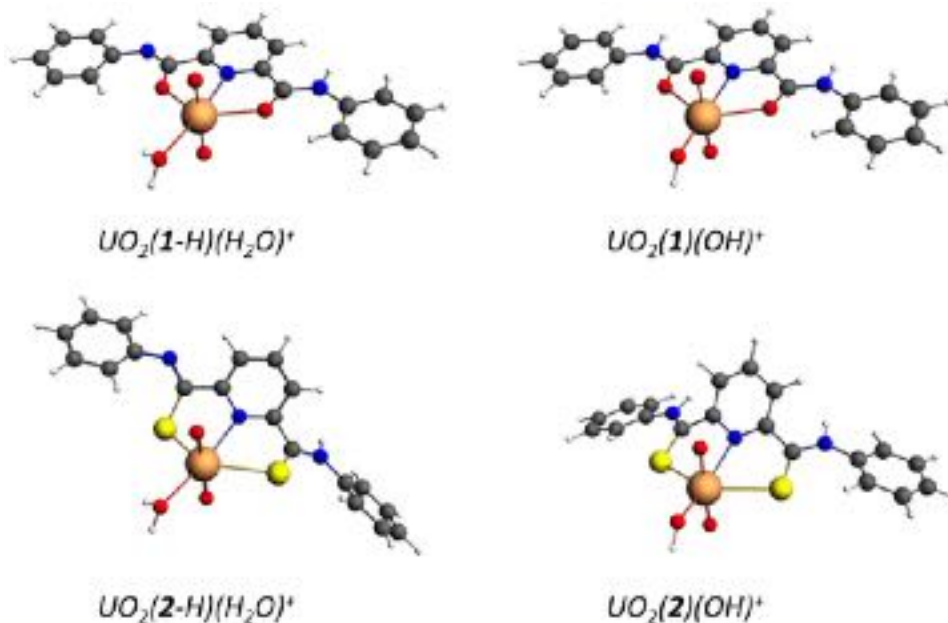


Figure 5.4. Optimized geometrical structures of $\text{UO}_2(\text{L-H})(\text{H}_2\text{O})^+$ and $\text{UO}_2(\text{L})(\text{OH})^+$ ($\text{L}=\mathbf{1},\mathbf{2}$), as derived by DFT calculations (LANL).

Multiphoton FT-IR dissociation spectra (Figure 5.5) were collected for **1** and uranyl at FELIX Lab Netherlands (Drs. Gibson and Martens). The frequency shift for uranyl asymmetric stretch indicates the ligand-uranyl interaction for the same charge state. Stronger bonding produces a more significant red-shift. The large red-shifts in ν_3 relative to bare uranyl (UO_2^{2+} $\nu_3 \approx 1100 \text{ cm}^{-1}$) indicate substantial charge transfer and strong binding of **1** to uranium. Studies with **2** could not be performed, due to time limitations at FELIX lab. The gas-phase ESI-CID-MS studies, together with multiphoton FT-IR spectroscopy and theory, showed evidence of 1:1 and 1:2 UO_2^{2+} /ligand complexation with an agreement between experimental and theoretical spectra. The computed structure and bonding for uranium and **1** was confirmed by isolating $\text{UO}_2(\mathbf{1})_2^{2+}$ in the gas phase and acquiring its IRMPD spectrum. The comparison between the experimental and the calculated IR spectra of $\text{UO}_2(\mathbf{1})_2^{2+}$ is displayed in Figure 5.5. The IR absorption peaks at

750, 968, and 1006 cm^{-1} are assigned to benzene ring C-H bending, O=U=O antisymmetric stretch, and pyridine ring symmetric breathing modes, respectively. The three strong peaks in the range of 1500 to 1650 cm^{-1} are assigned to amide N-H bending, the coupling of pyridine C=C stretching and C=N stretching, and C=O stretching modes, respectively.

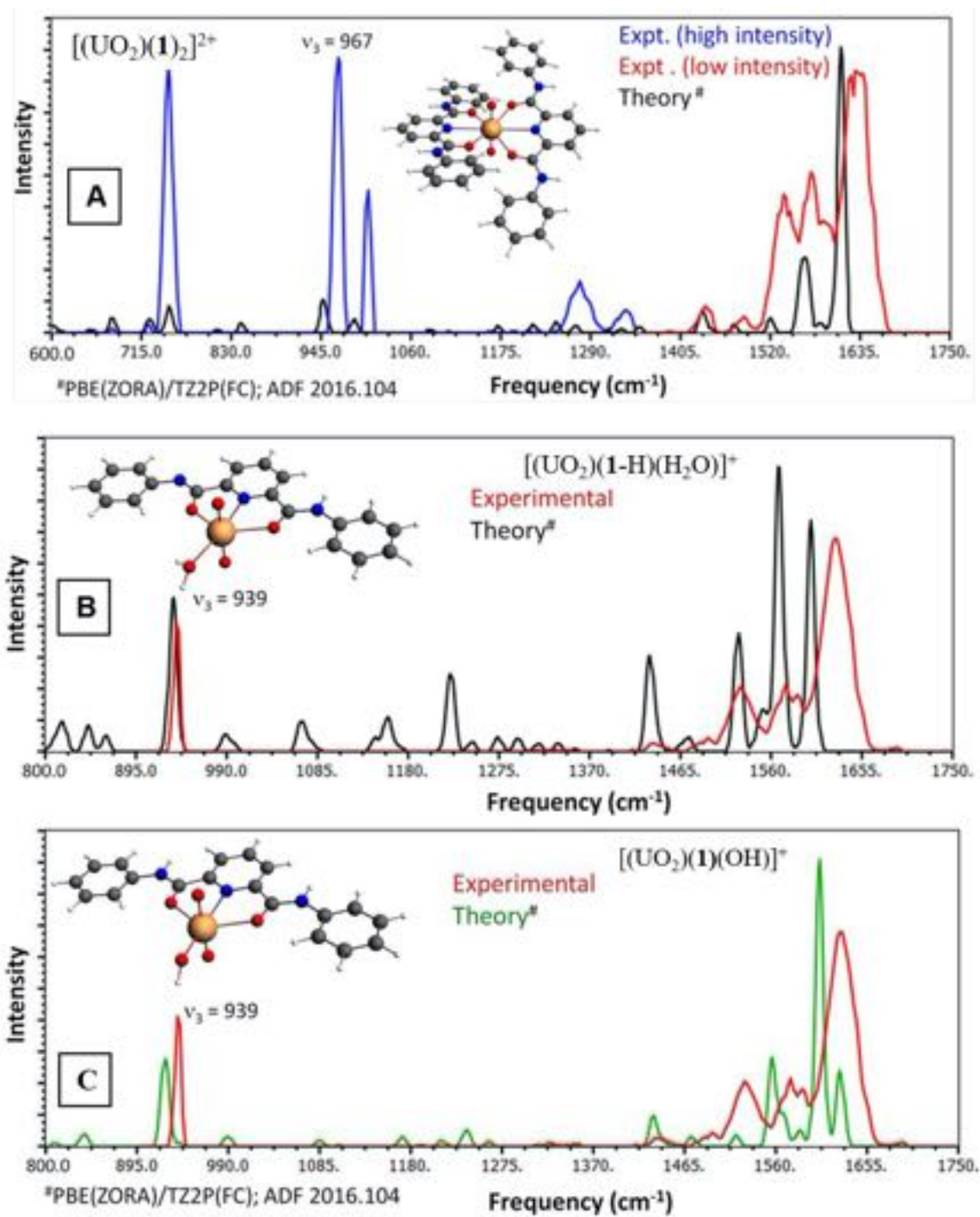


Figure 5.5. FT-IR Multiphoton Dissociation Spectra – A. Free electro-laser $[(\text{UO}_2)(\mathbf{1})_2]^{2+}$ infrared spectra. B. Infrared spectra of $[(\text{UO}_2)(\mathbf{1-H})(\text{H}_2\text{O})]^+$ C. Infrared spectra $[(\text{UO}_2)(\mathbf{1})(\text{OH})]^+$. (FELIX Lab, Netherlands)

FT-IR solvent drop grinding experiments were performed with ligand **1** and **2** with a drop of MeCN to confirm ligand-uranyl interaction (Figure 5.6). The pyridine ring vibrations for ligands **1** and **2** (red line on A and B) appear at 995 cm^{-1} (breathing) and 640 cm^{-1} (in-plane) for the free ligands.⁴ If any interaction between **1** and **2** and uranyl the pyridine ring vibration bands are expected to be observed at higher wavenumbers. In the spectra for the ligand:uranyl mixture (blue), we can observe a shift to 1041 cm^{-1} (**1**) and 1039 cm^{-1} (**2**) (breathing) vibrations and at 755 cm^{-1} (**1**) 750 cm^{-1} (**2**) (in-plane). The infrared spectra indicated bonding or interaction of the pyridine nitrogen to the metal ions of UO_2^{2+} for both ligands **1** and **2**.

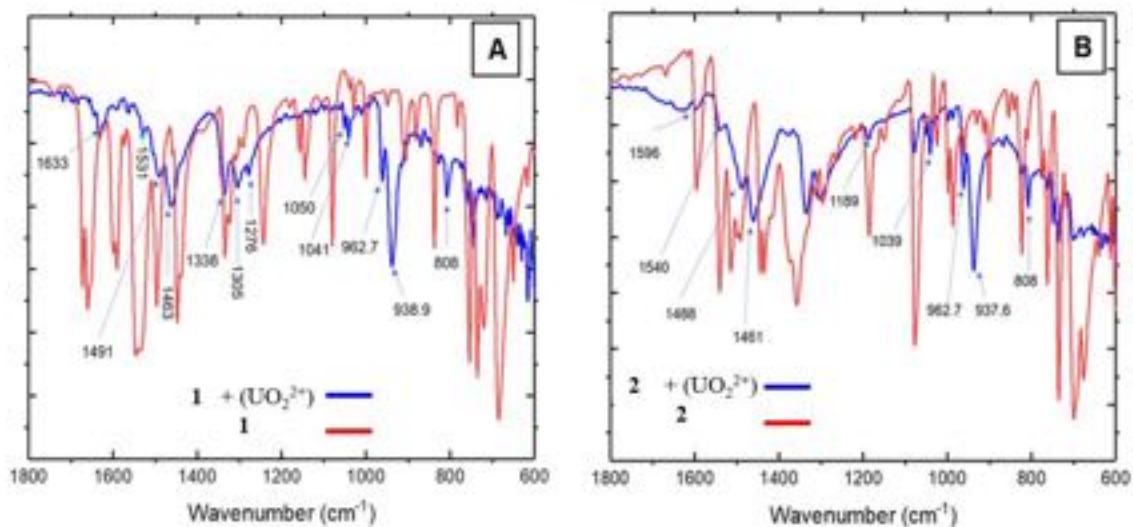


Figure 5.6. FT-IR solvent drop grinding experiments: A) Ligand **1** with $\text{UO}_2(\text{NO}_3)_3 \cdot 6\text{H}_2\text{O}$ B) Ligand **2** with $\text{UO}_2(\text{NO}_3)_3 \cdot 6\text{H}_2\text{O}$ vs. spectra of **1** and **2**.

5.4 Experimental section

5.4.1 Materials and Methods

All chemicals were purchased from Aldrich Chemical Company or ACROS Organics, were standard reagent grade and were used without further purification unless otherwise noted. (*N'*, *N''*-diphenyl)pyridine-2,6-dicarboxamide (**1**) was prepared from 2,6-pyridinedicarbonyl dichloride and aniline in DMF by a modification of a previously published procedure and was found spectroscopically identical to the published compound.^{14,15} (*N'*,*N''*-diphenyl)pyridine-2,6-bis(carbothioamide) (**2**) was prepared from **1** by improving a previously published method involving a reaction with Lawesson's reagent in toluene, and was found to be spectroscopically identical to the reported compound.¹⁵⁻¹⁷ ¹H and ¹³C NMR spectra recorded on a 400 MHz Bruker NMR spectrometer and referenced to the residual solvent resonances. All chemical shifts, δ , are reported in ppm. UV-Vis spectra on a Cary 100 UV-visible spectrophotometer. The gas phase experiments were performed using an Agilent 6340 quadrupole ion trap mass spectrometer (QIT/MS) with the ESI source located inside a radiological containment glovebox.¹⁸

5.4.2 UV-Visible titrations

Solutions of ligands **1** or **2** in CH₃CN were titrated with UO₂(NO₃)₂·6H₂O at constant ligand concentration. In a typical experiment, a solution of **1** (7.6×10^{-5} M) in CH₃CN (solution A) was titrated with a solution of UO₂(NO₃)₃·6H₂O (1.4×10^{-3} M) (solution B) prepared by dilution with solution A in a 5.00 mL volumetric flask, thus keeping a constant concentration of ligand upon titration of solution A with solution B. 2 mL of solution A were added to the UV-visible cuvette and solution B was added in 2-150 μ L increments

until a total of 1000 μL had been added. The absorbance changes were monitored, with the results plotted and fitted to the 1:1 binding isotherm (Equation 2) using non-linear regression analysis:

$$\Delta A = A_{\text{obs}} - A_2 = \frac{([\mathbf{1}]_t + [\mathbf{X}^-]_t + K_a^{-1} - ((([\mathbf{1}]_t + [\mathbf{X}^-]_t + K_a^{-1})^2 - 4[\mathbf{X}^-]_t [\mathbf{1}]_t)^{1/2})) \Delta A_{\text{max.}}}{2[\mathbf{1}]_t} \text{ (Eq.2)}$$

5.4.3 Solvent drop grinding Infrared spectroscopy

FT-IR experiments were performed in solid state (ATR mode) with ligand **1** or **2** with $\text{UO}_2(\text{NO}_3)_2 \cdot 6\text{H}_2\text{O}$ and one or two drops of acetonitrile. Ligand **1** (0.004 mmol) or **2** (0.003 mmol) in one drop of CH_3CN were grinded with $\text{UO}_2(\text{NO}_3)_3 \cdot 6\text{H}_2\text{O}$ (0.020 mmol) for 30 min in a mortar and pestle. When the solid is completely dry, infrared spectra were collected.

5.4.4 Gas-phase experiments (CID-ESI-MS) and infrared multiphoton dissociation spectroscopy

The gas-phase cation complex of interest was isolated and subjected to collision-induced dissociation (CID) whereby ions are excited and undergo multiple energetic collisions with helium to ultimately induce dissociation. As discussed elsewhere, the background H_2O and O_2 pressures in the ion trap are estimated to be on the order of 10^{-6} Torr, while the helium buffer gas pressure in the trap is constant at $\sim 10^{-4}$ Torr.¹⁹ Cation mass spectra were acquired using the following instrumental parameters: solution flow rate, $60 \mu\text{L min}^{-1}$; nebulizer gas pressure, 18 psi; capillary voltage, -3500 V; end plate voltage offset, -500 V; dry gas flow rate, 4 L/min; dry gas temperature, $325 \text{ }^\circ\text{C}$; capillary exit, 94.0 V; skimmer, 40.0 V; octopole 1 and 2 dc, 12.0 and 1.7 V; octopole RF amplitude,

171.0 Vpp; lens 1 and 2, -5.0 and -60.0 V; trap drive, 52.0. The high-purity nitrogen gas for nebulization and drying in the ion transfer capillary was the boil-off from a liquid nitrogen Dewar. Infrared multiphoton dissociation spectroscopy (IRMPD) of complexes acquired by coupled to Fourier transform ion cyclotron resonance mass spectrometry (FTICR-MS) using the high-intensity tunable FELIX IR laser.

5.4.5 Computational details

DFT calculations were performed on the following uranyl-**1/2** complexes: $\text{UO}_2(\text{L})_2^{2+}$ ($\text{L}=\mathbf{1}, \mathbf{2}$, see scheme 5.1), the deprotonated complexes $\text{UO}_2(\mathbf{1})(\mathbf{2}\text{-H})^+$ and $\text{UO}_2(\mathbf{1}\text{-H})(\mathbf{2})^+$ produced by ESI experiment, and ligand loss products $\text{UO}_2(\text{L}\text{-H})^+$, and one water addition complexes $\text{UO}_2(\text{L}\text{-H})(\text{H}_2\text{O})^+ / \text{UO}_2(\text{L})(\text{HO})^+$. Geometry optimizations were performed by employing the generalized gradient approximation (GGA) with the PBE²⁰ exchange-correlation functional as implemented in the Amsterdam Density Functional (ADF 2016.104).²¹ The Slater basis sets with the quality of triple- ζ plus two polarization functions (TZ2P) were used.^{22,23} The frozen core approximation was applied to the $[1s^2\text{-}4f^{14}]$ cores of U, and $[1s^2]$ cores of C, N, and O, and $[1s^2\text{-}2p^6]$ core of S, with the rest of the electrons, explicitly treated fluctuational. All the geometric structures were fully optimized by DFT/PBE at the scalar-relativistic (SR) zero-order-regular approximation (ZORA)²³ with the gradient convergence of 10^{-4} . The optimized structures were confirmed to be true minima by analytical vibrational frequency calculations. To verify the accuracy of PBE energies, single-point PBE0²¹ calculations were performed on PBE optimized ground-state geometries with all-electron TZ2P basis sets. Chemical bonding analyses were performed with the energy decomposition approach (EDA)²⁴ to evaluate the relative importance of

steric repulsion and orbital interactions between uranyl fragment and **1/2** ligand fragment in the $\text{UO}_2(\text{L})_2^{2+}$ compounds. And the U-O, -S, -N σ and/or π bonding components in the orbital interaction was further analyzed using an extended transition state energy decomposition scheme combined with the natural orbitals for chemical valence (ETS-NOCV).²⁵

5.5 Conclusion:

Experimental and theoretical data confirm stronger UO_2^{2+} binding affinity of **1** vs. **2**. Both theory and solution UV-Vis spectra for **1** or **2** with uranyl nitrate show a spectral change for **1** that is more pronounced than for **2**. Moreover, as we also observe on our previously reported dipicolinamide and dithiopicolinamide work (Chapter 2) the S-donor ligand **2** has a weaker binding affinity, but a stronger orbital interaction (or σ bonding).¹⁵ This enhanced bonding interaction with uranyl (used as AmO_2^{2+} surrogate) is also key in giving selectivity in actinide/lanthanide separations for **2** vs **1**. Compared to the successful generation of $\text{UO}_2(\mathbf{1})_2^{2+}$ by ESI experiment, the failure to obtain a similar $\text{UO}_2(\mathbf{2})_2^{2+}$ complex may indirectly substantiate weaker binding ability of **2**. Our study provides insights into the fundamental chemistry of O- vs. S-donor ligands with *f*-elements, which may help with new ligand design for extraction and binding of actinides. This provides possible future paths for application to reprocessing of acidic nuclear waste.

5.6 References:

- (1) Lapka, J. L.; Paulenova, A.; Zakharov, L. N.; Alyapyshev, M. Y.; Babain, V. A. Coordination of Uranium(VI) with *N*, *N'*-Diethyl-*N*, *N'*-Ditolyldipicolinamide. *IOP Conf. Ser.: Mater. Sci. Eng.* **2009**, *9*, 012029.
- (2) Ramos, M. L.; Justino, L. L. G.; Barata, R.; Costa, T.; Nogueira, B. A.; Fausto, R.; Burrows, H. D. Oxocomplexes of U(VI) with 8-Hydroxyquinoline-5-Sulfonate in Solution: Structural Studies and Photophysical Behaviour. *Dalton Trans.* **2017**, *46*, 9358–9368.
- (3) Sather, A. C.; Berryman, O. B.; Rebek, J. Selective Recognition and Extraction of the Uranyl Ion. *J. Am. Chem. Soc.* **2010**, *132*, 13572–13574.
- (4) Duval, P. B.; Kannan, S.; Barnes, C. L. Convenient Syntheses of Uranyl(VI) Cis-Dihalide Complexes as Anhydrous Starting Materials. *Inorganic Chemistry Communications.* **2006**, *9*, 426–428.
- (5) Dares, C. J.; Lapidés, A. M.; Mincher, B. J.; Meyer, T. J. Electrochemical Oxidation of ²⁴³Am(III) in Nitric Acid by a Terpyridyl-Derivatized Electrode. *Science.* **2015**, *350*, 652–655.
- (6) Orth, D. A. *Purex: Process and Equipment Performance*; Report DP-MS-86-28; Savannah River Laboratory: Aiken, SC. USA, **1986**.
- (7) Modolo, G.; Wilden, A.; Kaufholz, P.; Bosbach, D.; Geist, A. Development and Demonstration of Innovative Partitioning Processes (*i*-SANEX and *I*-Cycle SANEX) for Actinide Partitioning. *Progress in Nuclear Energy* **2014**, *72*, 107–114.
- (8) Whittaker, D. M.; Griffiths, T. L.; Helliwell, M.; Swinburne, A. N.; Natrajan, L. S.; Lewis, F. W.; Harwood, L. M.; Parry, S. A.; Sharrad, C. A. Lanthanide Speciation in Potential SANEX and GANEX Actinide/Lanthanide Separations Using Tetra-*N*-Donor Extractants. *Inorg. Chem.* **2013**, *52*, 3429–3444.
- (9) Bhattacharyya, A.; Mohapatra, P. K.; Manchanda, V. K. Separation of Americium(III) and Europium(III) from Nitrate Medium Using a Binary Mixture of Cyanex-301 with *N*-donor Ligands. *Solvent Extraction and Ion Exchange* **2006**, *24*, 1–17.
- (10) Veliscek-Carolan, J. Separation of Actinides from Spent Nuclear Fuel: A Review. *Journal of Hazardous Materials* **2016**, *318*, 266–281.

- (11) Pathak, P. N.; Kumbhare, L. B.; Manchanda, V. K. Effect of Structure of *N,N*-Dialkyl Amides on the Extraction of U(VI) and Th(IV): A Thermodynamic Study. *Radiochimica Acta*. **2001**, *89*, 447–452.
- (12) Suleimenov, O. M.; Seward, T. M.; Hovey, J. K. A Spectrophotometric Study on Uranyl Nitrate Complexation to 150 C. *J. Solution Chem.* **2007**, *36*, 1093–1102.
- (13) Lapka, J. L.; Paulenova, A.; Alyapyshev, M. Yu.; Babain, V. A.; Herbst, R. S.; Law, J. D. Extraction of Uranium(VI) with Diamides of Dipicolinic Acid from Nitric Acid Solutions. *Radiochimica Acta International journal for chemical aspects of nuclear science and technology*. **2008**, *97*, 291–296.
- (14) Zhang, X.; Yuan, L.; Chai, Z.; Shi, W. A New Solvent System Containing *N,N'*-Diethyl-*N,N'*-Ditolyl-2,9-Diamide-1,10-Phenanthroline in 1-(Trifluoromethyl)-3-Nitrobenzene for Highly Selective UO_2^{2+} Extraction. *Separation and Purification Technology*. **2016**, *168*, 232–237.
- (15) Lehman-Andino, I.; Su, J.; Papathanasiou, K. E.; Eaton, T. M.; Jian, J.; Dan, D.; Albrecht-Schmitt, T. E.; Dares, C. J.; Batista, E. R.; Yang, P.; Gibson, J. K.; Kavallieratos, K. Soft-Donor Dipicolinamide Derivatives for Selective Actinide(III)/Lanthanide(III) Separation: The Role of S- vs. O-Donor Sites. *Chem. Commun.* **2019**, *55*, 2441–2444.
- (16) Malone, J. F.; Murray, C. M.; Dolan, G. M.; Docherty, R.; Lavery, A. J. Intermolecular Interactions in the Crystal Chemistry of *N,N'*-Diphenylisophthalamide, Pyridine-2,6-Dicarboxylic Acid Bisphenylamide, and Related Compounds. *Chem. Mater.* **1997**, *9*, 2983–2989.
- (17) Komiyama, Y.; Kuwabara, J.; Kanbara, T. Deprotonation-Induced Structural Changes in SNS-Pincer Ruthenium Complexes with Secondary Thioamide Groups. *Organometallics*. **2014**, *33*, 885–891.
- (18) Suzuki, T.; Kajita, Y.; Masuda, H. Deprotonation/Protonation-Driven Change of the σ -Donor Ability of a Sulfur Atom in Iron(II) Complexes with a Thioamide SNS Pincer Type Ligand. *Dalton Trans.* **2014**, *43*, 9732–9739.
- (19) Rios, D.; Rutkowski, P. X.; Shuh, D. K.; Bray, T. H.; Gibson, J. K.; Van Stipdonk, M. J. Electron Transfer Dissociation of Dipositive Uranyl and Plutonyl Coordination Complexes. *J Mass Spectrom.* **2011**, *46*, 1247–1254.

- (20) Rios, D.; Michelini, M. C.; Lucena, A. F.; Marçalo, J.; Bray, T. H.; Gibson, J. K. Gas-Phase Uranyl, Neptunyl, and Plutonyl: Hydration and Oxidation Studied by Experiment and Theory. *Inorg Chem.* **2012**, *51*, 6603–6614.
- (21) Perdew, J. P.; Burke, K.; Ernzerhof, M. Generalized Gradient Approximation Made Simple. *Phys. Rev. Lett.* **1996**, *77*, 3865–3868.
- (22) te Velde, G.; Bickelhaupt, F. M.; Baerends, E. J.; Guerra, C. F.; Van Gisbergen, S. J. A.; Snijders, J. G.; Ziegler, T. Chemistry with ADF. *J. Comput. Chem.* **2001**, *22*, 931–967.
- (23) Lenthe, E. van; Leeuwen, R. van; Baerends, E. J.; Snijders, J. G. Relativistic regular two-component Hamiltonians. *International Journal of Quantum Chemistry.* **1996**, *57*, 281–293.
- (24) Lenthe, E. V.; Baerends, E. J. Optimized Slater-Type Basis Sets for the Elements 1–118. *Journal of Computational Chemistry.* **2003**, *24*, 1142–1156.
- (25) Ziegler, T.; Rauk, A. On the Calculation of Bonding Energies by the Hartree Fock Slater Method. *Theoret. Chim. Acta.* **1977**, *46*, 1–10.
- (26) Mitoraj, M. P.; Michalak, A.; Ziegler, T. A Combined Charge and Energy Decomposition Scheme for Bond Analysis. *J. Chem. Theory Comput.* **2009**, *5*, 962–975.

Chapter VI: General Conclusions

In this work, we have shown the role of dipicolinamide and dithiopicolinamide ligands in An(III)/Ln(III) separations and for toxic metal separation and sensing. We have investigated and demonstrated the binding and extraction properties of these ligands, establishing a comparison between the dipicolinamide (C=O) and the dithiopicolinamide (C=S), and showing how the soft-character of dithiopicolinamides can facilitate selective An(III)/Ln(III) separations and Hg(II) sensing. In Chapter II, we reported that the *S*-donor dithiopicolinamide ligand selectively extracts Am(III) over Ln(III) from highly acidic solutions. We also reported the gas-phase studies and theoretical DFT calculations; both showing stronger binding of An(III) *vs.* Ln(III) for the dithiopicolinamide *vs.* the dipicolinamide ligand in agreement with extraction results. These results lead us to conclude that the dithiopicolinamide ligand has suitable properties for selectively extracting Am(III) from acidic solutions with moderate to high separation factors in comparison to the amide analog. We accomplished excellent Am(III)/Eu(III) separation as well as a thorough understanding of *S*- vs *O*- site interactions with *f*-elements.

The dipicolinamide ligand was modified by structural changes for aqueous solubility (Chapter III). A selective dipyrindine-dipicolinamide (*N',N''*-bis(pyridin-2-ylmethyl)pyridine-2,6-dicarboxamide) was confirmed to act as a selective holdback reagent for Am(III) in the aqueous phase taking advantage of the difference on hardness between An(III) and Ln(III), while HDEHP complexes Ln(III) in the organic phase. The solvent extraction, UV-Vis, and gas-phase ESI-MS studies demonstrate a preferential binding of this ligand towards Am(III) at acidic conditions and effective separation for pH as low as 1.4. Strong selectivity for ²⁴¹Am *vs.* Eu(III) and Ce(III) was demonstrated even

at very low pHs of 0.5-2.0, with Eu/Am separation factors between 27 and 74 at TALSPEAK-like conditions. Slope analysis shows that a 3:1 ligand to metal binding stoichiometry is preferred for these dipicolinamide frameworks. This work suggests that the addition of soft-donor nitrogen atoms within appended pyridine groups increases the separation selectivity of dipicolinamide ligands towards An(III).

In Chapter IV, we exploited the ability of the dithiopicolinamide ligand (N^2, N^6 -diphenyl-2,6-pyridinedicarbothioamide) for sensing Hg(II). As Hg is present in the nuclear waste tanks at the Savannah River Site in several forms, including organic Hg, the mercury problem has been of concern. Specifically, we concluded that this thioamide ligand can extract and sense Hg(II) even in the presence of Na(I), K(I), Cs(I), Ca(II), and Sr(II) in alkaline conditions. The X-ray structure of this ligand with HgCl₂ shows a unique dinuclear complex, with coordination also confirmed by NMR and UV-Vis titrations, and a binding constant of $1.5 (\pm 0.9) \times 10^{16} \text{ M}^{-3}$.

Finally, in Chapter V, we reported a study that combines FT-IR, UV-Vis, ESI-MS, and DFT theoretical calculations to elucidate the binding properties of the dipicolinamide and dithiopicolinamide ligands with uranyl (UO_2^{2+}), used as surrogate for AmO_2^{2+} . Experimental and theoretical data confirm stronger binding of C=O vs. C=S ligand to uranyl, but a stronger orbital interaction (or σ bonding) for the dithiopicolinamide C=S ligand. Understanding the fundamental chemistry of O- vs. S-donor ligands with f -elements may help with new ligand design for the efficient extraction and binding of minor actinides.

In conclusion, the dipicolinamide and dithiopicolinamide ligands studied and presented over the five chapters of this dissertation can be used as potential An(III)/Ln(III) separation

extractants for used nuclear fuel. The dipicolinamide framework has been previously investigated, but we were now able to demonstrate successfully that the dithiopicolinamide framework, which has not been studied before, can achieve higher separation selectivity towards actinides. Moreover, the addition of nitrogen atoms to the dipicolinamide ligand, as appended pyridine groups, can increase selectivity towards An(III) by increasing the softness of the molecule. Overall this work demonstrates the capability of these ligands for An(III)/Ln(III) extraction and efficient separations. Furthermore, these dithiopicolinamide ligands have a potential impact on the alkaline mixed waste for separation and sensing of Hg(II). Further modification of these ligands needs to be achieved to increase the solubility either at organic or aqueous phase. By increasing solubility, the efficiency of the extraction process can be improved with high distribution ratios. Moreover, radiolytic studies of these ligands are needed to understand their stability under used nuclear fuel conditions and to allow practical application. These studies could provide possible future paths for the application of our dipicolinamide and dithiopicolinamide ligands for the reprocessing of acidic used nuclear fuel, as well as with other applications within the nuclear waste management field and beyond.

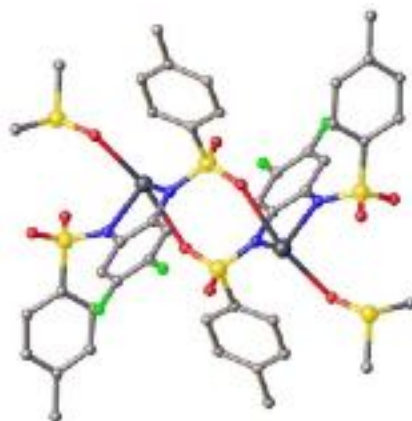
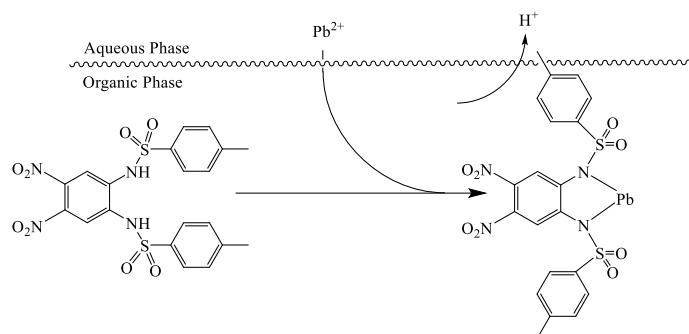
APPENDIX A

Selective Sensing and Binding Properties of Disulfonamide *o*-phenylenediamine Derivatives with Pb(II) and Other Toxic Metals

Ingrid Lehman-Andino, Gabriella G. Peña, Alvio J. Dominguez, Yadira Reynaldo,

Logesh Mathivathanan, Raphael G. Raptis, and Konstantinos Kavallieratos,^{1,*}

Department of Chemistry and Biochemistry, Florida International University, 11200 SW 8th Street, Miami, Florida 33199.



A.1 Abstract:

Selective extraction, sensing, and complexation of Pb(II) and other toxic metals is still a challenging problem. The presence of lead in the environment is a serious health concern. The growing concern for the toxicity of such metals calls upon new methods and techniques for their sensing and detection. Investigating the coordination properties of Pb(II) and other metals with sulfonamide derivatives can provide opportunities for selective sensing, via metal complexation and extraction into an organic phase. The 4-nitro-*N,N'*-bis-*p*-tolylsulphonyl-*o*-phenylenediamine (**1**) and the corresponding Pb(II) complex were successfully synthesized with 40% and 78% yields, respectively. Attempts to synthesize 1,2-Bis-(*p*-methylphenylsulfonamido)-4,5-bis-nitrobenzene (**2**) are also described. The synthesis of the 1,2-Bis-(*p*-methylphenylsulfonamido)-4,5-bis-fluorobenzene (**3**) was achieved and the Pb(II)-**3** complex was successfully isolated and crystallized, with the X-Ray crystal structure showing a dimeric complex. Extraction experiments showed that the mononitro analog **1** is not as capable for Pb(II) optical sensing as the previously studied dinitro derivative **2**. Analysis by ¹H-NMR, UV-Visible, and FT-IR also document Pb(II) complexation.

A.2 Introduction:

Lead (Pb) exposure, even at low levels, is a public health issue. It is the most abundant heavy metal pollutant on earth. Overall several years, researchers have found lead in cosmetics, toys, and paint.¹ Due to the solubility of many Pb(II) salts, divalent lead is the most environmentally mobile form of lead that can interfere with the nervous system and other enzymatic processes.² Thus there is a need to design ligands that can complex and

sense Pb(II) in environmental samples in very small quantities. The extraction, sensing, and complexation of Pb(II) can have many biological and environmental applications.² Recent literature for our group has shown the efficiency of a powerful extraction-based method based on disulfonamide ligands that complex Pb(II) and extract it to the organic phase^{3,4} with a concurrent change in their fluorescence⁵ and optical properties.

Extraction-based sensing of Pb(II) via an ion-exchange mechanism using ionizable chelates is easier, economical, and practical.^{6,7} Pb(II) complexes are formed upon deprotonation of the sulfonamide ligand by an organic base, resulting in metal extraction into an organic phase, and often into a fluorescence and/or optical change.^{3,4} (Figure A.1) In other previous studies, the dansyl group added on the sulfonyl part of the molecule was used as a fluorophore (Figure A.2).⁵ Our group has now undertaken a different approach by modifying the central aromatic ring of the ligand framework, instead, as the optical or fluorescent moiety, in order to increase the effects of binding on optical properties of the ligand.⁵

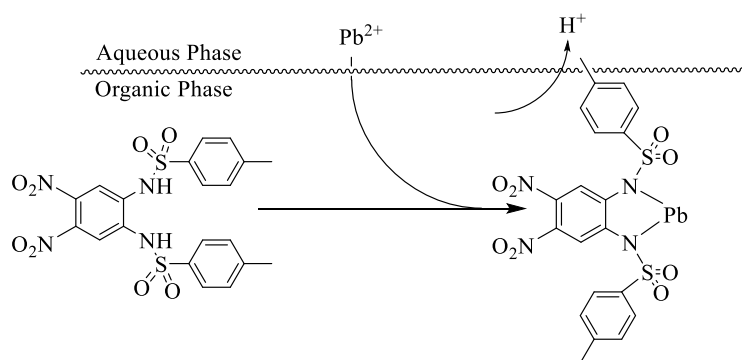


Figure A.1. Extraction-based sensing of Pb(II) via an ion-exchange mechanism using a dinitrosulfonamide analog, which leads to organic layer color-change (colorless to yellow) upon metal complexation.³

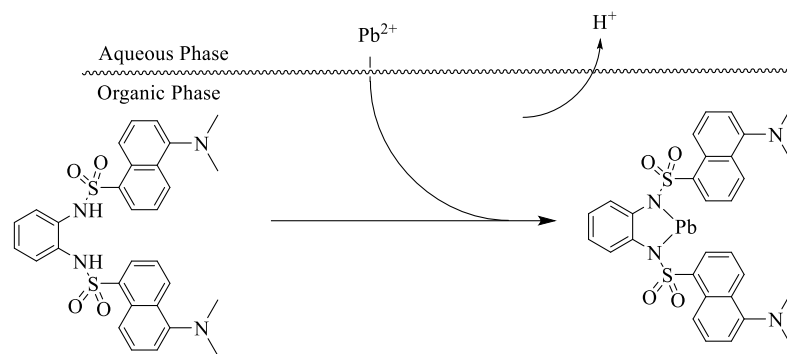


Figure A.2. Extraction-based sensing of Pb(II) via an ion-exchange mechanism using a sulfonamide analog, which leads to fluorescence change in the organic layer (strongly fluorescent to weakly fluorescent) upon metal complexation.⁵

Ligands for selective for Pb(II) have to be designed with special attention to the different geometries that Pb(II) can accommodate because of its unique coordination chemistry.⁸⁻¹⁰ The geometry on Pb(II) is often labeled as “hemidirected” or “holodirected” based on the presence or not, respectively, of a stereochemically active lone pair. Low coordination numbers (2-5) often show the lone pair as stereochemically active and result in a “hemidirected” ligand environment.^{8,11} In contrast, if the complexes have high coordination numbers (6-8) the lone pair will be stereochemically inactive and will result in a “holodirected” geometry. Such complexes often have bulky ligands and soft donors like sulfur or nitrogen.¹¹⁻¹³ Alvarado *et al.*³ demonstrated ionizable disulfonamide chelates, derived from *o*-phenylenediamine, that are successful at binding and extraction of Pb(II) via an ion-exchange mechanism (Figure A.3). Low-coordinate Pb(II) ion-exchangers have been developed for their ability to detect Pb(II) amongst other metals due to their preference for “hemidirected” geometries and a stereochemically active lone pair, which enhances selectivity for Pb(II).^{3,4}

We have now synthesized versatile disulfonamide ion-exchangers derived from *o*-phenylenediamine with electro-withdrawing and electro-donating groups on the main *o*-phenylenediamine central ring for sensing. These disulfonamide ligands are expected to quantitatively extract Pb(II) from H₂O into the organic phase under similar conditions as those previously reported.⁴ In this work it is shown that the ligand 1,2-Bis-(*p*-methylphenylsulfonamido)-4,5-bis-nitrobenzene **2** can act as an extraction-based Pb(II) optical sensor in the presence of 10-fold and 20-fold higher concentrations of Zn(II) and Ca(II), respectively. Work with newly-synthesized ligands **1** and **3** has been carried out under similar conditions.

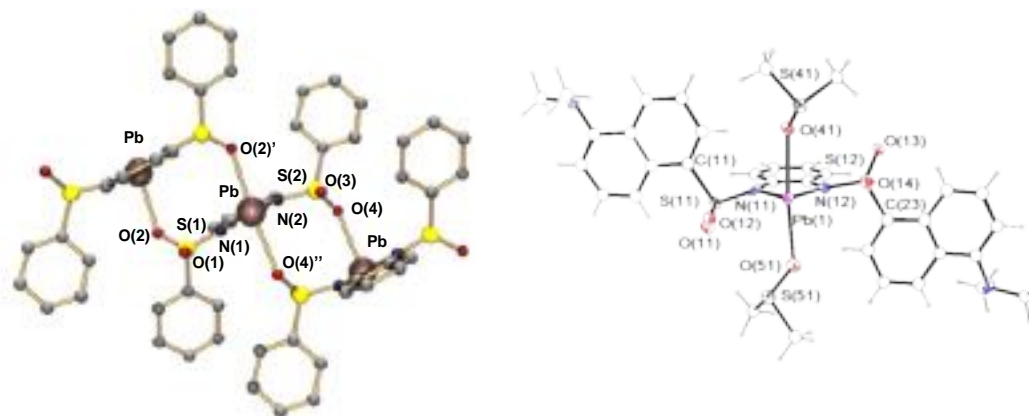


Figure A.3. A (left): PLUTO representation of the extended structure of Pb[1,2-C₆H₄(NSO₂C₆H₅)₂], indicating the formation of a coordination polymer. Hydrogen atoms have been omitted for clarity. B (Right): X-Ray structure of the complex of the dansylated derivative Pb[1,2-C₆H₄(N-dansyl)₂] which gives selective fluorescent sensing. [(dansyl = 5(N,N')-dimethyl amino-naphthylsulfonyl)].^{3,4}

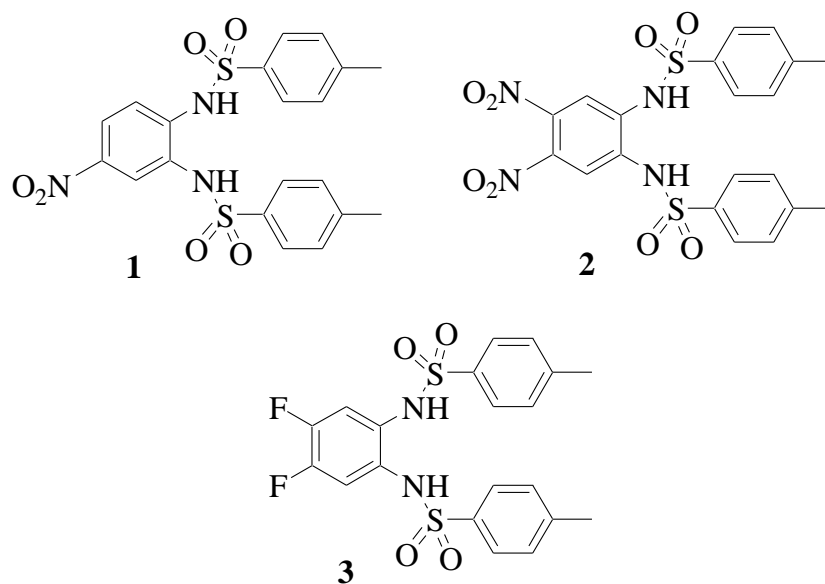


Figure A.4. Molecular structures of studied ligands 4-nitro-N,N'-bis-p-tolylsulphonyl-*o*-phenylenediamine (**1**), 1,2-Bis-(p-methylphenylsulfonamido)-4,5-bis-nitrobenzene (**2**), 1,2-Bis-(p-methylphenylsulfonamido)-4,5-bis-fluorobenzene (**3**).

A.3 Results and discussion

A.3.1 Extraction-based optical sensing by UV-Vis

Extraction-based optical sensing experiments were performed for ligands **1** - **3**. In this two-phase method the ligands are dissolved in CH_2Cl_2 and then is contacted with an aqueous solution of Zn(II), Pb(II), and Ca(II) (as nitrate or chloride salts).

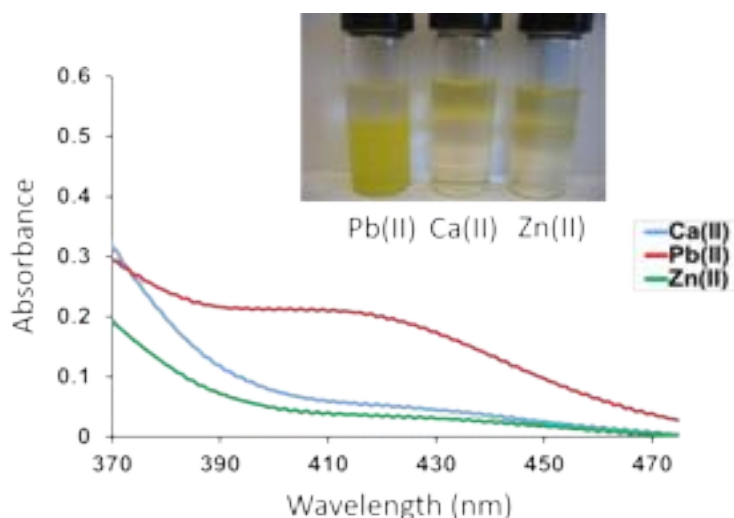


Figure A.5. UV-Vis spectra of **2** (0.0005 M) upon contact with Pb(II) (0.005M) vs. higher concentrations of Ca(II) (0.100 M) and Zn(II) (0.050 M) and a picture of the experiment.

The results (Figure A.5) show selective optical sensing in UV-Vis and an intense color change by dinitro ligand **2** for Pb(II) vs. Ca(II) and Zn(II) at much higher concentrations, (specifically 10-fold and 20-fold). Instead a very slight change in color was observed for **1** (Figure A.6) after addition of Pb(II), under the same conditions. The lack of a significant visible difference between the Pb(II), Ca(II), and Zn(II), even if the same concentrations are used for extraction, indicates no capability of **1** as an optical sensor. Similar results with

ligand **3** were obtained, with no significant spectroscopic changes in the visible region (Figure A.7).

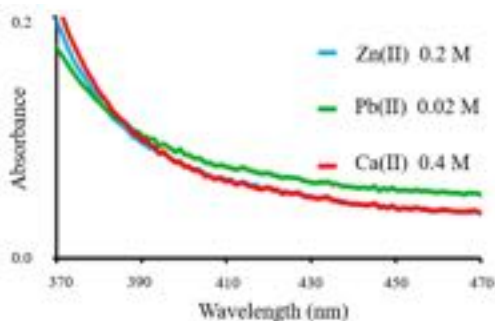


Figure A.6. UV-Vis spectra of **1** (0.002 M) upon contact with Pb(II) (0.02 M), Ca(II) (0.4 M) and Zn(II), 0.2 M).

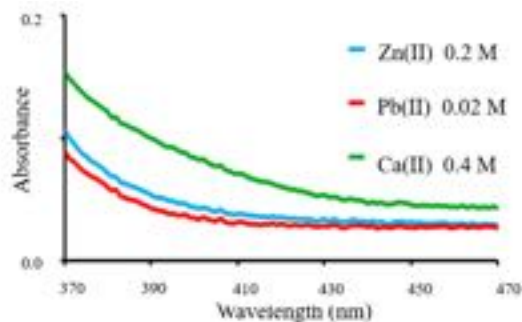


Figure A.7. UV-Vis spectra of **3** (0.002 M) upon contact with Pb(II) (0.02 M), Ca(II) (0.4 M) and Zn(II), 0.2 M).

A.3.2 Pb(II) complexation and X-Ray diffraction studies

The newly reported Pb-**1** complex was isolated and characterized by NMR and FT-IR (Section A.4.2); no crystals were obtained for diffraction analysis. However, ligand **3** and its Pb-**3** complex were successfully isolated and crystallized for X-Ray diffraction analysis. A crystal of ligand **3** was obtained by slow evaporation of methanol over a week. Figure

A.8 shows the diffraction in a triclinic *P-1* space group with a complete molecule in the asymmetric unit.

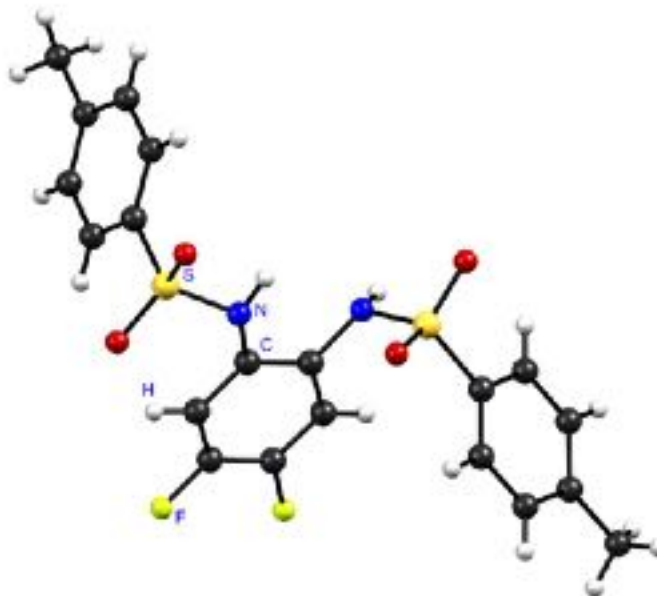


Figure A.8. X-ray diffraction of ligand **3** in a *P-1* space group.

Complex **Pb-3** was also recrystallized by slow evaporation from methanol, and its single crystal X-ray structure revealed a 2:2 metal:ligand neutral complex co-crystallizing with 2 molecules of DMSO. The **Pb-3** complex crystallized in a triclinic *P-1* space group with a complete molecule in the asymmetric unit. This X-Ray diffraction structure of **Pb-3** complex can be compared with the dansylated derivative $\text{Pb}[1,2\text{-C}_6\text{H}_4(\text{N-dansyl})_2]$, which was published by Alvarado in 2005.³ **Pb-3** also exhibits coordination with two DMSO molecules, but the **Pb-3** complex exhibits also a dimer instead of a monomer. The **Pb-3** complex (Fig. A.9) also shows a stereochemically active lone pair on Pb and a hemidirected geometry, consistent with what we observed for disulfonamide derivatives. The distances

between the Pb and the two O atoms of the DMSO molecules (2.501(5) and 2.525(3) Å) are also comparable to the Pb–O distances for the previously dansylated complex published by our research group.³

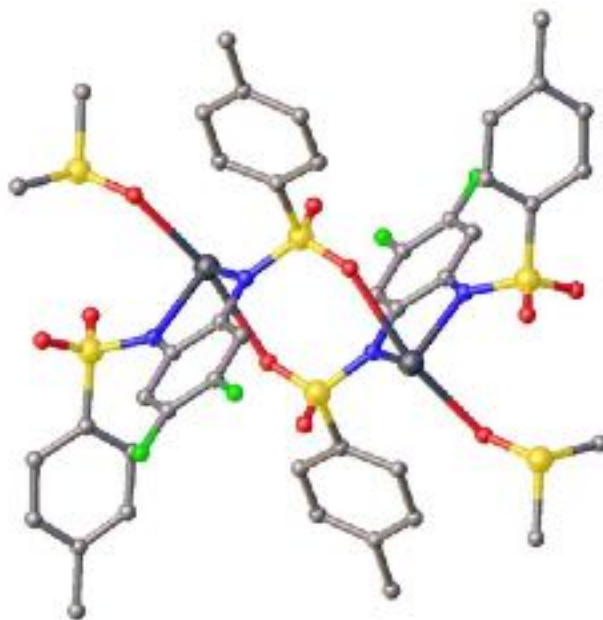


Figure A.9. X-ray crystallography of Pb-3 complex ($3 \cdot [2(\text{CH}_3)_2\text{SO}]$), *P-1* space group. Hydrogen atoms have been omitted for clarity.

A.4 Experimental Section

A.4.1 Materials and Methods

All chemicals and materials were purchased from Aldrich Chemical Co., ACROS Organics, or TCI. All chemicals were standard reagent grade and were used without further purification. $^1\text{H-NMR}$ spectra were recorded on a 400-MHz Bruker NMR spectrometer or on a 600-MHz Bruker NMR spectrometer. All chemical shifts are reported in ppm. UV-

Vis spectra were recorded on an Agilent Technologies Cary 8454 UV-Visible spectrophotometer. Diffractometer Bruker D8 with PHOTON 100 detector.

A.4.2 Synthetic procedures

4-nitro-*N,N'*-bis-*p*-tolylsulphonyl-*o*-phenylenediamine (1)²⁰

A solution of 4-nitro-*o*-phenylenediamine (315.0 mg, 2.10 mmol) and pyridine (1.3 mL, 16.25 mmol) in 20 mL of 1,2-dichloroethane was added dropwise to a solution of *p*-toluene-sulfonylchloride (1.36 g, 7.21 mmol) dissolved in 25 mL of 1,2-dichloroethane. The reaction mixture was refluxed for 72 h and was monitored by TLC (60:40, hexanes/EtOAc). The crude product was washed sequentially with 1 M HCl, 0.5 M NaHCO₃, and deionized H₂O. The resulting organic phase was then separated and dried with granular Na₂SO₄, then volatiles were evaporated, and the solid was recrystallized from MeOH/H₂O to give a brown powder (186.6 mg, 40% yield). ¹H-NMR (400 MHz, CD₂Cl₂) δ (ppm): 7.96 (dd, *J* = 9.0, 2.1 Hz, 1H), 7.80 (s, 1H), 7.73 (d, *J* = 7.8 Hz, 2H), 7.53 (d, *J* = 8.1 Hz, 2H), 7.43 (d, *J* = 9.3 Hz, 2H), 7.30 (t, *J* = 7.4 Hz, 4H), 6.54 (s, 1H), 2.41 (s, *J* = 2.1 Hz, 3H), 2.40 (s, *J* = 2.1 Hz, 3H). FT-IR: N-H, 3239 cm⁻¹; S=O, 1335 cm⁻¹. Other bands (cm⁻¹): 2922, 2857, 1586, 1520, 1446, 1413, 1394, 1278, 1081, 1015, 955, 894, 842, 815, 786, 745, 717, 660.

Pb(II) -1 complex (Pb[4-(NO₂)-1,2-C₆H₄(NSO₂C₆H₅CH₃)₂]):

A solution of Pb(NO₃)₂ (86.5mg, 0.261 mmol) in 10 mL of MeOH was added dropwise to a solution of (52.4 mg, 0.131 mmol) of **1** and NEt₃ (218.9 mg, 2.16 mmol) in 20 mL of MeOH. After stirring for 24 h, the reaction mixture was evaporated until 5 mL remained

and an equal volume of H₂O was added. A yellow-orange precipitate was collected (40.8 g, 78% yield). ¹H-NMR (400 MHz, MeOD) δ (ppm): 7.95 (dd, *J* = 9.8, 8.3 Hz, 4H), 7.55 (d, *J* = 2.5 Hz, 1H), 7.48 (dd, *J* = 9.0, 2.7 Hz, 1H), 7.38 (dd, *J* = 8.2, 3.0 Hz, 4H), 6.75 (d, *J* = 9.0 Hz, 1H), 2.41 (s, 6H). FT-IR: S=O 1273.67 cm⁻¹. Other bands (cm⁻¹): 2913; 1595; 1567; 1483; 1324; 1240; 1120; 1067; 1015; 997; 964; 894; 806; 745; 707; 660; 642.

1,2-Bis-(*p*-methylphenylsulfonamido)-4,5-bis-nitrobenzene (2)²¹

A solid amount of 7.08×10^{-4} mol (294.8 mg) 1,2-bis-*p*-substituted phenylsulfonamido-benzene was transferred into a three-neck flask and dissolved by adding 1.5 ml of acetic acid. To the stirring solution fuming acid was added by mixing 455 μL of nitric acid with 140 μL of sulfuric acid (on a cold ice bath). 60°C. The resulting solution in the three-neck flask was put under nitrogen and refluxed for 2 hours at 60°C. After 2 hours, the reaction was taken off and allowed to cool to room temperature. The product was then filtered using vacuum filtration and washed with 100 μL of acetic acid. The compound was left to dry until the following day, when it was recrystallized using dichloromethane and hexane. (49.3 mg, 14 %). ¹H-NMR (400 MHz, DMSO): δ 7.75 (s, 2H), 7.68 (d, 4H), 7.36 (d, 4H), 2.37 (s, 6H).

1,2-Bis-(*p*-methylphenylsulfonamido)-4,5-bis- fluorobenzene (3)²⁰

A solution of 1,2-diamino-4,5-difluorobenzene (139.8 mg, 1 mmol) and pyridine (0.4031 mL, 5.04 mmol) dissolved in 20.0 mL of 1,2-dichlorethane was added dropwise to another solution of *p*-toluenesulfonyl chloride (755 mg, 2mmol) which was also dissolved in 1,2- dichloroethane. The reaction mixture refluxed for 24 h and was monitored by TLC

(70:30, hexanes/EtOAc). The product was extracted sequentially with 1 M HCL, 0.2 M NaHCO₃, and deionized H₂O. The resulting organic phase was then separated and dried with granular MgSO₄. The solvent was evaporated to dryness using the rotovap, and the solution was recrystallized by adding hot dichloromethane and hexane. The final product was red crystals (310 mg, 68% yield). ¹H-NMR (δ/ppm vs. TMS in CD₃CN, 400 MHz) 7.66 (s, 2H) 7.55 (d, 4H) 7.33 (d, 4H) 6.88 (t, 2H). FT-IR: N-H(*m*)= 3264cm⁻¹, S=O(*s*)= 1157 cm⁻¹.

Pb-3 complex: (Pb[4,5-(Fluoro)-1,2-C₆H₄(NSO₂C₆H₅CH₃)₂·2(CH₃)₂SO)

A solution of Pb(NO₃)₂ (170mg, 0.520 mmol) in 5 mL of DMSO was added dropwise to a solution of (105.2 mg, 0.268 mmol) of **3** and NEt₃ (444.2 mg, 4.86 mmol) in 10 mL of DMSO. After stirring for 24 h, the reaction mixture was evaporated until 5 mL remained and an equal volume of H₂O was added. A yellow precipitate was collected (60.8 g, 58% yield). ¹H-NMR (400 MHz, MeOD) δ (ppm): 8.12 (dd, *J* = 9.8, 8.3 Hz, 4H), 7.89 (d, *J* = 2.5 Hz, 1H), 7.55 (dd, *J* = 9.0, 2.7 Hz, 1H), 6.88 (dd, *J* = 8.2, 3.0 Hz, 4H), 6.15 (d, *J* = 9.0 Hz, 1H), 2.28 (s, 6H). FT-IR: S=O 1120 cm⁻¹. Other bands (cm⁻¹): 2055, 1492, 1411, 1266, 1229, 1075, 928, 814, 668.

A.4.3 UV-Vis Extraction experiments

A 2.0 x 10⁻³ M solution of **1** or **3** was prepared in a 5.0 mL volumetric flask (Solution A). In a typical experiment, a 0.20 M aqueous solution of Zn(NO₃)₂ was prepared in a 10.0 mL volumetric flask (Solution B). A 0.02 M aqueous solution of Pb(NO₃)₂ was prepared in a 10.0 mL volumetric flask (Solution C). A 0.40 M aqueous solution of CaCl₂· 2H₂O

was prepared in a 10.0 mL volumetric flask (Solution D). 900 μ L of solution A was added to three empty vials. Then to each vial 900 μ L of solutions B, C, and D were added. The vials with the solutions were agitated for 5 min by Vortex. After 2 h the UV-Vis spectra were collected. To prepare the UV-Vis sample 200 μ L of the organic phases were diluted in 2,800 μ L of dichloromethane.

A.4.4 X-ray Crystallography

Light red-orange block-shaped crystals of Pb- **3** were obtained by slow evaporation of a methanolic solution. NMR characterization of the dissolved formed crystals perfectly matched the spectrum of the complex Pb-**3** formed by bulk synthesis. In case of ligand **3** and complex, a suitable crystal was selected and mounted on a Bruker D8 Quest diffractometer equipped with PHOTON II detector operating at $T = 298$ K. Data were collected with ω shutter less scan technique using graphite monochromated Mo- $K\alpha$ radiation ($\lambda = 0.71073$ Å). The total number of runs and images for both data collections was based on the strategy calculation from the program *APEX3* (Bruker)¹⁴. Cell parameters were retrieved using the *SAINT* (Bruker) software¹⁵ and refined using *SAINT* (Bruker) on 7113 reflections for **3** and on 9993 reflections for Pb-**3**. Data reduction was performed using the *SAINT* (Bruker) software, which corrects for Lorentz and polarization effects. Multi-scan absorption corrections were performed with both data sets using *SADABS* 2014/5.¹⁶ The structures for **3** and Pb-**3** were solved in the space group *P*-1 by intrinsic phasing using the *ShelXT* (Sheldrick, 2015)¹⁷ and the structure solution program and refined by full matrix least squares on F^2 using version 2016/6 of *ShelXL* (Sheldrick,

2015).¹⁸ One of such single crystals was selected for data collection upon the solution and refinement.

Calculations and molecular graphics were performed using *SHELXTL* 2014 and *Olex2*¹⁹ programs. Crystal data and structure refinement parameters are listed in Tables 1 and 2.

Table A.1. Crystal data and structure refinement parameters for ligand **3**.

Chemical formula	C ₂₀ H ₁₈ F ₂ N ₂ O ₄ S ₂
Crystal system, space group	Triclinic, P1
a, b, c (Å)	7.907 (4), 11.549 (6), 11.871 (6)
α, β, γ (°)	107.491 (12), 90.390 (12), 103.434 (12)
R _{int}	0.024
R[F ₂ > 2σ(F ₂)], wR(F ₂), S	0.039, 0.117, 1.06

Table A.2. Crystal data and structure refinement parameters for Pb-**3**.

Chemical formula	C ₄₄ H ₄₄ F ₄ N ₄ O ₁₀ Pb ₂ S ₆ MW 661.21g/mol
Crystal system, space group	Triclinic, P1
Temperature (K)	273
a, b, c (Å)	10.7539 (13), 11.2646 (15), 13.1056 (15)
α, β, γ (°)	109.164 (4), 109.375 (3), 97.044 (5)
Radiation type	Mo Kα
μ (mm ⁻¹)	6.36
Crystal size (mm)	0.22 × 0.04 × 0.04
R _{int}	0.024
R[F ₂ > 2σ(F ₂)], wR(F ₂), S	0.057, 0.165, 1.11

A.5 Conclusion

Disulfonamide analogs **1-3** were successfully synthesized and their Pb(II) extraction-based sensing properties were studied. The dinitro ligand **2** was found to be a selective extraction-based optical sensor for Pb(II). Complexes for ligands **1** and **3** were successfully isolated, but only the difluoro analog (**3**) gave us an insight into the structural coordination with Pb(II). The Pb-**3** complex coordinated with two DMSO molecules shows a stereochemically active lone pair on Pb and a hemidirected geometry, consistent with what we observed for disulfonamide derivatives.^{3,4} FT-IR spectra of these complexes show the S=O stretching frequency at lower wavelengths as expected for Pb(II) complexation. Unlike for **2**, the UV-Vis study of extraction-based sensing selectivity for the ligand **1** and **3**, demonstrate no capability for selective Pb(II) optical sensing. Future detailed characterization of these systems is expected for more detailed insight on toxic metal coordination and sensing by this ligand family.

A.6 References

- (1) Feng, T.; Keller, L. R.; Wang, L.; Wang, Y. Product Quality Risk Perceptions and Decisions: Contaminated Pet Food and Lead-Painted Toys. *Risk Analysis* **2010**, *30*, 1572–1589.
- (2) Godwin, H. A. The Biological Chemistry of Lead. *Current Opinion in Chemical Biology* **2001**, *5*, 223–227.
- (3) Alvarado, R. J.; Rosenberg, J. M.; Andreu, A.; Bryan, J. C.; Chen, W.-Z.; Ren, T.; Kavallieratos, K. Structural Insights into the Coordination and Extraction of Pb(II) by Disulfonamide Ligands Derived from o-Phenylenediamine. *Inorg. Chem.* **2005**, *44*, 7951–7959.

- (4) Kavallieratos, K.; Rosenberg, J. M.; Bryan, J. C. Pb(II) Coordination and Synergistic Ion-Exchange Extraction by Combinations of Sulfonamide Chelates and 2,2'-Bipyridine. *Inorg. Chem.* **2005**, *44*, 2573–2575.
- (5) Kavallieratos, K.; Rosenberg, J. M.; Chen, W.-Z.; Ren, T. Fluorescent Sensing and Selective Pb(II) Extraction by a Dansylamide Ion-Exchanger. *J. Am. Chem. Soc.* **2005**, *127*, 6514–6515.
- (6) Bajo, S.; Wyttenbach, A. Liquid-Liquid Extraction of Cadmium with Diethyldithiocarbamic Acid. *Anal. Chem.* **1977**, *49*, 158–161.
- (7) Battistuzzi, G.; Borsari, M.; Menabue, L.; Saladini, M.; Sola, M. Amide Group Coordination to the Pb²⁺ Ion. *Inorg. Chem.* **1996**, *35*, 4239–4247.
- (8) Claudio, E. S.; Godwin, H. A.; Magyar, J. S. Fundamental Coordination Chemistry, Environmental Chemistry, and Biochemistry of Lead(II). In *Progress in Inorganic Chemistry*; John Wiley & Sons, Ltd, **2003**, 1–144.
- (9) Parr, J. Tricoordinate complexes of lead(II) with innocent Schiff base ligands. *Polyhedron.* **1997**, *16*, 1853.
- (10) Harrison, P. G.; Stevens, A. T. J. Lead(II) carboxylate structures. *Organomet. Chem.* **1982**, *239*, 105.
- (11) Shimoni-Livny, L.; Glusker, J. P.; Bock, C. W. Lone Pair Functionality in Divalent Lead Compounds. *Inorg. Chem.* **1998**, *37*, 1853–1867.
- (12) Hancock, R. D.; Shaikjee, M. S.; Dobson, S. M.; Boeyens, J. C. A. *Inorg. Chim. Acta* **1989**, *154*, 229.
- (13) Magyar, J. S.; Weng, T.-C.; Stern, C. M.; Dye, D. F.; Rous, B. W.; Payne, J. C.; Bridgewater, B. M.; Mijovilovich, A.; Parkin, G.; Zaleski, J. M.; Penner-Hahn, J. E.; Godwin, H. A. Reexamination of Lead(II) Coordination Preferences in Sulfur-

Rich Sites: Implications for a Critical Mechanism of Lead Poisoning. *J. Am. Chem. Soc.* **2005**, *127*, 9495–9505.

- (14) *Bruker APEX 3*; Bruker AXS Inc.: Madison, Wisconsin, USA, **2014**.
- (15) *Bruker SAINT*; Bruker AXS Inc.: Madison, Wisconsin, USA, **2012**.
- (16) *Bruker SADABS*; Bruker AXS Inc.: Madison, Wisconsin, USA, **2014**.
- (17) Sheldrick, G. M. SHELXT – Integrated Space-Group and Crystal-Structure Determination. *Acta Cryst A.* **2015**, *71*, 3–8.
- (18) Sheldrick, G. M. Crystal Structure Refinement with SHELXL. *Acta Cryst C* **2015**, *71*, 3–8.
- (19) Dolomanov, O. V.; Bourhis, L. J.; Gildea, R. J.; Howard, J. A. K.; Puschmann, H. OLEX2: A Complete Structure Solution, Refinement and Analysis Program. *Journal of Applied Crystallography* **2009**, *42*, 339–341.
- (20) Saunders, A. Sprake, J.M. *J.Chem. Soc. (C)*, **1970**, 1161-1165.
- (21) X.; Lin, H.; Lin, H. *Journal of Fluorine chemistry.* **2007**, *128*, 530-534.

APPENDIX B

B. X-ray Crystallography and theoretical data

B.1 X-ray Crystallography

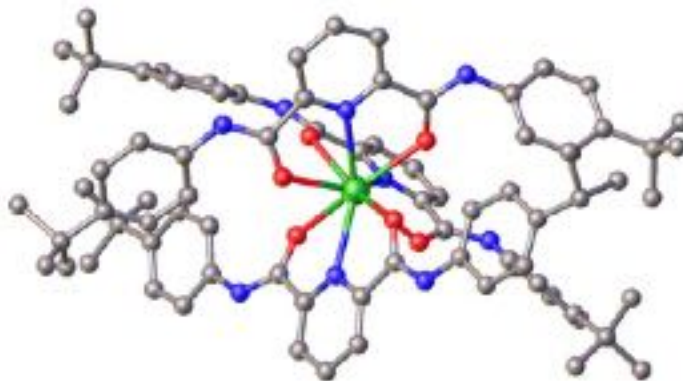


Figure B.1. Structure of $[\text{Nd}(\mathbf{3})_3]\text{I}_3 \cdot 3\text{CH}_3\text{CN}$. Hydrogens are omitted for clarity.

The bulky nature of the ligand creates challenges in packing three such ligands around a single metal center. One of the (**3**) ligands is relatively co-planar (labeled as the 0XX series in the CIF); whereas the other two ligands both have substantial distortions. For the (**3**) ligand labeled with the 200 series, there is substantial twisting of one of the peripheral phenyl rings by $55.08(5)^\circ$ with respect to the rest of the ligand, which is roughly co-planar. The second distorted (**3**) ligand (labeled as the 100 series in the CIF) accommodates the bulky ligand packing by twisting at one of the amide-pyridine linkages $23.69(5)^\circ$ with respect to the plane of the pyridine ring. These distortions allow for improved packing of the *t*-butyl groups on adjacent (**3**) ligands. Remarkably, even though there are substantial distortions of two of the three ligands, the Nd-N and Nd-O bond distances do not reflect

these features, and even in the most pronounced example, the Nd-O bond distances are not statistically different at the 3σ limit.

Table B.1. Crystal data and structure refinement for $[\text{Nd}(\mathbf{3})_3]\text{I}_3 \cdot 3\text{CH}_3\text{CN}$

Identification code	Nd(3)
Empirical formula	$\text{C}_{87.09}\text{H}_{105}\text{I}_3\text{N}_{12}\text{NdO}_6$
Formula weight	1940.90
Temperature/K	120
Crystal system	monoclinic
Space group	$\text{P}2_1/\text{c}$
$a/\text{\AA}$	18.754(3)
$b/\text{\AA}$	18.809(3)
$c/\text{\AA}$	25.655(4)
$\alpha/^\circ$	90
$\beta/^\circ$	108.127(3)
$\gamma/^\circ$	90
Volume/ \AA^3	8600(2)
Z	4
$\rho_{\text{calc}}/\text{cm}^3$	1.499
μ/mm^{-1}	1.739
F(000)	3914.0
Crystal size/ mm^3	$0.09 \times 0.08 \times 0.07$
Radiation	$\text{MoK}\alpha$ ($\lambda = 0.71073$)

2 Θ range for data collection/ $^{\circ}$	4.332 to 55.29
Index ranges	$-24 \leq h \leq 24, -24 \leq k \leq 24, -33 \leq l \leq 33$
Reflections collected	132580
Independent reflections	19967 [$R_{\text{int}} = 0.0472, R_{\text{sigma}} = 0.0298$]
Data/restraints/parameters	19967/0/1044
Goodness-of-fit on F^2	1.153
Final R indexes [$I \geq 2\sigma(I)$]	$R_1 = 0.0421, wR_2 = 0.1075$
Final R indexes [all data]	$R_1 = 0.0525, wR_2 = 0.1145$
Largest diff. peak/hole / $e \text{ \AA}^{-3}$	2.12/-0.99

Table B.2. Fractional Atomic Coordinates ($\times 10^4$) and Equivalent Isotropic Displacement Parameters ($\text{\AA}^2 \times 10^3$) for Nd(3). U_{eq} is defined as 1/3 of the trace of the orthogonalised U_{ij} tensor.

Atom	x	y	z	$U(\text{eq})$
Nd(1)	4865.0(2)	2593.4(2)	9572.2(2)	12.95(6)
I(2)	6198.7(2)	3908.0(2)	11606.2(2)	28.53(8)
I(3)	2754(9)	3186(11)	11479(2)	46(3)
I(3B)	2503(4)	2672(3)	11559(3)	30.8(7)
I(3A)	2585(4)	2841(11)	11532(2)	54(3)
I(1)	7188.3(2)	3690.0(2)	7610.4(2)	25.13(8)
O(201)	4567.9(15)	3780.3(14)	9833.3(11)	17.2(5)
O(102)	5187.6(16)	1333.0(15)	9783.7(12)	21.9(6)
O(101)	3848.0(14)	2989.5(14)	8753.1(11)	16.5(5)
O(2)	6071.8(15)	2621.8(15)	10322.5(11)	17.6(5)
O(1)	3618.4(15)	2395.3(15)	9702.3(11)	18.2(5)
N(201)	5358.0(17)	3672.1(17)	9157.3(12)	14.1(6)
O(202)	5838.9(16)	2383.7(15)	9127.9(11)	19.9(6)
N(1)	4837.7(17)	2362.3(17)	10560.6(13)	15.6(6)
N(101)	4232.7(18)	1659.3(17)	8825.1(14)	18.3(7)
N(3)	6827.1(18)	2245.8(17)	11158.5(14)	17.6(7)
N(102)	2810(2)	2820.0(19)	8021.4(16)	28.4(9)
C(17)	6159(2)	2393(2)	10792.0(16)	16.5(7)

C(106)	3444(2)	2602(2)	8391.3(16)	18.3(8)
C(107)	2430(2)	3473(2)	8006.8(17)	22.5(8)
C(6)	3514(2)	2379(2)	10158.5(16)	16.8(7)
N(2)	2846.5(18)	2456.9(19)	10234.2(14)	19.9(7)
N(203)	6613.0(19)	2682.5(19)	8638.7(15)	22.7(7)
C(7)	2133(2)	2547(2)	9820.5(16)	19.9(8)
C(105)	3659(2)	1833(2)	8384.2(17)	19.8(8)
C(205)	5110(2)	4329(2)	9217.3(15)	15.6(7)
N(202)	4090.5(17)	4849.9(17)	9486.1(14)	17.8(7)
C(5)	4179(2)	2251(2)	10658.1(16)	16.6(7)
C(206)	4563(2)	4312(2)	9539.6(15)	15.2(7)
C(104)	3303(2)	1337(2)	7986.3(18)	23.3(8)
C(204)	5365(2)	4924(2)	9019.2(17)	22.3(8)
C(3)	4810(2)	1880(2)	11571.6(17)	25.0(9)
C(2)	5486(2)	2003(2)	11478.7(17)	23.1(9)
C(201)	5847(2)	3594(2)	8876.6(16)	17.4(7)
C(208)	3205(2)	5568(2)	9758.3(17)	21.8(8)
C(19)	8154(2)	2128(2)	11552.2(16)	21.2(8)
C(23)	7683(2)	2521(3)	10620.2(19)	27.8(10)
C(4)	4146(2)	2005(2)	11158.7(17)	22.8(8)
C(209)	2616(2)	5639(2)	9973.5(19)	26.3(9)
C(207)	3498(2)	4902(2)	9724.5(17)	19.1(8)
C(1)	5474(2)	2247(2)	10965.9(16)	17.1(7)
C(202)	6115(2)	4164(2)	8651.8(17)	23.1(8)
C(220)	6990(2)	2013(2)	8698.8(19)	27.5(9)
C(203)	5875(2)	4839(2)	8733.7(19)	26.0(9)
C(221)	7080(3)	1672(3)	8249(2)	38.2(12)
C(18)	7549(2)	2315(2)	11098.4(16)	16.0(7)
N(103)	5564(2)	339.7(19)	9441.0(16)	26.8(8)
C(110)	1555(2)	4692(2)	7985.7(19)	26.6(9)
C(117)	5112(2)	889(2)	9410.0(17)	20.4(8)
C(21)	9019(2)	2310(3)	11032(2)	35.1(12)
C(103)	3551(2)	641(2)	8056.2(19)	28.9(10)
C(102)	4145(2)	456(2)	8514.5(19)	26.9(9)
C(101)	4476(2)	986(2)	8885.8(17)	20.8(8)
C(210)	2295(2)	5058(2)	10152(2)	29.8(10)
C(22)	8410(3)	2508(3)	10592(2)	44.9(15)
C(219)	6097(2)	2835(2)	8880.1(16)	18.5(8)
C(20)	8879(2)	2130(2)	11517.6(18)	24.4(9)
C(112)	2736(2)	4058(2)	8322.3(19)	29.0(10)
C(118)	6217(2)	190(2)	9902.8(19)	24.5(9)
C(121)	7530(2)	-155(2)	10743.8(19)	26.2(9)
C(119)	6401(3)	-506(2)	10028(2)	31.2(10)
C(12)	2049(2)	2834(2)	9308.2(18)	24.2(9)
C(122)	7330(3)	543(3)	10600(2)	40.7(13)
C(9)	797(3)	2449(3)	9589(2)	40.9(13)
C(11)	1328(2)	2931(2)	8945.9(18)	26.2(9)
C(213)	1638(3)	5133(3)	10387(3)	42.5(13)

C(124)	8271(2)	-318(2)	11188(2)	30.9(10)
C(108)	1689(2)	3506(2)	7669.7(19)	29.4(10)
C(114)	297(3)	5315(3)	7610(3)	50.1(16)
C(109)	1267(2)	4111(2)	7662.0(19)	29.2(10)
C(8)	1510(2)	2360(3)	9962.8(19)	36.4(12)
C(113)	1097(3)	5362(3)	8009(2)	41.4(13)
C(120)	7056(3)	-675(2)	10448(2)	33.0(11)
C(10)	686(2)	2730(3)	9070.6(18)	27.6(9)
C(123)	6684(3)	720(3)	10184(2)	40.9(13)
C(111)	2301(3)	4652(2)	8310(2)	32.7(11)
C(225)	7303(3)	1731(4)	9210(2)	50.9(17)
C(126)	8275(3)	44(3)	11724(2)	40.4(12)
C(211)	2602(3)	4402(3)	10110(3)	44.6(15)
C(13)	-93(2)	2838(3)	8652(2)	37.2(12)
C(212)	3195(3)	4318(2)	9898(3)	38.5(13)
C(223)	7804(3)	747(3)	8833(2)	44.1(14)
C(26)	10015(3)	2942(3)	10743(3)	46.3(14)
C(24)	9816(3)	2275(4)	10985(3)	71(3)
C(127)	8924(3)	-20(5)	11011(3)	62.3(19)
C(14)	-733(3)	2628(4)	8883(3)	56.2(17)
C(116)	1474(3)	6015(3)	7860(4)	69(2)
C(16)	-161(4)	2414(5)	8147(3)	74(3)
C(222)	7483(4)	1038(3)	8321(2)	49.8(16)
C(224)	7704(4)	1099(4)	9274(2)	58.8(19)
C(15)	-204(3)	3629(4)	8500(3)	63.3(19)
N(402)	4775(3)	2726(3)	7852(2)	49.4(13)
C(403)	4802(3)	2187(4)	7677(3)	49.1(15)
C(216)	1156(4)	4491(4)	10289(3)	66(2)
C(125)	8386(4)	-1104(3)	11303(3)	69(2)
C(115)	1049(4)	5439(5)	8587(3)	83(3)
C(226)	8277(4)	67(4)	8930(3)	65(2)
C(404)	4828(6)	1476(4)	7438(4)	90(3)
C(25)	10329(4)	1899(5)	11396(5)	105(4)
C(214)	1396(12)	5828(10)	10481(10)	85(9)
C(215)	1044(5)	5689(5)	9986(4)	33(3)
C(27)	9769(4)	1666(4)	10484(3)	68(2)
C(229)	9061(6)	248(6)	9224(10)	251(13)
C(227)	8252(16)	-284(10)	8436(6)	350(19)
C(218)	1912(5)	5462(5)	10919(4)	30(3)
C(217)	1961(8)	4821(8)	11085(6)	54(5)
C(405)	1338(5)	1226(5)	7199(4)	77(2)
N(403)	1386(6)	1726(5)	7485(4)	107(3)
C(406)	1300(7)	616(6)	6841(4)	109(4)
N(401)	4301(3)	4796(3)	6620(2)	48.1(12)
C(401)	4148(4)	4638(3)	6998(3)	52.2(15)
C(402)	3952(7)	4408(4)	7478(3)	94(3)
C(228)	8051(10)	-417(5)	9289(6)	172(8)

Table B.3. Anisotropic Displacement Parameters ($\text{\AA}^2 \times 10^3$) for Nd(3). The Anisotropic displacement factor exponent takes the form: $-2\pi^2[h^2a^2U_{11}+2hka*b*U_{12}+\dots]$.

Atom	U ₁₁	U ₂₂	U ₃₃	U ₂₃	U ₁₃	U ₁₂
Nd(1)	10.59(9)	13.70(10)	13.65(10)	0.21(7)	2.45(7)	1.82(7)
I(2)	32.93(16)	23.54(14)	28.31(15)	2.50(11)	8.36(12)	4.53(11)
I(3)	33(3)	84(5)	20.4(11)	-10.3(19)	6.0(13)	29(3)
I(3B)	21.0(11)	47.0(18)	24.7(9)	3.7(10)	7.4(7)	-1.2(9)
I(3A)	23.8(17)	112(7)	24.3(13)	-21(3)	4.8(9)	20(3)
I(1)	24.82(14)	32.71(15)	19.35(13)	-5.16(11)	9.01(11)	- 4.45(11)
O(201)	18.4(13)	16.0(13)	18.7(13)	-0.8(10)	8.0(11)	2.8(10)
O(102)	24.0(15)	15.3(13)	24.6(15)	0.8(11)	5.1(12)	3.4(11)
O(101)	13.3(12)	16.5(13)	16.9(13)	-0.3(10)	0.5(10)	1.6(10)
O(2)	12.9(12)	22.6(14)	15.8(13)	2.8(11)	2.2(10)	-1.7(10)
O(1)	12.1(12)	23.9(14)	17.7(13)	0.6(11)	3.4(10)	-1.5(11)
N(201)	10.2(14)	17.6(15)	13.5(14)	-2.9(12)	2.3(12)	1.5(12)
O(202)	20.6(14)	19.5(14)	21.5(14)	0.0(11)	9.2(11)	5.4(11)
N(1)	12.8(15)	15.8(15)	16.1(15)	-0.9(12)	1.7(12)	-2.0(12)
N(101)	14.9(15)	17.2(16)	21.9(17)	-1.4(13)	4.7(13)	2.2(12)
N(3)	15.1(15)	20.3(16)	17.9(16)	4.2(13)	6.1(13)	1.9(12)
N(102)	21.5(18)	20.4(17)	29(2)	-6.5(15)	-12.2(15)	4.9(14)
C(17)	15.7(17)	16.8(17)	16.4(18)	-0.4(14)	4.3(14)	-1.9(14)
C(106)	16.0(18)	17.6(18)	20.1(19)	-1.3(15)	3.9(15)	0.2(15)
C(107)	18.2(19)	19.0(19)	24(2)	-0.8(16)	-2.3(16)	2.1(15)

C(6)	11.9(17)	15.6(17)	22.4(19)	-2.3(15)	4.4(15)	-2.0(14)
N(2)	11.2(15)	31.7(19)	16.9(16)	-1.9(14)	4.7(13)	-1.7(13)
N(203)	20.1(17)	26.6(18)	24.8(18)	-1.1(14)	11.8(14)	6.1(14)
C(7)	10.0(17)	28(2)	20.7(19)	-6.2(16)	3.5(15)	-2.8(15)
C(105)	13.5(17)	21.0(19)	23(2)	-1.0(16)	2.7(15)	1.4(15)
C(205)	11.6(16)	18.6(18)	15.6(17)	-0.8(14)	2.6(14)	3.0(14)
N(202)	13.4(15)	15.1(15)	25.5(17)	-1.0(13)	6.8(13)	3.2(12)
C(5)	13.9(17)	18.9(18)	17.0(18)	-0.6(14)	4.6(14)	-0.3(14)
C(206)	12.2(16)	17.6(18)	14.6(17)	-5.3(14)	2.3(14)	0.3(14)
C(104)	18.2(19)	23(2)	26(2)	-3.2(17)	3.5(16)	-0.7(16)
C(204)	22(2)	18.0(19)	28(2)	2.8(16)	9.4(17)	2.7(16)
C(3)	22(2)	35(2)	19(2)	6.1(17)	7.1(16)	-1.2(17)
C(2)	16.2(19)	32(2)	17.2(19)	6.1(17)	-0.4(15)	-1.9(16)
C(201)	11.3(16)	22.7(19)	16.4(18)	-1.3(15)	1.6(14)	3.0(14)
C(208)	20.0(19)	20(2)	24(2)	-2.5(16)	5.2(16)	4.2(15)
C(19)	19.0(19)	27(2)	16.6(19)	2.2(16)	3.8(15)	0.3(16)
C(23)	20(2)	37(2)	29(2)	15.1(19)	10.4(17)	8.6(18)
C(4)	17.1(19)	29(2)	25(2)	0.5(17)	10.2(16)	-1.3(16)
C(209)	21(2)	23(2)	34(2)	-5.8(18)	7.6(18)	8.4(16)
C(207)	14.4(17)	17.9(19)	25(2)	-8.7(15)	5.6(15)	-0.8(14)
C(1)	12.0(17)	18.5(18)	20.2(19)	1.3(15)	4.1(14)	-1.9(14)
C(202)	18.6(19)	29(2)	25(2)	1.6(17)	11.6(16)	3.0(16)
C(220)	24(2)	32(2)	31(2)	1.5(19)	14.3(18)	13.6(18)
C(203)	23(2)	23(2)	34(2)	8.2(18)	13.7(18)	0.6(17)
C(221)	54(3)	36(3)	32(3)	6(2)	24(2)	20(2)
C(18)	11.5(17)	15.4(17)	20.7(19)	0.5(14)	4.6(14)	1.8(13)

N(103)	21.2(18)	18.6(17)	33(2)	-3.9(15)	-2.0(15)	5.7(14)
C(110)	20(2)	25(2)	29(2)	-2.9(18)	-1.1(17)	6.6(17)
C(117)	18.2(19)	14.2(18)	27(2)	3.0(16)	4.8(16)	0.7(15)
C(21)	14(2)	53(3)	41(3)	24(2)	12.3(19)	11(2)
C(103)	24(2)	25(2)	34(2)	-12.8(19)	2.9(18)	-3.4(17)
C(102)	23(2)	18(2)	36(2)	-4.5(17)	3.3(18)	4.1(16)
C(101)	17.0(18)	16.9(19)	27(2)	0.6(16)	4.8(16)	2.1(15)
C(210)	16.7(19)	26(2)	51(3)	-11(2)	18(2)	-0.1(17)
C(22)	23(2)	78(4)	39(3)	40(3)	17(2)	20(2)
C(219)	15.1(18)	21.9(19)	16.2(18)	-1.6(15)	1.5(14)	1.1(15)
C(20)	13.8(18)	30(2)	27(2)	6.7(18)	2.8(16)	2.8(16)
C(112)	14.7(19)	25(2)	35(2)	-5.9(18)	-9.5(17)	2.4(16)
C(118)	17.8(19)	16.8(19)	34(2)	-0.7(17)	1.4(17)	5.4(15)
C(121)	19(2)	19(2)	36(2)	-1.4(18)	2.0(18)	3.3(16)
C(119)	28(2)	17(2)	40(3)	-4.4(18)	-2(2)	0.2(17)
C(12)	17.1(19)	26(2)	30(2)	2.8(17)	6.8(17)	1.0(16)
C(122)	28(2)	20(2)	61(3)	-8(2)	-5(2)	0.7(19)
C(9)	13(2)	81(4)	30(2)	2(3)	7.8(18)	-4(2)
C(11)	20(2)	32(2)	25(2)	2.8(18)	4.6(17)	4.1(17)
C(213)	24(2)	40(3)	73(4)	-17(3)	29(3)	-2(2)
C(124)	20(2)	23(2)	42(3)	-3.6(19)	-2.3(19)	5.0(17)
C(108)	23(2)	25(2)	30(2)	-6.9(18)	-7.9(18)	2.4(17)
C(114)	25(2)	47(3)	63(4)	-17(3)	-9(2)	18(2)
C(109)	17(2)	29(2)	32(2)	-4.1(19)	-7.6(17)	4.1(17)
C(8)	15(2)	73(4)	19(2)	6(2)	3.7(17)	-3(2)
C(113)	23(2)	39(3)	49(3)	-20(2)	-7(2)	12(2)

C(120)	30(2)	15(2)	46(3)	1.0(19)	1(2)	5.8(17)
C(10)	15.4(19)	42(3)	22(2)	-4.8(19)	0.6(16)	1.2(18)
C(123)	31(3)	20(2)	60(3)	0(2)	-4(2)	5.2(19)
C(111)	24(2)	23(2)	40(3)	-8.4(19)	-7.2(19)	2.5(18)
C(225)	55(3)	71(4)	27(3)	1(3)	13(2)	41(3)
C(126)	33(3)	40(3)	42(3)	2(2)	1(2)	5(2)
C(211)	41(3)	21(2)	89(4)	-12(3)	45(3)	-6(2)
C(13)	14(2)	64(3)	29(2)	1(2)	-0.4(18)	5(2)
C(212)	32(3)	17(2)	78(4)	-11(2)	33(3)	-3.1(18)
C(223)	55(3)	43(3)	43(3)	11(2)	29(3)	28(3)
C(26)	24(2)	44(3)	78(4)	-1(3)	26(3)	-1(2)
C(24)	21(3)	116(6)	86(5)	75(5)	32(3)	35(3)
C(127)	20(3)	109(6)	56(4)	-4(4)	9(3)	2(3)
C(14)	16(2)	99(5)	47(3)	8(3)	0(2)	1(3)
C(116)	35(3)	26(3)	121(6)	-15(3)	-12(4)	13(2)
C(16)	36(3)	134(7)	36(3)	-30(4)	-12(3)	15(4)
C(222)	73(4)	47(3)	38(3)	1(2)	31(3)	34(3)
C(224)	68(4)	74(4)	36(3)	20(3)	20(3)	53(4)
C(15)	26(3)	85(5)	71(4)	22(4)	4(3)	16(3)
N(402)	47(3)	68(4)	32(2)	-5(2)	12(2)	-19(3)
C(403)	38(3)	71(4)	43(3)	14(3)	20(3)	-2(3)
C(216)	45(3)	73(5)	103(6)	-27(4)	54(4)	-19(3)
C(125)	54(4)	30(3)	84(5)	-5(3)	-34(4)	18(3)
C(115)	56(4)	112(7)	61(4)	-49(5)	-9(3)	40(4)
C(226)	87(5)	59(4)	63(4)	21(3)	43(4)	52(4)
C(404)	117(7)	55(4)	142(8)	-2(5)	103(7)	2(5)

C(25)	35(4)	124(8)	173(10)	78(7)	55(5)	42(4)
C(214)	87(14)	75(11)	130(20)	32(12)	89(16)	45(10)
C(215)	24(5)	42(6)	39(6)	9(4)	19(4)	15(4)
C(27)	57(4)	65(4)	98(6)	1(4)	45(4)	12(3)
C(229)	65(7)	68(7)	610(40)	38(14)	93(14)	49(6)
C(227)	690(50)	248(19)	120(11)	59(12)	137(19)	400(30)
C(218)	19(4)	41(6)	35(5)	-14(4)	18(4)	-3(4)
C(217)	54(8)	67(10)	52(8)	-8(7)	31(7)	2(7)
C(405)	89(6)	75(5)	70(5)	-10(4)	29(5)	-11(5)
N(403)	147(8)	74(5)	87(6)	-6(4)	19(5)	-10(5)
C(406)	166(11)	91(7)	96(7)	-18(6)	77(8)	-26(7)
N(401)	53(3)	36(3)	57(3)	6(2)	20(2)	-3(2)
C(401)	78(5)	29(3)	51(4)	-5(3)	21(3)	5(3)
C(402)	182(10)	58(5)	62(5)	3(4)	69(6)	24(6)
C(228)	320(20)	74(7)	181(13)	76(8)	171(14)	110(10)

Table B.4. Bond Lengths for Nd(3).

Atom	Atom	Length/Å	Atom	Atom	Length/Å
Nd(1)	O(201)	2.444(3)	C(220)	C(225)	1.366(7)
Nd(1)	O(102)	2.465(3)	C(221)	C(222)	1.393(7)
Nd(1)	O(101)	2.473(3)	N(103)	C(117)	1.323(5)
Nd(1)	O(2)	2.474(3)	N(103)	C(118)	1.442(5)
Nd(1)	O(1)	2.490(3)	C(110)	C(109)	1.378(6)
Nd(1)	N(201)	2.592(3)	C(110)	C(113)	1.536(6)

Nd(1)	O(202)	2.467(3)	C(110)	C(111)	1.390(6)
Nd(1)	N(1)	2.589(3)	C(117)	C(101)	1.506(6)
Nd(1)	N(101)	2.599(3)	C(21)	C(22)	1.385(7)
I(3)	I(3B)	1.12(2)	C(21)	C(20)	1.392(6)
I(3)	I(3A)	0.752(17)	C(21)	C(24)	1.538(6)
O(201)	C(206)	1.250(5)	C(103)	C(102)	1.388(6)
O(102)	C(117)	1.246(5)	C(102)	C(101)	1.385(6)
O(101)	C(106)	1.237(5)	C(210)	C(213)	1.537(6)
O(2)	C(17)	1.241(5)	C(210)	C(211)	1.379(6)
O(1)	C(6)	1.246(5)	C(112)	C(111)	1.378(6)
N(201)	C(205)	1.346(5)	C(118)	C(119)	1.366(6)
N(201)	C(201)	1.339(5)	C(118)	C(123)	1.375(6)
O(202)	C(219)	1.245(5)	C(121)	C(122)	1.384(6)
N(1)	C(5)	1.350(5)	C(121)	C(124)	1.529(6)
N(1)	C(1)	1.334(5)	C(121)	C(120)	1.378(6)
N(101)	C(105)	1.337(5)	C(119)	C(120)	1.395(6)
N(101)	C(101)	1.338(5)	C(12)	C(11)	1.394(6)
N(3)	C(17)	1.341(5)	C(122)	C(123)	1.383(7)
N(3)	C(18)	1.416(5)	C(9)	C(8)	1.391(6)
N(102)	C(106)	1.334(5)	C(9)	C(10)	1.385(7)
N(102)	C(107)	1.414(5)	C(11)	C(10)	1.391(6)
C(17)	C(1)	1.510(5)	C(213)	C(216)	1.483(8)
C(106)	C(105)	1.502(5)	C(213)	C(214)	1.429(17)

C(107)	C(112)	1.381(6)		C(213)	C(215)	1.636(10)
C(107)	C(108)	1.391(6)		C(213)	C(218)	1.439(10)
C(6)	N(2)	1.334(5)		C(213)	C(217)	1.801(16)
C(6)	C(5)	1.504(5)		C(124)	C(126)	1.531(7)
N(2)	C(7)	1.436(5)		C(124)	C(127)	1.540(8)
N(203)	C(220)	1.429(5)		C(124)	C(125)	1.509(7)
N(203)	C(219)	1.333(5)		C(108)	C(109)	1.382(6)
C(7)	C(12)	1.384(6)		C(114)	C(113)	1.533(7)
C(7)	C(8)	1.374(6)		C(113)	C(116)	1.524(9)
C(105)	C(104)	1.391(6)		C(113)	C(115)	1.520(9)
C(205)	C(206)	1.504(5)		C(10)	C(13)	1.535(6)
C(205)	C(204)	1.374(6)		C(225)	C(224)	1.389(8)
N(202)	C(206)	1.325(5)		C(211)	C(212)	1.391(7)
N(202)	C(207)	1.429(5)		C(13)	C(14)	1.545(8)
C(5)	C(4)	1.385(6)		C(13)	C(16)	1.495(8)
C(104)	C(103)	1.382(6)		C(13)	C(15)	1.536(9)
C(204)	C(203)	1.384(6)		C(223)	C(222)	1.377(8)
C(3)	C(2)	1.381(6)		C(223)	C(224)	1.373(8)
C(3)	C(4)	1.381(6)		C(223)	C(226)	1.533(7)
C(2)	C(1)	1.387(6)		C(26)	C(24)	1.497(9)
C(201)	C(202)	1.385(6)		C(24)	C(25)	1.381(9)
C(201)	C(219)	1.502(6)		C(24)	C(27)	1.704(12)
C(208)	C(209)	1.387(6)		N(402)	C(403)	1.117(8)

C(208)	C(207)	1.380(5)		C(403)	C(404)	1.477(11)
C(19)	C(18)	1.395(5)		C(226)	C(229)	1.468(16)
C(19)	C(20)	1.389(6)		C(226)	C(227)	1.418(14)
C(23)	C(18)	1.382(6)		C(226)	C(228)	1.447(12)
C(23)	C(22)	1.387(6)		C(405)	N(403)	1.179(11)
C(209)	C(210)	1.393(7)		C(405)	C(406)	1.458(12)
C(207)	C(212)	1.373(6)		N(401)	C(401)	1.132(8)
C(202)	C(203)	1.384(6)		C(401)	C(402)	1.457(10)
C(220)	C(221)	1.375(6)				

Table B.5. Bond Angles for Nd(3).

Atom	Atom	Atom	Angle/°	Atom	Atom	Atom	Angle/°
O(201)	Nd(1)	O(102)	151.55(9)	C(20)	C(19)	C(18)	120.3(4)
C218d	C(213)	C(210)	108.6(5)	C(18)	C(23)	C(22)	119.6(4)
O(201)	Nd(1)	O(101)	77.08(9)	C(3)	C(4)	C(5)	118.5(4)
O(201)	Nd(1)	O(2)	89.91(9)	C(208)	C(209)	C(210)	122.3(4)
C214c	C(213)	C(210)	119.1(8)	C(208)	C(207)	N(202)	117.8(4)
C214c	C(213)	C(216)	124.4(9)	C(212)	C(207)	N(202)	122.6(4)
C218d	C(213)	C(216)	122.0(6)	C(212)	C(207)	C(208)	119.6(4)
O(201)	Nd(1)	O(1)	78.25(9)	N(1)	C(1)	C(17)	112.2(3)
C218d	C(213)	C(215)	107.0(6)	N(1)	C(1)	C(2)	122.6(4)
C25a	C(24)	C(21)	115.1(5)	C(2)	C(1)	C(17)	125.2(3)
C25a	C(24)	C(26)	122.8(7)	C(203)	C(202)	C(201)	118.0(4)
C227d	C(226)	C(223)	112.8(7)	C(221)	C(220)	N(203)	120.4(4)
C229d	C(226)	C(223)	109.0(7)	C(225)	C(220)	N(203)	119.8(4)

O(201)	Nd(1)	N(201)	62.51(9)	C(225)	C(220)	C(221)	119.7(4)
O(201)	Nd(1)	O(202)	122.50(9)	C(204)	C(203)	C(202)	119.9(4)
O(201)	Nd(1)	N(1)	79.01(9)	C(220)	C(221)	C(222)	119.4(5)
O(201)	Nd(1)	N(101)	136.80(10)	C(19)	C(18)	N(3)	116.3(3)
O(102)	Nd(1)	O(101)	123.26(9)	C(23)	C(18)	N(3)	124.5(4)
O(102)	Nd(1)	O(2)	75.35(9)	C(23)	C(18)	C(19)	119.1(4)
O(102)	Nd(1)	O(1)	90.17(10)	C(117)	N(103)	C(118)	124.5(4)
C227d	C(226)	C(229)	108.4(14)	C(109)	C(110)	C(113)	123.8(4)
C227d	C(226)	C(228)	110.0(13)	C(109)	C(110)	C(111)	116.7(4)
O(102)	Nd(1)	N(201)	138.49(10)	C(111)	C(110)	C(113)	119.5(4)
O(102)	Nd(1)	O(202)	77.39(9)	O(102)	C(117)	N(103)	124.0(4)
O(102)	Nd(1)	N(1)	72.61(10)	O(102)	C(117)	C(101)	118.4(3)
O(102)	Nd(1)	N(101)	62.39(10)	N(103)	C(117)	C(101)	117.6(4)
O(101)	Nd(1)	O(2)	158.72(9)	C(22)	C(21)	C(20)	117.2(4)
O(101)	Nd(1)	O(1)	69.57(9)	C(22)	C(21)	C(24)	121.5(5)
O(101)	Nd(1)	N(201)	72.21(9)	C(20)	C(21)	C(24)	121.3(4)
O(101)	Nd(1)	N(1)	129.63(9)	C(104)	C(103)	C(102)	119.7(4)
O(101)	Nd(1)	N(101)	61.48(10)	C(101)	C(102)	C(103)	118.2(4)
O(2)	Nd(1)	O(1)	124.66(9)	N(101)	C(101)	C(117)	111.4(3)
O(2)	Nd(1)	N(201)	86.89(9)	N(101)	C(101)	C(102)	122.5(4)
O(2)	Nd(1)	N(1)	62.20(9)	C(102)	C(101)	C(117)	126.0(4)
O(2)	Nd(1)	N(101)	133.29(10)	C(209)	C(210)	C(213)	122.5(4)
O(1)	Nd(1)	N(201)	129.94(9)	C(211)	C(210)	C(209)	116.3(4)
O(1)	Nd(1)	N(1)	62.50(9)	C(211)	C(210)	C(213)	121.2(4)
O(1)	Nd(1)	N(101)	76.44(10)	C(21)	C(22)	C(23)	122.5(4)
N(201)	Nd(1)	N(101)	111.44(10)	O(202)	C(219)	N(203)	123.0(4)

O(202)	Nd(1)	O(101)	98.15(9)	O(202)	C(219)	C(201)	118.8(3)
O(202)	Nd(1)	O(2)	74.54(9)	N(203)	C(219)	C(201)	118.2(4)
O(202)	Nd(1)	O(1)	154.01(9)	C(19)	C(20)	C(21)	121.3(4)
O(202)	Nd(1)	N(201)	61.67(9)	C(111)	C(112)	C(107)	119.8(4)
O(202)	Nd(1)	N(1)	131.97(10)	C(119)	C(118)	N(103)	118.0(4)
O(202)	Nd(1)	N(101)	77.56(10)	C(119)	C(118)	C(123)	120.0(4)
N(1)	Nd(1)	N(201)	130.70(10)	C(123)	C(118)	N(103)	121.9(4)
N(1)	Nd(1)	N(101)	117.74(10)	C(122)	C(121)	C(124)	119.8(4)
I(3A)	I(3)	I(3B)	0.2(7)	C(120)	C(121)	C(122)	116.8(4)
C(206)	O(201)	Nd(1)	121.6(2)	C(120)	C(121)	C(124)	123.3(4)
C(117)	O(102)	Nd(1)	120.9(3)	C(118)	C(119)	C(120)	119.8(4)
C(106)	O(101)	Nd(1)	126.2(2)	C(7)	C(12)	C(11)	118.9(4)
C(17)	O(2)	Nd(1)	124.0(2)	C(123)	C(122)	C(121)	122.3(4)
C(6)	O(1)	Nd(1)	123.9(2)	C(10)	C(9)	C(8)	122.2(4)
C(205)	N(201)	Nd(1)	119.4(2)	C(10)	C(11)	C(12)	122.7(4)
C(201)	N(201)	Nd(1)	121.8(3)	C(210)	C(213)	C(215)	106.5(5)
C(201)	N(201)	C(205)	118.8(3)	C(210)	C(213)	C(217)	107.4(6)
C(219)	O(202)	Nd(1)	126.0(2)	C(216)	C(213)	C(210)	112.3(4)
C(5)	N(1)	Nd(1)	120.3(2)	C(216)	C(213)	C(215)	98.8(6)
C(1)	N(1)	Nd(1)	120.3(2)	C(216)	C(213)	C(217)	84.3(7)
C(1)	N(1)	C(5)	118.6(3)	C(121)	C(124)	C(126)	109.3(4)
C(105)	N(101)	Nd(1)	121.4(3)	C(121)	C(124)	C(127)	109.2(4)
C(105)	N(101)	C(101)	119.0(3)	C(126)	C(124)	C(127)	108.7(4)
C(101)	N(101)	Nd(1)	119.5(3)	C(125)	C(124)	C(121)	112.5(4)
C(17)	N(3)	C(18)	128.5(3)	C(125)	C(124)	C(126)	107.5(5)
C(106)	N(102)	C(107)	128.1(4)	C(125)	C(124)	C(127)	109.6(5)

O(2)	C(17)	N(3)	124.3(4)	C(109)	C(108)	C(107)	120.2(4)
O(2)	C(17)	C(1)	118.9(3)	C(110)	C(109)	C(108)	122.0(4)
N(3)	C(17)	C(1)	116.8(3)	C(7)	C(8)	C(9)	120.0(4)
O(101)	C(106)	N(102)	123.7(4)	C(114)	C(113)	C(110)	111.6(4)
O(101)	C(106)	C(105)	118.2(3)	C(116)	C(113)	C(110)	110.0(5)
N(102)	C(106)	C(105)	118.0(3)	C(116)	C(113)	C(114)	108.3(5)
C(112)	C(107)	N(102)	124.2(4)	C(115)	C(113)	C(110)	108.6(5)
C(112)	C(107)	C(108)	118.7(4)	C(115)	C(113)	C(114)	108.4(5)
C(108)	C(107)	N(102)	117.0(4)	C(115)	C(113)	C(116)	110.0(6)
O(1)	C(6)	N(2)	124.2(4)	C(121)	C(120)	C(119)	121.7(4)
O(1)	C(6)	C(5)	118.3(3)	C(9)	C(10)	C(11)	116.2(4)
N(2)	C(6)	C(5)	117.4(3)	C(9)	C(10)	C(13)	123.3(4)
C(6)	N(2)	C(7)	127.4(3)	C(11)	C(10)	C(13)	120.5(4)
C(219)	N(203)	C(220)	123.1(4)	C(118)	C(123)	C(122)	119.4(4)
C(12)	C(7)	N(2)	123.5(4)	C(112)	C(111)	C(110)	122.5(4)
C(8)	C(7)	N(2)	116.6(4)	C(220)	C(225)	C(224)	120.1(5)
C(8)	C(7)	C(12)	119.9(4)	C(210)	C(211)	C(212)	122.5(5)
N(101)	C(105)	C(106)	111.9(3)	C(10)	C(13)	C(14)	112.5(4)
N(101)	C(105)	C(104)	122.2(4)	C(10)	C(13)	C(15)	109.3(5)
C(104)	C(105)	C(106)	125.9(4)	C(16)	C(13)	C(10)	110.0(4)
N(201)	C(205)	C(206)	111.2(3)	C(16)	C(13)	C(14)	109.3(5)
N(201)	C(205)	C(204)	122.2(3)	C(16)	C(13)	C(15)	109.2(6)
C(204)	C(205)	C(206)	126.6(3)	C(15)	C(13)	C(14)	106.5(5)
C(206)	N(202)	C(207)	126.4(3)	C(207)	C(212)	C(211)	119.8(4)
N(1)	C(5)	C(6)	112.4(3)	C(222)	C(223)	C(226)	123.1(5)
N(1)	C(5)	C(4)	122.1(4)	C(224)	C(223)	C(222)	117.6(5)

C(4)	C(5)	C(6)	125.4(3)	C(224)	C(223)	C(226)	119.3(5)
O(201)	C(206)	C(205)	118.1(3)	C(21)	C(24)	C(27)	105.3(6)
O(201)	C(206)	N(202)	123.5(3)	C(26)	C(24)	C(21)	111.7(5)
N(202)	C(206)	C(205)	118.4(3)	C(26)	C(24)	C(27)	102.1(5)
C(103)	C(104)	C(105)	118.4(4)	C(223)	C(222)	C(221)	121.6(5)
C(205)	C(204)	C(203)	118.6(4)	C(223)	C(224)	C(225)	121.5(5)
C(2)	C(3)	C(4)	119.7(4)	N(402)	C(403)	C(404)	179.2(9)
C(3)	C(2)	C(1)	118.4(4)	C(228)	C(226)	C(223)	111.0(6)
N(201)	C(201)	C(202)	122.5(4)	C(228)	C(226)	C(229)	105.3(12)
N(201)	C(201)	C(219)	111.5(3)	N(403)	C(405)	C(406)	178.2(11)
C(202)	C(201)	C(219)	125.9(4)	N(401)	C(401)	C(402)	177.9(7)
C(207)	C(208)	C(209)	119.6(4)				

Table B.6. Hydrogen Atom Coordinates ($\text{\AA}\times 10^4$) and Isotropic Displacement Parameters ($\text{\AA}^2\times 10^3$) for Nd(**3**).

Atom	<i>x</i>	<i>y</i>	<i>z</i>	U(eq)
H(3)	6815.66	2089.32	11470.74	21
H(102)	2607.97	2527.54	7759.41	34
H(2)	2842.88	2453.21	10568.55	24
H(203)	6724.17	3002.19	8437.08	27
H(202)	4145.7	5202.4	9288.68	21
H(104)	2908.09	1469.78	7680.66	28
H(204)	5197.31	5373.96	9075.82	27
H(3A)	4801.28	1713.26	11910.99	30
H(2A)	5937.81	1924.53	11753.14	28
H(208)	3402.17	5965.77	9637.32	26
H(19)	8072.27	2001.47	11879.41	25
H(23)	7288.57	2668.61	10319.27	33
H(4)	3685.84	1926.12	11215.55	27
H(209)	2429.35	6091.21	9999.8	32
H(20A)	6446.82	4096.26	8451.75	28
H(20B)	6056.19	5233.74	8597.17	31
H(221)	6872.66	1862.78	7900.19	46
H(103)	5461.51	52.4	9166.87	32
H(10A)	3321.79	297.41	7797.52	35
H(10B)	4315.38	-10.17	8570.63	32
H(22)	8490.57	2636.6	10265.07	54
H(20)	9277.78	2008.32	11824.36	29

H(112)	3234.5	4051.63	8542.54	35
H(119)	6091.78	-866.33	9833.51	37
H(12)	2467.57	2960.83	9207.32	29
H(122)	7640.98	905.45	10788.71	49
H(9)	381.73	2315.7	9690.43	49
H(11)	1274.28	3138.68	8606.82	31
H(108)	1476.5	3120.6	7448.94	35
H(11A)	317.69	5251.71	7243.19	75
H(11B)	30.76	5744.55	7628.61	75
H(11C)	43.27	4917.57	7707.12	75
H(109)	773.85	4125.83	7431.49	35
H(8)	1563.98	2174.19	10308.99	44
H(120)	7175.12	-1149.73	10531.74	40
H(123)	6565.55	1194.7	10095.56	49
H(111)	2514.43	5040.44	8526.29	39
H(225)	7246.63	1962.02	9515.21	61
H(12A)	8220.52	547.91	11667.04	61
H(12B)	8740.91	-54.99	12002.91	61
H(12C)	7866.62	-134.72	11836.52	61
H(211)	2406.12	4001.98	10229.01	54
H(212)	3385.78	3867.16	9873.44	46
H(26A)	9655.66	3022.49	10388.85	69
H(26B)	10506.37	2893.61	10705.52	69
H(26C)	10010.42	3336.38	10979.14	69
H(12D)	8752.4	80.19	10624.83	93

H(12E)	9322.13	-363.62	11087.36	93
H(12F)	9106.32	409.74	11209.86	93
H(14A)	-715.68	2125.5	8950.17	84
H(14B)	-1207.48	2750.38	8622.03	84
H(14C)	-673.65	2878.61	9219.91	84
H(11D)	1982.51	6044.3	8097.57	103
H(11E)	1205.81	6434.53	7901.43	103
H(11F)	1472.52	5976.9	7486.18	103
H(16A)	260.48	2511.5	8020.61	111
H(16B)	-616.2	2540.5	7865.98	111
H(16C)	-170.37	1916.29	8228.2	111
H(222)	7537.66	806.04	8015.9	60
H(224)	7910.23	910.24	9624.07	71
H(15A)	-143.22	3905.36	8825.93	95
H(15B)	-699.51	3701.53	8250.29	95
H(15C)	160.47	3775.1	8329.52	95
H(21A)	952.97	4407.51	9901.74	99
H(21B)	753.8	4561.42	10440.84	99
H(21C)	1449.69	4087.66	10461.16	99
H(12G)	8011.08	-1277.7	11453.97	103
H(12H)	8875.1	-1182.9	11559.62	103
H(12I)	8345.18	-1351.23	10967.26	103
H(11G)	831.82	5017.34	8684.16	124
H(11H)	741.8	5842.2	8602.23	124
H(11I)	1543.33	5507.28	8839.59	124

H(40A)	5128.91	1496.44	7196.99	135
H(40B)	4328.1	1328.68	7235.65	135
H(40C)	5042.64	1141.58	7727.02	135
H(25A)	10440.25	2157.86	11734.25	157
H(25B)	10781.2	1832.77	11301.42	157
H(25C)	10122.03	1443.29	11438.11	157
H(21D)	1298.16	6124.08	9960.1	49
H(21E)	644.44	5785.23	10136.11	49
H(21F)	841.66	5483.17	9628.17	49
H(27A)	9665.08	1205.23	10603.37	103
H(27B)	10238.89	1654.06	10407.98	103
H(27C)	9375.91	1796.74	10156.84	103
H(22A)	9124.11	754.54	9220.09	377
H(22B)	9383.39	23.86	9046.71	377
H(22C)	9186.7	85.22	9595.86	377
H(22D)	8615.13	-661.61	8513.9	525
H(22E)	8365.4	48.96	8188.95	525
H(22F)	7760.26	-477.87	8269.21	525
H(21G)	2307.93	5177.57	11153.38	44
H(21H)	1510.56	5500.1	11075.07	44
H(21I)	2100.64	5927.62	10882	44
H(40D)	1362.08	772.38	6501.72	164
H(40E)	822.15	386.58	6769.68	164
H(40F)	1692.43	286.25	7016.96	164
H(40G)	4372.4	4167.09	7727.26	141

H(40H)	3531.18	4090.61	7366.51	141
H(40I)	3824.52	4814.98	7656.47	141
H(22G)	8069.51	-175.12	9622.4	258
H(22H)	7549.28	-578.84	9110.18	258
H(22I)	8386.04	-816.47	9371.98	258

Table B.7. Atomic Occupancy for Nd(3).

Atom	Occupancy	Atom	Occupancy	Atom	Occupancy
I(3)	0.192(17)	I(3B)	0.32(2)	I(3A)	0.48(2)
H(12D)	0	H(12E)	0	H(12F)	0
C(214)	0.46(2)	C(215)	0.54(2)	C(218)	0.534(18)
C(217)	0.466(18)				

Crystal structure determination of [Nd(3)]

Crystal Data for $C_{87.09}H_{105}I_3N_{12}NdO_6$ ($M=1940.90$ g/mol): monoclinic, space group $P2_1/c$ (no. 14), $a = 18.754(3)$ Å, $b = 18.809(3)$ Å, $c = 25.655(4)$ Å, $\beta = 108.127(3)^\circ$, $V = 8600(2)$ Å³, $Z = 4$, $T = 426.15$ K, $\mu(\text{MoK}\alpha) = 1.739$ mm⁻¹, $D_{\text{calc}} = 1.499$ g/cm³, 132580 reflections measured ($4.332^\circ \leq 2\theta \leq 55.29^\circ$), 19967 unique ($R_{\text{int}} = 0.0472$, $R_{\text{sigma}} = 0.0298$) which were used in all calculations. The final R_1 was 0.0421 ($I > 2\sigma(I)$) and wR_2 was 0.1145 (all data).

Refinement model description

Number of restraints - 0, number of constraints - unknown.

Details:

1. Fixed Uiso

At 1.2 times of:

All C(H) groups, All N(H) groups

At 1.5 times of:

All C(H,H,H) groups

2. Others

Sof(C215)=1-FVAR(1)

Sof(C214)=FVAR(1)

Sof(C217)=1-FVAR(2)

Sof(C218)=FVAR(2)

Fixed Sof: H12D(0) H12E(0) H12F(0)

3.a Me refined with riding coordinates:

C228(H22G,H22H,H22I)

3.b Aromatic/amide H refined with riding coordinates:

N3(H3), N102(H102), N2(H2), N203(H203), N202(H202), C104(H104), C204(H204),

C3(H3A), C2(H2A), C208(H208), C19(H19), C23(H23), C4(H4), C209(H209),

C202(H20A), C203(H20B), C221(H221), N103(H103), C103(H10A), C102(H10B),

C22(H22), C20(H20), C112(H112), C119(H119), C12(H12), C122(H122), C9(H9),
 C11(H11), C108(H108), C109(H109), C8(H8), C120(H120), C123(H123), C111(H111),
 C225(H225), C211(H211), C212(H212), C222(H222), C224(H224)

3.c Idealised Me refined as rotating group:

C114(H11A,H11B,H11C), C126(H12A,H12B,H12C), C26(H26A,H26B,H26C), C127(H12D,
 H12E,H12F), C14(H14A,H14B,H14C), C116(H11D,H11E,H11F), C16(H16A,H16B,H16C),
 C15(H15A,H15B,H15C), C216(H21A,H21B,H21C), C125(H12G,H12H,H12I), C115(H11G,
 H11H,H11I), C404(H40A,H40B,H40C), C25(H25A,H25B,H25C), C215(H21D,H21E,H21F),
 C27(H27A,H27B,H27C), C229(H22A,H22B,H22C), C227(H22D,H22E,H22F), C218(H21G,
 H21H,H21I), C406(H40D,H40E,H40F), C402(H40G,H40H,H40I)

This report has been created with Olex2, compiled on 2018.05.29 svn.r3508 for OlexSys.

B.2 Theoretical Additional Data

Table B.8. Cartesian coordinates of PBE0 optimized geometries of ligands and metal complexes

(1)	(2)
1.C 1.147414 -1.963562 -0.017753	1.C 1.154357 -2.132409 -0.089722
2.C 1.197775 -3.357892 -0.026719	2.C 1.197072 -3.528031 -0.099977
3.C 0.000054 -4.064000 -0.000340	3.C 0.000045 -4.226840 -0.000297
4.C -1.197688 -3.357934 0.026132	4.C -1.196992 -3.528064 0.099492
5.C -1.147368 -1.963602 0.017354	5.C -1.154288 -2.132442 0.089427
6.N 0.000011 -1.282604 -0.000152	6.N 0.000027 -1.466101 -0.000107
7.H 0.000072 -5.151049 -0.000413	7.H 0.000055 -5.313890 -0.000378
8.H 2.168348 -3.843040 -0.050026	8.H 2.158638 -4.023615 -0.182924
9.H -2.168248 -3.843114 0.049367	9.H -2.158552 -4.023671 0.182374
10.C 2.456664 -1.197069 -0.019383	10.C 2.420387 -1.310444 -0.162617
11.C -2.456647 -1.197157 0.019059	11.C -2.420339 -1.310516 0.162415
12.N 2.283087 0.142921 0.126029	12.N 2.174748 -0.024029 0.145169
13.C 3.237825 1.164955 0.199601	13.C 2.965057 1.129577 0.221364
14.C 4.611386 0.942653 0.035940	14.C 4.320969 1.195240 -0.123563
15.C 2.773334 2.465023 0.447818	15.C 2.313932 2.290113 0.674745

16.C	5.491895	2.018689	0.121700	16.C	4.996549	2.409222	-0.012835
17.H	4.969348	-0.061905	-0.151885	17.H	4.829434	0.304124	-0.469102
18.C	3.664208	3.527610	0.530628	18.C	3.000115	3.491236	0.780189
19.H	1.706967	2.639193	0.582440	19.H	1.262163	2.241531	0.953564
20.C	5.032215	3.310632	0.367507	20.C	4.350812	3.558286	0.435219
21.H	6.556094	1.837534	-0.007046	21.H	6.048627	2.449078	-0.283719
22.H	3.287033	4.528143	0.726091	22.H	2.479249	4.376286	1.135869
23.H	5.730838	4.140284	0.432631	23.H	4.892057	4.496850	0.517774
24.N	-2.283120	0.142860	-0.126156	24.N	-2.174752	-0.024072	-0.145288
25.C	-3.237901	1.164860	-0.199647	25.C	-2.965119	1.129499	-0.221427
26.C	-2.773448	2.464997	-0.447570	26.C	-2.314061	2.290085	-0.674774
27.C	-4.611471	0.942458	-0.036192	27.C	-4.321032	1.195078	0.123517
28.C	-3.664368	3.527552	-0.530300	28.C	-3.000311	3.491173	-0.780173
29.H	-1.707074	2.639248	-0.582027	29.H	-1.262293	2.241569	-0.953605
30.C	-5.492026	2.018463	-0.121869	30.C	-4.996679	2.409026	0.012833
31.H	-4.969403	-0.062153	0.151412	31.H	-4.829445	0.303924	0.469032
32.C	-5.032384	3.310474	-0.367387	32.C	-4.351009	3.558139	-0.435191
33.H	-3.287222	4.528141	-0.725535	33.H	-2.479496	4.376264	-1.135830
34.H	-6.556232	1.837227	0.006711	34.H	-6.048757	2.448815	0.283727
35.H	-5.731043	4.140099	-0.432452	35.H	-4.892307	4.496676	-0.517714
36.H	1.312164	0.413084	0.212947	36.H	1.190945	0.123863	0.356015
37.H	-1.312205	0.413078	-0.212995	37.H	-1.190959	0.123876	-0.356139
38.O	3.522654	-1.778326	-0.131500	38.S	-3.872972	-2.014434	0.579646
39.O	-3.522618	-1.778473	0.131055	39.S	3.873053	-2.014287	-0.579861
(3)				Nd(NO₃)₃(3)(H₂O)			
1.C	1.145962	-1.996875	0.056611	1.Nd	1.446295	1.728293	2.630807
2.C	1.196081	-3.391340	0.055034	2.H	-1.280616	6.346857	1.754506
3.C	-0.000323	-4.097527	-0.003148	3.C	-0.297335	4.598173	1.812752

4.C	-1.196706	-3.391191	-0.059956	4.N	1.778491	4.464621	2.944595
5.C	-1.146604	-1.996727	-0.057765	5.C	0.901064	5.305018	2.408019
6.N	-0.000340	-1.315632	0.000689	6.C	1.117829	6.684788	2.393187
7.H	-0.000326	-5.184621	-0.004470	7.H	0.424929	7.373529	1.918662
8.H	2.166176	-3.875827	0.100292	8.C	2.280424	7.177814	2.974619
9.H	-2.166763	-3.875561	-0.107229	9.H	2.486970	8.244372	2.969965
10.C	2.455148	-1.233419	0.127106	10.C	3.179864	6.291089	3.554615
11.C	-2.455682	-1.233123	-0.128845	11.H	4.089498	6.677496	4.004724
12.N	2.281655	0.112731	0.163219	12.C	2.885421	4.926055	3.516923
13.C	3.238098	1.133638	0.237009	13.C	3.741567	3.815648	4.084418
14.C	4.615663	0.902565	0.260136	14.H	5.060588	5.156069	4.788431
15.C	2.776678	2.456767	0.289855	15.N	2.783163	-0.886643	2.468223
16.C	5.496179	1.982206	0.334173	16.O	3.404106	0.201941	2.690193
17.H	4.987175	-0.113905	0.221159	17.O	1.527420	-0.766062	2.322299
18.C	3.669729	3.514115	0.363558	18.O	3.343874	-1.948140	2.403107
19.H	1.706169	2.656306	0.274797	19.N	0.115566	1.688249	5.248560
20.C	5.057569	3.307519	0.388047	20.O	0.720555	0.676958	4.778522
21.H	6.559115	1.762511	0.349798	21.O	-0.421511	1.681999	6.325751
22.H	3.269875	4.524389	0.403659	22.O	0.116567	2.719906	4.498406
23.N	-2.282337	0.113232	-0.157241	23.O	2.750519	2.884992	0.803623
24.C	-3.238577	1.134251	-0.232079	24.O	1.382911	1.356962	0.164852
25.C	-2.777523	2.458123	-0.266423	25.N	2.208287	2.268771	-0.164597
26.C	-4.615566	0.902536	-0.274936	26.O	2.450026	2.531277	-1.314659
27.C	-3.670346	3.515534	-0.342075	27.O	-0.776924	0.588788	1.882389
28.H	-1.707464	2.658220	-0.235237	28.H	-0.600724	-0.340311	2.083394
29.C	-5.495848	1.982235	-0.350864	29.H	-0.663149	0.658311	0.924690
30.H	-4.986793	-0.114470	-0.249634	30.O	3.363833	2.652268	3.956885
31.C	-5.057572	3.308260	-0.387122	31.O	-0.246937	3.385089	1.626080

32.H	-3.270787	4.526408	-0.367383	32.N	-1.365643	5.367356	1.533464
33.H	-6.558311	1.761991	-0.382604	33.N	4.878520	4.168716	4.705230
34.H	1.309982	0.392189	0.137680	34.C	5.862741	3.344587	5.298625
35.H	-1.310840	0.392734	-0.126019	35.C	6.839825	3.981506	6.066343
36.O	3.522956	-1.823109	0.149899	36.C	5.914762	1.956011	5.134332
37.O	-3.523256	-1.822910	-0.158961	37.C	7.855188	3.247083	6.668663
38.C	-6.010058	4.505045	-0.473708	38.H	6.808654	5.062169	6.200747
39.C	-5.711674	5.303603	-1.756236	39.C	6.939012	1.244112	5.746633
40.H	-6.380419	6.168922	-1.828653	40.H	5.173164	1.438945	4.537612
41.H	-4.681673	5.673339	-1.772539	41.C	7.929863	1.857595	6.526218
42.H	-5.859289	4.681498	-2.645458	42.H	8.594427	3.778919	7.258563
43.C	-5.803531	5.414657	0.751515	43.H	6.955779	0.167202	5.601183
44.H	-6.472132	6.281403	0.697149	44.C	-2.623379	5.000475	1.004942
45.H	-6.019275	4.873622	1.679045	45.C	-3.475689	6.036179	0.617274
46.H	-4.776085	5.786972	0.811220	46.C	-3.056620	3.676448	0.881713
47.C	-7.480473	4.072820	-0.508281	47.C	-4.740013	5.759569	0.108739
48.H	-7.699503	3.446156	-1.379372	48.H	-3.150756	7.071704	0.709498
49.H	-7.763134	3.521137	0.394625	49.C	-4.322892	3.423923	0.368257
50.H	-8.120382	4.959303	-0.568866	50.H	-2.417462	2.860391	1.193572
51.C	6.010307	4.504252	0.472588	51.C	-5.196172	4.445014	-0.032279
52.C	5.731116	5.288681	1.768083	52.H	-5.371231	6.593227	-0.180899
53.H	6.399808	6.154147	1.839290	53.H	-4.635195	2.386096	0.285824
54.H	4.700989	5.656627	1.804475	54.C	9.028202	1.013060	7.178014
55.H	5.893492	4.657291	2.648140	55.C	10.016862	1.869605	7.976978
56.C	7.481440	4.073156	0.479653	56.H	10.781781	1.224320	8.421550
57.H	7.714777	3.438154	1.340935	57.H	10.529911	2.599256	7.340947
58.H	7.750214	3.530683	-0.433014	58.H	9.523116	2.406666	8.794211
59.H	8.121489	4.959629	0.538922	59.C	8.382283	-0.005080	8.135793

60.C	5.784047	5.426679	-0.739515	60.H	7.825994	0.504035	8.930107
61.H	6.453022	6.293219	-0.686498	61.H	7.688380	-0.669711	7.612677
62.H	5.985383	4.895675	-1.676029	62.H	9.154989	-0.625755	8.602989
63.H	4.755656	5.799062	-0.779113	63.C	9.810295	0.262344	6.084518
				64.H	10.286150	0.964999	5.392075
				65.H	10.594113	-0.354121	6.538524
				66.H	9.161062	-0.397107	5.500984
				67.C	-6.578437	4.100109	-0.594137
				68.C	-7.387368	5.353720	-0.945575
				69.H	-8.365718	5.057797	-1.338350
				70.H	-7.561453	5.985079	-0.067487
				71.H	-6.892324	5.956235	-1.714859
				72.C	-7.368455	3.292153	0.451656
				73.H	-8.357168	3.031834	0.057760
				74.H	-6.858391	2.361351	0.716921
				75.H	-7.508384	3.872456	1.369861
				76.C	-6.409067	3.257397	-1.871711
				77.H	-5.857065	3.813989	-2.636565
				78.H	-5.865905	2.328197	-1.674809
				79.H	-7.390025	2.993203	-2.282226
Nd(NO ₃) ₃ (1)(H ₂ O)				Nd(NO ₃) ₃ (2)(H ₂ O)			
1.Nd	1.361230	1.699476	2.819075	1.Nd	1.461736	1.130969	2.343124
2.H	-1.359440	6.314323	1.786692	2.H	-0.636534	6.493738	1.876385
3.C	-0.362802	4.574044	1.936570	3.C	-0.345821	4.537350	1.682953
4.N	1.709436	4.449743	3.072533	4.N	1.854764	4.139372	2.648428
5.C	0.798172	5.289996	2.594142	5.C	1.110914	4.880712	1.825656
6.C	0.947930	6.674785	2.699856	6.C	1.636764	5.943733	1.079856
7.H	0.219806	7.370506	2.293627	7.H	1.017554	6.472693	0.361283

8.C	2.078564	7.172257	3.337409	8.C	2.983066	6.250535	1.216807
9.H	2.223531	8.243955	3.440687	9.H	3.439843	7.025371	0.607225
10.C	3.020306	6.283790	3.843111	10.C	3.736179	5.541721	2.142024
11.H	3.894717	6.670952	4.357834	11.H	4.794864	5.748695	2.268442
12.C	2.795139	4.915072	3.681781	12.C	3.123201	4.499375	2.851153
13.C	3.695426	3.804234	4.175592	13.C	3.918983	3.732684	3.870117
14.H	5.129820	5.134510	4.628364	14.H	4.586115	5.516843	4.446257
15.N	2.587805	-0.970937	2.891286	15.N	2.922058	-1.342115	1.831255
16.O	3.218615	0.092953	3.189793	16.O	3.500544	-0.221215	2.020316
17.O	1.384836	-0.791483	2.523881	17.O	1.654170	-1.306745	1.910650
18.O	3.091988	-2.060298	2.950326	18.O	3.529506	-2.350237	1.598369
19.N	-0.051102	1.721031	5.389872	19.N	0.430073	0.894951	5.077701
20.O	0.515885	0.679713	4.941476	20.O	0.966022	-0.085564	4.459817
21.O	-0.623249	1.747926	6.447840	21.O	0.025346	0.799661	6.205555
22.O	0.027436	2.750010	4.636896	22.O	0.356762	1.975200	4.413102
23.O	2.798203	2.712618	1.027453	23.O	2.430625	2.433967	0.439358
24.O	1.310050	1.320496	0.347507	24.O	1.120999	0.815615	-0.091350
25.N	2.221591	2.153699	0.042068	25.N	1.851087	1.778920	-0.485211
26.O	2.512771	2.399713	-1.099602	26.O	1.976933	2.060112	-1.647969
27.O	-0.877338	0.615372	2.040783	27.O	-0.781810	-0.125374	2.074586
28.H	-0.744032	-0.311243	2.282242	28.H	-0.675489	-0.840283	2.717066
29.H	-0.739582	0.644845	1.084280	29.H	-0.729014	-0.555691	1.211400
30.O	3.286131	2.646812	4.125228	30.N	-1.127248	5.634888	1.665493
31.O	-0.288294	3.363655	1.750900	31.N	4.736428	4.526961	4.587822
32.N	-1.425483	5.327728	1.594542	32.C	5.687536	4.257952	5.595369
33.N	4.905781	4.152260	4.643580	33.C	6.037323	5.340396	6.415911
34.C	5.942601	3.327236	5.139859	34.C	6.309630	3.019072	5.779974
35.C	7.042917	3.984579	5.705120	35.C	6.988088	5.186638	7.415345

36.C	5.917525	1.930186	5.068826	36.H	5.552473	6.304997	6.272954
37.C	8.114190	3.254094	6.202636	37.C	7.262981	2.879507	6.786370
38.H	7.058049	5.072483	5.757682	38.H	6.054093	2.176405	5.151320
39.C	7.000796	1.213509	5.573127	39.C	7.604946	3.950355	7.607520
40.H	5.077108	1.410521	4.625636	40.H	7.244387	6.032954	8.046681
41.C	8.096109	1.861165	6.139402	41.H	7.741448	1.913562	6.923810
42.H	8.961918	3.774675	6.639848	42.H	8.346858	3.824759	8.391250
43.H	6.978849	0.128730	5.513264	43.C	-2.514675	5.832185	1.512605
44.H	8.931988	1.285730	6.527574	44.C	-2.984093	7.118870	1.820286
45.C	-2.639095	4.931776	0.987489	45.C	-3.413435	4.859080	1.062918
46.C	-3.441631	5.950540	0.459664	46.C	-4.329796	7.429042	1.687828
47.C	-3.065446	3.601351	0.926030	47.H	-2.286866	7.878124	2.172128
48.C	-4.659586	5.644910	-0.134580	48.C	-4.762239	5.185515	0.934089
49.H	-3.107225	6.985710	0.508922	49.H	-3.066586	3.863245	0.822473
50.C	-4.287875	3.311015	0.324672	50.C	-5.229326	6.459148	1.244265
51.H	-2.456734	2.811926	1.347944	51.H	-4.676450	8.428856	1.934230
52.C	-5.086790	4.319896	-0.208252	52.H	-5.453500	4.423074	0.584956
53.H	-5.272702	6.443731	-0.542758	53.H	-6.284531	6.696642	1.141854
54.H	-4.617513	2.276445	0.280403	54.S	-0.845308	2.956711	1.533613
55.H	-6.037465	4.077090	-0.674740	55.S	3.785752	2.078392	4.008740
Eu(NO ₃) ₃ (1)(H ₂ O)				Eu(NO ₃) ₃ (2)(H ₂ O)			
1.Eu	1.318246	1.755740	2.917911	1.Eu	1.458467	1.123250	2.367072
2.H	-1.195083	6.317884	1.467034	2.H	-0.677051	6.521701	1.849899
3.C	-0.410265	4.550240	2.013781	3.C	-0.358264	4.564865	1.722019
4.N	1.673556	4.431234	3.135195	4.N	1.837073	4.194574	2.693021
5.C	0.750203	5.267432	2.672712	5.C	1.093146	4.927489	1.865562
6.C	0.871961	6.650058	2.831323	6.C	1.616790	5.988426	1.115022
7.H	0.115415	7.344599	2.478923	7.H	0.999735	6.512297	0.390713

8.C	1.992983	7.148254	3.485084	8.C	2.962105	6.300244	1.255070
9.H	2.111263	8.218051	3.632659	9.H	3.416929	7.076362	0.645585
10.C	2.954186	6.263165	3.959105	10.C	3.718376	5.591717	2.178244
11.H	3.820453	6.648361	4.488797	11.H	4.777493	5.799096	2.301085
12.C	2.749929	4.896675	3.760176	12.C	3.106560	4.548383	2.887205
13.C	3.657890	3.785086	4.238102	13.C	3.905018	3.762284	3.888395
14.H	5.100915	5.112391	4.681696	14.H	4.594780	5.530928	4.483939
15.N	2.838605	-0.669987	2.526333	15.N	2.893194	-1.335570	1.907477
16.O	3.361816	0.489186	2.475899	16.O	3.458785	-0.218784	2.162056
17.O	1.593767	-0.683033	2.773173	17.O	1.627153	-1.286685	1.861074
18.O	3.477811	-1.674623	2.356860	18.O	3.515593	-2.345274	1.726114
19.N	0.280934	1.788981	5.641333	19.N	0.528205	0.815236	5.069428
20.O	0.812188	0.758813	5.118086	20.O	1.061984	-0.141792	4.415704
21.O	-0.110601	1.807939	6.780079	21.O	0.153883	0.692513	6.204004
22.O	0.192601	2.798883	4.874755	22.O	0.423519	1.907138	4.426196
23.O	2.214067	2.803363	0.872614	23.O	2.429758	2.425971	0.537392
24.O	0.877851	1.148215	0.580330	24.O	1.087228	0.854202	-0.041270
25.N	1.592079	2.057480	0.052373	25.N	1.828449	1.818363	-0.407493
26.O	1.666375	2.208613	-1.139628	26.O	1.948088	2.143903	-1.558515
27.O	-0.892116	0.512430	2.763415	27.O	-0.759497	-0.055112	2.075964
28.H	-0.778317	-0.205909	3.399454	28.H	-0.625812	-0.856819	2.600080
29.H	-0.832338	0.094733	1.894361	29.H	-0.763518	-0.354609	1.157385
30.O	3.243938	2.628841	4.197281	30.N	-1.154560	5.649981	1.662877
31.O	-0.441752	3.324063	2.026929	31.N	4.736692	4.537749	4.610427
32.N	-1.357213	5.323975	1.448366	32.C	5.701277	4.246872	5.598485
33.N	4.880214	4.129277	4.675951	33.C	6.092589	5.321811	6.410467
34.C	5.921497	3.286399	5.136881	34.C	6.297710	2.993990	5.773627
35.C	6.944036	3.894250	5.874341	35.C	7.059782	5.147648	7.390506

36.C	5.973728	1.918420	4.851768	36.H	5.627739	6.297407	6.275555
37.C	8.015180	3.138579	6.335243	37.C	7.268341	2.834274	6.760438
38.H	6.896461	4.959834	6.094016	38.H	6.008893	2.156156	5.152929
39.C	7.053565	1.175230	5.322883	39.C	7.652279	3.897915	7.572192
40.H	5.193728	1.443180	4.268904	40.H	7.348241	5.988808	8.014862
41.C	8.071670	1.772372	6.063068	41.H	7.726608	1.857497	6.890022
42.H	8.803094	3.618392	6.909384	42.H	8.407296	3.756398	8.340518
43.H	7.093309	0.112885	5.097953	43.C	-2.541775	5.825002	1.484453
44.H	8.906548	1.177829	6.423633	44.C	-3.027403	7.120553	1.722368
45.C	-2.547656	4.948024	0.788413	45.C	-3.425943	4.821875	1.073361
46.C	-3.302161	5.983661	0.221757	46.C	-4.374205	7.410211	1.558218
47.C	-2.992458	3.625442	0.691224	47.H	-2.341900	7.903558	2.043912
48.C	-4.491176	5.704157	-0.438933	48.C	-4.775953	5.128103	0.911539
49.H	-2.954300	7.013021	0.296971	49.H	-3.066601	3.818651	0.888244
50.C	-4.186825	3.362045	0.024401	50.C	-5.258933	6.410899	1.151652
51.H	-2.413879	2.823107	1.129358	51.H	-4.733286	8.417555	1.750220
52.C	-4.939497	4.387853	-0.541555	52.H	-5.455456	4.342268	0.592440
53.H	-5.066050	6.516528	-0.875070	53.H	-6.314842	6.632636	1.024159
54.H	-4.528340	2.333136	-0.050333	54.S	-0.835140	2.972944	1.626732
55.H	-5.868200	4.165056	-1.059374	55.S	3.757705	2.107262	3.995526
Am(NO ₃) ₃ (1)(H ₂ O)				Am(NO ₃) ₃ (2)(H ₂ O)			
1.Am	1.340332	1.720465	2.888464	1.Am	1.488379	1.060960	2.353300
2.H	-1.227524	6.341607	1.561242	2.H	-0.673557	6.526402	1.903895
3.C	-0.387460	4.561016	1.979221	3.C	-0.343325	4.575158	1.732278
4.N	1.687642	4.421709	3.132435	4.N	1.869021	4.221037	2.671626
5.C	0.776086	5.263579	2.652421	5.C	1.107537	4.947705	1.855053
6.C	0.912646	6.646457	2.796771	6.C	1.610799	6.012093	1.095101
7.H	0.175366	7.346445	2.415984	7.H	0.977196	6.531282	0.381671

8.C	2.027693	7.141086	3.462354	8.C	2.955420	6.336012	1.214956
9.H	2.155448	8.211287	3.598613	9.H	3.393635	7.117609	0.600291
10.C	2.971454	6.251255	3.960557	10.C	3.732119	5.632029	2.124589
11.H	3.831294	6.632791	4.503066	11.H	4.791051	5.847998	2.234059
12.C	2.760424	4.884735	3.768419	12.C	3.139857	4.581678	2.839713
13.C	3.665045	3.779293	4.270751	13.C	3.968003	3.795593	3.816378
14.H	5.118526	5.114418	4.660387	14.H	4.584900	5.571832	4.462305
15.N	2.909505	-0.723919	2.539984	15.N	2.830466	-1.548969	2.233897
16.O	3.437813	0.431263	2.487531	16.O	3.385715	-0.476634	2.657119
17.O	1.658863	-0.733322	2.770965	17.O	1.642339	-1.403995	1.819753
18.O	3.544895	-1.733570	2.387013	18.O	3.401367	-2.604980	2.229995
19.N	0.035881	1.736406	5.542667	19.N	0.269223	0.755987	4.985888
20.O	0.577188	0.702112	5.033546	20.O	0.551288	-0.241493	4.240960
21.O	-0.477357	1.723802	6.632143	21.O	-0.236411	0.629731	6.067361
22.O	0.075750	2.779704	4.820342	22.O	0.565001	1.890344	4.493630
23.O	2.317046	2.785514	0.857655	23.O	2.535645	2.389330	0.543021
24.O	1.021453	1.115618	0.469474	24.O	1.240074	0.820416	-0.141215
25.N	1.750104	2.040013	-0.005089	25.N	1.981005	1.802221	-0.446029
26.O	1.891100	2.209689	-1.188760	26.O	2.149235	2.165623	-1.579804
27.O	-0.906870	0.434680	2.509367	27.O	-0.766095	-0.058172	1.727323
28.H	-0.854754	-0.308066	3.123948	28.H	-0.761688	-0.839513	2.295957
29.H	-0.770319	0.055016	1.631842	29.H	-0.645551	-0.384954	0.826813
30.O	3.248381	2.623569	4.266021	30.N	-1.148420	5.654622	1.709762
31.O	-0.400578	3.336595	1.923012	31.N	4.763681	4.581800	4.566255
32.N	-1.362277	5.346973	1.480196	32.C	5.734333	4.306628	5.552328
33.N	4.891877	4.133155	4.690900	33.C	6.108574	5.389924	6.361878
34.C	5.929871	3.300795	5.177934	34.C	6.347210	3.062594	5.734768
35.C	6.944496	3.923426	5.913971	35.C	7.074809	5.233115	7.345445

36.C	5.986552	1.927832	4.919137	36.H	5.630984	6.358702	6.222025
37.C	8.011349	3.177514	6.400276	37.C	7.316721	2.920359	6.725616
38.H	6.893736	4.992885	6.112986	38.H	6.070063	2.218196	5.117747
39.C	7.061591	1.194359	5.415911	39.C	7.683942	3.992272	7.533984
40.H	5.214077	1.441298	4.335589	40.H	7.349617	6.080681	7.967280
41.C	8.071300	1.806299	6.155518	41.H	7.787083	1.950145	6.861173
42.H	8.793066	3.668912	6.973129	42.H	8.438446	3.864215	8.305209
43.H	7.104891	0.128065	5.211184	43.C	-2.539679	5.823077	1.557030
44.H	8.902634	1.219442	6.536223	44.C	-3.030719	7.109205	1.831684
45.C	-2.561640	4.980128	0.830917	45.C	-3.422654	4.822550	1.137130
46.C	-3.332534	6.024951	0.304586	46.C	-4.381961	7.392264	1.694747
47.C	-3.002139	3.657789	0.710588	47.H	-2.345938	7.889877	2.160362
48.C	-4.532662	5.755134	-0.339967	48.C	-4.777148	5.122087	1.002800
49.H	-2.988390	7.054067	0.398082	49.H	-3.058506	3.826449	0.924394
50.C	-4.207853	3.404356	0.060482	50.C	-5.265487	6.395544	1.279290
51.H	-2.413158	2.847299	1.119068	51.H	-4.745408	8.392223	1.915078
52.C	-4.976167	4.439316	-0.466402	52.H	-5.455853	4.338492	0.676584
53.H	-5.119994	6.574791	-0.744735	53.H	-6.324857	6.612102	1.173020
54.H	-4.546252	2.375756	-0.031095	54.S	-0.808197	2.980727	1.603212
55.H	-5.913613	4.224020	-0.971433	55.S	3.894039	2.132143	3.855474
Eu(H ₂ O) ₉ ³⁺				Eu(NO ₃)(H ₂ O) ₈ ²⁺			
1.Eu	0.009192	0.000949	-0.007994	1.Eu	-0.030765	-0.005049	-0.423222
2.O	-0.934937	0.008207	-2.322430	2.O	0.461655	-0.387682	-2.819676
3.H	-0.636310	0.547137	-3.068964	3.H	1.302010	-0.113893	-3.211039
4.H	-1.677080	-0.516076	-2.656063	4.H	-0.061592	-0.781475	-3.527931
5.O	-1.498062	-0.000718	2.014041	5.O	0.045623	0.276843	3.588707
6.H	-1.392833	-0.525162	2.820712	6.H	1.009162	0.211607	3.651984
7.H	-2.301674	0.522293	2.146080	7.H	-0.281851	0.366254	4.493599

8.O	2.494077	-0.005192	0.249538	8.O	-2.244523	1.120766	-0.899179
9.H	3.128617	-0.543271	-0.245311	9.H	-2.849933	1.236719	-1.641613
10.H	3.020525	0.519800	0.869501	10.H	-2.602020	1.639223	-0.165802
11.O	-1.727242	1.775693	-0.206850	11.O	-0.643395	1.643708	1.314843
12.H	-2.406949	1.833335	-0.893956	12.H	-0.450459	1.354127	2.234365
13.H	-1.837299	2.569877	0.335542	13.H	-0.317637	2.549051	1.239812
14.O	0.687141	1.771530	1.590373	14.O	0.466484	2.294422	-1.269524
15.H	0.435058	1.821246	2.523862	15.H	1.395460	2.492125	-1.451671
16.H	1.191603	2.578094	1.411480	16.H	-0.060273	2.960696	-1.726991
17.O	1.019477	1.819842	-1.353540	17.O	-1.677132	-1.689644	-1.305162
18.H	1.950159	1.891603	-1.610580	18.H	-2.635731	-1.692319	-1.412515
19.H	0.591951	2.624477	-1.680452	19.H	-1.376730	-2.602324	-1.405868
20.O	-1.721310	-1.763245	-0.211708	20.O	-0.861138	-1.215825	1.525887
21.H	-2.544834	-1.811723	0.295178	21.H	-1.607367	-1.812714	1.646052
22.H	-1.695390	-2.568911	-0.747648	22.H	-0.588838	-0.887568	2.413040
23.O	0.687111	-1.780027	1.597302	23.O	0.909787	-2.352092	-0.563798
24.H	0.196240	-2.574507	1.852098	24.H	1.104181	-2.811863	0.263804
25.H	1.537072	-1.840420	2.057081	25.H	1.621096	-2.590491	-1.172811
26.O	1.015394	-1.816879	-1.356372	26.O	3.802553	0.232250	0.715565
27.H	1.449328	-2.621624	-1.038347	27.N	2.669060	0.173292	0.387312
28.H	0.999631	-1.888501	-2.321824	28.O	2.271278	0.338944	-0.827662
				29.O	1.703104	-0.064377	1.200292
Am(H ₂ O) ₉ ³⁺				Am(NO ₃)(H ₂ O) ₈ ²⁺			
1.Am	0.014412	0.000712	-0.015791	1.Am	-0.048914	0.015129	-0.439949
2.O	-0.902220	0.011538	-2.384519	2.O	0.507128	-0.418169	-2.882821
3.H	-0.597465	0.563705	-3.118914	3.H	1.364762	-0.163144	-3.248193
4.H	-1.633661	-0.515496	-2.737206	4.H	-0.018667	-0.755246	-3.618101
5.O	-1.525487	0.006046	2.055783	5.O	0.131018	0.233648	3.612432

6.H	-1.413700	-0.505631	2.869582	6.H	1.091384	0.123901	3.657728
7.H	-2.334643	0.521236	2.183856	7.H	-0.174667	0.327135	4.524466
8.O	2.545598	-0.016322	0.185881	8.O	-2.317514	1.227469	-0.775708
9.H	3.161804	-0.572081	-0.312719	9.H	-2.991349	1.343983	-1.456463
10.H	3.092966	0.511756	0.784890	10.H	-2.607354	1.743463	-0.011541
11.O	-1.788318	1.802035	-0.229690	11.O	-0.550743	1.684129	1.386790
12.H	-2.460347	1.856957	-0.924576	12.H	-0.343239	1.365194	2.293005
13.H	-1.923727	2.586451	0.321111	13.H	-0.217179	2.587780	1.329435
14.O	0.702385	1.807741	1.619634	14.O	0.461420	2.354719	-1.312102
15.H	0.452922	1.854724	2.553962	15.H	1.384861	2.564216	-1.507103
16.H	1.202183	2.617471	1.442146	16.H	-0.077451	3.030021	-1.741132
17.O	1.024706	1.895497	-1.352379	17.O	-1.773567	-1.659388	-1.362135
18.H	1.950231	1.981104	-1.623546	18.H	-2.732262	-1.656932	-1.468360
19.H	0.583832	2.701772	-1.656749	19.H	-1.481330	-2.573392	-1.473552
20.O	-1.757398	-1.798381	-0.201046	20.O	-0.889652	-1.219735	1.562063
21.H	-2.579628	-1.839871	0.308575	21.H	-1.616650	-1.836526	1.698525
22.H	-1.736155	-2.609822	-0.728364	22.H	-0.588412	-0.905524	2.443650
23.O	0.728076	-1.798177	1.656537	23.O	0.847728	-2.423919	-0.619024
24.H	0.236108	-2.580602	1.944350	24.H	1.063764	-2.900328	0.193351
25.H	1.585392	-1.855212	2.102980	25.H	1.506565	-2.699858	-1.269308
26.O	1.000253	-1.901329	-1.359031	26.O	3.832477	0.156635	0.663971
27.H	1.416238	-2.707410	-1.020894	27.N	2.693707	0.125008	0.351728
28.H	0.994301	-1.990583	-2.323118	28.O	2.278757	0.354843	-0.847446
				29.O	1.737448	-0.142404	1.166588
Nd(NO ₃) ₃ (H ₂ O) ₄							
1.O	1.518091	4.492986	5.545259				
2.O	0.827800	5.484392	7.346988				
3.N	1.725745	5.117393	6.545009				

4.Nd	2.293396	6.744762	8.926540
5.O	2.921647	5.473501	6.883200
6.O	5.350442	6.361634	6.423003
7.O	2.445699	4.170665	12.133890
8.O	2.257965	6.169256	11.310272
9.N	2.387464	4.902332	11.188595
10.O	2.460511	4.485292	9.986221
11.O	1.166257	8.621636	7.816016
12.O	0.126633	7.724004	9.468226
13.N	0.128500	8.622514	8.567800
14.O	-0.759905	9.411544	8.431910
15.O	4.767284	5.985811	9.147122
16.O	3.865616	8.314368	7.644325
17.O	3.134245	8.622923	10.417816
18.H	4.557491	5.836781	6.192713
19.H	5.241785	6.009849	8.296675
20.H	3.312845	8.924638	7.140781
21.H	3.195703	8.373516	11.347531
22.H	4.725597	5.056401	9.404482
23.H	6.019028	6.198426	5.752131
24.H	4.474950	7.872228	7.022824
25.H	3.931628	9.109248	10.185755

VITA

INGRID LEHMAN ANDINO

Born in Carolina, Puerto Rico

EDUCATION

PhD - Chemistry with Radiochemistry Track (2020)

Florida International University

MS-Master of Science in Chemistry (2018)

Florida International University

Specialization: Chemistry

Advisor: Konstantinos Kavallieratos

Bachelor of Science in Chemistry (2015)

University of Puerto Rico – Rio Piedras, PR, USA

Bachelor of Arts in Chemistry Education (2015)

University of Puerto Rico – Rio Piedras, PR, USA

PUBLICATIONS AND PRESENTATIONS:

1. Lehman-Andino, I.; Su, J.; Papathanasiou, K. E.; Eaton, T. M.; Jian, J.; Dan, D.; Albrecht-Schmitt, T. E.; Dares, C. J.; Batista, E. R.; Yang, P.; Gibson, J. K.; Kavallieratos, K. Soft-Donor Dipicolinamide Derivatives for Selective Actinide(III)/Lanthanide(III) Separation: The Role of S- vs. O-Donor Sites. *Chem. Commun.* 2019, 55 (17), 2441–2444. <https://doi.org/10.1039/C8CC07683A>.
2. Lehman-Andino, I.; Chakraborty, I.; Fortunato, M.T.; Panzer, R.; Raptis, R. G.; Kavallieratos, K. A dithiopicolinamide ligand complexes and senses Hg(II) selectively via a unique 2:2 Hg₂L₂ coordination pattern (In Preparation for *Chem. Comm.*).
3. Lehman-Andino, I., Chakraborty, I., Fortunato, M.T., Raptis, R. G., Kavallieratos, K.

4. Poster Presentation at the Waste Management Symposia (WM2020) at Phoenix, Arizona. *A Dithiopicolinamide Ligand Complexes and Senses Hg(II) Selectively Via a Unique 2:2 Coordination Pattern* March 2020.
5. Lehman-Andino, I., Su, J., Papathanasiou, K.E., Eaton, T. Jian, J., Dan, D., Albrecht-Schmitt, T.E., Grimes, T.S., Dares, C. J., Batista, E.R., Yang, P., Gibson, J. K., Kavallieratos, K. Oral presentation at Orlando ACS National Meeting & Expo. FL. *Oxoamide and thioamide ligands for solvent extraction applications from used nuclear fuel: Investigating actinide vs. lanthanide extraction selectivity.* April 2019.
6. Lehman-Andino, I., Grimes, T.S., Dares, C.J., Kavallieratos, K. Poster presentation at CAST Meeting Orlando Convention Center, FL *A water-soluble dipicolinamide holdback reagent for selective Am(III)/Ln(III) separation.* April 2019.
7. Lehman-Andino, I., Grimes, T.S., Dares, C.J., Kavallieratos, K. *A water-soluble dipicolinamide holdback reagent for selective Am(III)/Ln(III) separation.* 20th Symposium on Separation Science and Technology for Energy Applications. October 2018. Gatlinburg, Tennessee.
8. Lehman-Andino, I., Su, J., Papathanasiou, K. E, Eaton, T. Jian, J., Dan, D., Albrecht-Schmitt, T. E., Grimes, T. S., Dares, C. J., Batista, E. R., Yang, P., Gibson, J. K., Kavallieratos, K. *Investigation of Binding Properties of Actinides (An) and Lanthanides (Ln) for Nuclear Fuel Cycle Applications.* September 2018. Oral Presentation. Florida Inorganic & Material Symposium (FIMS), Gainesville FL.